DISSERTATION / DOCTORAL THESIS

Titel der Dissertation /Title of the Doctoral Thesis

„Single Phonon Quantum Optics
-
An experimental exploration of a
silicon photonics quantum memory"

verfasst von / submitted by

Ralf Riedinger, M.Sc.

angestrebter akademischer Grad / in partial fulfilment of the requirements for the degree of

Doktor der Naturwissenschaften (Dr. rer. nat.)

Wien, 2018 / Vienna 2018

für Vreni

Abstract

Acoustic phonons, the energy eigenstates of mechanical vibrations, possess a plethora of interesting features for quantum information processing. For example, they can serve as compact quantum memories with long life times, or can transduce quantum states between a variety of otherwise incompatible quantum systems. Particularly interesting among those are infrared photons in the telecommunication wavelength band, due to their widespread use in quantum communication. Using artificial optical and mechanical resonances, they can interact with phonons by radiation pressure. However, controlling individual excitations of motion in micromechanical resonators has thus far been restricted to the domain of microwave radiation, while optical control remained an outstanding goal. In this thesis, I describe how this can be achieved experimentally, employing quantum optics protocols. First, the operation of silicon optomechanical crystals in the quantum regime is demonstrated by creating non-classical photon-phonon pairs through optomechanical down conversion. This quantum interface is subsequently used to characterize heralded single phonons, and to generate quantum entanglement between two remote mechanical oscillators. The realization of these classic quantum optics experiments with single phonons establishes mechanical quantum memories in silicon photonics as a useful resource for future quantum networks.

Zusammenfassung

Akustische Phononen, die energetischen Eigenzustände von mechanischen Vibrationen, besitzen eine Vielzahl an interessanten Eigenschaften für die Verarbeitung von Quanteninformation. Beispielsweise können sie als langlebige und kompakte Quanteninformationsspeicher eingesetzt werden, oder Quantenzustände zwischen anderweitig inkompatiblen Systemen übertragen. Aufgrund ihrer technischen Relevanz sind hierbei Photonen im optischen Telekommunikations-Frequenzband von besonderem Interesse. Mit Hilfe von künstlich erzeugten optischen und akustischen Resonanzen, können die Photonen mit Phononen mittels Strahlungsdruck interagieren. Jedoch war die Kontrolle einzelner Bewegungsanregungen in mikromechanischen Resonatoren bisher auf den Mikrowellenbereich beschränkt, wohingegen das Ziel einer Manipulation durch Laser unerreicht blieb. In dieser Dissertation beschreibe ich, wie dies experimentell mithilfe von quantenoptischen Protokollen erreicht werden kann. Zunächst wird gezeigt, dass optomechanische Kristalle im Quantenbereich betrieben werden können, indem nichtklassische Photon-Phonon Paare mittels optomechanischer parametrischer Fluoreszenz erzeugt werden. Diese Quantenschnittstelle wird daraufhin verwendet um einzelne Phononen zu charakterisieren, sowie Quantenverschränkung zwischen zwei entfernten mechanischen Oszillatoren zu erzeugen. Die Demonstration dieser klassischen Quantenoptik Experimente mit einzelnen Phononen zeigt, dass mechanische Quanteninformationsspeicher eine vielversprechende Ressource für künftige Quantennetzwerke darstellen.

Contents

Contents

1. Introduction

Quantum optics is a field of research investigating and exploiting the consequences of the quantization of the electromagnetic field and its interaction with matter. Triggered by the invention of the laser, it experienced major advances, shaping our understanding of the foundations of physics and enabling new technologies for the manipulation of quantum systems. In this thesis, I employ quantum optical techniques to control individual excitations of motion, called phonons, in micromechanical oscillators. The experiments reported here demonstrate that optomechanical systems, in particular optomechanical crystals, can be a valuable resource for future optical quantum information architectures. They can serve as a quantum memory on an integrated silicon photonics platform, directly interfaced with photons in the conventional optical telecommunication wavelength band.

Quantum Optics

Early quantum optics experiments, such as the observation of particle-like features of light emitted by atoms [Cla74; KDM77], demonstrated the applicability of quantum field theory for optical experiments. Further, these non-classical emitters allowed to study quantum entanglement [FC72; AGR81], a counter-intuitive consequence of applying the superposition principle to correlations of particles [EPR35; Bel64]. Conversely, it was realized that light could be utilized to manipulate the internal [Kas50] and external degrees of freedom of atoms [Ash70]. Later on, the quantum optical control techniques were refined and extended to non-linear optical processes in bulk crystals [BW70; HM86] and various atom-like systems, such as defects in solid state materials [Gru+97] or superconducting qubits [Cla+88; NPT99; Wal+04a]. The ability to precisely manipulate these systems led to various applications, such as precision metrology, quantum simulation, quantum computation and quantum communication. Of particular interest is the coherent control of individual excitations in these systems. They can form the quantum analogue to a single bit of information, called qubit, which is the basis for the majority of quantum information protocols.

Cavity Optomechanics

Optical manipulation of massive objects has been demonstrated early on [Bet36; Ash70], however, it was limited to motion in the classical domain. Quantum control over motion was later on achieved in atomic systems [Die+89; Mee+96] using laser cooling techniques. In recent years, efforts to extend this quantum control to the motion of massive objects has attracted considerable attention [AKM14]. Relying on artificial instead of atomic resonances, this field of research was named cavity optomechanics. Technological advances in micromechanics and optics are promising to enable quantum control over massive, artificial degrees of freedom. On the one hand, this allows for an investigation on the

validity of quantum theory for macroscopic systems, some of them even visible to the naked eye [Tho+08].

On the other hand, the mechanical element can act as transducer [Rab+10] and memory [CG04; Fio+11; Cha+11b; Saf+11] in various quantum information applications. As the optical and mechanical resonances are artificially created, they can be designed to work at almost arbitrary frequencies. For example, a single mechanical element coupled to two electromagnetic resonances in vastly different frequency domains can act as bidirectional transducer between them [And+14; Vai+16].

Furthermore, the freedom of design can also be used to make mechanical quantum memories available for wavelength ranges with notoriously few usable atomic resonances. One such example is the conventional optical telecommunication band (C-band) around a wavelength of 1550 nanometers, which is of enormous interest for long distance quantum communication protocols, due to the high transmission of photons in this range in optical fibers. To expand quantum communication beyond the typical absorption length of these fibers, quantum repeaters have been proposed [Bri+98; Dua+01], which require memory elements interfaced to the traveling infrared photons. Particularly interesting is the possibility to have an array of optomechanical devices with closely spaced resonances in the C-band. This allows for wavelength division multiplexing of quantum communication channels, thereby achieving very high operational bandwidths. The individual mechanical elements can at the same time maintain long memory times, exceeding the current limitations of other broadband telecom quantum memory techniques, like rare earth ion doped crystals [Lau+10; Bus+14; Sag+15]. However, most protocols require control over individual excitations in the mechanical memory element, which remained elusive in the optical domain.

In a typical optomechanical system, the intensity of the light field couples to the mechanical displacement, exercising a force on the mechanical element known as radiation pressure. While this force is non-linear in the amplitude of the cavity field, as required for non-Gaussian control, it is very weak on the single photon level.

By driving the system strongly with an external laser, a considerable linear coupling between the cavity field and the mechanical interaction can be generated. A red detuned drive[1] allows for laser cooling of the mechanical element [Gig+06; Sch+06; Arc+06], eventually to its quantum ground state [Teu+11a; Cha+11a]. By further increasing the drive power, it is even possible to enter the regime of strong coupling between the mechanical and optical oscillator [Grö+09; Teu+11b; Ver+12], or to observe radiation pressure shot noise of a resonant optical field on the mechanical oscillator [PPR13]. While a blue detuned laser can generate Gaussian entanglement between the optical and the mechanical mode [Pal+13b], continuous driving leads to a parametric instability [Kip+05]. For technical reasons, this continuous variable entanglement was thus far only achieved in the microwave domain.

Single Phonon Control

In the driven system, the effective optomechanical interaction is linearized, preventing the direct generation of non-Gaussian states [Wie+15], such as single phonon excitations.

---

[1] In analogy to the visible spectrum, this corresponds to a drive laser with a frequency below that of the optical resonance.

In the microwave domain, it is instead possible to use an artificial non-linear resonance, i.e. a superconducting qubit, to generate a non-Gaussian quantum state, and use a linear interaction to transfer it to the mechanical element [OCo+10]. In addition to the previously described coupling in the driven system [Ree+17], this can also be achieved by a piezoelectric material, allowing for a direct generation and control of single phonons through the qubit [OCo+10]. Due to the smaller wavelength of mechanical waves, such a system could serve as compact memory also for superconducting quantum computation architectures [Chu+17].

In the optical domain, three main challenges prevented single phonon control so far: Compared to the microwave domain, (1) drive photons carry higher energy, thus increasing the absorption heating. (2) The higher frequency difference between the optical and the mechanical resonance imposes stricter requirements on their relative stability. (3) The optical domain lacks a tunable, strongly non-linear oscillator, akin superconducting qubits.

In the presented work, these points are addressed by choosing a monolithic optomechanical system that provides strong interactions and a high mechanical frequency. This is realized by nanofabricated resonators with a co-localized optical and mechanical mode, called optomechancial crystals and pioneered by the group of Oskar Painter [Eic+09; Cha+12]. (1) The high mechanical frequency of $\sim$ 5GHz allows for groundstate cooling by cryogenic means, eliminating absorption of an otherwise necessary cooling laser [Mee+14]. In addition, the high coupling strength reduces the drive power and therefore the absorption heating [Mee+15]. (2) The monolithic design of the cavity, along with the high mechanical frequency ensure that potential drifts in the cavity frequency are negligible, and enable the stabilization of the drive lasers to an external reference. Thus, the driven optomechanical interactions can be switched off completely when necessary. Furthermore, laser noise at the relevant sideband frequencies is small and can easily be further suppressed, in contrast to system involving low frequency oscillators. (3) While there is no comparable analogue to a superconducting qubit in the optical domain in terms of functionality[2], the strongly non-linear response of single photon detectors can be exploited to achieve non-Gaussian control over the mechanical element. In essence, probabilistic quantum optical protocols employ single photon detection events to distill quantum states from weakly driven system [Dua+01; Lee+11]. The use of single photon detectors for the detection of optomechanically generated photons, however, requires the complete suppression of the drive beams, which are separated from the signal by the mechanical frequency. As the latter is in the gigahertz range, this can conveniently be achieved by an array of optical filters [Coh+15].

The combination of optomechanical crystals with photon counting protocols enabled my coworkers and me to conduct a variety of quantum optics experiments with single phonons. First, we demonstrated the quantum nature of the optomechanical interface by observing non-classical correlations between photon-phonon pairs produced through optomechanical down-conversion [Rie+16]. Using this interface, we exerted non-Gaussian quantum control over the mechanical state, preparing a heralded single phonon, which was subsequently analyzed in a Hanbury Brown and Twiss interferometer [Hon+17]. Finally, we observed entanglement between two mechanical oscillators, by probabilistically preparing a single

---

[2] While there are plenty of effective two-level systems in the optical domain, too, they do not possess a comparable tunability, coherence time or ease-of-access as that of superconducting qubits.

phonon, and coherently erasing the information in which device it was generated [Rie+18].

Conclusion

Together, these three demonstrations of mechanical versions of quantum optical milestone experiments establish cavity optomechanics in the telecom band as new resource for future quantum networks. In particular the long lifetimes achievable in optomechanical crystals [Mee+15] and the integration in a silicon photonics platform are of interest for long distance quantum communication protocols.

Despite the impressive number of seminal experiments enabled by the development of linear optomechanical crystals [Eic+09; Cha+12], such as ground state cooling [Cha+11a], and phonon counting [Coh+15], amongst others [Saf+12; Hil+12; Mee+15; Fan+17; Pur+17], the devices are far from being mature. Further developments, which will be of great importance for the practical application of these devices, include the management of the heat load through integration in two dimensional structures [Saf+14]. This will allow for improvement of all relevant parameters of the experiments, by enabling laser cooling instead of cryogenic cooling, leading for example to significantly higher entanglement rates. Combining this with a full phononic bandgap shield to achieve long mechanical lifetimes will enable the realization of large area quantum networks based on silicon photonics.

Building on early experiments with phononic waveguides [Fan+16; Pat+18], it seems likely that these photon-phonon interfaces can be mechanically connected to other systems, in particular superconducting circuits [Vai+16]. This could allow for efficient transduction between microwave quantum processors and telecom optical photons. Applications thereof range from coherently linking separate quantum computers, to making a quantum network with error correcting nodes.

Structure of this Thesis

This thesis is structured as follows. The theoretical basis for this work is developed in chapter 2. After reviewing the standard treatment of the linearized optomechanical interactions and a characterization of the system components, the interaction between the flying optical mode and the mechanical memory element is described, and basic phonon counting protocols are explained. In chapter 3, the working principle of optomechanical crystals is briefly described. Thereafter, in the experimental part of this thesis, my manuscripts on optomechanical quantum correlations [Rie+16], intensity interferometry of single phonons [Hon+17], and mechanical entanglement [Rie+18] are presented in chapters 4 to 6. They are each preceded by an overview of the quantum optical context of the respective experiments. Finally, chapter 7 summarizes the results and gives a brief outlook over the potential of the presented optical single phonon control.

2. Theory of Cavity Optomechanics

Harmonic oscillators are omnipresent in physics and related fields of science. On the one hand, the equations of motion of a point-like mass on a spring are analytically easily solvable. This makes the harmonic oscillator in its classical and quantum version a textbook example in physics classes on all levels. On the other hand, it is a very good model for a vast number of physical systems. This can be understood by the fact that the equilibrium state of a system can often be described as local minimum of some effective potential. The system response to a small deviation from this state can be obtained from the first non-zero term of the Taylor expansion of this effective potential, usually quadratic in the deviation. This results in a linear restoring force, and thus in a harmonic oscillation around the equilibrium state.

The physical realization of such harmonic systems can differ drastically in nature. Mechanical oscillators, as used in this thesis, are manufactured solid state resonators. Their energy oscillates between the momentum $\hat{P}_p$ of the moving atoms, and the strain in the material or the local gravitational potential, both parametrized by a displacement $\hat{X}_p$ from the equilibrium position. In contrast, a light field confined by an optical resonator has the energy oscillate between an electric and a magnetic field. Despite no masses and spring being present in this system, it can be described in similar terms, with the magnetic field serving as a potential for the electric field or vice versa.

Cavity optomechanics studies the nonlinear coupling between those two vastly different systems. In addition to being an interesting toy system, it holds the promise to allow for quantum control of the mechanical element, using quantum optical control techniques. The standard example of an optomechanical system is a Fabry-Pérot Cavity with one movable mirror. The photons it reflects change the direction of propagation and thereby transfer momentum onto the movable mirror, an effect called radiation pressure. Con-

Photon   Mirror

$\vec{p}_i = \hbar\omega_{\mathrm{L}}/c\vec{e}_x$

$\Delta\vec{p} = 2\hbar\omega_{\mathrm{L}}/c\vec{e}_x$

$\vec{p}_f = -\hbar\omega_{\mathrm{L}}/c\vec{e}_x$
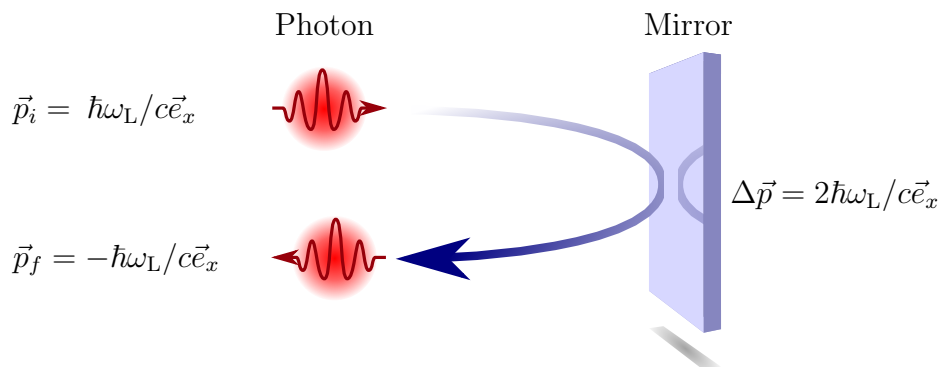
FIGURE 2.1.: **Radiation Pressure** When photons are reflected, e.g. by a mirror, their momentum $\vec{p}$ is reversed. As the total momentum is conserved, the mirror experiences a kick $\Delta\vec{p}$ ($\hbar$: reduced Planck constant, ω_{L} laser frequency, c: speed of light). The position of the mirror X_p is imprinted in the phase $\varphi = 2X_p\omega_{\mathrm{L}}/c$.

versely, a shift in the position of the mirror will change the distance the photons travel, thereby imposing a phase shift onto them, see figure 2.1.

In this chapter, I present the theoretical foundations of my work. Starting with a discussion of the basic equations of the optomechanical interaction in section 2.1, I continue reviewing the characteristics of the individual parts of the system in section 2.2. Note that those two topics are also covered elsewhere, for example in [AKM14]. Section 2.3 describes the primitives of the pulsed optomechanical control sequences used in the experimental part of this thesis. This is followed by an explanation of the basic protocols in section 2.4, employing the previously discussed control pulses.

In order to convey a feeling for the orders of magnitude, I will give examples using standard parameters of the devices used in chapters 4 to 6. The set of parameters used is given in table 2.1, along with an overview of frequently used operators.

This chapter is supposed to address inclined readers, as well as students, who are new to the field of optomechanics. Therefore, I included numerous footnotes, thereby offering the reader to go through the text at his or her own speed, suiting the interest and level of understanding of the respective topics.

Symbol	Description	Unit or Typical Value	See pg.
$\hat{c}^\dagger \ (\hat{c})$	creation (annihilation) operator of the optical cavity mode	$\sqrt{\text{photon}}$	7
$\hat{A}$	Amplitude quadrature of the optical mode	$\sqrt{\text{photon}}$	8
$\hat{Y}$	Phase quadrature of the optical mode	$\sqrt{\text{photon}}$	8
$\hat{m} \ (\hat{m}^\dagger)$	mechanical annihilation (creation) operator	$\sqrt{\text{phonon}}$	8
$\hat{P}$	Momentum quadrature of the mechanical mode	$\sqrt{\text{phonon}}$	8
$\hat{X}$	Displacement quadrature of the mechanical mode	$\sqrt{\text{phonon}}$	8
$\hat{o}_{\text{in}} \ (\hat{o}_{\text{out}})$	Optical input (output) field of the cavity	$\sqrt{\text{photon}/s}$	11
$\hat{o}_{\text{loss}}$	Incoupled loss channel of the cavity	$\sqrt{\text{photon}/s}$	11
$\hat{o}_{\text{loss,out}}$	Outcoupled loss channel of the cavity	$\sqrt{\text{photon}/s}$	11
$\hat{a}_{\text{in}}$	Discrete wave-packet inbound to cavity	$\sqrt{\text{photon}}$	33
$\hat{a}_{\text{out}}$	Discrete wave-packet outbound from cavity	$\sqrt{\text{photon}}$	34
$\chi_{\text{L}} \ (\chi_{\text{M}})$	Optical (mechanical) susceptibility	$2\pi \cdot \text{s}$	18/25
g_0	Optomechanical single photon coupling strength	$2\pi \cdot 825\,\text{kHz}$	9
Ω	Angular mechanical frequency	$2\pi \cdot 5.2\,\text{GHz}$	7
Γ	Mechanical energy decay rate	$2\pi\,\text{Hz}$	12
ω_c	Angular optical resonance frequency	$2\pi \cdot 193\,\text{THz}$	7
κ	Optical amplitude decay rate	$2\pi \cdot 450\,\text{MHz}$	11
ω_{L}	Angular frequency of the drive laser	$2\pi \cdot 193\,\text{THz}$	14
ϵ_{P}	Stokes scattering constant, pair-creation probability	1	39
ϵ_{R}	Anti-Stokes scattering constant, transfer efficiency	1	36
$g_{ab}^{(2)}$	Intensity cross-correlation between system a and b	1	48

TABLE 2.1.: This is a brief overview over the most important operators and constants used in this chapter. For relevant parameters, typical values for the devices used in this work are given. For a more extensive list, refer to appendix A.

2.1. The Optomechanical Interaction

The optomechanical interaction has been studied in detail theoretically as well as experimentally in a plethora of physical realizations [AKM14]. Here, I will give a short review of the basic equations, thereby clarifying the conventions and notations used throughout this thesis.

This section is structured as follows: First, I will introduce the Hamiltonian of the optomechanical system and its relation to the optical and mechanical environment. Paragraph 2.1.3 describes how the interaction can be enhanced and linearized by driving the system with an external laser. Finally, the transducing element, namely the optical cavity, is eliminated in paragraph 2.1.4, such that a relation between the flying optical fields and the stationary mechanical element is obtained. This description allows to identify the mechanical resonator as long lived quantum memory coupled to a traveling quantum field, as required for numerous quantum information protocols.

2.1.1. The Nonlinear System Hamiltonian

In a generic dispersive optomechanical system, the angular resonance frequency ω_c of an optical cavity is modified by a displacement $\hat{X}_p$ of a mechanical element. The Hamiltonian

$$\hat{\mathcal{H}} = \hbar\,\omega_c(\hat{X}_p)\,\left(\hat{c}^\dagger\hat{c} + \frac{1}{2}\right) + \frac{\hat{P}_p^2}{2m_{\text{eff}}} + V(\hat{X}_p) \tag{2.1}$$

thus gives rise to an interaction between the displacement $\hat{X}_p$ and the photon number $\hat{c}^\dagger\hat{c}$ in the optical resonator. Here, $\hbar$ is the reduced Planck constant, $\hat{P}_p = \frac{\hbar}{i}\frac{\partial}{\partial \hat{X}_p}$ is the momentum operator of the mechanical element with effective mass m_{eff}[1] and $V(\hat{X}_p)$ is the potential energy associated with the displacement $\hat{X}_p$. While the dependency of ω_c [Tho+08; San+10; Par+15] and V [AC05; GNQ13; Ric+17] on $\hat{X}_p$ can be more complex in general, we will only consider the lowest non-vanishing order of the Taylor expansion here. This results in a harmonic potential $V = m_{\text{eff}}\Omega^2\hat{X}_p^2/2$ for the mechanical element with the angular resonance frequency Ω_m, and the interaction term

$$\hat{\mathcal{H}}_{\text{int}} = \hbar\,\underbrace{\frac{\partial\omega_c}{\partial\hat{X}_p}}_{G}\,\hat{X}_p\left(\hat{c}^\dagger\hat{c} + \frac{1}{2}\right). \tag{2.2}$$

The transduction parameter $G/2\pi$ quantifies the linear shift of the optical resonance frequency per unit displacement, here in SI units of $[G/2\pi] = \text{Hz/m}$. To investigate the quantum effects of this system, it is convenient to use operators in natural (dimensionless) units. When considering individual quantized excitations in a harmonic oscillator, so-called ladder operators are a convenient choice, as they relate to jumps between neighboring Fock states $|n\rangle$ with a well defined number n of energy quanta:

$$\hat{a}\,|n\rangle_a = \sqrt{n}\,|n-1\rangle_a \qquad\qquad \hat{a}^\dagger\,|n\rangle_a = \sqrt{n+1}\,|n+1\rangle_a \tag{2.3}$$

---

[1] The mechanical elements employed in cavity optomechanics are in general macroscopic objects with a large number of normal modes. Here we consider a single mode with a unique frequency, such that it can be spectrally resolved. The effective mass m_{eff} of this mode allows to describe the kinetic and potential energy of this mode like for a point particle, see also paragraph 2.2.2.

2. Theory of Cavity Optomechanics

Here, $\hat{a}$ reduces the number of excitations in system a and is therefore called annihilation operator, whereas the so-called creation operator $\hat{a}^\dagger$ adds excitations to the system[2]. Throughout this thesis, annihilation operators will be represented by lowercase operators and creation operators as their Hermitian conjugates. For the excitations in the optical cavity mode, called photons, we will use the annihilation operator $\hat{c}$, as already introduced in eq. (2.1), and for the excitation in the mechanical mode, called phonons, the operator $\hat{m}$. For continuous variables, such as the displacement of the mechanical oscillator or the phase of the optical field, it is convenient to use a different set of operators,

$$\hat{Q}_{\hat{a}}^\theta = \frac{e^{-i\theta}\hat{a} + e^{i\theta}\hat{a}^\dagger}{\sqrt{2}}, \tag{2.4}$$

which are called quadratures. These self-adjoint operators, here for the generic system a, are characterized by a phase θ, and will be represented by capitalized operators. The system can completely be described by quadrature or ladder operators, with each set allowing for different intuitive access to the interaction. In this section, I will focus on a quadrature description, as it has a close correspondence to classical equations of motion. The important steps will be complemented by a ladder operator description, which is of importance for the final goal of understanding the single phonon control protocols.

In the mechanical system, the physical observables, the quadrature operators and the ladder operators relate to one another by

$$\hat{X} = \sqrt{\frac{m\Omega}{\hbar}}\hat{X}_p \qquad\qquad \hat{X} = \frac{\hat{m} + \hat{m}^\dagger}{\sqrt{2}} \tag{2.5a}$$

$$\hat{P} = \frac{1}{\sqrt{\hbar m\Omega}}\hat{P}_p \qquad\qquad \hat{P} = \frac{\hat{m} - \hat{m}^\dagger}{\sqrt{2}i} \tag{2.5b}$$

$$\hat{m} = \frac{\hat{X} + i\hat{P}}{\sqrt{2}} \qquad\qquad \hat{m}^\dagger = \frac{\hat{X} - i\hat{P}}{\sqrt{2}} \tag{2.5c}$$

The position (2.5a) and momentum (2.5b) quadrature operators $\hat{X} = \hat{Q}_{\hat{m}}^0$ and $\hat{P} = \hat{Q}_{\hat{m}}^{\pi/2}$ are rescaled versions of the physical displacement $\hat{X}_p$ and momentum $\hat{P}_p$ of the mechanical oscillator. As self-adjoint operators, they are observables. In contrast, the creation and annihilation operators $\hat{m}^\dagger$ and $\hat{m}$ are a Hermetian conjugate pair (2.5c), which cannot be measured experimentally. In close analogy, we define the optical quadratures $\hat{A}$ and $\hat{Y}$

$$\hat{A} = \frac{\hat{c} + \hat{c}^\dagger}{\sqrt{2}} \qquad\qquad \hat{Y} = \frac{\hat{c} - \hat{c}^\dagger}{\sqrt{2}i}, \tag{2.6}$$

which are associated with the oscillating electromagnetic field in the cavity. In paragraph 2.1.3 we will see that in a rotating frame, these two quadratures can be related to the amplitude ($\hat{A}$) and phase ($\hat{Y}$) of the optical field, and hence we will occasionally refer to them as amplitude, respectively, phase quadrature.

Using these relations[3], we can express the Hamiltonian (2.1) exclusively in terms of

---

[2] Note that the number operator $\hat{a}^\dagger\hat{a}\left|n\right\rangle_a = n\left|n\right\rangle_a$, is proportional to the free Hamiltonian of a harmonic oscillator and thus the Fock states are the eigenstates of the system.

[3] Note the commutation relations of these operators are

$$\left[\hat{X},\hat{P}\right] = i \qquad\qquad \left[\hat{A},\hat{Y}\right] = i \qquad\qquad [\hat{m},\hat{m}^\dagger] = 1 \qquad\qquad [\hat{c},\hat{c}^\dagger] = 1$$

quadratures

$$\hat{\mathcal{H}} = \frac{\hbar\omega_c}{2}\left(\hat{A}^2 + \hat{Y}^2\right) + \frac{\hbar\Omega}{2}\left(\hat{X}^2 + \hat{P}^2\right) + \frac{\hbar g_0}{\sqrt{2}}\hat{X}\left(\hat{A}^2 + \hat{Y}^2\right) \tag{2.7a}$$

or in terms of ladder operators

$$\hat{\mathcal{H}} = \hbar\omega_c\,\hat{c}^\dagger\hat{c} + \hbar\Omega\,\hat{m}^\dagger\hat{m} + \hbar g_0\left(\hat{c}^\dagger\hat{c} + \frac{1}{2}\right)\left(\hat{m} + \hat{m}^\dagger\right), \tag{2.7b}$$

neglecting constant energy offsets due to the vacuum energy of the optical and mechanical modes $\hbar\omega_c/2$ and $\hbar\Omega/2$. The offset in the interaction term, $\hbar g_0/2\left(\hat{m} + \hat{m}^\dagger\right)$, gives rise to a force based on the photonic vacuum fluctuations, as we will see in the next paragraph, in analogy to the Casimir-Polder force. Here, the single photon coupling rate

$$g_0 = G x_{\mathrm{zpf}} \tag{2.8a}$$

$$x_{\mathrm{zpf}} = \sqrt{\langle 0|\,\hat{X}_p^2\,|0\rangle} = \sqrt{\frac{\hbar}{2m_{\mathrm{eff}}\Omega}} \tag{2.8b}$$

describes how far the optical resonance is shifted by a displacement equivalent to the zero point fluctuations x_{zpf} of the mechanical mode. This nonlinearity is typically very weak, i.e. the optical frequency shift due to a single phonon is small compared to the spectral width of the optical resonance, which is the topic of the next paragraph. Nevertheless, the nonlinearity can be used to generate significant linear interaction between the mechanical and the optical mode, by driving the system with an auxiliary laser beam, as described in paragraph 2.1.3.

Before we introduce the coupling to the environment, we can estimate what type of interaction we can expect. In the Schrödinger picture, or more precisely in the interaction picture, we obtain the unitary state evolution $\hat{\mathcal{U}}(t)$ after time t by integrating the interaction term of (2.7b)[4]. For short interaction times $\sqrt{\epsilon} = g_0 t \ll 1$ we can neglect higher order terms and find the state after the interaction $|\psi(t)\rangle \approx (1 + i\sqrt{\epsilon}\hat{c}^\dagger\hat{c}\hat{m} + i\sqrt{\epsilon}\hat{m}^\dagger\hat{c}^\dagger\hat{c})\,|\psi(0)\rangle$. Concentrating on the last term $\propto \hat{m}^\dagger\hat{c}^\dagger\hat{c}$, we find, that with probability ϵ, a cavity photon will be annihilated under the creation of another cavity photon and a phonon. Energy conservation, or a rotating wave approximation, suggests that the reemitted photon will be downshifted by the mechanical frequency with respect to the annihilated photon. This process is called Stokes scattering, a phenomenon commonly associated with the Raman effect, i.e. the inelastic scattering of photons e.g. by molecules or crystals. The opposite process, anti-Stokes scattering, is associated with the second term $\propto \hat{c}^\dagger\hat{c}\hat{m}$, i.e. the up-conversion of a photon under annihilation of a phonon. As Raman scattering reveals the intrinsic vibrational frequencies of a substance, which are usually in the terahertz regime, this effect is employed e.g. for spectroscopic purposes. When the involved vibrations are not of molecular origin, but traveling waves in the bulk material, i.e. from the acoustic

---

and therefore we can express the number operators as

$$\hat{m}^\dagger\hat{m} = \frac{\hat{X}^2 + \hat{P}^2 - 1}{2} \qquad\qquad \hat{c}^\dagger\hat{c} = \frac{\hat{A}^2 + \hat{Y}^2 - 1}{2}.$$

[4] With the formal integration $\hat{\mathcal{U}}(t) = \exp(-i/\hbar\int_{t_0}^{t}\mathrm{d}t\,\hat{\mathcal{H}})$, we find $|\psi(t)\rangle = \hat{\mathcal{U}}(t)\,|\psi(t_0)\rangle$.

instead of optical phonon branch, the effect is usually called Brillouin scattering. Consequently, cavity optomechanics can be characterized as low frequency Raman scattering, or doubly resonant Brillouin scattering.

2.1.2. Langevin Equations

In order to quantitatively study the interaction rates, we need to take into account the coupling to the environment. For example, the finite lifetime $1/\kappa$ of photons in the optical resonator will result in an effective interaction time $t \sim 1/\kappa$ and thus scattering probability $\epsilon \sim g_0^2/\kappa^2$ for each cavity photon. In addition, the optical bandwidth will modify the spectral behavior of the Stokes and anti-Stokes processes.

For the treatment of open quantum systems, the system of interest is embedded in an environment, i.e. coupled to large number of auxiliary systems, the so called 'bath'. To reduce the complexity of the system, some assumptions on the bath are made, such that an effective equation of motion can be recovered. While a more complex approach, based on quantum stochastic calculus [Lin76; Bar90] will be used later on [Hon+17] to capture the full dynamics of the experiment, in most cases a simpler approach is sufficient to understand the basic effects of the system. Here, we use quantum Langevin equations for the operator equations of motion, based on chapter 3 of reference [GZ04].

We assume a white bath of independent harmonic oscillators[5], represented by the cumulative quadrature operator $\hat{\beta}_Q(t) \propto \sum_i \hat{Q}_i$, summing over some quadrature Q_i of all individual bath systems i. The oscillators are evenly and densely spaced in frequency, and are all coupling linearly with the same strength to a self-adjoint operator $\hat{C}$ of the system. This is called the first Markov approximation [GC85] and is never exactly fulfilled, but is a good model for narrow resonances (see also paragraph 2.2.2). As eventually only modes with frequencies close to the system eigenfrequency are relevant, colored mode densities and coupling strengths, e.g. by a finite bandwidth of the optical mirrors, can usually be modeled by using the mode density and coupling strength close to the resonance frequency for all bath modes. Note that in the first Markov approximation, the bath operator $\hat{\beta}_Q(t)$ can have an arbitrary time development. It is extrinsic to our system, i.e. its dynamics can not be derived from the resulting model, but is instead part of the description of the experiment. The equation of motion for a system operator $\hat{S}$ in the Heisenberg picture, can then be derived as

$$\frac{\mathrm{d}}{\mathrm{d}t}\hat{S} = \frac{i}{\hbar}\left[\hat{\mathcal{H}}, \hat{S}\right] + \frac{i}{2}\left[\frac{1}{q_C}\frac{\mathrm{d}}{\mathrm{d}t}\hat{C} - \hat{\beta}_C, \left[\hat{C}, \hat{S}\right]\right]_+ \tag{2.9}$$

with the coupling strength γ_C and the anti-commutator $[.,.]_+$[6]. To illustrate how this results in the dynamics we expect for a damped harmonic oscillator, we assume a bare, one sided optical cavity with the free Hamiltonian $\hat{\mathcal{H}}_{\mathrm{free}} = \hbar\omega_0(\hat{A}^2 + \hat{Y}^2 + 1)/2$. We can imagine a single mode in a Fabry-Pérot cavity consisting of one perfectly reflective back mirror and one semi-transparent input coupler mirror, see figure 2.2. The bath in this case is the continuum of frequencies in the optical mode impinging on the input coupler.

---

[5] The free Hamiltonian of the bath $\hat{\mathcal{H}} = \int_0^\infty \mathrm{d}\omega\,\hbar\omega\,\hat{o}_{\mathrm{in},\omega}^\dagger\hat{o}_{\mathrm{in},\omega}$ is defined in the limit of infinitely dense spacing of modes, i.e. the ladder operators fulfill the commutation relation $[\hat{o}_{\mathrm{in},\omega}, \hat{o}_{\mathrm{in},\omega'}^\dagger] = \delta(\omega - \omega')$. Consequently, their formal, free solution is $\hat{o}_{\mathrm{in},\omega}(t) = \hat{\tilde{o}}_{\mathrm{in},\omega}e^{-i\omega t}$.

[6] For two operators $\hat{a}$ and $\hat{b}$, the anti-commutator is $[\hat{a}, \hat{b}]_+ = \hat{a}\hat{b} + \hat{b}\hat{a}$.
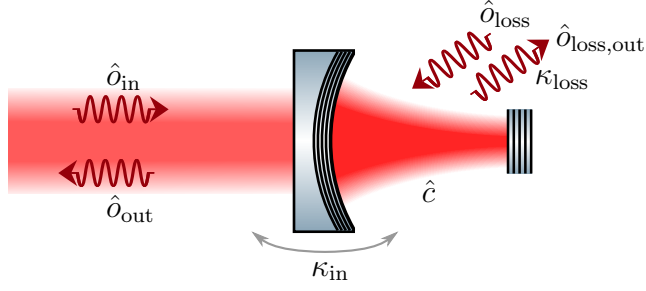
FIGURE 2.2.: **Coupling to the Environment.** The field inside a Fabry-Pérot cavity ($\hat{c}$) is coupled to an input mode $\hat{o}_{\mathrm{in}}$ with rate κ_{in} and emits into the mode $\hat{o}_{\mathrm{out}}$. Additionally, undesired losses in the optical resonator, such as scattering, leak with rate κ_{loss} into the mode $\hat{o}_{\mathrm{loss,out}}$. In the reverse direction, vacuum fluctuations from mode $\hat{o}_{\mathrm{loss}}$ enter the cavity.

Coupling $\hat{A}$ ($\hat{Y}$) with strength $1/q_A$ ($1/q_Y$) to the bath quadratures $\hat{\beta}_A$ ($\hat{\beta}_Y$), equation (2.9) leads to a system of linear equations. Solving this for the time derivatives, we obtain the quantum Langevin equations of motion

$$\frac{\mathrm{d}}{\mathrm{d}t}\hat{A} = \frac{1}{1+1/q_A q_Y}\left(\omega_0\hat{Y} - \frac{\omega_0}{q_Y}\hat{A} - \hat{\beta}_Y + \frac{1}{q_Y}\hat{\beta}_A\right) \tag{2.10a}$$

$$\frac{\mathrm{d}}{\mathrm{d}t}\hat{Y} = \frac{1}{1+1/q_A q_Y}\left(-\omega_0\hat{A} - \frac{\omega_0}{q_A}\hat{Y} + \hat{\beta}_A + \frac{1}{q_A}\hat{\beta}_Y\right). \tag{2.10b}$$

As expected, we obtain the equations of motion for a damped harmonic oscillator with a slightly modified eigenfrequency $\omega_c = \omega_0/(1+1/q_A q_Y)$ and driven by the external fields. In the usual case of a cavity with narrow linewidth, i.e. $q_A = q_Y \ll 1$, we can neglect the renormalization as well as the coupling of the input fields to the respective other cavity quadrature. We find the amplitude damping $\kappa_{\mathrm{in}} \approx \omega/q_Y$ and thus can interpret the previously introduced coupling strength of the cavity to the external field as the inverse quality factor $1/Q_{\mathrm{opt}} \approx 1/q_A + 1/q_Y$ of the resonance.

In order to relate the abstract bath operators $\hat{\beta}_{A,Y}$ to the photon flux $\hat{n}_{\mathrm{in}}(t) = \hat{o}_{\mathrm{in}}^\dagger(t)\hat{o}_{\mathrm{in}}(t)$ of the optical mode coupled to the cavity[7], we change to annihilation operators using (2.6). This results in [GC85]

$$\frac{\mathrm{d}}{\mathrm{d}t}\hat{c} = -i\omega\hat{c} - \kappa_{\mathrm{in}}\hat{c} + \sqrt{2\kappa_{\mathrm{in}}}e^{i\theta_{\mathrm{in}}}\hat{o}_{\mathrm{in}}. \tag{2.11}$$

The output field is defined by the interference of the reflected input field and the emission of the cavity as

$$\hat{o}_{\mathrm{out}} = e^{i\theta_{\mathrm{out}}}\left(e^{i\theta_{\mathrm{in}}}\hat{o}_{\mathrm{in}} - \sqrt{2\kappa_{\mathrm{in}}}\hat{c}\right). \tag{2.12}$$

---

[7] The creation (anihilation) operators are defined as the integral over the implicit solutions of the bath annihilation operators $\hat{o}_{\mathrm{in}}(t) = \int_0^\infty \hat{\tilde{o}}_{\mathrm{in},\omega} e^{-i\omega t} d\omega/\sqrt{\pi}$ and fulfill the relations

$$\left[\hat{o}_{\mathrm{in}}(t), \hat{o}_{\mathrm{in}}^\dagger(t')\right] = \delta(t-t') \qquad\qquad [\hat{o}_{\mathrm{in}}(t), \hat{o}_{\mathrm{in}}(t')] = 0,$$

see also [5]. Note that the operator can also formally be defined by extending the bath to negative frequencies, $\hat{o}_{\mathrm{in}}(t) = \int_{-\infty}^\infty \hat{\tilde{o}}_{\mathrm{in},\omega} e^{-i\omega t} d\omega/\sqrt{2\pi}$. While it is harder to motivate physically, the results remain the same and it is easier to treat analytically. For this reason, this definition is preferred in many theoretical derivations.

2. Theory of Cavity Optomechanics

Note that there can be a arbitrary phase θ_{in} and θ_{out} between input field, the resonator and the output field, depending on the exact cavity properties and the definition of the location of the input and output operators. Without loss of generality, we will set those phases to $\theta_{\text{in}} = \theta_{\text{out}} = 0$ in the following.

In a realistic optomechanical system, we have to consider the coupling to multiple environments. The optical cavity will, in addition to the desired coupling to the input mode, also loose energy by scattering, absorption and leakage into undesired modes. Conversely, fields can also couple into the cavity through these loss channels. We will summarize all these inbound fields into one artificial super-mode represented by the creation operator $\hat{o}_{\text{loss}}$, coupled with the rate κ_{loss}. We also define the respective quadratures $\hat{A}_{\text{loss}} = \hat{Q}^0_{\hat{o}_{\text{loss}}}$ and $\hat{Y}_{\text{loss}} = \hat{Q}^{\pi/2}_{\hat{o}_{\text{loss}}}$ of the inbound fields (see equation (2.4)).

The mechanical oscillator usually experiences damping only in its momentum quadrature, due to friction and mechanical clamping losses to the substrate (see also paragraph 2.2.2). These losses are characterized by the mechanical energy damping rate Γ. They couple the resonator to a bath of thermal phonons represented by the creation operator $\hat{m}^\dagger_{\text{loss}}$, respectively the quadrature $\hat{P}_{\text{loss}} = \hat{Q}^{\pi/2}_{\hat{m}_{\text{loss}}}$ [8].

From the system Hamiltonian (2.7a) we obtain the operator equation of motion[9]

$$\frac{\mathrm{d}}{\mathrm{d}t}\hat{A} = \omega_c \hat{Y} + \sqrt{2}g_0 \hat{X}\hat{Y} - \kappa\hat{A} + \sqrt{2\kappa_{\text{in}}}\hat{A}_{\text{in}} + \sqrt{2\kappa_{\text{loss}}}\hat{A}_{\text{loss}} \tag{2.13a}$$

$$\frac{\mathrm{d}}{\mathrm{d}t}\hat{Y} = -\omega_c \hat{A} - \sqrt{2}g_0 \hat{X}\hat{A} - \kappa\hat{Y} + \sqrt{2\kappa_{\text{in}}}\hat{Y}_{\text{in}} + \sqrt{2\kappa_{\text{loss}}}\hat{Y}_{\text{loss}} \tag{2.13b}$$

$$\frac{\mathrm{d}}{\mathrm{d}t}\hat{X} = \Omega\hat{P} \tag{2.13c}$$

$$\frac{\mathrm{d}}{\mathrm{d}t}\hat{P} = -\Omega\hat{X} - \sqrt{2}g_0 \frac{\hat{A}^2 + \hat{Y}^2}{2} - \Gamma\hat{P} + \sqrt{2\Gamma}\hat{P}_{\text{loss}} \tag{2.13d}$$

with the cavity amplitude decay rate

$$\kappa = \kappa_{\text{in}} + \kappa_{\text{loss}}. \tag{2.14}$$

Note that the right hand side of equation (2.13d) does not vanish, even if the mechanical and optical modes are in their respective groundstate. This becomes clear when transforming it to creation and annihilation operators[9], where the optical ground state energy shows up explicitly in the optomechanical force term. It results in a force $\langle d\hat{P}_p/dt \rangle = \sqrt{\hbar m_{\text{eff}} \Omega} g_0 / \sqrt{2}$ exerted by the optical vacuum fluctuations on the mechanical

---

[8] In a thermal environment, the input state approximately fulfills $\langle \hat{m}^\dagger_{\text{loss}}(t)\hat{m}_{\text{loss}}(t')\rangle = n_{\text{th}}\delta(t - t')$ [Hof15]. This is the case when the mean occupation number of all individual modes of the bath[5] is n_{th}. Computing the cross spectral density of the mechanical oscillator (see also paragraph 2.2.2), one finds that this results in the expected thermal state with the variance $\text{Var}(X) = \text{Var}(P) = n_{\text{th}} + \frac{1}{2}$.

[9] The equivalent Langevin equations for the creation and annihilation operators are

$$\frac{\mathrm{d}}{\mathrm{d}t}\hat{c} = -i\omega_c\hat{c} - ig_0\left(\hat{m} + \hat{m}^\dagger\right)\hat{c} - \kappa\hat{c} + \sqrt{2\kappa_{\text{in}}}\hat{o}_{\text{in}} + \sqrt{2\kappa_{\text{loss}}}\hat{o}_{\text{loss}}$$

$$\frac{\mathrm{d}}{\mathrm{d}t}\hat{m} = -i\Omega\hat{m} - ig_0\left(\hat{c}^\dagger\hat{c} + \frac{1}{2}\right) - \frac{\Gamma}{2}\left(\hat{m} - \hat{m}^\dagger\right) + i\sqrt{\Gamma}\hat{P}_{\text{loss}}.$$

object, known as Casimir effect[10].

We can identify different parameter regimes of the optomechanical system by comparing the various terms in equations (2.13). To this end, we use the standard deviation of fluctuations typically appearing in the system to replace the operators. For example, the vacuum fluctuations of the optical field justify the replacement $\hat{A} \to (\langle 0| \hat{A}^2 |0\rangle)^{1/2} = 1/2$.

In order to sense the mechanical motion, e.g. of a thermal state with average phonon number n_{th}, its effect $\sqrt{2}g_0\hat{X}\hat{Y} \sim \sqrt{2}g_0\sqrt{n_{\text{th}}n_{\text{opt}}}$ on the optical quadrature (2.13a) should exceed the quantum fluctuations of the field $\kappa\hat{A} \sim \kappa/2$. Hence, this sets a lower limit $8g_0^2 n_{\text{opt}}n_{\text{th}}/\kappa^2 > 1$ for the average number of intracavity photons n_{opt}.

If the force exerted by the optical field on the mechanical element is supposed to dominate (2.13d), it requires $\sqrt{2}g_0 n_{\text{opt}} > \Gamma\sqrt{n_{\text{th}}}$. In contrast to the previous regime, this requires more photons for larger thermal states.

Optomechanical back action means that the fluctuations of $\hat{A}$ induced by the thermal mechanical motion in eq. (2.13a) $\sim \sqrt{2}g_0\sqrt{n_{\text{th}}n_{\text{opt}}}/\kappa$ act back on the mechanical system in eq. (2.13d). The resulting back action force exceeds the mechanical damping force if the single phonon cooperativity $C_0 = 2g_0^2 n_{\text{opt}}/(\kappa\Gamma) > 1$ exceeds unity.

Despite the quantum treatment of the equations of motion, all of these effects are still classical. In order to reach the quantum regime, the back action from the mechanical ground state fluctuations in eq. (2.13a) should dominate not only the thermal amplitude decay $\sim \Gamma\sqrt{n_{\text{th}}}$ in eq. (2.13d), but also the phonon exchange rate with the environment $\sim \Gamma(n_{\text{th}}+1)$. This results in the condition termed strong cooperativity, with the optomechanical cooperativity $C = 2g_0^2 n_{\text{opt}}/(\kappa\Gamma(n_{\text{th}}+1)) > 1$ exceeding unity.

As mentioned in the previous paragraph, the non-linearity g_0 is relatively weak compared to the optical linewidth κ in all state of the art systems. Consequently, thus far in all experimentally interesting cases, it is necessary to work with a sizable number of photons in the cavity $n_{\text{opt}} \gg 1$, i.e. the cavity must be driven by an external laser field.

2.1.3. Linearization of the Interaction

Weak nonlinear interactions, such as the one discussed in equations (2.13), can be enhanced by driving the system, to become strong, yet linear interactions. The idea is to replace one of the operators in the nonlinear interaction term $\hat{X}\hat{A}$, by its mean value of the driven system, e.g. $\bar{A} = \langle\hat{A}\rangle$. This is achieved by splitting $\hat{A} \to \bar{A} + \delta\hat{A}$ into its mean value and some fluctuations, and subsequently neglecting the small residual nonlinear term. The resulting interaction is linear ($\propto \hat{X}$), enhanced by a factor $\bar{A}$, and couples the mechanical motion to the fluctuations, that is the sidebands of the drive laser.

We typically drive the system with a coherent laser beam, characterized by a carrier frequency ω_{L} and a slowly varying envelope $\alpha_0(t)$. Although laser beams are not exactly displaced vacuum states, also called coherent states, they can conveniently predict and reproduce experiments with laser beams [Møl97]. A coherent state with complex amplitude α in a mode associated with the annihilation operator $\hat{a}$ is generated by displacing

---

[10] This results in a steady state deflection of $\langle X_p \rangle = -x_{\text{zpf}}g_0/\Omega = \frac{G\hbar}{2m_{\text{eff}}\Omega^2}$, see also (2.20). Note that all possible electromagnetic modes contribute to the full Casimir-Polder force, and the attractive force originating from the decrease in the energy of the vacuum fluctuation dominates over the potentially repulsive force described here.
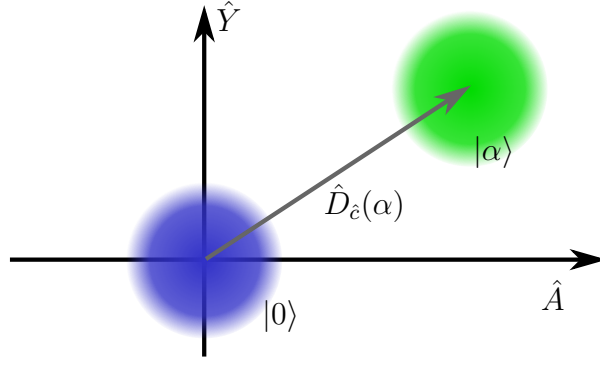
FIGURE 2.3.: **Coherent State.** The displacement operator $\hat{D}_{\hat{c}}(\alpha)$ shifts the state it is applied to in quadrature phase space by the complex amplitude α. Thus, its representation as quasi-probability distribution, such as the Glauber Sudarshan P-function, is displaced by the vector $\sqrt{2}(\mathcal{R}e[\alpha], \mathcal{I}m[\alpha])^T$ in a quadrature basis $(\hat{A}, \hat{Y})$. This is scatched for a vacuum state $|0\rangle$ of the optical cavity field, resulting in the coherent state $|\alpha\rangle$ in the resonator.

the vacuum state

$$|\alpha\rangle = \hat{D}_{\hat{a}}(\alpha)|0\rangle = e^{-|\alpha|^2/2} \sum_{n=0}^{\infty} \frac{\alpha^n}{\sqrt{n!}}|n\rangle. \tag{2.15}$$

using the displacement operator [Gla63a; CG69]

$$\hat{D}_{\hat{a}}(\alpha) = \exp\big(\alpha\hat{a}^\dagger + \alpha^\dagger\hat{a}\big) = e^{-|\alpha|^2/2} e^{\alpha\hat{a}^\dagger} e^{-\alpha^\dagger\hat{a}}, \tag{2.16}$$

see also figure 2.3. They behave (i.e. propagate and interfere) like classical fields with an additional noise term, corresponding to the optical shot noise[11]. Driving the system (2.13) with a coherent input state

$$|\psi_{\text{drive}}\rangle_{\text{in}} = \hat{D}_{\hat{o}_{\text{in}}}\big(\alpha_0(t)e^{-i\omega_{\text{L}}t}\big)|0\rangle \tag{2.17}$$

will induce a (classical) response, represented by the ensemble mean values of the system operators. In order to access the quantum properties of the system, we will eliminate these dynamics by moving to a well suited reference frame. In essence, we can achieve this by splitting the operators into their mean value and their excess quantum fluctuations $\hat{a} \rightarrow \langle\hat{a}\rangle + \delta\hat{a}$.

In a first step, we transform the operators to a frame rotating at the frequency of the optical field, making use of the knowledge that a driven harmonic system will oscillate at the drive frequency. This is achieved by introducing new operators

$$\hat{o}_{\text{a},\omega_{\text{L}}} = e^{-i\omega_{\text{L}}t\,\hat{o}_{\text{a}}^\dagger\hat{o}_{\text{a}}}\,\hat{o}_{\text{a}}\,e^{i\omega_{\text{L}}t\,\hat{o}_{\text{a}}^\dagger\hat{o}_{\text{a}}} = \hat{o}_{\text{a}}\,e^{i\omega_{\text{L}}t} \tag{2.18a}$$

$$\hat{c}_{\omega_{\text{L}}} = e^{-i\omega_{\text{L}}t\,\hat{c}^\dagger\hat{c}}\,\hat{c}\,e^{i\omega_{\text{L}}t\,\hat{c}^\dagger\hat{c}} = \hat{c}\,e^{i\omega_{\text{L}}t} \tag{2.18b}$$

---

[11] Using the Baker Campbell Hausdorff formula, we find that the subsequent displacement by two complex numbers α and β

$$\hat{D}_{\hat{a}}(\alpha)\,\hat{D}_{\hat{a}}(\beta) = \hat{D}_{\hat{a}}(\alpha+\beta)\,e^{(\alpha\beta^\dagger - \alpha^\dagger\beta)/2}$$

results in the displacement by the sum $\alpha + \beta$ and a global phase $\mathcal{I}m(\alpha\beta^\dagger)$, such that the interference between coherent states $|\alpha\rangle$ and $|\beta\rangle$ essentially recreates the interference we expect from classical light fields with the complex amplitudes α and β. It also immediately follows that $D_a^\dagger(\alpha) = D_a(-\alpha) = (D_a(\alpha))^{-1}$.

by the unitary transformation $\hat{U}_{\mathrm{L}} = \exp(i\omega_{\mathrm{L}}t\,\hat{o}_{\mathrm{a}}^{\dagger}\hat{o}_{\mathrm{a}})\exp(i\omega_{\mathrm{L}}t\,\hat{c}^{\dagger}\hat{c})$[12] where $\hat{o}_{\mathrm{a}}$ stands for either input field $\hat{o}_{\mathrm{in}}$, $\hat{o}_{\mathrm{loss}}$[13]. We also label the corresponding quadrature operators (2.4) with an additional index ω_{L}, e.g. $\hat{A}_{\omega_{\mathrm{L}}} = \hat{Q}_{\hat{c}_{\omega_{\mathrm{L}}}}^{0}$ and $\hat{Y}_{\omega_{\mathrm{L}}} = \hat{Q}_{\hat{c}_{\omega_{\mathrm{L}}}}^{\pi/2}$. Using the product rule, we obtain the equations of motion for the rotating operators

$$\frac{\mathrm{d}}{\mathrm{d}t}\hat{c}_{\omega_{\mathrm{L}}} = \frac{d\hat{c}}{dt}e^{i\omega_{\mathrm{L}}t} + \hat{c}\frac{d}{dt}e^{i\omega_{\mathrm{L}}t} \tag{2.19}$$

which shift the rotation frequency of the optical field to $\omega_c - \omega_{\mathrm{L}}$, leaving the other terms unchanged.

In the second step, we displace all operators by their mean values. In the adiabatic limit, i.e. the change in the drive amplitude $\alpha_0(t)$ is slow compared to all relevant time scales (primarily κ and Ω), we can find the mean values by setting their derivative to zero, using (2.13):

$$\langle\hat{A}_{\omega_{\mathrm{L}}}\rangle = \frac{\sqrt{2\kappa_{\mathrm{in}}}}{\kappa^2 + \Delta^2}\left(\kappa\bar{A}_{\mathrm{in}} + \Delta\bar{Y}_{\mathrm{in}}\right) \qquad \langle\hat{Y}_{\omega_{\mathrm{L}}}\rangle = \frac{\sqrt{2\kappa_{\mathrm{in}}}}{\kappa^2 + \Delta^2}\left(\kappa\bar{Y}_{\mathrm{in}} - \Delta\bar{A}_{\mathrm{in}}\right) \tag{2.20a}$$

$$\langle\hat{X}\rangle = -\frac{\sqrt{2}g_0}{\Omega}\left(\frac{\kappa_{\mathrm{in}}}{\kappa^2 + \Delta^2}\left(\bar{A}_{\mathrm{in}}^2 + \bar{Y}_{\mathrm{in}}^2\right) + \frac{1}{2}\right) \qquad \langle\hat{P}\rangle = 0 \tag{2.20b}$$

$$\Delta = \left(\omega_c + \sqrt{2}g_0\langle\hat{X}\rangle\right) - \omega_{\mathrm{L}}. \tag{2.20c}$$

Here, we introduced the effective detuning Δ of the drive laser relative to the optical resonance, see (2.20c), which is shifted by $\sqrt{2}g_0\langle\hat{X}\rangle$ due to the optomechanical force acting on the cavity[14] Note that inserting the expression for the detuning (2.20c) into equation (2.20b), we obtain an expression which is cubic in steady state displacement $\bar{X}$. As a consequence, for high intracavity powers, multiple steady state values for the mean displacement are possible. This bistability of the optical cavity can limit the maximum intracavity power [Dor+83; PPR13; Hof15]. By choosing the phase of the input beam, we can set $\kappa\bar{Y}_{\mathrm{in}} = \Delta\bar{A}_{\mathrm{in}}$ without loss of generality, and thereby eliminate $\langle\hat{Y}_{\omega_{\mathrm{L}}}\rangle = 0$. We thereby define $\hat{A}$ as the amplitude quadrature of the cavity field: $\langle\hat{A}_{\omega_{\mathrm{L}}}\rangle = \sqrt{2}\alpha_0$

---

[12] We define a unitary transformation $\exp(i\xi\hat{B})$ with the observable $\hat{B}$ and a phase ξ. Next, we employ an equality derived from the Baker Campbell Hausdorff formula, using the function $\mathcal{K}_{\hat{B}}(\hat{b}) = [\hat{B}, \hat{b}]$:

$$e^{i\xi\hat{B}}\,\hat{b}\,e^{-i\xi\hat{B}} = \sum_{n=0}^{\infty}\frac{(i\xi)^n}{n!}\mathcal{K}_{\hat{B}}^n(\hat{b})$$

With $\mathcal{K}_{\hat{c}^{\dagger}\hat{c}}(\hat{c}) = -\hat{c}$ and thus $\mathcal{K}_{\hat{c}^{\dagger}\hat{c}}^n(\hat{c}) = (-1)^n\hat{c}$, we obtain the unitary rotating frame transformation by setting $\xi = \omega t$.

[13] The definition of the transformation requires that $[\hat{o}_{\mathrm{a}}(t), \hat{c}(t)] = 0$, which is not strictly true [GZ04]. However, we know that due to causality, $[\hat{o}_{\mathrm{a}}(s), \hat{c}(t)] = 0$ for all $s > t$, such that we can use an infinitesimal shift in the definition of the time of the input field $\lim_{\delta t \to 0^+}[\hat{o}_{\mathrm{a}}(t + \delta t), \hat{c}(t)] = 0$

[14] For the creation and annihilation operators, we find

$$\langle\hat{c}_{\omega_{\mathrm{L}}}\rangle = \frac{\sqrt{2\kappa_{\mathrm{in}}}}{i\Delta + \kappa}\alpha_0 = \frac{\sqrt{2\kappa_{\mathrm{in}}}}{\sqrt{\Delta^2 + \kappa^2}}\frac{\kappa - i\Delta}{\sqrt{\Delta^2 + \kappa^2}}\alpha_0$$

$$\langle\hat{m}\rangle = -\frac{g_0}{\Omega}\left(\frac{2\kappa_{\mathrm{in}}|\alpha_0|^2}{\Delta^2 + \kappa^2} + \frac{1}{2}\right).$$

corresponds to the amplitude of a classical oscillating field, and the phase quadrature $\hat{Y} \sim \langle \hat{A}_{\omega_\mathrm{L}} \rangle \varphi$ relates to its phase φ. This choice of input phase is arbitrary, i.e. if it is more convenient to describe the equations in terms of amplitude and phase of the input or output fields, a different phase convention can be chosen.

Now we can subtract the classical dynamics from the equations of motion by displacing the mechanical state with the unitary operation $\hat{D}_{\hat{m}}(-\langle \hat{X} \rangle / \sqrt{2})$, defining the mechanical position fluctuation operator

$$\delta \hat{X} = \hat{D}_{\hat{m}}^\dagger \left(-\langle \hat{X} \rangle / \sqrt{2} \right) \hat{X} \hat{D}_{\hat{m}} \left(-\langle \hat{X} \rangle / \sqrt{2} \right) = \hat{X} - \langle \hat{X} \rangle. \qquad (2.21)$$

Equivalently, we define the fluctuation operators for the rotating optical quadratures $\delta \hat{A}_{\omega_\mathrm{L}}$ and $\delta \hat{Y}_{\omega_\mathrm{L}}$ by displacing the optical state by $\hat{D}_{\hat{c}_{\omega_\mathrm{L}}}(-[\langle \hat{A}_{\omega_\mathrm{L}} \rangle + i \langle \hat{Y}_{\omega_\mathrm{L}} \rangle] / \sqrt{2})$, as well as the input field fluctuations $\delta \hat{A}_{\mathrm{in},\omega_\mathrm{L}}$ and $\delta \hat{Y}_{\mathrm{in},\omega_\mathrm{L}}$ by the transformation $\hat{D}_{\hat{o}_{\mathrm{in},\omega_\mathrm{L}}}(-\alpha_0(t))$. Note that we use the indication δ that the operators refer to the fluctuations only in this paragraph, and will drop them in the rest of the thesis. Hence, we obtain the linearized equations of motion[15]

$$\frac{\mathrm{d}}{\mathrm{d}t} \delta \hat{A}_{\omega_\mathrm{L}} = \Delta \delta \hat{Y}_{\omega_\mathrm{L}} + g_Y \delta \hat{X} - \kappa \delta \hat{A}_{\omega_\mathrm{L}} + \sqrt{2\kappa_\mathrm{in}} \delta \hat{A}_{\mathrm{in},\omega_\mathrm{L}} + \sqrt{2\kappa_\mathrm{loss}} \delta \hat{A}_{\mathrm{loss},\omega_\mathrm{L}} + \mathcal{O}(g_0 \delta^2) \quad (2.22\mathrm{a})$$

$$\frac{\mathrm{d}}{\mathrm{d}t} \delta \hat{Y}_{\omega_\mathrm{L}} = -\Delta \delta \hat{A}_{\omega_\mathrm{L}} - g_A \delta \hat{X} - \kappa \delta \hat{Y}_{\omega_\mathrm{L}} + \sqrt{2\kappa_\mathrm{in}} \delta \hat{Y}_{\mathrm{in},\omega_\mathrm{L}} + \sqrt{2\kappa_\mathrm{loss}} \delta \hat{Y}_{\mathrm{loss},\omega_\mathrm{L}} + \mathcal{O}(g_0 \delta^2) \quad (2.22\mathrm{b})$$

$$\frac{\mathrm{d}}{\mathrm{d}t} \delta \hat{X} = \Omega \hat{P} \qquad (2.22\mathrm{c})$$

$$\frac{\mathrm{d}}{\mathrm{d}t} \hat{P} = -\Omega \delta \hat{X} - g_A \delta \hat{A}_{\omega_\mathrm{L}} - g_Y \delta \hat{Y}_{\omega_\mathrm{L}} - \Gamma \hat{P} + \sqrt{2\Gamma} \hat{P}_\mathrm{loss} + \mathcal{O}(g_0 \delta^2). \qquad (2.22\mathrm{d})$$

We find a linear interaction between the mechanical and the optical mode with the enhanced linear coupling rate

$$g = g_0 \bar{c} = (g_A + i g_Y)/2 \qquad g_A = \sqrt{2} g_0 \langle \hat{A}_{\omega_\mathrm{L}} \rangle \qquad g_Y = \sqrt{2} g_0 \langle \hat{Y}_{\omega_\mathrm{L}} \rangle \qquad (2.23)$$

and in the case of weak single photon coupling $g_0 \ll \kappa, g$, we can neglect the non-linear terms $\mathcal{O}(g_0 \delta^2)$. With the previous convention for the phase and amplitude quadrature ($\langle \hat{Y}_{\omega_\mathrm{L}} \rangle \equiv 0$), we find that the mechanical oscillator experiences a force originating from the amplitude fluctuations $\delta \hat{A}_{\omega_\mathrm{L}}$ of the light field (2.22d), whose phase $\sim \delta \hat{Y} / \langle \hat{A}_{\omega_\mathrm{L}} \rangle$ is in turn changed by the mechanical displacement $\delta \hat{X}$ (2.22b). If the life time of the cavity $1/\kappa$ is long enough, these phase shifts can turn into amplitude fluctuations, which will again interact with the mechanical element. This back-action of the mechanical element on itself can be understood by eliminating the mediating cavity field, as we will see in the next paragraph.

---

[15] Using the same transformation $\hat{U} = \hat{D}_{\hat{m}}(-\langle \hat{m} \rangle) \hat{D}_{\hat{c}_{\omega_\mathrm{L}}}(-\langle \hat{c}_{\omega_\mathrm{L}} \rangle) \hat{D}_{\hat{o}_{\mathrm{in},\omega_\mathrm{L}}}(-\alpha_0)$ to define the annihilation operators of the fluctuations, we obtain their corresponding Langevin equations of motion, with the linearized coupling rate (2.23):

$$\frac{\mathrm{d}}{\mathrm{d}t} \delta \hat{c}_{\omega_\mathrm{L}} = -i\Delta \delta \hat{c}_{\omega_\mathrm{L}} - ig(\delta \hat{m} + \delta \hat{m}^\dagger) - \kappa \delta \hat{c}_{\omega_\mathrm{L}} + \sqrt{2\kappa_\mathrm{in}} \delta \hat{o}_{\mathrm{in},\omega_\mathrm{L}} + \sqrt{2\kappa_\mathrm{loss}} \hat{o}_{\mathrm{loss},\omega_\mathrm{L}} + \mathcal{O}(g_0 \delta^2)$$

$$\frac{\mathrm{d}}{\mathrm{d}t} \delta \hat{m} = -i\Omega \delta \hat{m} - i(g^\dagger \hat{c}_{\omega_\mathrm{L}} + g \hat{c}_{\omega_\mathrm{L}}^\dagger) - \frac{\Gamma}{2}(\delta \hat{m} - \delta \hat{m}^\dagger) + i\sqrt{\Gamma} \hat{P}_\mathrm{loss} + \mathcal{O}(g_0 \delta^2)$$

2.1.4. Adiabatic Elimination of the Cavity

While the equations (2.22) describe the driven system well, often times we want to understand the interaction between the extrinsic light mode $\hat{o}_{\text{in,out}}$ and the mechanics $\hat{m}$. Whereas we can control the optical input and measure the optical output, we have no direct access to the cavity field itself, and it merely is the mediator and amplifier of the interaction between the free space mode and the mechanical element. In order to obtain the equations of the direct interaction between the extrinsic light field and the mechanical oscillator, we want to eliminate the cavity field from the equations. This can be achieved in various parameter regimes [Van+11; Hof+11]. Here we will focus on the adiabatic limit, i.e. where the bandwidth the drive field $\alpha_0(t)$ is small[16] compared to the relevant time scales κ and Ω. Note that from here on we drop the prefix δ of the displaced operators, which indicated that they refer to the fluctuations on top of the steady state mean value of the original operators, as defined in the previous paragraph.

First, we introduce a super mode $\hat{o} = \sqrt{\kappa_{\text{in}}/\kappa}\,\hat{o}_{\text{in}} + \sqrt{\kappa_{\text{loss}}/\kappa}\,\hat{o}_{\text{loss}}$ to combine the optical input fields. It will mostly appear as Fourier transform $\hat{\tilde{o}}_{\omega_{\text{L}}} = \int \mathrm{d}\tau \hat{o}_{\omega_{\text{L}}}(\tau)e^{i\omega\tau}/\sqrt{2\pi}$ of the time domain operator $\hat{o}_{\omega_{\text{L}}}(\tau)$ in a frame rotating with the drive frequency (2.18). Next, we also transform the mechanical field to a rotating frame $\hat{U} = \exp(-i\tilde{\Omega}t\,\hat{m}^\dagger\hat{m})$, where the frequency $\tilde{\Omega}$ describes the dynamical frequency of the mechanical oscillator, i.e. including the optical spring effect, as we will see later. For now we can simply assume that it is sufficiently close to the mechanical frequency Ω, such that the new operator $\hat{m}_{\tilde{\Omega}} = \hat{m}e^{i\tilde{\Omega}t}$ evolves slow compared to κ.

With this, we formally integrate the Langevin equation (2.22) for the cavity annihilation operator[17]

$$
\hat{c}_{\omega_{\text{L}}} = -ig\left(\underbrace{\frac{\hat{m}_{\tilde{\Omega}}e^{-i\tilde{\Omega}t}}{i(\Delta - \tilde{\Omega}) + \kappa}}_{①} + \underbrace{\frac{\hat{m}_{\tilde{\Omega}}^\dagger e^{i\tilde{\Omega}t}}{i(\Delta + \tilde{\Omega}) + \kappa}}_{②} \right) + \sqrt{\frac{\kappa}{\pi}}\underbrace{\int_{-\infty}^{\infty}\frac{\hat{\tilde{o}}(\omega)e^{-i\omega t}}{i(\Delta - \omega) + \kappa}d\omega}_{③}. \qquad (2.24)
$$

This already offers us insight into the effects of the optomechanical interaction. The first two terms show, that the mechanical motion will generate sidebands on the optical field. The first term (①), associated with the annihilation of a phonon, will create a tone at $-i(\omega_{\text{L}} + \tilde{\Omega})$, i.e. upconvert photons from the drive laser. We will later see that this corresponds to an anti-Stokes scattering process. The second term (②), associated with the creation of a phonon, downconverts drive photons to $-i(\omega_{\text{L}} - \tilde{\Omega})$ in a Stokes scattering process. The last term (③) describes the modification of the optical input field by the cavity. For the protocols considered in this thesis, we will usually assume no input power at the optical side bands, such that we can essentially assume the optical vacuum as input state.

---

[16] More explicitly, at high frequencies, the Fourier transform $\tilde{\alpha}_0(\omega) = \int_{-\infty}^{\infty}\frac{\mathrm{d}t}{\sqrt{2\pi}}\,\alpha_0(t)e^{i\omega t}$ should fall off steeper than the optical susceptibility $\chi_{\text{L}}(\omega_c+\omega)$. A bandwidth smaller than the mechanical frequency Ω is necessary to resolve the optomechanical sidebands.

[17] We employ the formal integration $\frac{da(t)}{dt} = -\Xi a(t) + f(t) \rightarrow a(t) = \int_{-\infty}^{t}\mathrm{d}\tau\,f(\tau)e^{\Xi(\tau-t)}$. With the assumption that $\hat{m}_\Omega$ and $\hat{o}_{\omega_{\text{L}}}(\omega)$ evolve slowly on the relevant time scales, we can approximate them to be constant and pull them out from the integral. For example for the first term, this results in the formal solution $\hat{c}_{\omega_{\text{L}}}e^{(i\Delta+\kappa)t} \approx -ig\hat{m}_{\tilde{\Omega}}\int_{-\infty}^{t}\mathrm{d}\tau\,e^{(i\Delta+\kappa-i\tilde{\Omega})\tau}$.

2. Theory of Cavity Optomechanics

The denominators $\chi_{\omega_{\mathrm{L}}}(\omega) = 1/(i(\Delta-\omega)+\kappa)$ describe the spectral filtering by the optical cavity and can be understood as the rotating frame form of the cavity susceptibility

$$\chi_{\mathrm{L}}(\omega) = \frac{1}{i(\omega_c - \omega) + \kappa} \qquad (2.25)$$

describing the spectral response of the resonator to a drive field[18]. For a resonant drive ($\Delta \approx 0$), both sidebands have equal strength, i.e. the optical state is proportional to a generalized quadrature (2.4) $\hat{c}_{\omega_{\mathrm{L}}} \tilde{\propto} \hat{Q}_{\hat{m}}^\theta$ of the mechanical mode, with the quadrature phase depending on the sideband resolution. In the resolved sideband limit ($\tilde{\Omega} \gg \kappa$), we can use the cavity response $\chi_{\omega_{\mathrm{L}}}$ to select individual optomechanical sidebands. By setting the detuning to the mechanical frequency $\Delta \approx \pm\tilde{\Omega}$, we obtain a resonant enhancement for one sideband, while suppressing the other sideband. For example, when choosing $\Delta = -\tilde{\Omega}$, the Stokes sideband $|\chi_{\omega_{\mathrm{L}}}(-\tilde{\Omega})| \approx 1/\kappa$ is dominating over the anti-Stokes term $|\chi_{\omega_{\mathrm{L}}}(+\tilde{\Omega})| \approx 1/(2\tilde{\Omega}) \ll |\chi_{\omega_{\mathrm{L}}}(-\tilde{\Omega})|$.

While we have no direct access on the intra-cavity field, it couples directly to the output field (2.12):

$$\hat{o}_{\mathrm{out},\omega_{\mathrm{L}}} = \sqrt{2\kappa_{\mathrm{in}}} ig \left(\chi_{\omega_{\mathrm{L}}}(+\tilde{\Omega})\hat{m}_{\tilde{\Omega}} e^{-i\tilde{\Omega}t} + \chi_{\omega_{\mathrm{L}}}(-\tilde{\Omega})\hat{m}_{\tilde{\Omega}}^\dagger e^{i\tilde{\Omega}t} \right) \qquad (2.26a)$$

$$+ \int_{-\infty}^{\infty} \frac{\mathrm{d}\omega}{\sqrt{2\pi}} \frac{\left[i(\Delta - \omega) + \kappa_{\mathrm{loss}} - \kappa_{\mathrm{in}}\right]\hat{\tilde{o}}_{\mathrm{in}}(\omega) - 2\sqrt{\kappa_{\mathrm{in}}\kappa_{\mathrm{loss}}}\hat{\tilde{o}}_{\mathrm{loss}}(\omega)}{i(\Delta - \omega) + \kappa} e^{-i\omega t} \qquad (2.26b)$$

In the first line, we can identify the optomechanical sidebands. The second line shows the unitary, frequency-dependent mixing between the intended coupling to the inbound mode and the unintended coupling to the loss channel. Note that if both optical input fields are in their respective ground state, the entire line (2.26b) simply represents an effective field in its ground state. This is a typical setting for many optomechanical protocols, see also paragraph 2.3.1.

Beyond the effect of the mechanical element on the optical field, we would also like to know the influence of the optical field on the motional state. To this end, we insert equation (2.24) in eq. (2.22) to obtain the effective mechanical equations of motion[19].

---

[18] The optical susceptibility $\chi_{\mathrm{L}}(\omega)$ is obtained by Fourier transform of (2.13) when neglecting the optomechanical interaction $g_0 \approx 0$ and describes the response of the optical cavity oscillator

$$\langle \hat{c}(t) \rangle = \int \frac{d\omega}{\sqrt{2\pi}} \chi_{\mathrm{L}}(\omega) \xi(\omega) e^{-i\omega t}$$

to a driving field $\xi(\omega) = \sqrt{2\kappa_{\mathrm{in}}} \int_{-\infty}^{\infty} \frac{\mathrm{d}t}{\sqrt{2\pi}} \langle \hat{o}(t) \rangle e^{i\omega t}$. Consequently, in a frame rotating with ω_{L}, the cavity response to a sideband frequency $\omega' = \omega - \omega_{\mathrm{L}}$ is described by $\chi_{\omega_{\mathrm{L}}}(\omega') = \chi_{\mathrm{L}}(\omega)$.

[19] The full equation is relatively bulky and contains several fast rotating terms:

$$\frac{\mathrm{d}}{\mathrm{d}t}\hat{m}_{\tilde{\Omega}} = -i(\Omega - \tilde{\Omega})\hat{m}_{\tilde{\Omega}} - \frac{\Gamma}{2}\left(\hat{m}_{\tilde{\Omega}} - \hat{m}_{\tilde{\Omega}}^\dagger e^{i2\tilde{\Omega}t}\right) + i\sqrt{\Gamma}\hat{P}_{\mathrm{loss}} e^{i\tilde{\Omega}t}$$

$$- |g|^2 \left(\chi_{\omega_{\mathrm{L}}}(\tilde{\Omega})\hat{m}_{\tilde{\Omega}} + \chi_{\omega_{\mathrm{L}}}(-\tilde{\Omega})\hat{m}_{\tilde{\Omega}}^\dagger e^{i2\tilde{\Omega}t} - \chi_{\omega_{\mathrm{L}}}(-\tilde{\Omega})^\dagger\hat{m}_{\tilde{\Omega}} - \chi_{\omega_{\mathrm{L}}}(\tilde{\Omega})^\dagger\hat{m}_{\tilde{\Omega}}^\dagger e^{i2\tilde{\Omega}t} \right)$$

$$- i\sqrt{\frac{\kappa}{\pi}} \int_{-\infty}^{\infty} g^\dagger \chi_{\omega_{\mathrm{L}}}(\omega)\hat{o}_{\omega_{\mathrm{L}}}(\omega) e^{-i(\omega-\tilde{\Omega})t} + g\chi_{\omega_{\mathrm{L}}}(\omega)^\dagger \hat{o}_{\omega_{\mathrm{L}}}^\dagger(\omega) e^{i(\omega+\tilde{\Omega})t} d\omega$$

They become negligible for integration times much longer than a mechanical period $T = 2\pi/\tilde{\Omega}$, for (sideband-)frequencies close to the mechanical frequency, and can thus be neglected in resonant proto-

After neglecting the fast rotating terms [Hof15] and sorting for real and imaginary parts of the backaction, we find the phonon annihilation operator dynamics to be

$$\frac{\mathrm{d}}{\mathrm{d}t}\hat{m}_{\tilde{\Omega}} = - i \left(\Omega + |g|^2 \mathcal{I}m \left(\chi_{\omega_{\mathrm{L}}}(+\tilde{\Omega}) \right) + |g|^2 \mathcal{I}m \left(\chi_{\omega_{\mathrm{L}}}(-\tilde{\Omega}) \right) - \tilde{\Omega} \right) \hat{m}_{\tilde{\Omega}} \tag{2.27a}$$

$$- \left(\frac{\Gamma}{2} + |g|^2 \mathcal{R}e \left(\chi_{\omega_{\mathrm{L}}}(+\tilde{\Omega}) \right) - |g|^2 \mathcal{R}e \left(\chi_{\omega_{\mathrm{L}}}(-\tilde{\Omega}) \right) \right) \hat{m}_{\tilde{\Omega}} \tag{2.27b}$$

$$- i \sqrt{\frac{\kappa}{\pi}} \int_{-\infty}^{\infty} g^\dagger \chi_{\omega_{\mathrm{L}}}(\omega) \hat{\bar{o}}_{\omega_{\mathrm{L}}}(\omega) e^{-i(\omega - \tilde{\Omega})t} + g \chi_{\omega_{\mathrm{L}}}(\omega)^\dagger \hat{\bar{o}}_{\omega_{\mathrm{L}}}^\dagger(\omega) e^{i(\omega + \tilde{\Omega})t} d\omega \tag{2.27c}$$

$$+ i \sqrt{\Gamma} \hat{\bar{m}}_{\mathrm{loss}} e^{i\tilde{\Omega}t}. \tag{2.27d}$$

In the first line, the spring constant is modified by the presence of the optical field. This effect, called the optical spring, has its cause in the dynamic change of the optical force in phase with the mechanical motion. As the mechanical element is displaced, it changes the detuning and thus the amount of light in the cavity, thereby changing e.g. the radiation pressure force, see e.g. [Cor+06; Teu+08; Nor14; Edg+16; Cri+18b]. We find as implicit equation for the dynamic frequency

$$\tilde{\Omega} = \Omega + 2|g|^2 \Delta \frac{\tilde{\Omega}^2 - \Delta^2 - \kappa^2}{(\tilde{\Omega}^2 + \Delta^2 + \kappa^2)^2 - 4\Delta^2 \tilde{\Omega}^2} \tag{2.28}$$

where $|g|^2$ is also a function of κ and Δ (see figure 2.4). Note that in many cases, the optical spring effect is small compared to the mechanical spring, i.e. it is a good approximation to replace on the right hand side of equation (2.28) $\tilde{\Omega}$ by Ω. It therefore offers a convenient way to calibrate the coupling strength $|g|$.

In the second line of equation (2.27b), we find that the damping of the mechanical resonator is modified. This relates to the linear coupling of the mechanical resonator to the optical field. When tuning the system to the red side of the optical cavity, we bias the interaction towards upconversion of drive photons, thereby extracting energy from the system and damping the mechanical motion. This effect increases the effective linewidth

$$\tilde{\Gamma} = \Gamma + \frac{8|g|^2 \Delta \kappa \tilde{\Omega}}{(\tilde{\Omega}^2 + \Delta^2 + \kappa^2)^2 - 4\Delta^2 \tilde{\Omega}^2} \tag{2.29}$$

for positive detunings $\Delta > 0$ (see figure 2.4). Driving the optical cavity on the other side $\Delta < 0$, the downconversion of the drive photons is enhanced, pumping energy into the system. This process is related to phonon lasing, thus reducing the linewidth. In fact the damping (2.29) can become negative, i.e. amplifying the motion of the mechanical motion instead of damping it. Note that this configuration is not stable for long times, as the resulting large mechanical amplitudes will break the perturbation Ansatz used for the linearization of the equations of motion and thus eventually run into some non-linearity. Theoretically, this can result in non-classical limit cycles [BSV01; Kip+05], yet experimentally, the typically relevant non-linearities are much stronger and sometimes irreversible, e.g. losing the lock of the optical cavity or fracturing of the mechanical

---

cols in the adiabatic regime. Note that this also requires to approximate the mechanical environment operator $\hat{P}_{\mathrm{loss}} e^{i\tilde{\Omega}t} \approx \hat{\bar{m}}_{\mathrm{loss}}$ by a time averaged version $\hat{\bar{m}}_{\mathrm{loss}}(t) \sim \int_t^{t+\delta t} \mathrm{d}\tau \, \hat{m}_{\mathrm{loss}}(\tau) e^{i\tilde{\Omega}\tau} / \delta t$, for details see e.g. [Hof15]
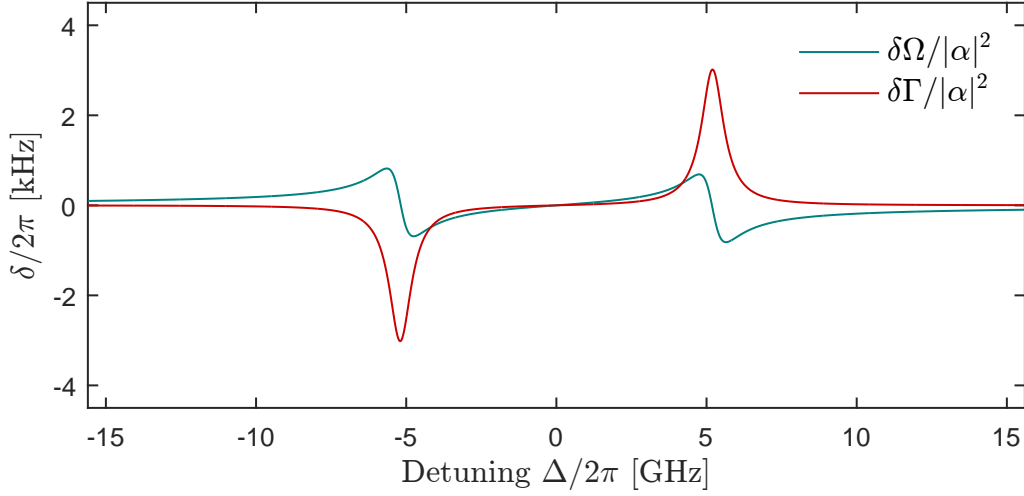
FIGURE 2.4.: **Optical Spring.** The optomechanical interaction modifies the mechanical response. This can be characterized by a change in the mechanical frequency $\delta\Omega = \tilde{\Omega} - \Omega$ (cyan) and the engergy damping rate $\delta\Gamma = \tilde{\Gamma} - \Gamma$ (red). The parameters used are specified in table 2.1. Note that for a mechanical quality factor of $Q_{\mathrm{mech}} = 10^7$, a single photon in the cavity is enough to generate mechanical gain, i.e. $\Gamma < 0$, for a blue detuned drive laser ($\Delta = -\tilde{\Omega}$).

element. These undesirable effects can be circumvented by limiting the time during which this interaction is driven [Hof+11; Pal+13b], thus resorting to a quasi-continous drive of the system, see section 2.3.

The third (2.27c) and forth line (2.27d) of the effective mechanical equation of motion describe the coupling to the optical and mechanical bath. To understand it better, we artificially split up the individual terms of the modified mechanical dissipation relation and assign a bath to each of them. For this, we introduce the root coupling

$$\mu_\pm = -g^\mp \sqrt{\mathcal{R}e\left(\chi_{\omega_{\mathrm{L}}}(\mp\tilde{\Omega})\right)} = -\frac{g^\mp \sqrt{\kappa}}{\sqrt{(\Delta \pm \tilde{\Omega})^2 + \kappa^2}} \tag{2.30}$$

with μ_+ relating to the Stokes process (with the effective interaction Hamiltonian $\hat{\mathcal{H}}_{\mathrm{S}} = \hbar g \hat{c}^\dagger \hat{m}^\dagger + \text{h.c.}[20]$) and μ_- relating to the anti-Stokes process ($\hat{\mathcal{H}}_{\mathrm{aS}} = \hbar g^\dagger \hat{c} \hat{m}^\dagger + \text{h.c.}$). The optomechanical coupling constant $g = g^- = g_0 \bar{c}$ is complex conjugated only for the anti-Stokes process ($g^+ = (g)^\dagger$). The phase of the root coupling, however, only plays a role for the coupling to the optical input field and thus can be neglected in most cases. We can now rewrite equation (2.27) in the Langevin form of fluctuation dissipation relations

$$\frac{\mathrm{d}}{\mathrm{d}t}\hat{m}_{\tilde{\Omega}} = -\frac{\Gamma}{2}\hat{m}_{\tilde{\Omega}} + i\sqrt{\Gamma}\hat{\tilde{m}}_{\mathrm{loss}}e^{i\tilde{\Omega}t} \tag{2.31a}$$

$$- |\mu_-|^2 \hat{m}_{\tilde{\Omega}} + i\sqrt{2}\mu_- \hat{\tilde{o}}_{\mathrm{eff}}^{(-)} \tag{2.31b}$$

$$+ |\mu_+|^2 \hat{m}_{\tilde{\Omega}} + i\sqrt{2}\mu_+ \hat{\tilde{o}}_{\mathrm{eff}}^{(+)} \tag{2.31c}$$

$$\hat{\tilde{o}}_{\mathrm{eff}}^{(\pm)} = \int_{-\infty}^{\infty} \frac{\chi_{\omega_{\mathrm{L}}}^{\pm}(\omega \mp \tilde{\Omega})}{|\chi_{\omega_{\mathrm{L}}}(\mp\tilde{\Omega})|} \hat{o}_{\omega_{\mathrm{L}}}^{\pm}(\omega \mp \tilde{\Omega})e^{\pm i\omega t} \frac{d\omega}{\sqrt{2\pi}} \tag{2.31d}$$

---

[20] This effective Hamiltonian recreates the relevant terms of the linearized equations of motion (2.22).

finding that the mechanical system couples to three different baths. Note that we now eliminated the optical spring effect by choosing the actual mechanical frequency (2.28) for the rotating mechanical frame. The first two terms describe a standard damping and coupling to the phononic (2.31a) and optical bath (2.31b). The third term (2.31c), however, can on its own not be understood by a fluctuation dissipation theorem, as there is no finite steady state temperature associated with it, due to the inverted sign of the damping. The optical baths (2.31d) are not in general independent. In the adiabatic regime, i.e. when the interaction is long enough to spectrally resolve the mechanical modes, only the resonant part of the drive, i.e. $\omega \approx 0$ will play a role. In this case, the prefactor becomes a simple phase shift and we find that the relevant baths are the upper sideband $\hat{\tilde{o}}_{\omega_{\mathrm{L}}}(+\tilde{\Omega})$ for the anti-Stokes term (2.31b), and the lower sideband $\hat{\tilde{o}}^{\dagger}_{\omega_{\mathrm{L}}}(-\tilde{\Omega})$ for the Stokes term (2.31c). The relevant bandwidth of the optical input will roughly correspond to the maximum of the mechanical damping Γ, the optomechanical coupling $|\mu_{\pm}|^2$ and the bandwidth of the drive pulse $\alpha_0(t)$.

Note that so far, we neither made an assumption on the sideband resolution $\tilde{\Omega}/\kappa$ nor the conventional rotating wave approximation of neglecting either term (2.31b) or (2.31c). Thus, the full dynamics of the system are covered, as long as the envelope of the drive pulse is slow on the relevant time scales κ and $\tilde{\Omega}$.

So far, we focused on the derivation of the equations of motion of the optomechanical system. In the following section, we complement this by discussing the system parameters and the mechanisms of the optomechanical system more specifically.

2.2. Characterization of the Components

In the previous section, we derived and described the effective interaction between an itinerant optical field coupled to a mechanical oscillator via an optomechanical system. We linearized the equations of motion and eliminated the cavity field, which is mediating and enhancing the interaction between the traveling light wave and the mechanical element. In this section, we will interpret the system dynamics, characterizing first the optical and mechanical resonators individually. In paragraph 2.2.3, we will turn to the optomechanical coupling, describing specific relevant examples of driven interactions.

2.2.1. The Optical Resonator

In order to describe the experiments, we need to characterize the optical cavity. This can be done by scanning the drive laser across the resonance and monitoring the reflected light. We defined the input light field by the flux operators

$$\left\langle \hat{n}_{\mathrm{in}}(t) \right\rangle = \left\langle \hat{o}^{\dagger}_{\mathrm{in}}(t)\hat{o}_{\mathrm{in}}(t) \right\rangle = |\alpha_0(t)|^2 = \frac{P_{\mathrm{in}}(t)}{\hbar\omega_{\mathrm{L}}} \tag{2.32}$$

where we made the approximation[21] of a monochromatic light source of frequency ω_{L} and power $P_{\mathrm{in}}(t)$ at the cavity input coupler. Using the steady state values (2.20), we find for

---

[21] More precisely, the full expression for the input power $\hat{P}_{\mathrm{in}} = \int_0^\infty \mathrm{d}\omega\, \hbar\omega\, \hat{o}^{\dagger}_{\mathrm{in}}(\omega)\hat{o}_{\mathrm{in}}(\omega)$ is based on the original bath definition, see also [5]. For a monochromatic light source (2.17), we in essence limit the integration range of the power expression. Using the commutator relation $[\hat{D}_{\hat{o}_{\mathrm{in}}(\omega_{\mathrm{L}})}(\alpha_0), \hat{o}_{\mathrm{in}}(\omega')] = \delta(\omega_{\mathrm{L}} - \omega')\alpha_0 \hat{D}_{\hat{o}_{\mathrm{in}}(\omega_{\mathrm{L}})}(\alpha_0)$, we obtain the above equation.
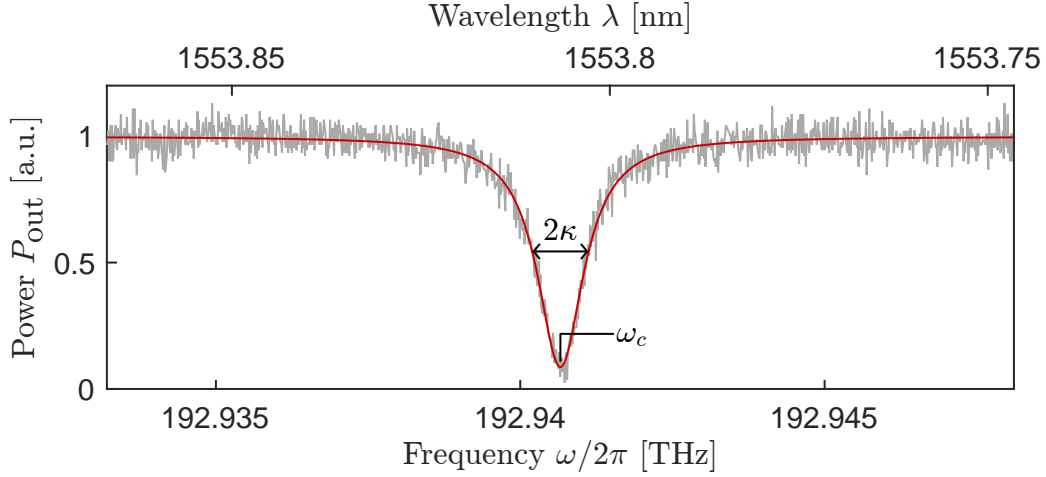
FIGURE 2.5.: **Optical Resonance Scan** The frequency of a laser with constant power is swept over the optical resonance. Light coupled into the cavity can be scattered, reducing the reflected power. From this dip, the exact resonance frequency ($\omega_c/2\pi = c/1553.806\,\text{nm}$) and amplitude decay rate $\kappa/2\pi = 463\,\text{MHz}$ can be extracted. To avoid strong optomechanical effects, the scan is performed at low power (grey) and the resulting noisy data is numerically fitted (red). The resonance characterized here belongs to device A in chapter 6.

the intracavity photon number

$$\langle \hat{c}^\dagger \hat{c} \rangle = \left\langle \frac{\bar{A}^2 + \bar{Y}^2 - 1}{2} \right\rangle = |\bar{c}|^2 = \frac{2\kappa_{in}}{\kappa^2 + \Delta^2}|\alpha_0|^2. \tag{2.33}$$

To scan the cavity, we change the detuning Δ, keeping the input power $\propto |\alpha_0|^2$ constant. With the input output relation of the cavity (2.12) we obtain the reflected power

$$P_{\text{out}}(\Delta) = \hbar\omega_{\text{L}} \left\langle \hat{o}_{\text{out}}^\dagger \hat{o}_{\text{out}} \right\rangle = P_{\text{in}} \left(1 - \underbrace{\frac{4\kappa_{\text{in}}\kappa_{\text{loss}}}{\kappa^2 + \Delta^2}}_{I(\Delta)} \right), \tag{2.34}$$

see also figure 2.5. Here, we introduced the cavity dip $I(\Delta) \propto |\chi_{\text{L}}(\omega_{\text{L}})|^2$, which is proportional to the absolute square of the cavity susceptibility (2.25), and can thus be used for the basic characterization of the cavity. Its half width half maximum (in angular frequency space) corresponds to the amplitude decay κ, i.e. $I(0) = 2I(\kappa)$. Note that the resonance scan has to be performed at low input powers, in order to keep the steady state shift $\bar{X}$ of the mechanical element negligible, such that $\Delta \approx \omega_c - \omega_{\text{L}}$. Consequently, these measurements can be noisy, such that numeric fitting the Lorenzian shape of $I(\Delta)$ is required to determine the exact optical resonance frequency and line width, see figure 2.5.

We know from equation (2.11) that the cavity field decays with rate κ, e.g. when turning off the drive field instantly at time t_0, the cavity field will ring down as $\langle \hat{c}_{\omega_{\text{L}}}(t) \rangle \approx \langle \hat{c}_{\omega_{\text{L}}}(t_0) \rangle e^{-\kappa t}$. For the emitted power this means that $\hbar\omega_{\text{L}} \left\langle \hat{o}_{\text{out}}^\dagger \hat{o}_{\text{out}} \right\rangle \propto e^{-2\kappa t}$, i.e. the power decay rate is $\kappa_{\text{power}} = 2\kappa$. Thus the optical quality factor is defined as $Q_{\text{opt}} = \omega_c/(2\kappa)$.

Note that from the Lorenzian reflection dip, we cannot generally distinguish between the decay into internal losses κ_{loss} and the coupling to the optical mode κ_{in}, as equation (2.34) is symmetric in those two variables. While a ring down measurement of the reflection could in principle provide a distinction, it is usually experimentally impractical for our integrated devices due to the fast ring down times $1/\kappa \sim 0.4$ns. Instead, a more viable way is to probe the phase response of the reflected field [22], e.g. by an off resonance reference beam. An important exception is the case of a critically coupled cavity, that is when the internal and external losses are degenerate $\kappa_{\text{in}} = \kappa_{\text{loss}} = \kappa/2$ and a distinction is not necessary to determine the individual values. Under those circumstances, $I(0) = 0$ and thus the reflection vanishes on resonance. It turns out that this configuration is the optimal trade-off between a narrow linewidth κ and maximum transduction $|\mu|^2 \approx |g|^2/\kappa^2$ for most of our protocols, given the usual restrictions of the device fabrication in terms of scattering losses, see also paragraph 2.4.2.

In paragraph 2.1.3, we introduced the notion of amplitude and phase quadrature. It is important to keep in mind that the cavity imposes a phase shift on the reflected optical field, which depends on its detuning. Therefore, different quadrature angles correspond to the physical amplitude quadrature for the input, output and cavity field. Setting the global phase of the complex input amplitude α_0 (2.17) accordingly, allows for choosing a convenient basis for one of these fields, e.g. setting the cavity quadrature $\langle \hat{Y}_{\omega_{\text{L}}} \rangle = 0$, making $\hat{Y}_{\omega_{\text{L}}}$ the phase and $\hat{A}_{\omega_{\text{L}}}$ the amplitude quadrature.

2.2.2. The Mechanical Resonator

In cavity optomechanics, a huge variety of mechanical oscillators are used, ranging from clouds of cold atoms to massive pendulums in gravitational wave detectors. The majority of experiments employ solid state resonators, comprising a large number of normal eigenmodes [AKM14]. Here, we consider a single, well isolated normal mode with a non-degenerate frequency, which can be spectrally resolved. This mode is described by a displacement field $\vec{\hat{d}}(\vec{r}) = \hat{X}_p \cdot \vec{d}_0(\vec{r})$, which is parametrized by the scalar operator $\hat{X}_p$. Using the effective mass $m_{\text{eff}} = \int \mathrm{d}^3 r\, \rho(\vec{r}) |\vec{d}_0(\vec{r})|^2$, the kinetic and potential energy of the mode can be described by[23]

$$\hat{\mathcal{H}}_{\text{mech}} = \frac{\hat{P}_p^2}{2m_{\text{eff}}} + m_{\text{eff}}\Omega^2 \hat{X}_p^2/2, \tag{2.35}$$

corresponding to the Hamiltonian of a point particle in a harmonic potential. The scalar momentum operator parametrizes the momentum field $\vec{\hat{p}}(\vec{r}) = \hat{P}_p \cdot \vec{d}_0(\vec{r})$ and relates to the displacement operator as expected for a point particle, with $\hat{P}_p = \frac{\hbar}{i}\frac{\partial}{\partial \hat{X}_p}$ and $\langle \hat{P}_p \rangle = m_{\text{eff}}\frac{\mathrm{d}}{\mathrm{d}t}\langle \hat{X}_p \rangle$. Note that $\hat{P}_p$ does not necessarily correspond to the total momentum $\int \mathrm{d}^3 r\, \vec{\hat{p}}(\vec{r})$, which can be zero for example for breathing modes.

---

[22] Inserting the steady state (2.20) into the input output relation (2.12), we obtain the reflected field

$$\langle \hat{o}_{\text{out},\omega_{\text{L}}} \rangle = \left(1 - \frac{2\kappa_{\text{in}}}{\sqrt{\Delta^2 + \kappa^2}}\frac{\kappa - i\Delta}{\sqrt{\Delta^2 + \kappa^2}}\right)\alpha_0$$

which exhibits a phase response linear in the input coupling rate κ_{in} for small detunings Δ.

[23] Furthermore, we assume small oscillation amplitudes, such that nonlinearities can be neglected, for example the coupling to other normal modes.

The equations of motion (2.13) of the mechanical oscillator differ from those of the optical field, also when the interaction is neglected $g_0 \approx 0$. In contrast to the cavity, ideally only one quadrature of the mechanical oscillator, the position $\hat{X}$, couples to the environment. Consequently, the dissipative term only appears in the derivative of the orthogonal quadrature, the momentum $\hat{P}$ (2.13d). Here, we will quickly review the causes, limits and consequences of this trait. For further details, please refer to one of the excellent reviews covering this topic [CR02; ER05; UFK10; GPI12; AKM14].

In a typical solid state harmonic oscillator, there are various damping mechanisms, making a complete description and analysis of them difficult [PZ12]. Some examples of known and at least partially understood mechanisms are gas friction, clamping or radiative phonon losses [Wil08; Col+11; VS14], thermoelastic damping [Zen37; Cag+17] and nonlinear phonon scattering [TRA09; KA11], coupling to localized defects in the bulk [UFK10; Bas+13; Bil+17] and on the surface [VS14] amongst others [Bar+12]. Loss mechanisms are sometimes categorized as extrinsic or intrinsic, with the first relating to mechanisms that can be controlled, e.g. by resonator geometry or gas pressure, and the second refers to properties of the bulk material. As the latter are typically hard to determine, the term intrinsic material losses also sometimes is a phenomenological summation of unidentified and less understood damping mechanisms [Sau90; Num+02; Mar+14b].

For some mechanisms, it is straight forward to see that only the displacement quadrature couples to the environment. Clamping losses couple the displacement of the oscillator to a small displacement of the supporting substrate [Wil08; Col+11]. Thermoelastic damping describes the dissipation of temperature gradients generated by inhomogeneous strain fields [Zen37; LR00]. This mechanism also couples to the mechanical displacement, as the material strain is directly related to the potential energy of the mechanical oscillator. Friction by residual gas in the viscous or molecular regime [Kok+87; Pal07b] is a velocity dependent force, i.e. the bath is coupled to the displacement. The same holds for eddy current damping of the motion of magnetic objects or of conductors in a magnetic field. Two level systems in the material, e.g. crystal defects, can be coupled to the strain, as investigated in the context of nitrogen vacancy defects in diamond [Mac+13; Tei+14; Ova+14]. Other mechanisms, in particular coupling to intrinsic environments, can couple also to the orthogonal quadrature and are thus better described by a general loss angle [Sau90], much like the decay of the optical cavity. This can for example be related to the relaxation of intrinsic bistable states [ZH46; Eti+03; Mar+14b], or, as an extrinsic mechanism, adsorption and desorption of gas molecules from the surface [EYR04; Pal07a]. In summary, an accurate model of the damping of a mechanical oscillator is highly complex and depends on the microscopic processes responsible for the dissipation [AW01b; AW01a]. The topic gets even more complicated when taking into account frequency dependent coupling to the bath. However, all of these effects mainly alter the mechanical response far off its resonance [Sau90] or in strongly damped systems. Consequently, they are of importance primarily for off-resonant detection schemes [Kra+12; Mar+16] and when precise fitting of the mechanical spectrum is required [Cri+18a]. For resonant processes, as considered in this thesis, the first Markov approximation and a viscous damping model are a reasonable assumption. In fact, as argued in [Hof15], the difference to a damping model that equally couples to both quadratures is negligible for a strongly under-damped oscillator, when measurements average over many oscillation
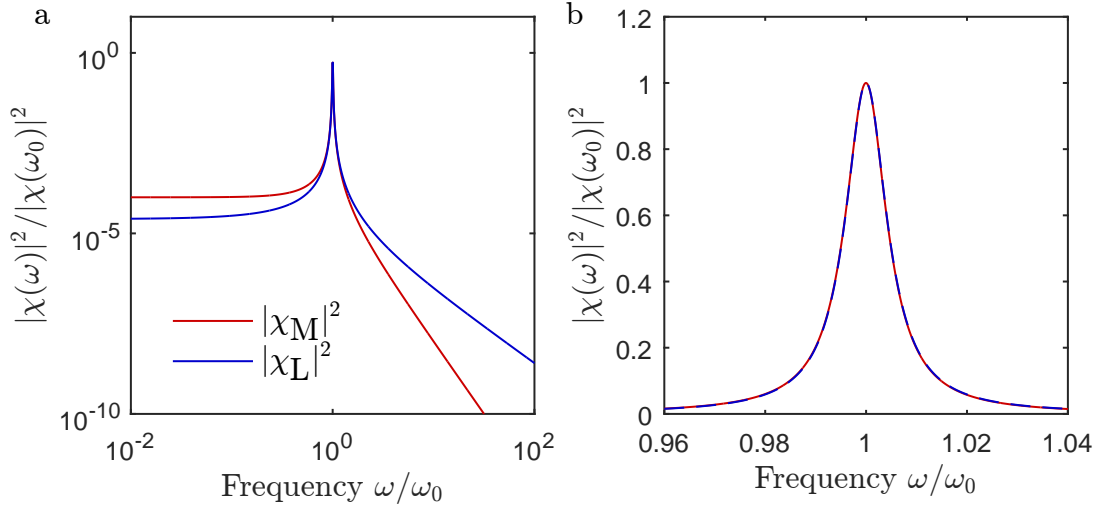
FIGURE 2.6.: **Optical and Mechanical Susceptibilities** The power susceptibilities of a resonance with viscous and symmetric damping are compared. In both cases a resonance frequency ω_0 and a quality factor $Q = 100$ is assumed. For viscous damping, only one quadrature experiences a coupling to the environment. This is approximately the case for a mechanical oscillator, resulting in the power susceptibility $|\chi_M|^2$ (red). In a symmetric damping model, as used for the optical power susceptibility $|\chi_L|^2$ (blue), both quadratures are coupled to loss channels. **a** On a logarithmic scale, we can see that far off resonance, the response functions differ strongly. **b** For the zoom onto the resonance on a linear scale, the lines are dashed to facilitate the comparison. Close to the resonance they are nearly identical. Consequently, it is justified to approximate a symmetric damping model for resonant protocols.

periods.

This effectively has been applied in the previous section when neglecting the fast rotating terms in the derivation of the effective mechanical equation of motion (2.31a) in the rotating frame. From this we can see, that the mechanical amplitude damping rate is $\Gamma/2$ and the energy decay is thus described by $e^{-\Gamma t}$. The mechanical quality factor, i.e. the ratio of stored energy H to energy dissipated per cycle L is therefore

$$Q_{\text{mech}} = 2\pi \frac{H}{L} \approx \frac{\Omega}{\Gamma} \tag{2.36}$$

in the limit of low damping. In order to extract the basic properties of the mechancial resonator, i.e. the resonance frequency Ω and the damping Γ we introduce the mechanical susceptibility

$$\chi_M(\omega) = \frac{\Omega}{\Omega^2 - \omega^2 - i\Gamma\omega}, \tag{2.37}$$

which we can obtain by Fourier transformation of (2.13). It describes the spectral response of the displacement to an external driving force[24].

---

[24] The displacement of the mechanical oscillator reacts with

$$\left\langle \hat{X}(t) \right\rangle = \int_{-\infty}^{\infty} \frac{d\omega}{\sqrt{2\pi}} \, \chi_M(\omega) \tilde{f}(\omega) e^{-i\omega t}$$

to a driving force $\sqrt{2\Gamma} \langle \hat{P}_{\text{loss}}(t) \rangle = \int_{-\infty}^{\infty} \frac{d\omega}{\sqrt{2\pi}} \tilde{f}(\omega) e^{-i\omega t}$, similar as the optical susceptibility (2.25). Note

2. Theory of Cavity Optomechanics

Note the difference to the optical susceptibility $\chi_{\mathrm{L}}(\omega) = (i(\omega_c - \omega) + \kappa)^{-1}$ (2.25), originating from simultaneous damping of both quadratures, see figure 2.6. Close to the resonance Ω we find similar behavior, with the energy decay rate corresponding to the full width half maximum of the power susceptibility $|\chi_{\mathrm{M}}(\Omega \pm \Gamma/2)|^2 \approx |\chi_{\mathrm{M}}(\Omega)|^2/2$ and $|\chi_{\mathrm{L}}(\omega_c \pm \kappa)|^2 = |\chi_{\mathrm{L}}(\omega_c)|^2/2$. In contrast, the off-resonant behavior can vary strongly. The response to a low frequency drive $\omega \approx 0$ differs by a factor 4 with $|\chi_{\mathrm{M}}(0)|^2/|\chi_{\mathrm{M}}(\Omega)|^2 = 1/Q_{\mathrm{mech}}^2$ and $|\chi_{\mathrm{L}}(0)|^2/|\chi_{\mathrm{L}}(\omega_c)|^2 \approx 1/(4Q_{\mathrm{opt}}^2)$. At high frequencies $\omega \gg \Omega$, the scaling for the mechanical response $|\chi_{\mathrm{M}}(\omega)|^2 \tilde{\propto} 1/\omega^4$ is a lot steeper than for the optical response $|\chi_{\mathrm{L}}(\omega)|^2 \tilde{\propto} 1/\omega^2$. We can therefore see, that the microscopic damping model is predominantly only important for off-resonant mechanical protocols. In this case, the contributions from other mechanical modes also need to be considered.

In case of the optical cavity, we had access to the power susceptibility $|\chi_{\mathrm{L}}(\omega)|^2$ by scanning the optical resonance with the drive laser. As we do not always have a narrow band actuator for the mechanical element, we need other ways to determine the basic parameters. A first alternative is to use broadband noise to excite the cavity and directly investigate the spectral response of the oscillator. Using noise which is approximately white around the resonance, such as the excitations by the thermal environment, all frequency components are driven equally and we can suspect the response to be proportional to $|\chi_{\mathrm{M}}(\omega)|^2$.

In order to formally discuss the mechanical spectrum, we first introduce the power spectral density (PSD). Using the finite-time-normalized Fourier transform[25] $\tilde{z}_T(\omega) = \int_0^T \mathrm{d}t\, z(t) e^{i\omega t}/\sqrt{T}$ of a signal $z(t)$ in a system subject to a stationary process, we define the power spectral density as

$$S_{\mathrm{zz}}(\omega) = \lim_{T \to \infty} \left\langle |\tilde{z}_T(\omega)|^2 \right\rangle \tag{2.38}$$

which describes the distribution of power[26] over the frequency range. For a random process, such as a thermally driven oscillator, there is by definition no knowledge about any Fourier component of the signal $\langle \tilde{z}_{T \to \infty} \rangle = 0$, i.e. the components of a sequence of independent measurements are expected to average out and we cannot predict the individual components of future trials. However, the higher statistical momenta of the random process are non-vanishing. We can thus understand the PSD as the variance of the distribution of finite-time-normalized Fourier components of our signal. The same argument holds for the power spectrum of a random noise source $\xi(t) = \sqrt{2\Gamma}\langle \hat{P}_{\mathrm{loss}}(t) \rangle$, and using the susceptibility (2.37), we can infer the PSD of the mechanical system driven by this source, $S_{\mathrm{XX}}(\omega) = |\chi_{\mathrm{m}}(\omega)|^2 S_{\xi\xi}(\omega)$. For a Markovian thermal bath in the first Markov approximation of white coupling, $S_{\xi\xi} = 2\Gamma(n_{\mathrm{th}} + 1/2)$ is white[27], i.e. constant over all frequencies, and therefore the resulting thermal spectrum can be used to to extract the mechanical power susceptibility. The mean thermal occupation number corresponds to the Bose distribution $n_{\mathrm{th}} = (e^{\hbar\omega/k_{\mathrm{B}}T} - 1)^{-1}$, with the Boltzmann constant k_{B} and the effective temperature T.

---

    that the mean value of the driving force needs to be real (2.13d), and with $\chi_{\mathrm{M}}(-\omega) = \chi_{\mathrm{M}}(\omega)^\dagger$ (2.37) we can see immediately that $\langle \hat{X}(t) \rangle$ is also real valued at all times.

[25] This ensures a finite value of the Fourier transform for continuous signals.

[26] In the signal processing sense, that is $\propto z^2$

[27] We find for a Markovian bath that the force noise is uncorrelated at different times $\langle \hat{P}_{\mathrm{loss}}(t) \hat{P}_{\mathrm{loss}}(t') \rangle = \delta(t - t')(n_{\mathrm{th}} + 1/2)$, which results in the white PSD, as can be seen using the Wiener-Khinchin theorem (2.39).

Ideally we would like to relate the thermal spectrum to the temperature of the bath of the oscillator. For this, we invoke the Wiener-Khinchin theorem, which relates the PSD to the Fourier transform of the autocorrelation function[28] $\gamma_z(\tau) = \langle z(t)z(t+\tau) \rangle$ by

$$S_{zz}(\omega) = \int_{-\infty}^{\infty} d\tau \, \gamma_z(\tau) e^{i\omega\tau}. \tag{2.39}$$

Thus, we obtain the variance of the displacement by transforming its PSD back for $\tau = 0$, which is equivalent to $\langle \hat{X}^2 \rangle = \int_{-\infty}^{\infty} \frac{d\omega}{2\pi} S_{XX}(\omega) = n_{\text{th}} + 1/2$, see also appendix B.1.

However, in many cases we will find that the full width half maximum of the thermal or white noise driven peak will not correspond to the mechanical life time. This is due to dispersive effects of the environment, that is fluctuations of the environmental conditions will change the resonance frequency. Consequently, the power spectral density will be convoluted with the likelyhood function of the resonance frequencies and thus smeared out. There are numerous processes effecting the resonance frequency [CR02; EYR04], such as temperature changes, adsorption and desorption of background gas molecules [Pal07a], changes of material defects, mechanical nonlinearities [GNQ13] or fluctuations in the optical drive power, thereby changing the optical spring (2.28), to name some of the known effects. Frequency fluctuations can be translated into additional phase noise $\delta\phi = \int \delta\Omega(t)dt$ but has ideally no effect on the amplitude noise of the oscillator. Thus, to probe the bare energy decay rate Γ, the measurement protocol needs to be insensitive to the mechanical phase. Two important methods, both realizing this condition by employing mechanical energy measurements[29], are ring-down- and autocorrelation measurements.

In a ring down measurement, the mechanical oscillator is initially excited by an external force to a mean phonon number n_{init} and after rapidly turning the external force off, the mechanical energy decay is observed. The excitation can be provided for example by optomechanically driving the Stokes transition, rapidly switching on and off a thermal bath [Rie+16; Jai+16], or externally actuated by a piezoelectric transducer [Col+14] or electrostatic forces [Sch+16]. Once the excitation ceased, the energy stored in the mechanical oscillator will decay as

$$\langle \hat{m}^\dagger \hat{m} \rangle(\tau) = (n_{\text{init}} - n_{\text{th}})e^{-\Gamma\tau} + n_{\text{th}}, \tag{2.40}$$

with the mean occupation number n_{th} in the steady state of the system. In optomechanical devices with narrow optical resonances, a measurement of the mechanical state can easily act back on the system, modifying the mechanical damping rate (2.29). In order to obtain the intrinsic damping rate, the optomechanical drive laser can be switched off for a time τ between the excitation and the actual energy measurement, thereby varying τ to obtain a full ring down measurement [Rie+16]. Alternatively, an auxiliary laser beam can be used to measure the mechanical state, ideally accessing the mechanical element without resonant enhancement, for example operating in a different wavelength regime or probing the mechanical oscillator at a different angle.

An autocorrelation measurement is useful when no external force can be provided or switched rapidly enough. It relies exclusively on the coupling to the thermal environment,

---

[28] As the processes is stationary, the autocorrelation function $\gamma_z(\tau)$ is independent of the initial time t.
[29] In most cases, the mechanical state will be deeply in the classical regime, thus the energy can be computed from the root mean squared of a position measurement.

exploiting that the typical time scale for changes in the thermal state of the oscillator also is given by the energy exchange rate with its environment Γ. Using the results from paragraph 2.3.2, we find that the normalized autocorrelation of the mechanical energy $\hat{\mathcal{H}}_{\mathrm{m}}(t) = \hbar\Omega\hat{m}^\dagger(t)\hat{m}(t)$

$$g_{\mathrm{mm}}^{(2)}(\tau) = \frac{\langle :\hat{\mathcal{H}}_{\mathrm{m}}(t)\hat{\mathcal{H}}_{\mathrm{m}}(t+\tau): \rangle}{\langle\hat{\mathcal{H}}_{\mathrm{m}}(t)\rangle^2} \approx \left(g_{\mathrm{mm}}^{(2)}(0) - 1\right)e^{-\Gamma\tau} + 1. \tag{2.41}$$

For large equilibrium occupation numbers $n_{\mathrm{th}} \gg 1$, the normal ordering $: \cdot :$ can be neglected (see paragraph 2.4.2). The autocorrelation of a thermal state is $g_{\mathrm{mm}}^{(2)}(0) \approx 2$, yielding a decent visibility of the decay.

2.2.3. The Linearized Interaction

After describing the properties of the optical and the mechanical resonator, I turn to discussing the coupling between these two systems. As the nonlinear parametric coupling is weak on the relevant scales of the system, we need to enhance the interaction by driving the system with an external laser beam. In this case, we obtain the linearized interaction, described by the effective Hamiltonian

$$\hat{\mathcal{H}}_{\mathrm{eff}} = 2\hbar g\hat{X}\hat{A} = \hbar g\left(\hat{m} + \hat{m}^\dagger\right)\left(\hat{c} + \hat{c}^\dagger\right), \tag{2.42}$$

which recreates[30] the operator equations of motion (2.22). After the linearization, the cavity operators correspond to fluctuations on the drive beam, that is the mechanical motion interacts with the optical sidebands, which are separated from the carrier frequency ω_{L} by the mechanical frequency. The enhanced interaction rate $g = g_0\bar{c}$, see equation (2.23), can be understood in the following way: The single photon coupling g_0^2 can be related to the (constant) scattering probability per photon in the drive beam. In contrast, $|g|^2$ relates to the probability of generating a photon in the sidebands, and thus it can be enhanced by supplying more photons in the drive beam.

The effective interaction Hamiltonian (2.42) describes the Stokes ($\hat{m}^\dagger\hat{c}^\dagger$) as well as the anti-Stokes scattering ($\hat{m}\hat{c}^\dagger$) due to the optomechanical interaction. By taking into account the cavity response in paragraph 2.1.4, we found that the nature of the interaction is influenced by the detuning of the drive beam with respect to the cavity. In the following I will briefly discuss the cases when (a) the drive laser, (b) the higher frequency anti-Stokes sideband, and (c) the lower frequency Stokes sideband is on resonance with the cavity.

Resonant Drive

When the drive beam is on resonance, i.e. the detuning $\Delta = 0$, the cavity susceptibility of both sidebands has the same magnitude $|\chi_{\omega_{\mathrm{L}}}(+\tilde{\Omega})| = |\chi_{\omega_{\mathrm{L}}}(-\tilde{\Omega})|$. Consequently, we can express the optical output field (2.26) as

$$\hat{o}_{\mathrm{out},\omega_{\mathrm{L}}} = i\frac{2\sqrt{\kappa_{\mathrm{in}}}g}{\sqrt{\kappa^2 + \tilde{\Omega}^2}}\hat{Q}_{\hat{m}}^\theta + \hat{o}_{\mathrm{in,eff},\omega_{\mathrm{L}}} \tag{2.43}$$

---

[30]Here, we set the global phase such that the intracavity field $\bar{c} \in \mathbb{R}$ is real.

with the phase $\theta = \arg(\chi_{\omega_{\mathrm{L}}}(-\tilde{\Omega}))$ and the normalized effective input field $\hat{o}_{\mathrm{in,eff},\omega_{\mathrm{L}}}$, which we assume to be in the vacuum state. We thus find that the cavity output field is proportional to a mechanical quadrature, with a phase depending on the sideband resolution of the system. In the bad cavity limit, that is $\kappa \gg \tilde{\Omega}$, the phase is $\theta \approx 0$ and thus the instantaneous mechanical displacement $\hat{X}$ is measured. In the resolved sideband limit, that is $\kappa \ll \tilde{\Omega}$, $\theta \approx -\pi/2$ as a result of the delay induced by the cavity, corresponding to a measurement of the momentum $\hat{P}$. As the proportionality in eq. (2.43) is purely imaginary, the signal is on the phase quadrature of the optical output.

While a resonant drive does neither induce an optical spring (2.28), nor modify the mechanical damping (2.29), the vacuum fluctuations of the input beam act as an additional bath, as can be seen in eq. (2.31). This force noise, called radiation pressure shot noise in reference to the vacuum fluctuations of the drive beam, limits the accuracy with which the displacement of an oscillator can be measured [Ede+78; Cav80]. This noise can in fact exceed the thermal noise and become the dominant noise contribution [PPR13].

Red Drive

By tuning the drive beam to a frequency that is lower than the optical resonance by exactly the mechanical frequency, that is $\Delta = \tilde{\Omega}$, the anti-Stokes sideband becomes resonant. In analogy to the visible spectrum, such a configuration is referred to as 'driving the cavity on the red side', and the corresponding drive beam is labeled 'red'. For a sideband resolved system, this yields a maximum enhancement of the anti-Stokes process, while at the same time strongly suppressing the off-resonant Stokes process $|\mu_+| \ll |\mu_-|$, see (2.30). Neglecting the latter is called rotating wave approximation, referring to the fast rotation of the off-resonant term in the frame of the cavity resonance. The interaction generated by the red drive can be approximated as exclusively involving the anti-Stokes process, corresponding to an effective interaction Hamiltonian of

$$\hat{\mathcal{H}}_{\mathrm{antiStokes}} = \hbar g \left(\hat{c}^\dagger \hat{m} + \hat{c}\hat{m}^\dagger \right). \tag{2.44}$$

It transfers phonons to resonant photons and vice versa, corresponding to a state transfer in the weak coupling regime. When the optical sideband frequency is in its vacuum state, that is there are no resonant photons injected into the cavity, mechanical excitations are first transferred to the optical domain and then rapidly leave the system at the optical decay rate κ. Consequently, the mechanical oscillator is cooled[Gig+06; Sch+08], potentially to its ground state [Teu+11a; Cha+11a].

In a scattering picture, low energy drive photons are upconverted to resonant photons of a higher energy, thus extracting energy from the system. The red drive thus couples the mechanical element to an additional, optical bath, which is in its ground state and thus appears very cold. This is reflected in an increased linewidth[31] of the mechanical resonances, see (2.29).

Alternatively, the interaction can be interpreted as a (partial) state transfer between the mechanical and the optical resonance. As we will see in paragraph 2.3.2, the red drive

---

[31] In a continuous variable pictures, the cavity response shifts the phase of optomechanical position measurement by $-\pi/2$, generating a cavity field and thus radiation pressure force proportional to $-\hat{P}$. In other words, resolved sideband cavity cooling is similar to feedback cooling, with the optical resonator computing the feedback signal [HM13].

mixes the optical and the mechanical input similarly to the way an optical beamsplitter mixes its input modes. Here, the state transfer fidelity, or the mixing ratio, corresponds to the power of the drive laser. For this reason, (2.44) is also referred to as beamsplitter interaction.

When the exchange rate of photons and phonons g exceeds the cavity decay rate κ, the transferred phonons do not necessarily leave the cavity, but can be transferred back into phonons again. This regime is called strong coupling [Grö+09; Teu+11b], leading to a hybridization of the optical and the mechanical excitations. As the new hybrid modes are split by the coupling rate $g > \kappa$ and are thus spectrally distinguishable, it is also referred to as normal mode splitting. This regime would be ideal for rapid and deterministic state transfers between the mechanical and the optical resonances, exploiting Rabi oscillations between the two domains. However, this regime has thus far not been accessible in the nanofabricated optomechanical crystals used in the experimental part of this thesis.

While the rotating wave approximation (2.44) is good for understanding the cooling and state transfer mechanism, it neglects the residual heating due to the off-resonant Stokes scattering. As will be discussed in paragraph 2.3.4, the ratio between the Stokes and anti-Stokes process is fixed by the sideband resolution $\tilde{\Omega}/\kappa$. This results in a minimal achievable phonon number of $\langle \hat{m}^\dagger \hat{m} \rangle \sim \kappa^2/(4\tilde{\Omega}^2) \ll 1$ by laser cooling [Sch+08], corresponding to the effective temperature of the optical bath.

For typical parameters of the devices used in the experimental part of this work, the sideband cooling limit $\kappa^2/(4\tilde{\Omega}^2) \sim 2 \cdot 10^{-3}$ is well below the observed residual absorption heating.

Blue Drive

When the drive laser is tuned to a frequency, which is higher than the optical resonance, that is the 'blue' side in the analogy of the visible spectrum, the Stokes process is enhanced. As in this case the high energy drive photons are downconverted to lower energy scattered photons, we expect a heating of the system. In the resolved sideband regime with $\Delta = -\tilde{\Omega}$, the effective interaction Hamiltonian is

$$\hat{\mathcal{H}}_{\text{Stokes}} = \hbar g \left(\hat{c}^\dagger \hat{m}^\dagger + \hat{c}\hat{m} \right). \tag{2.45}$$

in the rotating wave approximation, i.e. when neglecting the off-resonant anti-Stokes process. In this case, resonant photons and phonons are created or annihilated in pairs. Due to the proportionality of the ladder operators (2.3), phonons are more likely to be generated, independent of the optical input, i.e. the energy in the mechanical mode is generally increased. In fact, as $\hat{m}^\dagger |n\rangle = \sqrt{n+1}\,|n+1\rangle$, this heating rate is proportional to the number of mechanical excitations. Once it exceeds the internal mechanical damping, this corresponds to an exponential growth of the mechanical state, corresponding to a negative mechanical decay rate (2.29). Thus the optomechanical system is unstable for a continuous blue drive [BSV01; Kip+05].

Despite depositing energy in the system, which naively[32] resembles thermal heating, the process is coherent and can be employed as an active gain medium, once the self-amplifying property of the interaction is limited. In this case, the blue drive provides a gain for the

---

[32]That is, when tracing over the optical output.

optical and the mechanical mode, allowing for amplification of input signals [Mas+11; Nun+14; Lec+15b; Mal+18], respectively spontaneous emission [Gru+10; Coh+15].

Beyond a simple gain, the optical and mechanical states generated by eq. (2.45) are highly correlated. When decoherence and thermal noise is negligible, the pairwise occurrence of excitations in the two resonances corresponds to a two-mode-squeezed state. That is, a linear combination of a mechanical and an optical quadrature exhibits fluctuations below those of the optomechanical vacuum state. The properties of this state cannot be reproduced by describing the systems individually, hence the two subsystems are 'not separable' or 'entangled' [Hof+11; Pal+13a]. Referring to this important continuous variable state, the interaction (2.45) is also termed two-mode-squeezing interaction.

A different way of interpreting the optomechanical correlations [Rie+16] is to focus on the interaction on the single particle level. In essence, a blue detuned drive photon decays into a resonant photon and a phonon. This is similar to spontaneous parametric down conversion in non-linear crystals [BW70; Mol73], an important source of non-Gaussian states in quantum optics. While non-Gaussian states, i.e. states with a quasi-probability distribution that is not a multi-dimensional Gaussian function, are of great importance for quantum information protocols, they cannot be generated from initial Gaussian states through linear interactions and linear detection[33]. With thermal states, including the ground state, having Gaussian distributions, the linearized optomechanical interaction is thus unable to generate non-Gaussian states on its own. Probabilistic quantum optical protocols exploit the strong non-linearity of single photon detectors to conditionally prepare highly non-classical states. For example, single phonon Fock states can be generated in a heralding scheme [HM86], where the detection of a resonant signal photon, indicates the presence of a single idler phonon [Hon+17], see also chapter 5. By driving two optomechanical systems and erasing the information from which one the signal photon originated, the idler phonon can be projected into a superposition of being in either one device [Dua+01], thus entangling the two remote mechanical oscillators [Rie+18], see also chapter 6.

2.3. Single Phonon Quantum Optics

In the previous sections, we reviewed the basic equations describing the optomechanical interaction and then characterized the individual components of the system. Now we turn to formulating a precise theoretical description for optical control of the mechanical motion with slowly varying drive pulses. This method, called quasi-continuous control, allows for individually addressing Stokes or anti-Stokes transitions in the resolved sideband regime, as is the case for continuous drives, but also allows to limit the interaction strength. Thereby, for example, the parametric instability associated with the continuous driving of the Stokes transition can be avoided, providing access to its entangling property between the light field and the mechanical mode. Furthermore, it allows for control of the optomechanical state on a timescale which can be faster than the slow thermal processes related to optical absorption, allowing e.g. for low-noise, high-fidelity transfer of the state from the mechanical oscillator to the optical field.

---

[33] This also explains why non-Gaussian states are important to obtain a quantum advantage in information processing: Gaussian states can be very efficiently simulated, as they stay Gaussian under linear interactions and measurements [Kal60; Wie+15].

First, we will treat the time-varying effective coupling of the mechanical oscillator to a bath in general terms in paragraph 2.3.1, followed by the specific case for the anti-Stokes (paragraph 2.3.2) and Stokes scattering term (paragraph 2.3.3). These three paragraphs are strongly based on references [Hof+11; Hof15], where important, complimentary technical details can be found. Here, the framework is developed further by creating a quantitative description for the experimentally important scenario of arbitrary pulse shapes and lossy optical resonators. Thereafter, we will investigate contributions by the usually neglected off-resonant scattering terms in paragraph 2.3.4, and describe how the quasi-continuous protocols can be extended from the control of the amplitude of the mechanical state to the control of its phase (paragraph 2.3.5).

2.3.1. Generalized Quasi-Continuous Drives

For a continuously driven system, the input power of the drive laser is fixed, resulting in a constant coupling strength. Thus, the system will reach a steady state and remain in it indefinitely. In a quasi-continuous drive, the input power is varied slowly compared to the cavity bandwidth and the mechanical frequency, such that the same approximations, e.g. for addressing individual Stokes or anti-Stokes transitions can be made. Yet, by using time scales which are fast compared to the mechanical damping, coherent manipulation of the mechanical state is possible.

We start by investigating the individual terms of the fluctuation dissipation form of the mechanical equation of motion (2.31)

$$\frac{\mathrm{d}}{\mathrm{d}t}\hat{m}_{\tilde{\Omega}} = \pm\tilde{s}_{\pm}(t)\hat{m}_{\tilde{\Omega}} + ie^{i\phi_{\pm}}\sqrt{2\tilde{s}_{\pm}(t)}\hat{\zeta}_{\tilde{s}_{\pm}}^{(\pm)} \tag{2.46}$$

with a coupling constant $\tilde{s}_{\pm}(t) \geq 0$ (which can vary in time) and an input noise operator $\hat{\zeta}_{\tilde{s}_{\pm}}$. For the mechanical damping (2.31a), this would correspond to a negative sign with $(\tilde{s}_{-}, \phi_{-}, \hat{\zeta}^{(-)}) = (\Gamma/2, 0, \hat{\tilde{m}}_{\text{loss}})$. For the anti-Stokes interaction (2.31b), the parameters are $(\tilde{s}_{-}, \phi_{-}, \hat{\zeta}^{(-)}) = (|\mu_{-}(t)|^2, \arg(\mu_{-}), \hat{o}_{\text{eff}}^{(-)})$, and for the Stokes interaction term (2.31c) they are $(\tilde{s}_{+}, \phi_{+}, \hat{\zeta}^{(+)}) = (|\mu_{+}(t)|^2, \arg(\mu_{+}), \hat{o}_{\text{eff}}^{(+)})$.

In the following we will consider an interaction $\tilde{s}_{\pm}(t)$, which is limited to the time interval $t \in [0, T]$, i.e. we assume $\tilde{s}_{\pm}(t) = 0 \, \forall \, t \notin [0, T]$. For the subsequent steps, it will be convenient to define the accumulated interaction rate

$$\tilde{G}_{\pm}(t) = \pm\int_0^t \mathrm{d}\tau \, \tilde{s}_{\pm}(\tau). \tag{2.47}$$

Using the same type of formal integration as in the adiabatic elimination of the cavity (see also [17]), this allows us to express the mechanical annihilation operator in the rotating frame as

$$\hat{m}_{\tilde{\Omega}}(t) = \underbrace{e^{\tilde{G}_{\pm}(t)}\hat{m}_{\tilde{\Omega}}(0)}_{①} + ie^{i\phi_{\pm}}\underbrace{e^{\tilde{G}_{\pm}(t)}\int_0^t \mathrm{d}\tau \, e^{-\tilde{G}_{\pm}(\tau)}\sqrt{2\tilde{s}_{\pm}(\tau)}\,\hat{\zeta}_{\tilde{s}_{\pm}}^{(\pm)}(\tau)}_{②}. \tag{2.48}$$

We can see that the final mechanical operator (and thus state) $\hat{m}_{\tilde{\Omega}}(t)$ is a mix of the initial mechanical operator in the homogenous solution term ① and the integrated noise input in the inhomogenous solution term ②.

The latter is a discrete wavelet mode of the input flux operator $\hat{\zeta}_{\tilde{s}_\pm}(t)$. In other words, it is localized in time and frequency domain, allowing to address individual sidebands as well as manipulations that are fast compared to the mechanical life time. This will be discussed in more detail below. The mode shape in term ② can be normalized by ensuring that the commutation relation of its annihilation and creation operator is the identity[34]. We thus define the normalized input mode operator as

$$\hat{a}_{\text{in}} = \frac{1}{\sqrt{\pm\left(1 - e^{-2\tilde{G}_\pm(T)}\right)}} \int_0^T \mathrm{d}\tau \, e^{-\tilde{G}_\pm(\tau)} \sqrt{2\tilde{s}_\pm(\tau)} \left(\hat{\zeta}_{\tilde{s}_\pm}^{(\pm)}(\tau)\right)^\pm, \qquad (2.49)$$

which fulfills $[\hat{a}_{\text{in}}, \hat{a}_{\text{in}}^\dagger] = 1$ and describes the time envelope of an excitation in the input mode which can interact with the mechanical system. This yields for the final mechanical annihilation operator (2.48) the simple expression

$$\hat{m}_{\tilde{\Omega}}(T) = e^{\tilde{G}_\pm(T)}\hat{m}_{\tilde{\Omega}}(0) + ie^{i\phi_\pm}\sqrt{\pm\left(e^{2\tilde{G}_\pm(T)} - 1\right)}\hat{a}_{\text{in}}^\pm. \qquad (2.50)$$

While we will discuss more detailed implications of this equation in the subsequent paragraphs, we can immediately see that the part of the mechanical operator which is influenced by the optical mode $\hat{a}_{\text{in}}$ inherits the phase $\phi_\pm$ of the drive beam. This reflects the fact that the optomechanical interaction is a three body process, as described in paragraph 2.1.1, involving the annihilation of one and creation of another photon, while creating or annihilating a phonon. Hence, despite the linearization of the interaction in the weak coupling limits discussed here, the phase information of the drive field is not lost. This is employed, for example, to control the phase of the mechanical state in chapter 6 and discussed further in appendix B.4. The phase coherence between the drive and scattered fields is a common trait of parametric processes in quantum optics [Ou+90].

After keeping the discussion so far in general terms, in order to also treat the mechanical coupling to the environment, we will now focus explicitly on the optomechanical interaction. We start by relating the cumulative coupling, which characterized the interaction between the optical and the mechanical input (2.50), to the extra-cavity control beam driving the system[35]:

$$|\tilde{G}_\pm(T)| = \underbrace{\frac{g_0^2 \kappa}{(\Delta \pm \tilde{\Omega})^2 + \kappa^2}}_{①} \underbrace{\frac{2\kappa_{\text{in}}}{\Delta^2 + \kappa^2}}_{②} \underbrace{\int_0^T \mathrm{d}t \, |\alpha_0(t)|^2}_{=N_{\text{in},\pm}} \qquad (2.51)$$

---

[34] We know that the pulse shape of the optical input $\hat{a}_{\text{in}}$ is proportional to the inhomogeneous part ② of the solution (2.48). We normalize it by introducing a factor $\mathcal{N}$ to the input mode $\hat{a}_{\text{in}} = \mathcal{N} \cdot \int_0^T \mathrm{d}\tau \, e^{-\tilde{G}_\pm(\tau)}\sqrt{2\tilde{s}_\pm(\tau)}\hat{\zeta}(\tau)$ and setting the commutator to unity. Using the approximation $\left[\hat{\zeta}(\tau), \hat{\zeta}^\dagger(\tau')\right] \approx \delta(\tau - \tau')$, which is justified in the limit of a large bandwidth of the cavity $\kappa \to \infty$ [Hof15], we find

$$\left[\hat{a}_{\text{in}}, \hat{a}_{\text{in}}^\dagger\right] \overset{!}{=} 1 = \mathcal{N}^2 \int_0^T \mathrm{d}\tau \, e^{-2\tilde{G}_\pm(\tau)} \underbrace{2\tilde{s}_\pm(\tau)}_{=\pm\frac{\mathrm{d}}{\mathrm{d}\tau}2\tilde{G}_\pm(\tau)} = \pm\left(1 - e^{\mp 2|\tilde{G}_\pm(T)|}\right)\mathcal{N}^2$$

[35] We use the definition (2.47) of $\tilde{G}_\pm$ and the optomechanical coupling rate (2.30) and (2.23), together with the steady state of the intra-cavity field (2.20) and obtain a direct proportionality of the cumulative coupling to the extra-cavity photon number $N_{\text{in},\pm}$.

2. Theory of Cavity Optomechanics

We find that it is directly proportional to the number of photons in the drive pulse $N_{\mathrm{in},\pm}$ as well as to the optical susceptibility at the frequency of the generated sideband ① and the drive itself ②.

Next, we investigate the explicit form of the optical input and output pulses. Using the full expression (2.31d) for the optical input field $\hat{\tilde{o}}_{\mathrm{eff}}$, the input mode (2.49) becomes

$$\hat{a}_{\mathrm{in}} = \int_{-\infty}^{\infty} \frac{\mathrm{d}\omega}{\sqrt{2\pi}} \int_0^T \mathrm{d}\tau\, \mathcal{W}_{(\pm)}^{\mathrm{in}}(\omega, \tau) \hat{\tilde{o}}_{\omega_{\mathrm{L}}}(\omega \mp \tilde{\Omega}). \tag{2.52a}$$

The normalized wavelet envelope

$$\mathcal{W}_{(\pm)}^{\mathrm{in}}(\omega, \tau) = \frac{1}{\sqrt{\pm\left(1 - e^{-2\tilde{G}_\pm(T)}\right)}} \frac{\chi_{\omega_{\mathrm{L}}}(\omega \mp \tilde{\Omega})}{|\chi_{\omega_{\mathrm{L}}}(\mp \tilde{\Omega})|} e^{-\tilde{G}_\pm(\tau)} \sqrt{2\tilde{s}_\pm(\tau)} e^{-i\omega\tau} \tag{2.52b}$$

is localized in frequency space around the mechanical sideband frequency $\omega \sim 0$ (that is in absolute frequency $\omega_{\mathrm{L}} \mp \tilde{\Omega}$) with the bandwidth of the input mode shape. Consequently, the input operators for the Stokes and anti-Stokes transition from the same drive field are approximately orthogonal, despite occupying similar temporal envelopes.

For the output mode, we similarly define the super-mode

$$\hat{u} = \sqrt{\kappa_{\mathrm{in}}/\kappa}\,\hat{o}_{\mathrm{out}} + \sqrt{\kappa_{\mathrm{loss}}/\kappa}\,\hat{o}_{\mathrm{loss,out}}$$

and its Fourier transform $\hat{\tilde{u}}_{\omega_{\mathrm{L}}}$ in a frame rotating at the drive frequency. With this, we can define an output mode (see appendix B.2 for details) in analogy to (2.52)

$$\hat{a}_{\mathrm{out}} = \int_{-\infty}^{\infty} \frac{\mathrm{d}\omega}{\sqrt{2\pi}} \int_0^T \mathrm{d}\tau\, \mathcal{W}_{(\pm)}^{\mathrm{out}}(\omega, \tau) \hat{\tilde{u}}_{\omega_{\mathrm{L}}}(\omega \mp \tilde{\Omega}) \tag{2.53a}$$

$$\mathcal{W}_{(\pm)}^{\mathrm{out}}(\omega, \tau) = \frac{1}{\sqrt{\pm(e^{2\tilde{G}_\pm(T)} - 1)}} \frac{\chi_{\omega_{\mathrm{L}}}(\omega \mp \Omega)^\dagger}{|\chi_{\omega_{\mathrm{L}}}(\mp \Omega)|} e^{\tilde{G}_\pm(\tau)} \sqrt{2\tilde{s}_\pm(\tau)} e^{-i\omega\tau}, \tag{2.53b}$$

using the wavelet $\mathcal{W}_{(\pm)}^{\mathrm{out}}$. The mode is, in close analogy to the input mode, a narrow band mode located on the respective sideband of the drive. It can be interpreted as the mode with maximal overlap with the optomechanically generated photon. Using (2.26), this allows to write the interaction as

$$\hat{a}_{\mathrm{out}} = -ie^{\pm i\phi_\pm} \sqrt{\pm\left(e^{2\tilde{G}_\pm(T)} - 1\right)}\,\hat{m}_{\tilde{\Omega}}^\pm(0) - e^{\tilde{G}_\pm(T)}\hat{a}_{\mathrm{in}}. \tag{2.54}$$

The optical and mechanical output modes are orthonormal[36], i.e. the final operators after the interaction are a unitary transformation of the initial operators.

So far, we restricted our analysis to optical super-modes $\hat{o}$ and $\hat{u}$ which couple to the cavity. However, they combine the accessible fields $\hat{o}_{\mathrm{in}}$ and $\hat{o}_{\mathrm{out}}$ and the inaccessible stray fields $\hat{o}_{\mathrm{loss}}$ and $\hat{o}_{\mathrm{loss,out}}$. Additionally, there is also a set of decoupled, orthogonal modes for the optical input $\hat{o}_{\mathrm{d,in}} = \sqrt{\kappa_{\mathrm{loss}}/\kappa}\,\hat{o}_{\mathrm{in}} - \sqrt{\kappa_{\mathrm{in}}/\kappa}\,\hat{o}_{\mathrm{loss}}$ and the output $\hat{o}_{\mathrm{d,out}} = \sqrt{\kappa_{\mathrm{loss}}/\kappa}\,\hat{o}_{\mathrm{out}} - \sqrt{\kappa_{\mathrm{in}}/\kappa}\,\hat{o}_{\mathrm{loss,out}}$. Employing the input-output relations (2.12), we find $\hat{o}_{\mathrm{d,out}} = \hat{o}_{\mathrm{d,in}}$, i.e. the field is, as expected, decoupled from the cavity dynamics and thus does not participate

---

[36] Using equations (2.50) and (2.54), we find $[\hat{m}_{\tilde{\Omega}}(T), \hat{m}_{\tilde{\Omega}}^\dagger(T)] = [\hat{a}_{\mathrm{out}}, \hat{a}_{\mathrm{out}}^\dagger] = 1$ and $[\hat{m}_{\tilde{\Omega}}(T), \hat{a}_{\mathrm{out}}^\pm] = 0$.

in the optomechanical interaction. Defining the corresponding discrete mode $\hat{a}_{\mathrm{dec}}$ ($\hat{a}_{\mathrm{wg,out}}$, $\hat{a}_{\mathrm{loss,out}}$) belonging to the field $\hat{o}_{\mathrm{d,in}}$ ($\hat{o}_{\mathrm{out}}$, $\hat{o}_{\mathrm{loss,out}}$) in analogy to (2.53)[37], we find that the decoupled mode $\hat{a}_{\mathrm{dec}}$ mixes with the mode emitted from the cavity $\hat{a}_{\mathrm{out}}$ to form the experimentally accessible ($\hat{a}_{\mathrm{wg,out}}$) and inaccessible ($\hat{a}_{\mathrm{loss,out}}$) mode:

$$\hat{a}_{\mathrm{wg,out}} = \sqrt{\frac{\kappa_{\mathrm{in}}}{\kappa}}\hat{a}_{\mathrm{out}} + \sqrt{\frac{\kappa_{\mathrm{loss}}}{\kappa}}\hat{a}_{\mathrm{dec}} \tag{2.55a}$$

$$\hat{a}_{\mathrm{loss,out}} = \sqrt{\frac{\kappa_{\mathrm{loss}}}{\kappa}}\hat{a}_{\mathrm{out}} - \sqrt{\frac{\kappa_{\mathrm{in}}}{\kappa}}\hat{a}_{\mathrm{dec}} \tag{2.55b}$$

This description is similar to a directional coupler with splitting ratio $\kappa_{\mathrm{in}}:\kappa_{\mathrm{loss}}$. In the experimental work presented in this thesis, the optical input field at the mechanical sideband frequencies is always in its groundstate. In this case, the directional coupler (2.55) can be interpreted as a simple loss mechanism [Yur85; Sha85], in which a fraction $\kappa_{\mathrm{loss}}/\kappa$ of the optomechanical signal is immediately lost to the environment and only a fraction $\kappa_{\mathrm{in}}/\kappa$ couples into the desired mode $\hat{a}_{\mathrm{wg,out}}$, e.g. confined in a waveguide and thus accessible for measurements.

In applications where there is a non-vacuum optical input, we find that the accessible input mode $\hat{a}_{\mathrm{wg,in}}$[38] influences the mechanical state

$$
\begin{aligned}
\hat{m}_{\tilde{\Omega}}(T) =& e^{\tilde{G}_{\pm}(T)}\hat{m}_{\tilde{\Omega}}(0) \\
&+ ie^{i\phi_{\pm}}\sqrt{\frac{\kappa_{\mathrm{in}}}{\kappa}}\sqrt{\pm\left(e^{2\tilde{G}_{\pm}(T)} - 1\right)}\hat{a}_{\mathrm{wg,in}}^{\pm} \\
&+ ie^{i\phi_{\pm}}\sqrt{\frac{\kappa_{\mathrm{loss}}}{\kappa}}\sqrt{\pm\left(e^{2\tilde{G}_{\pm}(T)} - 1\right)}\hat{a}_{\mathrm{loss}}^{\pm}
\end{aligned}
\tag{2.56}
$$

with an amplitude reduced by $\sqrt{\kappa_{\mathrm{in}}/\kappa}$. Furthermore, in such protocols it needs to be considered that the pulse shape of the decoupled mode $\mathcal{W}_{(\pm)}^{\mathrm{out}}$ differs from the coupled optical input $\mathcal{W}_{(\pm)}^{\mathrm{in}}$, in particular for large cumulative couplings $|\tilde{G}_{\pm}(T)|$. Consequently, protocols which are based on the interference of the interacting and non-interacting parts of the optical beam, such as a quasi-continuous version of optomechanically induced transparency [Wei+10] need to take into account a finite visibility of this interference.

2.3.2. Anti-Stokes Scattering

After deriving a general description of the optomechanical interaction driven by a slowly varying laser pulse in the previous paragraph, we will now specifically investigate the anti-Stokes scattering term before turning to the Stokes term in the next paragraph. As described in paragraph 2.2.3, the anti-Stokes term, corresponding to the effective interaction Hamiltonian $\hat{\mathcal{H}}_{\mathrm{AntiStokes}} \propto \hat{c}^{\dagger}\hat{m} + \mathrm{h.c.}$, can be made dominant by detuning the

---

[37] That is $\hat{a}_{\mathrm{dec}} = \int_{-\infty}^{\infty}\frac{\mathrm{d}\omega}{\sqrt{2\pi}}\int_0^T\mathrm{d}\tau\,\mathcal{W}_{(\pm)}^{\mathrm{out}}(\omega,\tau)\hat{\tilde{o}}_{\mathrm{d},\omega_{\mathrm{L}}}(\omega\mp\tilde{\Omega})$ for the Fourier transform $\hat{\tilde{o}}_{\mathrm{d},\omega_{\mathrm{L}}}$ of the field $\hat{o}_{\mathrm{d,in}}$ in a reference frame rotating at the drive frequency ω_{L}. Similarly, we define $\hat{a}_{\mathrm{wg,out}} = \int_{-\infty}^{\infty}\frac{\mathrm{d}\omega}{\sqrt{2\pi}}\int_0^T\mathrm{d}\tau\,\mathcal{W}_{(\pm)}^{\mathrm{out}}(\omega,\tau)\hat{\tilde{o}}_{\mathrm{out},\omega_{\mathrm{L}}}(\omega\mp\tilde{\Omega})$ and $\hat{a}_{\mathrm{loss,out}} = \int_{-\infty}^{\infty}\frac{\mathrm{d}\omega}{\sqrt{2\pi}}\int_0^T\mathrm{d}\tau\,\mathcal{W}_{(\pm)}^{\mathrm{out}}(\omega,\tau)\hat{\tilde{o}}_{\mathrm{loss,out},\omega_{\mathrm{L}}}(\omega\mp\tilde{\Omega})$

[38] As described in [37] and (2.52), we define $\hat{a}_{\mathrm{wg,in}} = \int_{-\infty}^{\infty}\frac{\mathrm{d}\omega}{\sqrt{2\pi}}\int_0^T\mathrm{d}\tau\,\mathcal{W}_{(\pm)}^{\mathrm{in}}(\omega,\tau)\hat{\tilde{o}}_{\mathrm{in},\omega_{\mathrm{L}}}(\omega\mp\tilde{\Omega})$ and $\hat{a}_{\mathrm{loss}} = \int_{-\infty}^{\infty}\frac{\mathrm{d}\omega}{\sqrt{2\pi}}\int_0^T\mathrm{d}\tau\,\mathcal{W}_{(\pm)}^{\mathrm{in}}(\omega,\tau)\hat{\tilde{o}}_{\mathrm{loss},\omega_{\mathrm{L}}}(\omega\mp\tilde{\Omega})$

2. Theory of Cavity Optomechanics

drive laser frequency $\omega_\mathrm{L} \approx \omega_c - \Omega$ to the red, i.e. lower frequency side of the optical cavity by the frequency of the mechanical oscillator. This corresponds to the detuning $\Delta = \tilde{\Omega}$, rendering the coupling constant of the anti-Stokes term $\tilde{s}_- = |g|^2/\kappa$ much larger than for the Stokes term $\tilde{s}_+ = |g|^2/(\kappa + 4\tilde{\Omega}^2/\kappa)$ for $\tilde{\Omega} \ll \kappa$, i.e. in the resolved sideband regime. We can define the probability

$$\epsilon_\mathrm{R} = 1 - e^{-2|\tilde{G}_\pm(T)|} \tag{2.57}$$

to rewrite the input output form of the interaction (2.50) and (2.54) as

$$\hat{m}_{\tilde{\Omega}}(T) = \sqrt{1 - \epsilon_\mathrm{R}}\, \hat{m}_{\tilde{\Omega}}(0) + ie^{-i\theta}\sqrt{\epsilon_\mathrm{R}}\, \hat{a}_\mathrm{in} \tag{2.58a}$$

$$\hat{a}_\mathrm{out} = -ie^{i\theta}\sqrt{\epsilon_\mathrm{R}}\, \hat{m}_{\tilde{\Omega}}(0) - \sqrt{1 - \epsilon_\mathrm{R}}\, \hat{a}_\mathrm{in}, \tag{2.58b}$$

with $\theta = \arg(-g_0\alpha_0)$ defined by the phase of the drive beam and the sign of the optomechanical coupling constant g_0. This is equivalent to the description of an optical beam splitter or directional coupler with reflectivity ϵ_R, with one input and one output port being the mechanical mode before and after the pulsed interaction, see figure 2.7. This mixing of the optical and mechanical modes can be interpreted in multiple ways. First, we consider the case where the optical input is in the vacuum state and the mechanical mode initially is in a thermal state. The average number of phonons in the system $\bar{n}(t) = \left\langle \hat{m}_{\tilde{\Omega}}^\dagger \hat{m}_{\tilde{\Omega}}(t) \right\rangle$ after the interaction (at $t = T$) is reduced to a fraction $1 - \epsilon_\mathrm{R}$ of the initial $(t = 0)$ phonon number $\bar{n}(T) = (1 - \epsilon_\mathrm{R})\bar{n}(0)$. The extracted phonons are converted to photons in the optical output mode $\left\langle \hat{a}_\mathrm{out}^\dagger \hat{a}_\mathrm{out} \right\rangle = \epsilon_\mathrm{R}\bar{n}(0)$. Note that here we neglected heating by absorption of drive photons and Stokes scattering, which in practical experiments sets a limit to the minimal achievable phonon number.

The same setting can also be interpreted as a partial or lossy state swap: A beam splitter with vacuum on one input port, here the optical input, can be used to model loss in a transmission channel [Yur85; Sha85]. Thus, the state of the optical output mode after the interaction is equivalent to the initial mechanical state going through a lossy element with transmission ϵ_R. Note that the remaining part of the initial mechanical state is not actually lost in this case, but simply remains in the mechanical oscillator, and can in principle be retrieved by a subsequent pulse. Taking into account the additional loss due to the inaccessible scattered light field, see equation (2.55), the equivalent transmission after an ideal state transfer from the mechanical to the accessible optical mode drops to $\epsilon_\mathrm{R}\kappa_\mathrm{in}/\kappa$.

Another scenario is to have the mechanical mode initially in its ground state and sending an optical state with envelope $\mathcal{W}_{(-)}^\mathrm{in}$ (2.52) to the device. In this case, the pulsed state transfer of the anti-Stokes term converts the flying optical state in mode $\hat{a}_\mathrm{in}$ to a stationary mechanical state in mode $\hat{m}_{\tilde{\Omega}}(T)$ after the interaction. This again happens with a fidelity of $\epsilon_\mathrm{R}\kappa_\mathrm{in}/\kappa$, for a state sent in via the accessible input mode (2.56). The fidelity is composed of the cavity input impedance $\kappa_\mathrm{in}/\kappa$ and the fidelity of the actual optomechanical state transfer ϵ_R. This storage of the optical input state, controlled by the strength of the drive field, modifies the interference between the different field contributions in the cavity[39]. This can lead to an observed increase or decrease in the transmission of the probe beam $\hat{a}_\mathrm{wg,in}$ similarly to optomechanically induced transparency. The main difference here is

---

[39] For $\epsilon_\mathrm{R} \ll 1$, the envelope of the incoming and emitted wave are approximately the same $\mathcal{W}_{(-)}^\mathrm{out} \approx \tilde{\chi}\mathcal{W}_{(-)}^\mathrm{in}$, where $\tilde{\chi} = \chi_{\omega_\mathrm{L}}^\dagger(\tilde{\Omega})/\chi_{\omega_\mathrm{L}}(\tilde{\Omega})$ is a phase shift. We find for the wave package emitted into the accessible
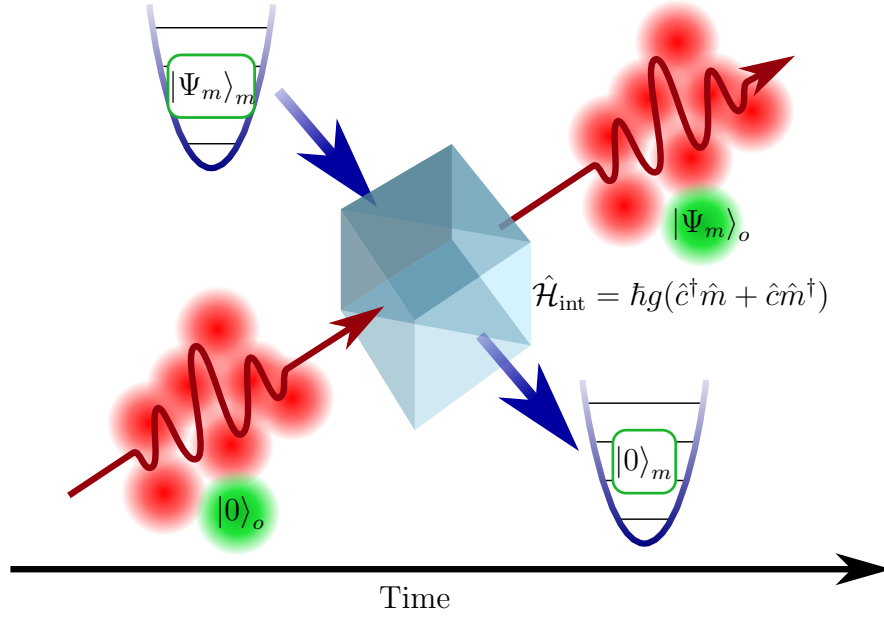
FIGURE 2.7.: **Optomechanical Beamsplitter Interaction.** The description of the anti-Stokes interaction (2.58) is equivalent to that of an optical beamsplitter with reflectivity ϵ_{R}. A strong red detuned drive field (red dots) generates a linear interaction $\hat{\mathcal{H}}_{\mathrm{int}}$ between the optical (green dot) and the mechanical resonance (harmonic potential), symbolized by a beamsplitter cube. For $\epsilon_{\mathrm{R}} \sim 1$, the input states (left side) of the optical and mechanical state are swapped, i.e. the final state (right side) of the optical mode is the inital mechanical state and vice versa. This state swap allows to optically read out the mechanical state. If the resonant optical sideband initially was in the vacuum state, the mechanical resonance will be cooled to the ground state, neglecting detrimental heating effects.

that we consider a mode which is matched to the emitted transferred state $\mathcal{W}^{\mathrm{out}}_{(-)}$, while OMIT protocols use a stored and retrieved state to generate an interference effect, i.e. the initial mechanical state should not play a role. To recreate such protocols, the pulse envelopes $\mathcal{W}^{\mathrm{in}}_{(-)}$ and $\mathcal{W}^{\mathrm{out}}_{(-)}$ need to be adjusted to reduce the overlap with the transferred state[40], which however is beyond the scope of this thesis.

So far we discussed the effect of the anti-Stokes process with a general state transfer fidelity ϵ_{R}. We now turn to a specific example of a system with the drive frequency tuned to $\Delta = \tilde{\Omega}$, i.e. the scattered field is resonant with the optical cavity. In this case, using

---

optical mode

$$\hat{a}_{\mathrm{wg,out}} = -ie^{i\theta}\sqrt{\frac{\kappa_{\mathrm{in}}}{\kappa}\epsilon_{\mathrm{R}}}\, \hat{m}_{\tilde{\Omega}}(0) - \left(\frac{\kappa_{\mathrm{in}}}{\kappa}\sqrt{1-\epsilon_{\mathrm{R}}} - \tilde{\chi}\frac{\kappa_{\mathrm{loss}}}{\kappa}\right)\hat{a}_{\mathrm{wg,in}} - \frac{\sqrt{\kappa_{\mathrm{in}}\kappa_{\mathrm{loss}}}}{\kappa}\left(\sqrt{1-\epsilon_{\mathrm{R}}} + \tilde{\chi}\right)\hat{a}_{\mathrm{loss}}.$$

Note that the optomechanical coupling modifies the impedance matching of the cavity. For example, an impedance matched cavity ($\kappa_{\mathrm{in}} = \kappa_{\mathrm{loss}}$) has no contribution of $\hat{a}_{\mathrm{wg,in}}$ to $\hat{a}_{\mathrm{wg,out}}$ on resonance, when the drive beam is off ($\epsilon_{\mathrm{R}} = 0$), but has finite reflection for $\epsilon_{\mathrm{R}} > 0$.

[40] This can be seen for example in equation (B.16) in appendix B.2. By keeping the drive on after the initial state is transferred, the optical output field is mainly correlated with the optical input field. Matching the mode envelopes to this time-domain part of the field will result in OMIT like features.
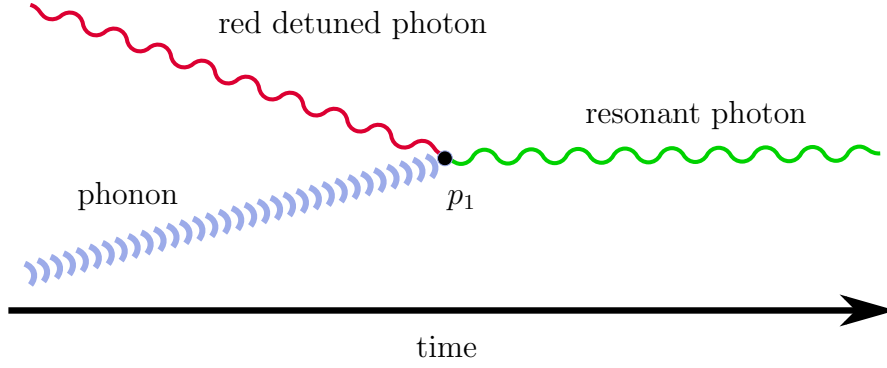
FIGURE 2.8.: **Anti-Stokes Scattering.** On a single particle level, one red detuned drive photon (red) and a phonon (blue) are annihilated, and a resonant photon (green) is created. If a single photon and phonon is present, this scattering process happens with a probability $p_1 \sim 5 \cdot 10^{-8}$ for the parameters given in table 2.1. In order to achieve an efficient state transfer, a large number of drive photons are necessary.

(2.51) we find the explicit form for the fidelity

$$\epsilon_{\mathrm{R}} = 1 - \exp\left(-\frac{\kappa_{\mathrm{in}}}{\kappa} \frac{4g_0^2 N_{\mathrm{in,-}}}{\tilde{\Omega}^2 + \kappa^2}\right) \tag{2.59a}$$

$$\approx \frac{\kappa_{\mathrm{in}}}{\kappa} \frac{4g_0^2 N_{\mathrm{in,-}}}{\tilde{\Omega}^2 + \kappa^2} \quad \text{for } \epsilon_{\mathrm{R}} \ll 1 \tag{2.59b}$$

with the average number of photons in the drive pulse $N_{\mathrm{in,-}}$. For small transfer efficiencies, it scales linearly with the number of photons in the drive pulse and saturates asymptotically to an ideal state transfer of $\epsilon_{\mathrm{R}} \to 1$ for larger numbers. The drop in fidelity per drive photon can be understood by artificially splitting the drive pulse into several smaller pulses. After the first fictitious drive transfers e.g. 50% of the mechanical state, the second drive can only transfer 50% of the remaining state, i.e. 25% of the initial state, leading to an exponential drop in the efficiency of per drive photon. Note that in the case of a sideband resolved cavity, i.e. $\Omega \ll \kappa$ the optical linewidth κ does not change the fidelity ϵ_{R}, but only the relative impedance $\kappa_{\mathrm{in}}/\kappa$. However, the off-resonant intracavity photon number $\langle \hat{c}_{\omega_{\mathrm{L}}}^\dagger \hat{c}_{\omega_{\mathrm{L}}} \rangle \propto \kappa_{\mathrm{in}}$ decreases, thereby reducing the power deposited in the system due to absorption of drive photons in the cavity[41]. Note that the formalism used here assumes weak coupling, i.e. $|g| \ll \kappa$, which sets a limit to the peak power of the drive pulse. While this does not prevent us from asymptotically reaching an ideal state transfer $\epsilon_{\mathrm{R}} \to 1$, it sets a lower limit to the time required to reach a certain fidelity. While the experiments presented in this thesis are well within this regime, strong coupling has been achieved in optomechanical systems [Grö+09; Teu+11b; Ver+12], which allows for an ideal state transfer in finite time.

For a small fidelity $\epsilon_{\mathrm{R}} \ll 1$, every drive photon contributes equally and we can recover the non-linear interaction picture introduced in paragraph 2.1.1. Introducing the single

---

[41] Assuming a fixed absorption rate κ_{abs} as part of the undesired cavity losses κ_{loss}, we find for the deposited energy $E_{\mathrm{abs}} \approx 4\hbar\omega_{\mathrm{L}}\kappa_{\mathrm{abs}}\kappa_{\mathrm{in}}N_{\mathrm{in,-}}/\tilde{\Omega}^2$ using the cavity input output relation (2.12) and the mean cavity field (2.20). In real systems non-linear effects, such as saturation of the absorption centers or two-photon absorption can also play a role.

photon scattering probability

$$p_1 = \frac{\kappa_{\text{in}}}{\kappa} \frac{4g_0^2}{\tilde{\Omega}^2 + \kappa^2} \tag{2.60a}$$

we can approximate the interaction for individual scattering events as[42]

$$|\psi_{\text{opt}}, \psi_{\text{m}}, \psi_{\text{drive}}\rangle_{\text{final}} \sim \left(1 + i\sqrt{p_1}\hat{a}_{\text{out}}^\dagger \hat{a}_{\text{drive}}\hat{m}_{\tilde{\Omega}} + i\sqrt{p_1}\hat{a}_{\text{drive}}^\dagger \hat{m}_{\tilde{\Omega}}^\dagger \hat{a}_{\text{in}}\right)|\psi_{\text{opt}}, \psi_{\text{m}}, \psi_{\text{drive}}\rangle_{\text{initial}} \tag{2.60b}$$

with $\hat{a}_{\text{drive}}$ the annihilation operator of a photon in the drive mode and the wavefunction $|\psi_{\text{opt}}, \psi_{\text{m}}, \psi_{\text{drive}}\rangle$ containing the state of the resonant optical field, mechanical oscillator and the red detuned optical drive mode. This crude approximation (see also figure 2.8) is not intended for calculations, as it does not properly comprise, for example, the effects of a lossy cavity $\kappa_{\text{loss}} \neq 0$ or situations in which multiple scattering events take place. It is rather supposed to guide the intuition for the anti-Stokes process. We find that for the transfer of the mechanical state to the optical mode, a drive photon is upconverted, i.e. it is annihilated by $\hat{a}_{\text{drive}}$ and a higher frequency resonant photon $\hat{a}_{\text{out}}$ is created, while simultaneously annihilating a mechanical phonon. In the scenario of storing an inbound optical state, the resonant photon is downconverted, i.e. it is annihilated by $\hat{a}_{\text{in}}$ and a lower frequency photon is generated by $\hat{a}_{\text{drive}}$, and simultaneously a phonon is created. Both processes can equivalently be enhanced by increasing the number of initial excitations, bearing in mind that the description (2.60b) is based on the assumption that the number of drive photons $\langle \hat{a}_{\text{drive}}^\dagger \hat{a}_{\text{drive}} \rangle = N_{\text{in,-}}$ is much larger than the number of resonant input photons $\langle \hat{a}_{\text{in}}^\dagger \hat{a}_{\text{in}} \rangle$. The systems presented in chapters 4 to 6 typically exhibit a single photon scattering rate of $p_1 \sim 5 \cdot 10^{-8}$. Consequently, to approach a high fidelity state transfer, on the order of $N_{\text{in,-}} \sim 2 \cdot 10^7$ drive photons are necessary.

2.3.3. Stokes Scattering

In the resolved sideband regime, the Stokes scattering term $\hat{\mathcal{H}}_{\text{Stokes}} \propto \hat{c}^\dagger \hat{m}^\dagger + \text{h.c.}$ becomes dominant when tuning the drive laser to the blue side of the optical resonance $\omega_{\text{L}} \approx \omega_c + \Omega$, corresponding to the detuning $\Delta = -\tilde{\Omega}$. In this case, the coupling constant for the Stokes scattering process $\tilde{s}_+ = |g|^2/\kappa$ by far exceeds the one for the anti-Stokes scattering $\tilde{s}_- = |g|^2/(\kappa + 4\tilde{\Omega}^2/\kappa)$. We define the constant

$$\epsilon_{\text{P}} = e^{2|\bar{G}_\pm(T)|} - 1 \tag{2.61}$$

and use it to express equations (2.50) and (2.54) as

$$\hat{m}_{\tilde{\Omega}}(T) = \sqrt{1 + \epsilon_{\text{P}}}\,\hat{m}_{\tilde{\Omega}}(0) + ie^{i\theta}\sqrt{\epsilon_{\text{P}}}\,\hat{a}_{\text{in}}^\dagger \tag{2.62a}$$

$$\hat{a}_{\text{out}} = -ie^{i\theta}\sqrt{\epsilon_{\text{P}}}\,\hat{m}_{\tilde{\Omega}}^\dagger(0) - \sqrt{1 + \epsilon_{\text{P}}}\,\hat{a}_{\text{in}}, \tag{2.62b}$$

---

[42] The unitary evolution operator $\hat{U}$ allows to change from an interaction picture, evolving the wavefunction $|\psi\rangle_f = \hat{U}|\psi\rangle_i$, to the Heisenberg picture, evolving the operator $\hat{o}_f = \hat{U}^\dagger \hat{o}_i \hat{U}$. For the anti-Stokes scattering, $\hat{U} = \exp(i\xi[e^{-i\theta}\hat{m}_{\tilde{\Omega}}^\dagger \hat{a}_{\text{in}} + \text{h.c.}])$ recreates the discrete mode formulation described in eq. (2.58). Here, $\xi = \sin^{-1}(\sqrt{\epsilon_{\text{R}}}) \approx \sqrt{p_1}\sqrt{N_{\text{in,-}}}$ for small ϵ_{R} and the exact pulse shape evolution is hidden in the approximation $\hat{a}_{\text{out}} = -\hat{a}_{\text{in}}$ in the interaction picture. We approximately map this linearized evolution Hamiltonian back to the non-linear case by the replacement $\sqrt{N_{\text{in,-}}}e^{i\theta} \to \hat{a}_{\text{drive}}$ under the assumption of a coherent input state (2.17) $|\psi_{\text{drive}}\rangle = \hat{D}_{\hat{o}_{\text{in}}}(\alpha_0(t)e^{-i\omega_{\text{L}}t})|0\rangle$.

2. Theory of Cavity Optomechanics

with $\theta = \arg(-g_0\alpha_0)$. Note that $\sqrt{1 + \epsilon_P} > 1$ and thus there is always a gain for the mechanical and optical mode. This can be understood by considering that the effective damping (2.29) can become negative for detunings $\Delta < 0$, in particular as we currently neglect the mechanical damping $\Gamma \approx 0$. For this reason, continuous driving under these conditions can easily turn the system unstable and drive it out of the linearized regime into a parametric instability [BSV01; Kip+05]. For a pulsed interaction, ϵ_P is finite and the system can stay linear [Hof+11; Pal+13b]. In this case, the interaction (2.62) constitutes a combined squeezing of the optical and mechanical mode, entangling them with each other. Accessing this type of two mode squeezed entanglement directly requires low noise and a high readout fidelity [Hof+11; Pal+13b]. Tracing over one of the modes, the phase information of the two-mode-squeezed or entangled state is lost and thus the interaction appears like a gain for the individual modes. This can be exploited to generate states by amplified spontaneous emission of photons respectively phonons, also termed phonon lasing [Gru+10; Coh+15]. The optomechanical gain can alternatively be employed to amplify mechanical [Lec+15b] and microwave signals [Mas+11; Nun+14; Mal+18] instead of spontaneous emission. The interaction can also be interpreted as the pairwise creation or annihilation of photons and phonons, as can be seen from the corresponding effective interaction Hamiltonian $\hat{\mathcal{H}}_{\text{eff}} = \hbar g \hat{c}^\dagger \hat{m}^\dagger + \text{h.c.}$[43]. If both the mechanical and optical modes are in their respective ground state, the creation operators in eq. (2.62) will still generate excitations and we find $\langle \hat{m}^\dagger_{\tilde{\Omega}} \hat{m}_{\tilde{\Omega}}(T) \rangle = \langle \hat{a}^\dagger_{\text{out}} \hat{a}_{\text{out}} \rangle = \epsilon_P$. Hence, for small $\epsilon_P \ll 1$ the scattering constant ϵ_P corresponds to the probability of the creation of a photon-phonon pair (see also figure 2.9). As the vacuum-seeded pair creation process is spontaneous and thus random, a small probability $p_1 \approx \epsilon_P \ll 1$ of creating a single pair implies that the creation of multiple pairs is drastically more unlikely, with a probability of approximately $p_2 \approx \epsilon_P^2$. Consequently, the emission of a photon in mode $\hat{a}_{\text{out}}$ heralds the existence of a single phonon stored in the mechanical resonator [HM86; Hon+17].

This type of probabilistic pair creation process also occurs in other systems, such as non-linear crystals [BW70], atomic vapors [Kuz+03] or lattice or molecular vibrations in bulk materials [AS71; LLK72]. It is a standard tool in quantum optics, called spontaneous parametric down conversion, parametric fluorescence or parametric frequency splitting, amongst others. Beyond the creation of high-quality single-excitation Fock states [HM86], this process is used for example in non-linear crystals to generate complex entangled states involving multiple excitations [Wal+04b; Wal+05; Giu+15].

For an optomechanical system with the drive laser tuned to $\Delta = -\tilde{\Omega}$ on the blue side of the cavity, i.e. the Stokes scattered field being resonant with the optical cavity, we find

---

[43] Alternatively we can go from the Heisenberg picture, where the operator evolves with the time, with the final operator $\hat{o}_f = \hat{U}^\dagger \hat{o}_i \hat{U}$ being a unitary transformation of the initial operator, to an interaction picture, where the wavefunction evolves with this unitary transformation $|\psi\rangle_f = \hat{U} |\psi\rangle_i$ from its initial to final state. For (2.62), we find that the transformation

$$\hat{U} = \exp\left(ir\left[e^{i\theta}\hat{a}^\dagger_{\text{in}}\hat{m}^\dagger_{\tilde{\Omega}} + \text{h.c.}\right]\right) \qquad \text{with } r = \sinh^{-1}(\sqrt{\epsilon_P})$$

approximately generates the desired behavior, where we exploit the equality also used in [12]. Note that here we approximated $\hat{a}_{\text{out}}(T) \approx -\hat{a}_{\text{in}}(T)$, neglecting the deformation of the envelope by the interaction.
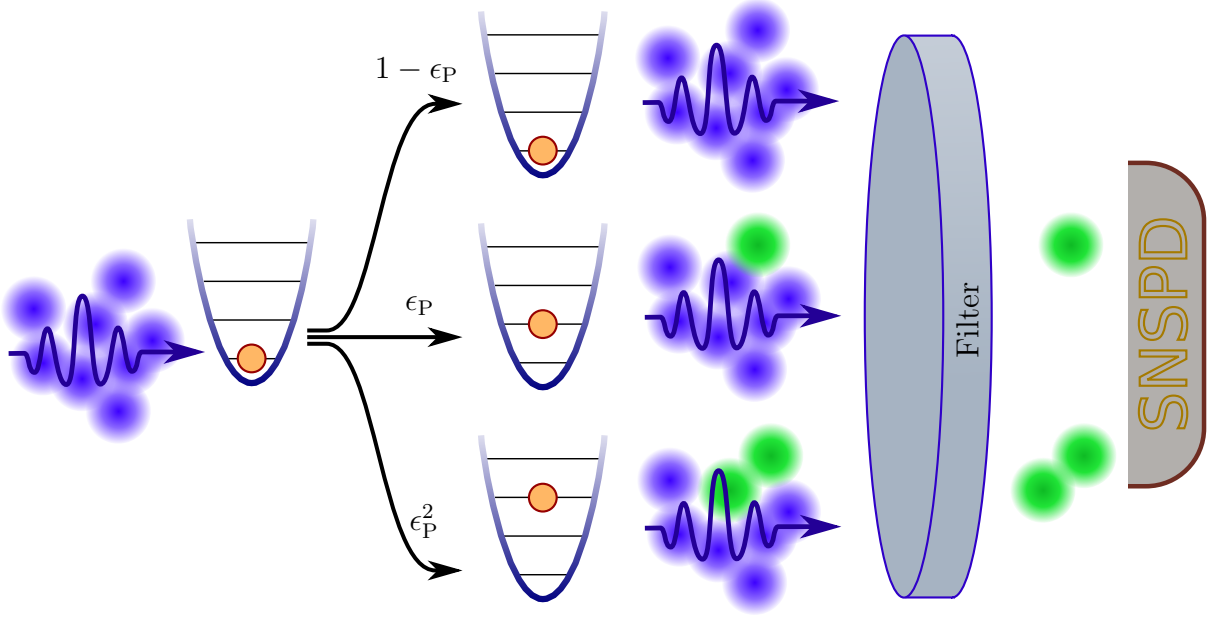
FIGURE 2.9.: **Optomechanical Down Conversion.** The Stokes interaction leads to a correlated amplification of the input states, as in an optical parametric amplifier. This also holds if the optical and mechanical mode initially are in their groundstate: A high energy drive photon (blue dots) is down converted to a resonant signal photon (green dots) and an idler phonon (orange dots). For low probabilities $\epsilon_P \ll 1$ of this spontaneous down conversion, multiple scattering events are highly unlikely ($\sim \epsilon_P^2$). Thus, the detection of a signal photon, e.g. with a superconducting nanowire single photon detector (SNSPD) heralds the presence of a single idler phonon.

by employing (2.51) the Stokes scattering constant

$$\epsilon_P = \exp\left(\frac{\kappa_{\mathrm{in}}}{\kappa} \frac{4g_0^2 N_{\mathrm{in},+}}{\tilde{\Omega}^2 + \kappa^2}\right) - 1 \tag{2.63a}$$

$$\approx \frac{\kappa_{\mathrm{in}}}{\kappa} \frac{4g_0^2 N_{\mathrm{in},+}}{\tilde{\Omega}^2 + \kappa^2} \quad \text{for } \epsilon_P \ll 1. \tag{2.63b}$$

The exponential scaling of ϵ_P with the number of photons in the drive pulse $N_{\mathrm{in},+}$ in eq. (2.63a) corresponds to the amplification of the spontaneous pair creation, as mentioned above. For low pump strengths, this amplification does not play a significant role and the pair creation probability (2.63b) is approximately linear in the number of pump photons. In this regime, we can again recover the interaction picture of the non-linear dynamics. In this case the interaction changes the initial wavefunction by the transformation[44]

$$|\psi_{\mathrm{opt}}, \psi_{\mathrm{m}}, \psi_{\mathrm{drive}}\rangle_{\mathrm{final}} \propto \left(1 + i\sqrt{p_1}\,\hat{a}_{\mathrm{in}}^\dagger \hat{m}_{\tilde{\Omega}}^\dagger \hat{a}_{\mathrm{drive}} + i\sqrt{p_1}\,\hat{a}_{\mathrm{drive}}^\dagger \hat{a}_{\mathrm{out}} \hat{m}_{\tilde{\Omega}}\right)|\psi_{\mathrm{opt}}, \psi_{\mathrm{m}}, \psi_{\mathrm{drive}}\rangle_{\mathrm{initial}} \tag{2.64a}$$

$$p_1 = \frac{\kappa_{\mathrm{in}}}{\kappa} \frac{4g_0^2}{\tilde{\Omega}^2 + \kappa^2} \tag{2.64b}$$

---

[44] As in paragraph 2.3.2, we use the evolution operator described in [43] to approximately map the linearized problem back to the non-linear process described in paragraph 2.1.1, by replacing $\sqrt{N_{\mathrm{in},+}}e^{i\theta} \rightarrow \hat{a}_{\mathrm{drive}}$.

where p_1 stands for the scattering probability of each drive photon[45] (see also figure 2.10). Note that as in the case of anti-Stokes scattering in paragraph 2.3.2, this approximation is mainly intended to guide the intuition of the process, as it does not properly capture losses and finite coupling of the drive photons to the cavity. We find that for the photon-phonon pair creation, an off-resonant, high frequency drive photon is annihilated by $\hat{a}_{\text{drive}}$ and a low frequency, resonant photon is created by $\hat{a}_{\text{out}}^{\dagger}$ along with a mechanical phonon $\hat{m}_{\tilde{\Omega}}$. In the Hermitian conjugate process, a resonant photon and a phonon both annihilate to add a photon to the drive beam. Both processes can be enhanced by increasing the number of excitations, bearing in mind the assumption made in the approximation (2.64a), that the number of drive photons $\langle \hat{a}_{\text{drive}}^{\dagger} \hat{a}_{\text{drive}} \rangle = N_{\text{in},+}$ greatly exceeds the number of photons on resonance $\langle \hat{a}_{\text{in}}^{\dagger} \hat{a}_{\text{in}} \rangle$. In the optomechanical crystals used in chapters 4 to 6 the single photon Stokes scattering rate is $p_1 \sim 5 \cdot 10^{-8}$. Hence, using approximately $N_{\text{in},+} \sim 2 \cdot 10^5$ drive photons results in a probability of about $\epsilon_{\text{P}} \sim 1\%$ of a single pair creation event per pulse, keeping the probability of generating multiple pairs negligible.
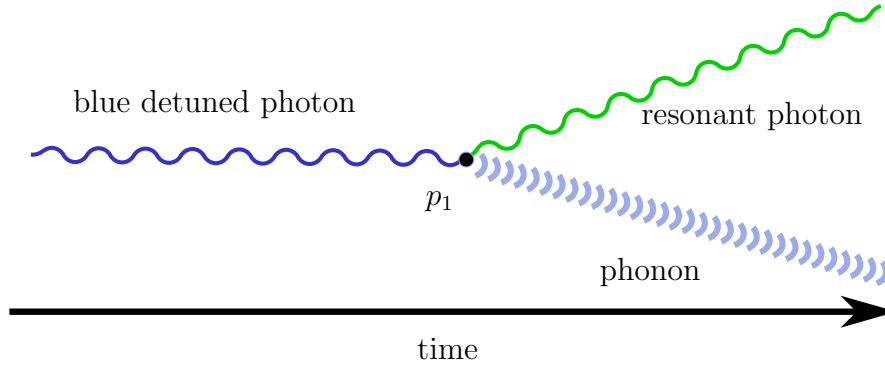
FIGURE 2.10.: **Stokes Scattering.** A blue detuned drive photon (dark blue) decays into a resonant photon (green) and a phonon (light blue). The probability of this process for each drive photon is $p_1 \sim 5 \cdot 10^{-8}$ for the parameters given in table 2.1.

2.3.4. Combined Scattering Processes

In the previous paragraphs, we treated each interaction term independently. While this is a good approximation for many experimental protocols in the resolved sideband regime, there will always be a residual contribution by all types of interactions, Stokes and anti-Stokes scattering, as well as mechanical decay. Here, we will treat the previously ignored interaction terms as small perturbations to the dominant term, in order to estimate the magnitude and scaling of their influence. First, I will treat the influence of the mechanical decay during the protocol, followed by the influence of the simultaneous Stokes and anti-Stokes scattering.

The mechanical oscillator is coupled to the thermal environment, allowing excitations to escape the resonator and thermal phonons to enter it. This coupling $\tilde{s}_- = \Gamma/2$ is usually constant over time, such that we cannot define a single input or output mode by

---

[45]As in the previous paragraph, $\hat{a}_{\text{drive}}$ is the annihilation operator of a photon in the drive mode and the wavefunction $|\psi_{\text{opt}}, \psi_{\text{mech}}, \psi_{\text{drive}}\rangle$ contains the state of the resonant optical field, mechanical oscillator and the blue detuned optical drive mode.

an envelope with a finite localization in the time domain, as we did in paragraph 2.3.1 for the optical baths (2.49) and (2.53). However, as we are not primarily interested in the pulse shape of the phonon emitted into the environment, but rather in the phonon loss during the dominant optical interaction, it is a good approximation to consider the mechanical coupling constant during the interaction for a characteristic time τ_{eff} and zero outside of this time window. The proper choice of this characteristic time depends on the exact goal of the calculation[46], but is typically between the full width half maximum of the optical pulse envelope $\tau_{\mathrm{FWHM}} \leq \tau_{\mathrm{eff}}$ and the total pulse length $T \geq \tau_{\mathrm{eff}}$. For a more precise computation of the influence of the mechanical environment, a master equation in the Lindblad form can be used, as detailed in section 5.3. In analogy to the anti-Stokes process for small fidelities (2.59b), we find the fidelity of a state transfer with the thermal environment

$$\epsilon_{\mathrm{R}}^{\mathrm{mech}} \approx \Gamma \tau_{\mathrm{eff}}. \tag{2.65}$$

Consequently, during the pulsed optical interaction, a thermal environment with average occupation number n_{th} adds $\epsilon_{\mathrm{R}}^{\mathrm{mech}} n_{\mathrm{th}}$ phonons to the system. A state transfer by Stokes scattering will asymptotically be limited to $1 - \epsilon_{\mathrm{R}}^{\mathrm{mech}}$, also for large numbers of drive photons. Hence, it is advantageous to use short drive pulses, theoretically limited by the condition of adiabaticity and weak coupling[47]. Practically, the pulse length T or τ_{FWHM} is effectively limited by the bandwidth of the drive rejection filters, as discussed in paragraph 2.4.2.

In addition to mechanical losses and heating by the thermal environment, there is also a secondary optical scattering term. In the resolved sideband regime, this term is off-resonant, i.e. the scattered photons are not close to the optical resonance, and it is therefore much weaker than the dominant, resonant scattering term. We will first look at the example of an off-resonant Stokes term, which causes heating during a resonant, anti-Stokes based state transfer, as described in paragraph 2.3.2. For a single adiabatic drive beam, we found in paragraph 2.3.1 that the optical baths for Stokes-process and the anti-Stokes process are orthogonal modes, as they are separated in frequency. We thus treat both processes independently[48] and find for the Stokes pair creation probability

$$\epsilon_{\mathrm{P}}^{\mathrm{red}} = \frac{\kappa_{\mathrm{in}}\kappa}{\kappa^2 + 4\tilde{\Omega}^2} \frac{4g_0^2 N_{\mathrm{in,-}}}{\tilde{\Omega}^2 + \kappa^2} \tag{2.66a}$$

$$\approx \frac{1}{1 + 4\tilde{\Omega}^2/\kappa^2} \epsilon_{\mathrm{R}} \quad \text{for } \epsilon_{\mathrm{R}} \ll 1. \tag{2.66b}$$

For small transfer fidelities ϵ_{R}, the sideband resolution $\tilde{\Omega}/\kappa$ determines the optomechanical heating induced by the anti-Stokes drive pulse. For the devices used in chapters 4 to 6,

---

[46] A proper effective time will be slightly different when estimating e.g. the influx of phonons from the thermal bath during a Stokes scattering based pair creation process or the reduction of state transfer fidelity in a anti Stokes scattering based state transfer.

[47] This limit is only with regard to the presented anti-Stokes state transfer. Of course, high fidelity state transfer can also be achieved in the strong coupling regime, using a Rabi oscillations between the mechanical and optical mode.

[48] Scattering from the drive pulse into the optomechanical sidebands is independent, which is the case described here. When there are initially coherent excitations in both of the sidebands, interference can occur when they are scattered onto the drive frequency, and thus care must be taken when considering this specific example, which is, however, beyond the scope of this work.

the Stokes scattering probability $\epsilon_P^{\mathrm{red}} \sim 2 \cdot 10^{-3} \epsilon_R$ is significantly smaller than the desired anti-Stokes probability, and for a typical fidelity of $\epsilon_R \sim 10\%$ leads to a heating by $\sim 2 \cdot 10^{-4}$ phonons. As the heating only occurs during the optomechanical interaction, approximately $\epsilon_R^2/(1 + 4\tilde{\Omega}^2/\kappa^2)/2$ photons are added to the anti-Stokes sideband. Note that these additional resonant photons correspond to a transferred phonon created by a Stokes scattering event, before being transferred to the optical domain. Hence, they are highly correlated with the corresponding Stokes photons at the off-resonant optical frequency $\omega_L - 2\tilde{\Omega}$. While this contribution is negligible in the off-resonant driving schemes applied in chapters 4 to 6, the residual Stokes interaction of an anti-Stokes state transfer is exploited for example in references [Vit+07; BNG11] and [Kas+15; Kas+16][49].

When driving the Stokes transition, i.e. $\Delta = \tilde{\Omega}$ as described in paragraph 2.3.3, the off-resonant anti-Stokes fidelity is $\epsilon_R^{\mathrm{blue}} = \epsilon_P/(1 + 4\tilde{\Omega}^2/\kappa^2)$ for a small Stokes pair creation probability $\epsilon_P \ll 1$. It thus scales in the same way with the sideband resolution as in the previous example. Consequently, in both cases, the only way to reduce the secondary optical scattering terms is to increase the sideband resolution $\tilde{\Omega}/\kappa$, which in most cases is limited by the unintentional losses of the cavity. Note that while a Stokes scattering event can happen spontaneously, the anti-Stokes transition requires an input in the optical anti-Stokes sideband or the mechanical resonator. The anti-Stokes scattering can thus be suppressed if all input modes, except for the drive, initially are in their respective ground state. Hence, photon-phonon pairs can be created also in the unresolved sideband regime, as long as the mechanical resonator was previously cooled to the ground state. For the creation of photon-phonon pairs by Stokes scattering, the undesired anti-Stokes transition mainly represents a loss channel for the thereby created phonons. As this loss scales with the pair creation probability ϵ_P, keeping the latter small reduces this effect. For sideband resolved systems, $\epsilon_R \ll \epsilon_P$ and therefore the quality of the photon-phonon pairs will always be limited by the emission of multiple pairs, see also chapter 4.

When the system is driven by multiple lasers, in particular when some of the optomechanical sidebands are close in frequency, these sidebands can interact and non-trivial effects can occur [Qiu+18]. In particular, when the system is driven at $\Delta = \pm\tilde{\Omega}$ simultaneously, the interference between Stokes transition of the blue drive and the anti-Stokes transition of the red drive represents an engineered bath which can lead to squeezing of the mechanical state [BVT80; Cir+93; CMJ08; Suh+14; Wol+15; Pir+15; Lec+15a].

2.3.5. Phase Control

So far, we focused on the discussion of the addition and subtraction of phonons by means of Stokes and anti-Stokes transitions. Complementary to this optical control of the amplitude of the mechanical motion, the drive laser also influences the phase of the mechanical resonator. The dynamical backaction of the optomechanical interaction modifies the mechanical resonance frequency from the natural frequency Ω to the effective frequency $\tilde{\Omega} = \Omega + \delta\Omega$. As the interaction, and therefore the frequency shift is finite in time, this results in a finite accumulated phase $\delta\Phi = \int\mathrm{d}t\,\delta\Omega(t)$ during the interaction.

---

[49] In other experiments with optical phonons [Lee+11; Lee+12], distinct read and write pulses are used in order to obtain temporal resolution.

Using the expression for the optical spring (2.28), we obtain a phase shift

$$\delta\Phi = 2g_0^2 \Delta \frac{\tilde{\Omega}^2 - \Delta^2 - \kappa^2}{(\tilde{\Omega}^2 + \Delta^2 + \kappa^2)^2 - 4\Delta^2\tilde{\Omega}^2} \frac{2\kappa_{\text{in}}}{\Delta^2 + \kappa^2} \underbrace{\int_0^T dt \, |\alpha_0(t)|^2}_{=N_{\text{in},\pm}}, \qquad (2.67)$$

which the mechanical mode accumulates relative to the evolution with its natural frequency Ω. This expression is not easily accessible by intuition in its general form, as it contains higher order polynomials in its numerator and denominator. We can see for example, that the phase shift can become zero for various detunings ($\Delta = 0, \pm\sqrt{\tilde{\Omega}^2 - \kappa^2}$) in the resolved sideband regime. Moreover, the expression implicitly still depends on the mechanical frequency modified by the optical spring $\tilde{\Omega}$. We will therefore restrict the discussion to some cases relevant for the optical control of the mechanical quantum state.

The main focus of this thesis lies on off-resonant drives in the resolved sideband regime with weak optomechanical coupling ($\tilde{\Omega} > \kappa > g$). In this limit, the frequency shift $\delta\Omega$ is small compared to the natural frequency Ω, i.e. we can set $\tilde{\Omega} \approx \Omega$ in equation (2.67), rendering the expression explicit. As a drive laser will always induce Stokes and anti-Stokes scattering, it is of interest how the phase shift relates to the scattering probability. Note that the phase shift $\delta\Phi \propto g_0^2 N_{\text{in},\pm}$ is proportional to the squared single photon coupling strength and the number of drive photons, just as the scattering cross sections ϵ_{P} and ϵ_{R} in the limit of a weak drive. It is thus instructive to compare the phase shift with the cumulative coupling

$$\frac{\delta\Phi}{2|\tilde{G}_\pm(T)|} = \frac{\Delta}{\kappa} \frac{\left(\tilde{\Omega}^2 - \Delta^2 - \kappa^2\right)\left((\Delta \pm \tilde{\Omega})^2 + \kappa^2\right)}{(\tilde{\Omega}^2 + \Delta^2 + \kappa^2)^2 - 4\Delta^2\tilde{\Omega}^2} \qquad (2.68a)$$

$$= \pm\frac{\kappa\tilde{\Omega}}{\kappa^2 + 4\tilde{\Omega}^2} \qquad \text{for } \Delta = \mp\tilde{\Omega}. \qquad (2.68b)$$

For protocols in which one sideband is resonant (2.68b), i.e. selective Stokes or anti-Stokes scattering, we thus find that the phase shift is weak compared to the pair creation probability, respectively state transfer fidelity, with $\delta\Phi/|2\tilde{G}_\pm(T)| \approx \kappa/(4\tilde{\Omega}) \ll 1$. For the systems described in chapters 4 to 6, a state transfer fidelity of $\epsilon_{\text{R}} = 10\%$ typically would lead to a negligible phase shift of $-\delta\Phi \approx 5 \cdot 10^{-3} = 0.3°$. Thus, sideband scattering protocols result in almost pure amplitude control of the mechanical state, justifying that phaseshifts by the interaction are typically neglected (see also figure 2.4 on page 20).

In order to achieve predominant phase control, other detuning regimes need to be considered. In the resolved sideband regime, the relative phase shift for very small or very large detunings $|\Delta|$ is

$$\frac{\delta\Phi}{2|\tilde{G}_\pm(T)|} \approx +\frac{\Delta}{\kappa} \qquad \text{for } |\Delta| \ll \tilde{\Omega} \qquad (2.69a)$$

$$\approx -\frac{\Delta}{\kappa} \qquad \text{for } |\Delta| \gg \tilde{\Omega}. \qquad (2.69b)$$

Efficient phase control with small detunings sets strict requirements for the sideband resolution, as it requires $\tilde{\Omega} \gg |\Delta| \gg \kappa$. For large detuning, efficient phase control is also possible for moderate sideband resolution, but requires large drive powers, as the

cavity is driven far off resonance. In both cases, the optical control of the phase requires a significant amount of intracavity photons and can thus generate undesired side effects such as absorption heating[50]. Consequently, while in principle this optomechanical analogue to the AC Stark shift allows for phase control over the mechanical mode, in absorption limited systems other solutions are preferable. For example, in chapter 6 the phase of the mechanical state is altered during the transfer to the optical domain through the phase of the optical drive pulse.

2.4. Basic Protocols

In the previous section, we investigated the interaction between the optical and the mechanical mode driven by a quasi-continuous control pulse. It was followed by a description of the possibilities and limitations of pulsed optical control of mechanical motion in the quantum regime. In this section, we specify some basic protocols that allow to characterize the optomechanical state.

First, we will describe a method to measure the effective mode temperature of the mechanical oscillator, exploiting the asymmetry in the scattering rate of the Stokes and anti-Stokes transition for low phonon numbers in paragraph 2.4.1. Thereafter, we turn to the correlation between the optical and the mechanical state, describing in paragraph 2.4.2 how to measure the second order coherence between the two modes, also called normalized cross-correlations.

Finally, we will investigate a non-adiabatic protocol, briefly discussing the possibilities and limitations of instantaneous, stroboscopic position measurements to achieve quantum non-demolition measurements of a mechanical quadrature.

2.4.1. Sideband Asymmetry Thermometry

The effective temperature of the mechanical oscillator, or more precisely its mean occupation number $\bar{n} = \langle \hat{m}^\dagger \hat{m} \rangle$ is an important characteristic of the mechanical state. It quantifies how well the resonator is thermalized, either to its mechanical environment or the effective bath of a sideband cooling laser. In many quantum applications, $\bar{n}$ relates to the noise added to a pure quantum state in an operation involving the mechanical oscillator, possibly masking its quantum properties such as entanglement or squeezing.

As we saw in paragraph 2.3.2, the optomechanical sideband created by anti-Stokes scattering is a (usually incomplete) mapping of the mechanical state, and hence its intensity is proportional to the mean occupation number $\bar{n}$. Consequently, an intensity measurement of this sideband can be converted to $\bar{n}$, given that a proper normalization of the anti-Stokes sideband is available. This can for example be a measurement at a known mode temperature [Teu+11a], e.g. room temperature, or a complete and independent characterization of all system parameters, primarily the linearized coupling strength g and the

---

[50] The efficiency of the phase shift $\delta\Phi$ with respect to the deposited energy E_{abs} by absorption of drive photons, see also [41], scales with $\delta\Phi/E_{\mathrm{abs}} \propto \Delta/\tilde{\Omega}^2$ for small detunings and $\propto 1/\Delta$ for large detunings. When quantifying the condition of small detuning as $|\Delta| = \tilde{\Omega}/k$ and large detuning as $|\Delta| = \tilde{\Omega} \cdot k$, with $k \gg 1$, both cases become $\delta\Phi/E_{\mathrm{abs}} \propto 1/(k\tilde{\Omega})$. Hence, they are similarly vulnerable to absorbtion heating, and the choice of protocol will likely depend on the available sideband resolution and laser power.

losses in the optical path [Cha+11a]. Oftentimes, those two options are not possible, for example when operating the experiment at cryogenic temperatures and not all system parameters are accessible. When operating close to the mechanical ground state, luckily, a new possibility arises, namely normalizing the anti-Stokes by the Stokes sideband intensity [Die+89; Saf+12; Wei+14].

We consider quasi-continous control pulses, as described in section 2.3, driving a Stokes transition with scattering probability ϵ_{P} and an anti-Stokes transition with a transfer fidelity ϵ_{R}. The control pulses are weak and of the same strength, such that $\epsilon_{\mathrm{P}} = \epsilon_{\mathrm{R}} \ll 1$. This can for example be achieved with a single drive pulse on resonance ($\Delta = 0$) or with two independent drive pulses with opposite detuning on the blue and red side. In the resolved sideband regime, the latter configuration (with $\Delta = \pm\Omega$) is preferable, as it minimizes the residual heating due to absorption of drive photons.

We now define the optical mode of the detection channel

$$\hat{d}_{\mathrm{w(r)}} = \sqrt{\eta_{\mathrm{d}}}\hat{a}_{\mathrm{out}}^{w(r)} + \sqrt{1 - \eta_{\mathrm{d}}}\hat{l} \tag{2.70}$$

for the Stokes (anti-Stokes) sideband $\hat{a}_{\mathrm{out}}^w$ ($\hat{a}_{\mathrm{out}}^r$) emitted from the cavity, as described by eq. (2.62) (respectively (2.58)). We model the absolute quantum efficiency η_{d} of the detection, which is the same for both channels, by a directional coupling to an auxiliary input mode $\hat{l}$ which is in the ground state [Yur85; Sha85]. Further assuming the input mode $\hat{a}_{\mathrm{in}}$ of the optical sidebands to be in the vacuum state, we find with eq. (2.62) and (2.58)

$$\langle \hat{d}_{\mathrm{w}}^\dagger \hat{d}_{\mathrm{w}} \rangle = \eta_{\mathrm{d}}\epsilon_{\mathrm{R}} \, \langle \hat{m}\hat{m}^\dagger \rangle = \eta_{\mathrm{d}}\epsilon_{\mathrm{R}}\langle \hat{m}^\dagger \hat{m} + 1 \rangle \tag{2.71a}$$

$$\langle \hat{d}_{\mathrm{r}}^\dagger \hat{d}_{\mathrm{r}} \rangle = \eta_{\mathrm{d}}\epsilon_{\mathrm{R}} \, \langle \hat{m}^\dagger \hat{m} \rangle. \tag{2.71b}$$

Here, all mechanical operators are evaluated before the interaction $\hat{m} = \hat{m}(0)$. For the anti-Stokes transition (2.71b), we find the expected proportionality of the number of photons in the sideband to the number of phonons in the mechanical oscillator. For the Stokes transition (2.71a), the inverted order of the mechanical operators results in an offset given by the commutation relation of the ladder operators, see also [3], equivalent to exactly one phonon. We can thus use this natural scale bar to normalize the anti-Stokes scattering rate and obtain the mean phonon number

$$\bar{n} = \frac{\left\langle \hat{d}_{\mathrm{r}}^\dagger \hat{d}_{\mathrm{r}} \right\rangle}{\left\langle \hat{d}_{\mathrm{w}}^\dagger \hat{d}_{\mathrm{w}} \right\rangle - \left\langle \hat{d}_{\mathrm{r}}^\dagger \hat{d}_{\mathrm{r}} \right\rangle}. \tag{2.72}$$

As this natural scale bar given by the asymmetry in the scattering rates is equivalent to a single phonon, this method is most reliable for small mean occupation numbers $\bar{n} \lesssim 1$. While in principle it also works for larger $\bar{n}$, in this case a good relative precision is necessary, as single phonon resolution is required.

Note that this thermometry technique relies on several assumptions, which should be checked to verify that the result is reliable. For a single, resonant drive, the detection efficiency η_{d} of both sidebands needs to be the same, despite them being at different absolute frequencies. In the case of two independent drives, the scattered photons are at the same frequency ω_c, however, the average photon number in both of them needs to be

identical in order to ensure that both scattering parameters $\epsilon_P = \epsilon_R$ are the same, see (2.59b), (2.63b). Furthermore, the optical input modes need to be in the vacuum state, as photons originating from residual laser noise can corrupt the measurement [KSG13; Saf+13b].

Furthermore, for low phonon numbers $\bar{n} \ll 1$, the measurement of background photons can modify the apparent sideband intensity. For example, when using single photon detectors, it is necessary to filter out the drive pulses (see also paragraph 2.4.2), as the detectors cannot distinguish the drive from the signal photons. Realistic filters only have a finite suppression η_{leak} at the drive frequency, such that in addition to the optomechanical sideband signal, the detectors also register leaked drive photons, for example $\langle \hat{d}_r^\dagger \hat{d}_r \rangle = \eta_d \epsilon_R \, \langle \hat{m}^\dagger \hat{m} \rangle + \eta_{\text{leak}} \langle \hat{a}_{\text{drive}}^\dagger \hat{a}_{\text{drive}} \rangle$. This can be characterized and subratcted, e.g. by an offresonant measurement $\langle \hat{d}_o^\dagger \hat{d}_o \rangle = \eta_{\text{leak}} \langle \hat{a}_{\text{drive}}^\dagger \hat{a}_{\text{drive}} \rangle$ suppressing the optomechanical sideband. Hence, an accurate estimate for the true mean phonon occupation number is

$$\bar{n} = \frac{\left\langle \hat{d}_r^\dagger \hat{d}_r \right\rangle - \left\langle \hat{d}_o^\dagger \hat{d}_o \right\rangle}{\left\langle \hat{d}_w^\dagger \hat{d}_w \right\rangle - \left\langle \hat{d}_r^\dagger \hat{d}_r \right\rangle}. \tag{2.73}$$

This method can of course be refined by taking separate leak measurements for both sidebands, in order to also compensate dispersion in the optical filtering setup [Rie+16; Hon+17].

2.4.2. Second Order Coherence

Many quantum properties constitute themselves in correlations between different observables of a system. For example, Heisenberg's uncertainty relation predicts a correlation between the variances of orthonormal quadratures such as momentum and position, and quantum entanglement describes correlations between two systems which are stronger than classically possible, thereby rendering the description of the states inseparable.

Here we discuss a specific type of correlation measurement, which is very useful for the characterization of the interaction in an optomechanical system. The normalized intensity cross-correlation, also called second order coherence, describes the intensity-intensity correlations between two modes, represented by their annihilation operators $\hat{a}$ and $\hat{b}$, normalized to the average intensity of each mode [Gla63b]. It is defined as

$$g_{ab}^{(2)}(\tau) = \frac{\langle :\hat{a}^\dagger(t)\hat{a}(t)\hat{b}^\dagger(t+\tau)\hat{b}(t+\tau): \rangle}{\langle \hat{a}^\dagger(t)\hat{a}(t) \rangle \langle \hat{b}^\dagger(t+\tau)\hat{b}(t+\tau) \rangle}, \tag{2.74}$$

with $:\hat{O}:$ standing for normal ordering of operator $\hat{O}$[51]. Due to its normalization, this quantity is invariant under losses in the detection path, and therefore is convenient for experiments with small detection efficiency. For classical fields, the Cauchy–Schwarz inequality sets an upper limit to the cross-correlation [Cla74; MW95; Kuz+03]. A violation of this bound thus offers a simple possibility to identify if the system operates in the quantum regime. Due to this property, the cross-correlation also serves as a benchmark

---

[51] Normal ordering $:\hat{O}:$ of an operator $\hat{O}$ relates to expressing the operator in terms of annihilation and creation operators, e.g. $\hat{O} = \hat{a}\hat{b}^\dagger\hat{c} + \hat{d}\hat{e}^\dagger$, and sorting it such that all creation operators are on the right side, and annihilation operators are on the left side, i.e. in this case $:\hat{O}:= \hat{b}^\dagger\hat{a}\hat{c} + \hat{e}^\dagger\hat{d}$.

for various quantum information protocols. In many cases, a condition for the feasibility of a protocol can be formulated in terms of a minimum value of the cross-correlation.

In the following, we will address each of these points, first describing a typical measurement protocol, then explaining the loss tolerance and giving an intuition for the classicality bound. Finally, we review the properties of the normalized cross-correlation in the optomechanical context, as well as the technical requirements for the measurement. Note that chapter 4 describes the experimental work on optomechanical cross-correlations, and contains complementary information on the topic.

Measurement Protocol

As we saw in paragraph 2.3.3, driving the optomechanical Stokes transition should lead to the correlated creation of resonant photons and phonons. To characterize this interaction, we measure the cross-correlation $g_{om}^{(2)}$ between the optical mode containing the Stokes scattered photons and the mechanical mode. While we have direct access to the emitted photon, we first need to transfer the mechanical state to the optical domain in order to measure its intensity, which we achieve by driving the anti-Stokes transition, see also paragraph 2.3.2. Here, we consider a sideband resolved cavity, such that we can selectively drive the Stokes and anti-Stokes transition, with the mechanical oscillator close to, and the optical sideband input in their respective ground state. As detectors, we will assume single photon detectors, though this is not strictly necessary [BNG11].

We first send a blue detuned drive pulse at $\Delta = -\tilde{\Omega}$ with a scattering constant ϵ_P, called "write pulse". After a short period τ, we swap the mechanical state onto the optical mode, using a red detuned drive at $\Delta = +\tilde{\Omega}$ with scattering constant ϵ_R, called "read pulse". Both scattered fields, the Stokes sideband $\hat{a}_{\text{out}}^w$ and the anti-Stokes sideband $\hat{a}_{\text{out}}^r$ have the same carrier frequency ω_c and will thus experience the same loss $1 - \eta_d$ on their path to the detector. Modeling the loss as described in eq. (2.70), we find the total detection quantum efficiency for the Stokes scattered photons to be $\eta_d = \eta_{\text{qe}} \eta_{\text{path}} \kappa_{\text{in}}/\kappa$, with the quantum efficiency η_{qe} of the detector, η_{path} the transmission of the optical path from the device to the detector, and $\kappa_{\text{in}}/\kappa$ the loss due to the cavity impedance. For the mechanical mode, we also need to take into account the finite state transfer fidelity ϵ_R, yielding the detection efficiency $\eta_r = \eta_d \epsilon_R$ of the mechanical mode $\hat{m}$.

We can thus write the annihilation operator of the detection mode for the write pulse $\hat{d}_w = \sqrt{\eta_d}\hat{a}_{\text{out}}^w + \sqrt{1 - \eta_d}\hat{l}_w$ and for the read pulse $\hat{d}_r = \sqrt{\eta_r}\hat{m} + \sqrt{1 - \eta_r}\hat{l}_r$, with the effective loss mode $\hat{l}_r \propto \sqrt{\eta_d(1 - \epsilon_R)}\hat{a}_{\text{in}}^r + \sqrt{1 - \eta_d}\hat{l}_d$. The loss modes $\hat{l}_w$, $\hat{l}_r$, and $\hat{l}_d$ are vacuum ports, see also eq. (2.70). As the mode envelopes of $\hat{l}_w$ and $\hat{l}_d$ are defined at distinct times, $\hat{l}_w$ and $\hat{l}_r$ can be considered orthogonal. Consequently, we find in analogy to (2.71b) that the cross-correlation between the two detection channels

$$g_{d_w d_r}^{(2)} = \frac{\langle \eta_d \eta_r : \hat{a}_{\text{out}}^{w\dagger} \hat{a}_{\text{out}}^w \hat{m}^\dagger \hat{m} : \rangle}{\langle \eta_d \ \hat{a}_{\text{out}}^{w\dagger} \hat{a}_{\text{out}}^w \rangle \langle \eta_r \ \hat{m}^\dagger \hat{m} \rangle} = g_{om}^{(2)} \tag{2.75}$$

is equivalent to the cross-correlation between the photon mode and phonon mode of the Stokes scattering process. Hence, we see that detection losses do not modify the cross-correlation, allowing e.g. for measurements with low optomechanical state transfer fidelity.

Note that in a realistic experiment, the detectors will also detect signals which do not originate from the scattering process, but for example relate to photons of the drive

pulse, leaked through the filter setup. In order to understand the effect of these false positive detection events, we reformulate the definition (2.74) of the cross-correlation by introducing the notion of heralded states. The heralded state of the mechanical oscillator, represented by the statistical operator $\hat{\rho}_{\mathrm{m,her}}$, e.g. after a Stokes scattering process, is obtained by conditioning the state on a detection event in the optical mode. The state therefore can be expressed as $\hat{\rho}_{\mathrm{m,her}} = \mathrm{Tr}_{d_{\mathrm{w}}}(\hat{d}_w^\dagger \hat{d}_w \hat{\rho}_w)/\mathrm{Tr}(\hat{d}_w^\dagger \hat{d}_w \hat{\rho}_w)$ with the statistical operator of optomechanical state $\hat{\rho}_w$ after the write pulse. The index in $\mathrm{Tr}_{d_{\mathrm{w}}}(\,\cdot\,)$ indicates that the trace is only taken over the optical part, here the detection channel associated with $\hat{d}_w$, in contrast to $\mathrm{Tr}(\,\cdot\,)$ tracing over all systems. Consequently, $\hat{\rho}_{\mathrm{m,her}}$ is properly normalized, such that we can deduce

$$g_{d_{\mathrm{w}}d_{\mathrm{r}}}^{(2)} = \frac{\mathrm{Tr}\left(\hat{d}_r^\dagger \hat{d}_r \hat{\rho}_{\mathrm{m,her}}\right)}{\mathrm{Tr}\left(\hat{d}_r^\dagger \hat{d}_r \hat{\rho}_w\right)} = \frac{\langle \hat{d}_r^\dagger \hat{d}_r \rangle_{\mathrm{heralded}}}{\langle \hat{d}_r^\dagger \hat{d}_r \rangle_{\mathrm{unheralded}}} \tag{2.76a}$$

$$\approx \frac{\langle \hat{m}^\dagger \hat{m} \rangle_{\mathrm{heralded}}}{\langle \hat{m}^\dagger \hat{m} \rangle_{\mathrm{unheralded}}} \approx g_{om}^{(2)}, \tag{2.76b}$$

i.e. that the cross-correlation describes the ratio of the expectation value of excitations in the conditional state versus excitations in the unconditional state. Uncorrelated false positive counts thus add a constant offset $\langle \hat{d}_r^\dagger \hat{d}_r \rangle \propto \langle \hat{m}^\dagger \hat{m} \rangle + \mathrm{const.}$ to the numerator and denominator, regressing $g_{d_{\mathrm{w}}d_{\mathrm{r}}}^{(2)}$ towards 1. Consequently, the measured $g_{d_{\mathrm{w}}d_{\mathrm{r}}}^{(2)}$ is typically a conservative estimate of the pure optomechanical $g_{om}^{(2)}$.

Classical Cauchy–Schwarz Inequality

For classical waves, it is possible to describe their joint state by a well-behaved probability distribution for their amplitudes and phases. This corresponds to a positive square integrable Glauber Sudarshan phase space function[52], which allows to bound the cross-correlation of a classical system using a Cauchy-Schwarz inequality

$$g_{ab}^{(2)} \leq \sqrt{g_{aa}^{(2)} g_{bb}^{(2)}} \tag{2.77}$$

by the mean value of the auto-correlations of the subsystems. We can understand this from the following picture (see also figure 2.11): Due to the loss tolerance of the second order coherence, the autocorrelation corresponds to the cross-correlation between the two output ports of a 50:50 beamsplitter. Such a beamsplitter creates the highest classically possible correlations, as the two outputs are identical copies of the input wave, albeit with smaller amplitude. Thus, whatever the interaction driven by the laser pulse was exactly, the correlations it creates cannot be higher than the (multiplicative) mean of the auto-correlations. Note that this classicality bound only restricts the property of the common system of mode $\hat{a}$ and $\hat{b}$, in our case the optical and mechanical mode. It is sufficient for one system to exhibit quantum properties to violate this inequality. For example, if one system ($\hat{a}$) is a decent single photon source, it's autocorrelation will be

---

[52] The statistical operator is expressed by the quasi-probability distribution $P(\alpha, \beta)$, named after Glauber and Sudarshan, as $\hat{\rho} = \iint \mathrm{d}^2\alpha\,\mathrm{d}^2\beta\, P(\alpha, \beta)\,|\alpha, \beta\rangle\langle\alpha, \beta|$ and is considered classical if $P(\alpha, \beta) \geq 0 \,\forall \alpha, \beta$, in which case it corresponds to a well-behaved probability distribution for the phase and amplitude of the classical waves.
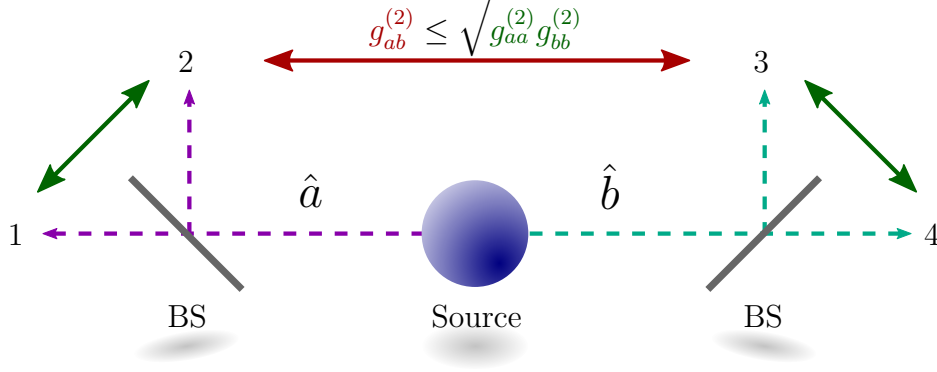
FIGURE 2.11.: **Classical Cauchy–Schwarz Inequality.** A classical source emits fields into two modes $\hat{a}$ and $\hat{b}$. The intensity correlation between them $g_{ab}^{(2)} = g_{23}^{(2)}$ is given by the correlation between ports 2 and 3 (red arrow). It cannot exceed the correlation of a mode with an identical copy of itself (green arrows), such as the correlation between ports 1 and 2 $g_{12}^{(2)} = g_{aa}^{(2)}$. For unequal fields, this bound is given by the multiplicative mean value $(g_{aa}^{(2)} g_{bb}^{(2)})^{1/2}$. Quantum fields can violate this inequality.

$g_{aa}^{(2)} \ll 1/2$. Therefore, any uncorrelated system $\hat{b}$ with thermal properties, that is $g_{bb}^{(2)} = 2$, and showing statistical independence, that is $g_{ab}^{(2)} = 1$, will violate the inequality (2.77). This example also highlights, that it specifically is a bound against classical wave-like behavior. Classical particles, like a football, can also violate the inequality, as they can trivially be in a state with an autocorrelation $g_{\text{ball,ball}}^{(2)} = 0$, i.e. not being detected at two places simultaneously.

Experimental Requirements

We now turn back to the optomechanical system described above, to analyze the properties of the cross-correlation. As we learned in paragraph 2.3.3, the Stokes transition driven by the write pulse should create photon-phonon pairs with a probability $\epsilon_{\text{P}} \ll 1$, which we assume here to be small. Consequently, the heralded state should contain a single phonon, while the unheralded state has a mean phonon number of $n_f = \epsilon_{\text{P}} + \bar{n}$ with the initial mean occupation $\bar{n} \ll 1$ of the mechanical mode. Thus, when starting close to the ground state and using a weak write pulse, we expect a large violation $g_{om}^{(2)} \sim (1 + n_f)/n_f \nleq 2$ of inequality (2.77), given a thermal property $g_{oo}^{(2)} = g_{mm}^{(2)} = 2$ of both subsystems. In appendix B.3, we find as full expression

$$g_{d_{\text{w}}d_{\text{r}}}^{(2)}(\tau) = \frac{e^{-\Gamma\tau}}{n_f(\tau) + P_B} + 1 \tag{2.78}$$

for a delay τ between the write and the read pulse, an the mean occupation number $n_f(\tau) \ll 1$ of the mechanical oscillator at this time. The normalized background counts $P_B \ll 1$, i.e. the count rate of false positive events converted to an equivalent phonon number P_B expected from the read pulse[53], can be characterized as described in the

---

[53] The normalize count rate $P_B = P(\text{false positive})/\eta_{\text{r}}$ corresponds to the probability of a false positive detection event $P(\text{false positive})$ during the time window of the read pulse, normalized by the detection quantum efficiency of a phonon η_{r}, as defined at equation (2.75). Compare also to the compensation of false positive events in the sideband asymmetry protocol (2.73).

previous paragraph. Thus, a cross-correlation measurement allows for a self-calibrated determination of the mean phonon number $n_f(\tau)$.

The approximation (2.78) also helps to understand why the cross-correlation can be used as a benchmark for other probabilistic protocols. The denominator quantifies the added noise contributions from the thermal environment, the state preparation by the write pulse, the read out noise of the stored state, all normalized to an equivalent phonon number $n_{\mathrm{Noise}} = n_f + P_B$. Thus, the normalized cross-correlation can be used to estimate if the system under investigation has low enough added noise such that it can potentially yield a successful measurements of a more involved protocol. For example, the generation of remote entanglement requires $g_{om}^{(2)} \geq 5.8$ [BNG11][54], the violation of a Bell inequality $g_{om}^{(2)} \geq 5.8$ [Rie+06] and the autocorrelation of the heralded phonon can be approximated as $g_{mm,\mathrm{heralded}}^{(2)} \sim 4/(g_{om}^{(2)} - 1)$ for $g_{om}^{(2)} \gg 1$ [Gal+14; Rie+16].

Note that for simple thermometry, the single-fold count rate based sideband asymmetry measurement described in paragraph 2.4.1 is more resource efficient, as the second order correlation is a two-fold coincidence measurement. From the losses described in equation (2.75), we can deduce the average number of repetitions necessary to observe one uncorrelated coincidence event as $N_{\mathrm{tries/coincidence}} \approx 1/P(W \cup R) = 1/(\epsilon_P \epsilon_R \eta_d^2)$. Hence, assuming Gaussian counting statistics, a statistical uncertainty of $\sigma = 0.1$ in units of the normalized cross-correlation requires $\sim 100 \cdot N_{\mathrm{tries/coincidence}}$. Using this scaling, we can estimate the optimal coupling to the cavity κ_{in}. In most measurements, the usable range of ϵ_P and ϵ_R is limited by absorption of photons in the cavity, and the intrinsic loss rate κ_{loss} is limited by fabrication. Consequently, fixing the intracavity photon number $|\bar{c}|^2$ and κ_{loss}, we find the minimum $N_{\mathrm{tries/coincidence}}$ for $\kappa_{\mathrm{in}} = \kappa/2$[55].

The classical bound requires slightly more measurements with a mean repetition number per uncorrelated coincidence of $N_w \approx 1/(\epsilon_P^2 \eta_d^2)$ for the write pulse and $N_r \approx 1/(n_f^2 \epsilon_R^2 \eta_d^2)$ for the read pulse. Furthermore, we can estimate the minimum filter suppression $1/\eta_f$ of the drive pulses required to achieve a maximum contribution to the normalized background counts $P_{\mathrm{B,leak,max}}$ by leaked drive photons, see also [53]. As the drive pulses experience the same loss in the optical path to the detectors, the residual transmission of drive photons is bound by

$$\eta_f \leq P_{\mathrm{B,leak,max}} \frac{\kappa_{\mathrm{in}}}{\kappa} \frac{\epsilon_R}{N_{\mathrm{in,-}}} \approx P_{\mathrm{B,leak,max}} \frac{\kappa_{\mathrm{in}}^2}{\kappa^2} \frac{4 g_0^2}{\tilde{\Omega}^2 + \kappa^2}. \tag{2.79}$$

In the second step, small state transfer fidelities $\epsilon_R \ll 1$ are assumed. For larger fidelities, the transfer efficiency per drive photon is reduced (2.59a), and thus even stronger suppression $1/\eta_f$ is required. In order to also allow for high bandwidths of the drive pulse, typically concatenated filters are required. Using n_{filter} identical filters with a bandwidth κ_{filter}[56], all resonant with the optomechanically scattered photons, we find for the residual transmission

$$\eta_f = \left(\frac{1}{1 + \tilde{\Omega}^2/\kappa_{\mathrm{filter}}^2} \right)^{n_{\mathrm{filter}}}. \tag{2.80}$$

---

[54] In a different estimation, reference [Usm+12] requires $g_{om}^{(2)} \geq 7.8$.

[55] In the case that the absorption is low enough such that multiple Stokes scattering events are limiting the usable range of ϵ_P, i.e. ϵ_P contributes significantly to n_f, slight over-coupling $\kappa_{\mathrm{in}} = 2\kappa_{\mathrm{loss}}$ becomes optimal.

[56] The bandwidth corresponding to the amplitude decay rate of the filters, see also (2.34).

For the typical parameters in chapters 4 to 6, the drive suppression (2.79) needs to exceed $1/\eta_f \sim (\tilde{\Omega}/\kappa_{\text{filter}})^{2n_{\text{filter}}} \geq 4 \cdot 10^8$. For a mechanical frequency $\tilde{\Omega}/2\pi \sim 5.2\text{GHz}$, this can be achieved with $n_{\text{filter}} = 2$ filters with a linewidth $\kappa_{\text{filter}}/2\pi \sim 35\text{MHz}$. Note that the free spectral range of these filters must exceed 2Ω, and mode-matching to other spatial and polarization modes of the filter must be taken into account.

2.4.3. Stroboscopic Measurements

The previous sections focused on optical control pulses with an envelope that changes slowly compared to the mechanical oscillation frequency. For low frequency oscillators, it is also possible to adiabatically drive the cavity, yet keep the pulse length much shorter than the mechanical period. In this case, the free mechanical operator can be approximated as remaining stationary during the presence of the drive pulse, such that the interaction corresponds to a measurement of the instantaneous position of the mechanical element [Van+11]. This in principle allows to evade the measurement back action on the observed quadrature, allowing e.g. for conditional squeezing of the state [Van+13; Vas+15]. As the quantum formalism for these stroboscopic measurements can be found in details elsewhere [BVK78; Tho+78; BVT80; Kha+10; Van+11], I will restrict the explanation of the measurement protocols to a basic level and focus on the practical limitations with respect to stroboscopic quantum control of mechanical oscillators.

If an interaction only reveals information on one quadrature of the system under investigation, e.g. $\hat{X}$, the unitary operator describing the evolution of the wavefunction[57] due to this interaction, $\hat{U} = \hat{U}(\hat{X})$, can only be a function of this quadrature. In other words, the unitary $\hat{U}$ must be independent of the non-commuting orthogonal quadrature, in this case $\hat{P}$, and consequently commute with the measured quadrature $[\hat{U}(\hat{X}), \hat{X}] = 0$. Thus, a measurement that principally only allows to access a single property of the system will not impart measurement back action on this property.

We can intuitively understand this by considering the radiation pressure interaction, neglecting the mediating optical cavity. When a short laser pulse is reflected by an object, the optical phase relates to its (instantaneous) position. The reversal of the propagation direction of the laser pulse corresponds to change in its momentum, which is compensated by transferring momentum difference to the object, an effect called radiation pressure. Consequently, while information on the position is obtained, the measurement back action only affects the momentum of the investigated object. This example also allows to grasp the limits of this measurement scheme. Firstly, if the pulse is not infinitesimally short, it can be split in two equal halves, with the difference of the two position measurements revealing information on the momentum of the object. This corresponds to the transition between an instantaneous optical phase measurement and a resolvable continuous Doppler shift of the optical frequency. Secondly, the transferred momentum will change the position of the object immediately. Thus, even though there is no back action imparted to the instantaneous position, the free evolution of the object prevents a continuous observation the position, such that the protocol cannot strictly be described as a quantum non-demolition (QND) measurement. For a harmonic oscillator, the initial position and momentum state will recur after a full mechanical period, allowing for a repeated measurement of the same instantaneous position. For this reason, the (rotating)

---

[57]Respectively the evolution of the operators in the Heisenberg picture.

quadratures are called stroboscopic QND observables [BVT80]. However, this requires the mechanical state to remain unaltered by the thermal environment for a full mechanical period, setting strict bounds for the mechanical decoherence rate. Practically, the stroboscopic nature of the QND observables leads to a third challenge. Massive mechanical oscillators possess a plethora of mechanical modes at various frequencies. Thus, the measured position of the object does not correspond to the recurring, stroboscopic QND observable of a single mode, but the non-recurring total displacement of the mechanical oscillator.

These three limitations render the stroboscopic measurement scheme vulnerable to corruption by thermal noise. In the following I will briefly quantify the conditions for a stroboscopic QND measurement arising from these classical noise contributions.

Pulse Length

If the measurement pulse is too long, it contains information on the change of position and thus the momentum of the object. For simplicity, we will consider two consecutive, ideal, and instantaneous position measurements and investigate the resulting uncertainty due to the thermal momentum distribution. Assuming the back action noise imparted on the momentum quadrature is negligible compared to its thermal distribution, we can treat the system classically, defining the measurement $M_i = X(t_i)$, $i = 1, 2$ at time $t_1 = 0$ and $t_2 = \delta t$. For a harmonic evolution of the mechanical oscillator with angular frequency Ω and neglecting the mean momentum transfer by the measurement pulse, as well as the thermal decoherence, we find for the harmonic evolution $X(t) = X_0 \cos(\Omega t) + P_0 \sin(\Omega t)$, with the parameters X_0 and P_0 having a thermal distribution with the uncertainty $\sigma_{X_0} = \sigma_{P_0} = \sqrt{n_{\text{th}} + 1/2}$. For the difference $\delta M = M_2 - M_1$ we thus find the variance $\langle \delta M^2 \rangle \approx (\Omega \delta t)^2 \langle P_0^2 \rangle$. Consequently, in order to achieve a variance smaller than the ground state fluctuations $\langle 0 | \hat{X}^2 | 0 \rangle$, that is allowing for conditional squeezing of the state, the time difference needs to be smaller than

$$\delta t \leq \frac{1}{\Omega \sqrt{2 n_{\text{th}} + 1}}. \tag{2.81}$$

On the one hand, this set an upper limit for the pulse length. On the other hand, when using pulses which are much shorter than this bound, it describes a time scale during which two consecutive measurements can in principle resolve conditional squeezing of the position quadrature. Note that the effective phonon number of the thermal state describing the variance of the instantaneous position and momentum quadrature X_0 and P_0 does not have to correspond to the actual phonon number of the oscillator. Knowledge on the instantaneous momentum quadrature previous measurements can be used to obtain a conditional state of a lower temperature with $\sigma_{P_0} = \sqrt{\langle P_0^2 \rangle - \langle P_0 \rangle^2}$.

Thermal Decoherence

For a truly stroboscopic measurement of the instantaneous position, it is necessary to wait until the original instantaneous quadratures recur. While this happens after every full period $T = 2\pi/\Omega$, after half a period, the quadratures are recovered with an inverted sign. In the high temperature limit, i.e. the fluctuations of the thermal environment $n_{\text{env}} \gg 1/2$ exceeding the vacuum fluctuations by far, we can approximate the rethermalization of

the conditional position variance after a measurement at $t = 0$ as $\langle P_0^2(\delta t)\rangle - \langle P_0(0)\rangle^2 \approx (1 - e^{-\Gamma \delta t}) \cdot (n_{\text{env}} + 1/2)$. Thus, to enable a variance between measurements, delayed by half a mechanical period $\delta t = T/2$, to be smaller than the vacuum fluctuations $\langle (M_1 + M_2)^2 \rangle \leq 1/2$, the mechanical quality factor needs to exceed $Q \geq 2\pi(n_{\text{env}} + 1/2)$. For a mechanical oscillator with a frequency of $\Omega/2\pi \sim 100\text{kHz}$ at a temperature of 4K, this corresponds to a minimum quality factor of $Q \geq 5 \cdot 10^6$.

Spectator Modes

Massive oscillators have a series of normal vibrational modes, of which all except of one are typically neglected. However, a short pulse measures the displacement of the oscillator at a large bandwidth, thus not allowing for spectrally selecting the mode of interest, as is done in the quasi-continuous protocols described in the previous paragraphs. For simplicity, we assume two mechanical modes, with the measurement being normalized to the mode of interest at the angular frequency Ω_0. The second mode, called spectator mode, is transduced differently to the measurement signal by a factor μ, such that we can express the time evolution of the observed displacement $X(t) = X_0 \cos(\Omega_0 t) + P_0 \sin(\Omega_0 t) + \mu X_1 \cos(\Omega_1 t) + \mu P_1 \sin(\Omega_1 t)$. For a stroboscopic measurement of the primary mode, i.e. $\delta t = 2\pi/\Omega_0$, this results in a variance of the measurement difference

$$\langle \delta M^2 \rangle \approx 2\mu^2 \sigma_{X_1}^2 \left(1 - \cos\left(2\pi \, \Omega_1/\Omega_2 \right) \right). \tag{2.82}$$

Here, we assumed equipartition of the uncertainty between the two instantaneous quadratures of the spectator mode $\sigma_{X_1} = \sigma_{P_1} = \sqrt{n_1 + 1/2}$, with the conditional variance of the mode $n_1 + 1/2$. Unfortunately, in contrast to the two previous cases, this does not result in a simple condition indicating when a measurement uncertainty below the mechanical shot noise limit is possible. It is further complicated by the fact that not just a single spectator mode but all of them contribute to the added noise, i.e. if it is possible to cancel out the contribution of one spectator mode, another one will still contribute to the measurement noise. In the following, I will describe mitigation strategies addressing the individual factors of equation (2.82).

First, the conditional variance $\sigma_{X_1}^2$ can be reduced by cryogenic cooling and the use of knowledge obtained from previous measurements to further lower the temperature of the conditional state. This is effective for a broad frequency range. Note that the requirements for conditional cooling-by-measurement [Van+13] of spectator modes to below the shot noise limit of the primary mode are typically similar to the requirements necessary to prepare a conditional pure state in the primary mode [Wie+15]. In other words, this strategy to reach the quantum regime is usually only promising if feedback cooling to the ground state is possible, which has only recently been achieved experimentally [Ros+18].

Secondly, the last term indicates that ideal higher harmonics of the primary mode do not contribute to the noise. Therefore, it can be of interest to use a system with a simple geometry, such as a vibrating string. As nanofabricated devices typically exhibit some unintentional asymmetries, this approach is limited in its effectiveness. Furthermore, it only works for full periods between pulses. When considering half periods between the measurement pulses, which is advantageous for the thermal decoherence, even-numbered higher harmonics will not cancel out.

Thirdly, the transduction to the spectator modes can be engineered. The transduction parameter $\mu = g_1/g_0$ used here corresponds to the ratio of single photon coupling strengths

of the primary mode g_0 to the spectator mode g_1. This can be reduced for some modes by exploiting symmetries, for example by coupling the optical cavity in the middle of a vibrating string, even higher harmonics will be canceled out, similarly to out of plane modes. To also address the odd higher order modes, it can be beneficial to increase the stiffness of the middle part of the resonator compared to the supporting tethers. In the extreme limit, the higher order modes can then be interpreted as string modes of the tether, while the primary mode is the center of mass mode of the test mass in the middle. While this reduces the coupling strength of the spectator modes, it will also cause the spectrum to deviate strongly from the form of higher harmonics, which were found to be beneficial in the previous point. Another way to reduce the coupling of spectator modes is to increase the sampling area of the optical probe compared to the size of the mechanical oscillator. In the limit of large oversampling, that is a beam spot much larger than the test object, exclusively the center of mass motion will couple to the optical field, while contributions of the higher order modes will in first order cancel out.

A promising approach therefore is the use of optically levitated nano-particles. Due to the absence of mechanical support, they do not exhibit spectator modes associated with tethering of the mass. Bulk modes of the nano particles are several orders of magnitude higher in frequency than the center of mass motion, such that usually only three distinct modes can be observed, corresponding to the center of mass motion in each dimension of space. By probing only one direction, an effective single mode oscillator can be obtained [Mag+18].

3. Physical realization

While cavity optomechanics in the weak coupling regime is very accessible from a theoretical perspective, reaching the quantum regime in experiments is challenging. The reason is, that the non-linear nature of the interaction allows for coupling between two engineered degrees of freedom in vastly different frequency regimes. On the one hand, this is an intriguing feature for many applications in quantum information science and beyond, allowing e.g. for a direct interface between long lived mechanical quantum memories and photons in the conventional fiber telecommunication band. On the other hand, using large numbers of high-energy optical excitations to control individual low-energy mechanical excitations can lead to undesired side effects: A single absorbed drive photon carries enough energy to potentially generate several hundred thousand phonons. Despite low conversion efficiency between absorption centers and the mechanical mode, this incoherent quasi-thermal contribution can easily mask all quantum effects.

A large single photon coupling strength reduces the number of drive photons required to achieve a certain interaction strength and thus the number of photons that can potentially be absorbed. The coupling strength can be boosted by reducing the mode volume of the optical and the mechanical resonator, that is increasing the field per photon, respectively phonon. As described in section 3.1, nanophotonic cavities based on interference in regularly patterned waveguides, called photonic crystal cavities, allow for small mode volumes and at the same time narrow cavity linewidths.

The same principle, that is modulating the speed of propagation of a guided wave to form strongly confined resonances, can also be applied to vibrations. In section 3.2 the similarities and differences to photonic cavities are explored and the possibilities of co-localizing and coupling photonic and phononic resonances are explained. A co-localized photonic and phononic crystal resonance is called optomechanical crystal, a type of device used in the experiments reported in chapters 4 to 6. These optomechanical crystals were initially designed and realized in seminal works in the group of Oskar Painter [Eic+09; Cha+11a; Cha+12] and were only slightly adapted in the present work.

3.1. Photonic Crystal Cavities

Photonic crystals are nanofabricated devices, which exhibit an artificial structural periodicity on the order of the wavelength [Sak05; Joa+08]. The light scattered by the periodic structures interferes and can therefore form a complex dispersion relation. Due to the spatial periodicity, it can be mapped into a band diagram of the first irreducible Brillouin zone of momentum space, in the same way as electronic and vibrational dispersion relations of single crystals are described in solid state physics [Yab87; Joh87], see figure 3.1a. Similarly to semi-conductors, the artificial photonic crystals can exhibit band gaps, that is optical frequencies to which no real wave vector in the reciprocal space corresponds [YG89; Yab93]. The origin of these photonic band gaps can be understood as normal

3. Physical realization
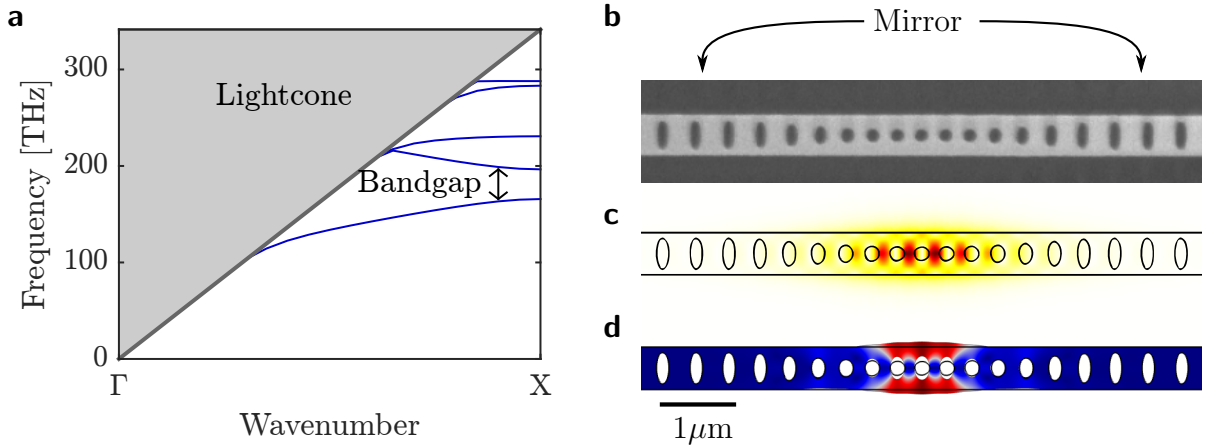
FIGURE 3.1.: **Photonic and Phononic Crystal.** Periodic structures on the wavelength scale create non-trivial dispersion relations, as the scattered fields can interfere. **a** The band band diagram shows the relation of the wavenumber to the frequency of horizontally polarized Bloch modes in an infinite lattice of unit cells (blue). The unit cell for the waveguide photonic crystal with (longitudinal length, width, height, [longitudinal, transverse] hole diameter)=(439, 550, 250, [160, 403])nm exhibits a band gap at optical telecom frequencies. In this frequency region, no light can propagate and will be reflected. Inside the lightcone (grey), the waveguide cannot confine the light in the transverse direction. **b** In the scanning electron microscope picture of a device as used in chapter 4 to 6 a pattern of such cells is used to generate mirrors in a waveguide. **c** In the region between the mirrors, an optical resonance can form. The simulated absolute field strength of the resonance is shown in arbitrary units. **d** The same principle also holds for sound waves. By choosing the right geometry, a mechanical mode can be co-localized with the optical resonance. The simulated displacement field of the breathing mode used in chapter 4 to 6 is shown in arbitrary units.

mode splitting due to strong coupling of the forward and backward propagating waves, induced by the periodic sub-wavelength structures. At frequencies within the band gap, destructive interference in the forward direction does not allow for lossless transmission of the wave, called Bloch mode, as it is the case on the photonic bands. Instead, the wave number acquires a complex part, corresponding to exponential attenuation in the band gap material [Joa+08; QDL10]. If scattering to the side is suppressed, inbound light is reflected on the boundary of a photonic crystal exhibiting a band gap at the right frequency, in close analogy to a distributed Bragg reflector.

We now consider a dielectric waveguide, radially confining the light by total internal reflection. A photonic crystal mirror can be created by patterning the waveguide periodically, for example by etching holes of the right size and spacing into the material. Similarly to a Fabry-Pérot cavity, an optical resonator can be formed by two such mirrors, separated at the right distance, see figure 3.1b-c. The space between them is called defect, as it breaks the periodicity of the crystal. Such devices are called nano beam photonic crystal cavities and can at the same time exhibit very high optical quality factors and small mode volumes when properly designed and fabricated [SP02; Vuc+02; SP03; LMH04; EFV05; QDL10; QL11]. A fundamental condition for narrow optical resonances is to avoid off-axis scattering, that is ensuring axial guidance of the wave by total internal reflection of the waveguide. As scattered waves would have to propagate in vacuum, this

can be achieved by avoiding spatial Fourier components in the light cone, i.e. at angular wave numbers below $k \leq \omega_c/c$, with the resonance frequency $\omega_c/2\pi$ and the speed of light c. In other words, a smooth transition from the defect to the mirror region is required [Aka+03], allowing for a smooth envelope of the resonant field, thereby localizing the spatial Fourier transform narrowly around the carrier wave number $k = n\omega_c/c$, with the effective refractive index n of the photonic crystal waveguide. Consequently, it is necessary to strike a compromise between strong real-space localization and strong wavenumber-space localization, something reasonably achieved for example by a Gaussian envelope. Practically, high performance resonators need to be optimized in numerical simulations, which is easily possible with dedicated software, even on modern notebook computers.

Nanobeam photonic crystals have a strong geometric asymmetry between the horizontal and vertical axial direction. Consequently, they have a strong birefringence, typically only allowing for large bandgaps only for the horizontal polarization. While photonic crystal cavities thus only work for a single polarization, the other polarization is for the same reason strongly decoupled and has therefore no negative influence, e.g. in the form of an additional loss channel for the resonance.

3.2. Phononic Crystal Resonators

A periodic pattern in a material does not only modulate the speed of propagation of optical waves, but also of mechanical waves, that is vibrations. Consequently, the principles described in the previous section can be applied to phononic crystals. Artificial materials with high reflectivity for vibrations can be designed and employed to strongly localize mechanical modes, in this case called phononic crystal resonators [Gor+05], see also figure 3.1d. However, there are a number of differences to the optical case, which are worth highlighting.

Firstly, the speed of sound c_S is much slower than that of light c_L in a material, with $c_S/c_L \sim 10^{-4}$ for longitudinal waves in silicon [HNK10]. Consequently, feature sizes of telecom band *photonic* crystals[1], result in *phononic* crystals with typical frequencies in the gigahertz (GHz) range. Thus, devices with common photonic and phononic band gaps will exhibit resonances in these drastically disparate frequency regimes. While the freedom of the design allows to shift the relative frequencies by about an order of magnitude [Eic+09; SP10; Cha+12; Saf+14], accessing e.g. lower relative frequencies will require a separation of the optical and mechanical functionality of the artificial crystal [Ale+11; Kra+12; Saf+13a; Yu+14; Tsa+17].

Secondly, while light can propagate in vacuum, vibrations cannot, thereby lifting the necessity of smoothly transferring from a defect to the phononic mirror material. As a consequence, the requirements on the design of the resonator defect is significantly relaxed for the phononic case, leaving leeway to optimize a co-localized optical resonance. In addition, this means that a dedicated phononic bandgap material can suppress the coupling to the support [Saf+11; Ale+11].

In contrast to light, which only has two polarizations, vibrations can be of many more

---

[1]More specifically, photonic crystals with a band gap covering the conventional telecommunication band, that is infrared radiation with a free space wavelength close to $\lambda \sim 1550\,\text{nm}$.

types. Compression and shearing of the material creates a plethora of categories of vibrational waves, leading to complex band diagrams [Cha+12]. While it is possible to create full band gaps, i.e. frequency regions where all vibrational types are reflected, quasi-bandgaps, inhibiting only the propagation of vibrational modes with a certain symmetry are already enough to strongly localize modes of the same symmetry. Quasi-bandgaps can further be employed to precisely engineer the coupling of the mechanical resonator to the substrate by a controlled perturbation of one of these symmetries [Pat+17; Pat+18]. In case of the breathing mode of the optomechanical crystals used in chapters 4 to 6, this allows to reduce the mechanical quality factor from $Q \sim 10^7$ for a symmetric device with a quasi bandgap nanobeam to $Q \sim 10^5$ by slightly offsetting all holes of the device to the side[2].

The localized mechanical modes can couple in different ways to a co-localized optical mode. In optomechanical crystals, there are two dominating mechanisms, related to the deformation and the strain in the material induced by the mechanical motion [Cha+12]. The deformation of the material leads to a change of the boundaries of the optical cavity, thereby changing its resonance frequency. This effect is similar to radiation pressure on a movable end mirror in a macroscopic Fabry-Perot cavity [Cav80; Arc+06] or the optical gradient force on dielectrics in an optical resonator [Tho+08; Kie+13; Mag+18]. For photonic crystals it can be quantified by perturbation theory on the surface fields [Joh+02; SP10]. In addition, the strain due to the compressive part of the breathing modes changes the refractive index of the material, a mechanism called photo-elastic effect. This changes the effective length of the optical resonator, and thus its frequency. This effect is relatively strong in silicon [CPB59; Bie74] and exceeds the effect of the moving boundary in the investigated optomechanical crystals by far [Cha+12].

---

[2]The symmetry can also be broken by shifting only the center hole. However, this increases the coupling to asymmetric tilting modes drastically and therefore is not as controllable as shifting all holes at once. In both cases the optical resonance is barely influenced by the shift.

4. Non-classical correlations between single photons and phonons from a mechanical oscillator

The second order coherence describes the correlation of the fluctuations of two systems, and can therefore be quantified via a cross-correlation measurement. It carries a wealth of information on the quality of bimodal quantum sources and has therefore become a benchmark measurement in quantum optics. Here, I will report on my work on non-classical photon-phonon correlations, first published as reference [Rie+16], preceded by a summary of the scientific context of this manuscript. More details can be found in paragraph 2.4.2.

While the first order coherence relates to the interference visibility of two modes, a concept with close correspondence between the classical and quantum description, the cross-correlation of a quantum system can assume values outside of the classical realm [Lou80; RW86]. This motivated initial investigations by Clauser on the cross-correlation between two light beams originating from cascaded fluorescence, trying to unambiguously disprove semi-classical theories of light [Cla74].

Semi-classical theories assume a quantum description of atoms, but treat electromagnetic radiation classically. They were met with interest, as they could reproduce many experimental observations that were up to then considered to be genuine quantum effects, including the photoelectric effect [MSW64; CJ69].

While it was not the first experimental falsification of semi-classical theories [Gav28; Cla72; Gib72; WAR72; GCS73][1], the simplicity of Clauser's experiment is striking. His distinction to classical field theory is based on a Cauchy Schwartz inequality for probability distributions [Gla63b; TG65]. If two fields a and b with the complex amplitudes $\alpha, \beta \in \mathbb{C}$ can be described by the probability distribution $P(\alpha, \beta)$, then the correlation between their intensities I_a and I_b is bound by $\langle I_\mathrm{a} I_\mathrm{b} \rangle^2 \leq \langle I_\mathrm{a}^2 \rangle \langle I_\mathrm{b}^2 \rangle$, respectively its normalized form (2.77). The experimental determination of the classicality bound allowed Clauser to omit making assumption on the source, which limited the conclusiveness of previous correlation experiments [ÁJV55] with respect to semi-classical theories. The classical Cauchy-Schwarz inequality is therefore valid independent of the source, or more specifically how the latter is modeled [Cla74].

Clauser's experiment, employing cascaded decays in mercury atoms, was followed up by theoretical prediction of violations of the Cauchy-Schwarz inequality in various other systems [Zub82; MG83; RW84]. However, as the incompatibility of semi-classical field

---

[1] Note that the experiment in reference [Gav28] was conducted well before the advent of semi-classical theories in the 1960s, but was rediscovered and identified to falsify them only in the 1970s [ARW73] after the newer experimental test were published. It was originally intended to disprove a theory by Schrödinger, which would nowadays also be classified as semi-classical.

theories with correlation experiments was demonstrated, the experimental focus shifted to Bell's inequality, as well as a variety of the Cauchy-Schwarz inequality involving a single spatial mode at different times. Demonstration of this property, called anti-bunching, allows to demonstrate the non-classicality of a radiation field from a single mode [KDM77], see also chapter 5.

Aside from allowing for a distinction of quantum field theory and semi-classical theories, coincidence measurements were used as a standard method for the characterization of bimodal sources [Cam+70; BW70]. In particular the coincidence measurements in spontaneous parametric down conversion in reference [BW70] suggest that the classical inequality could have been violated, but the classical bound was not determined.

The interest in the normalized second order coherence was renewed with proposals for long range quantum communication. In order to overcome the exponential degradation of distributed entanglement related to loss in the transmission channel, quantum repeaters were suggested to distribute entanglement more efficiently [Bri+98; Dua+01]. Quantum repeaters are based on a chain of local nodes, which interface a quantum memory, typically a cloud of atoms, with a movable quantum state, typically a photon.

A violation of the classical Cauchy-Schwarz inequality allowed to demonstrate that the node could operate in the quantum regime [Kuz+03][2]. As in the normalized form (2.77) the classical bound is close to $\sqrt{g^{(2)}_{aa} g^{(2)}_{bb}} \sim 2$, corresponding to a thermal state of the individual modes, subsequent experiments rarely measured this bound specifically [Cha+05; Mat+05; Fel+05; Mat+06a].

Instead it was realized that the measurement of the normalized cross-correlation realistically captures the noise in the generation of excitations pairs, in quantum memories [Rie+06; Lau+06; Lau+07; Usm+12] and other bimodal sources [Boc+09; För+13]. Thus, it can be measured to predict whether more involved experiments, such as a test of Bell's inequality or subpoissonian statistics of a heralded single phonon, can be successful.

In the context of bulk lattice vibrations, the normalized cross-correlation was measured and used to characterize the Stokes and anti-Stokes scattering of naturally occurring optical phonons in diamond [Lee+11; Lee+12], yet without testing the classicality bound.

In the following I will present my work demonstrating a quantum interface between a nanofabricated, integrated quantum memory in the form of an optomechanical crystal, and an itinerant photon with a wavelength in the conventional telecommunication band [Rie+16]. I contributed to this work by conceiving, building and automating the experiment, taking and analyzing the data and writing the manuscript.

In brief, a blue drive pulse probabilistically induces a Stokes scattering event, creating a pair of a resonant photon and phonon. To measure the correlations between the emitted optical mode and the mechanical mode, a red drive pulse transfers the mechanical state to the optical domain, see also figure 4.1.

With the demonstration of non-classical optomechanical correlations, we show that optomechanical crystals with their designed resonance frequencies act as a quantum interface between the optical and the mechanical domain. Thus, the long lived mechanical resonance can serve as quantum memory for quantum information processing protocols with telecom photons, such as the DLCZ quantum repeater scheme [Dua+01]. Optomechanical down conversion of blue detuned drive photons is shown to work in the single

---

[2]Operation in the quantum regime can also be shown by other correlation measurements, e.g. the observation of sub-shotnoise correlations in the Fourier domain [Wal+03].
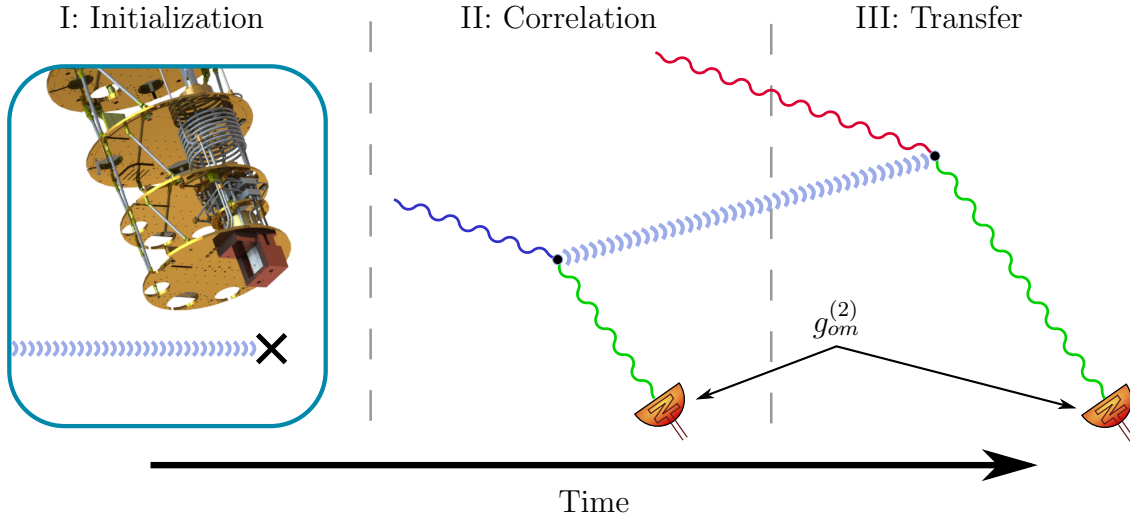
FIGURE 4.1.: **Optomechanical Cross–Correlations.** First, the device is initialized in its ground state by cryogenic cooling, leaving enough time for residual phonons to decay. Then, a driven Stokes interaction (fig. 2.10)generates correlated photons and phonons. The latter transferred to the optical domain by an anti-Stokes interaction (fig. 2.8) and the intensity correlation $g_{om}^{(2)}$ between the optical and the mechanical mode is measured using superconducting nanowire single photon detectors.

quantum regime, thereby enabling a plethora of probabilistic quantum protocols at the heart of quantum information science, as well as for studies of fundamental questions in macroscopic quantum physics. Examples are the generation of single phonon Fock state [Hon+17], the generation of remote mechanical entanglement [Rie+18], or the violation of Bell inequality between a stored mechanical phonon and an itinerant optical photon [Mar+18].

Non-classical correlations between single photons and phonons from a mechanical oscillator

Ralf Riedinger*,a, Sungkun Hong*,a, Richard A. Norteb, Joshua A. Slatera, Juying Shangc, Alexander G. Krauseb, Vikas Anantc, Markus Aspelmeyera, Simon Gröblacherb

* These authors contributed equally to this work.

a Vienna Center for Quantum Science and Technology (VCQ), Faculty of Physics, University of Vienna

b Kavli Institute of Nanoscience, Delft University of Technology

c Photon Spot Inc.

4.1. Abstract

Interfacing a single photon with another quantum system is a key capability in modern quantum information science. It allows quantum states of matter, such as spin states of atoms [Wil+07; Stu+13], atomic ensembles [Kuz+03; Wal+03] or solids [YFI10], to be prepared and manipulated by photon counting and, in particular, to be distributed over long distances. Such light-matter interfaces have become crucial to fundamental tests of quantum physics [Hen+15] and realizations of quantum networks [Kim08]. Here we report non-classical correlations between single photons and phonons – the quanta of mechanical motion – from a nanomechanical resonator. We implement a full quantum protocol involving initialization of the resonator in its quantum ground state of motion and subsequent generation and read-out of correlated photon-phonon pairs. The observed violation of a Cauchy-Schwarz inequality is clear evidence for the non-classical nature of the mechanical state generated. Our results demonstrate the availability of on-chip solid-state mechanical resonators as light-matter quantum interfaces. The performance we achieved will enable studies of macroscopic quantum phenomena [Rom11] as well as applications in quantum communication [Sta+10], as quantum memories [Cha+11b] and as quantum transducers [Bar+12; Boc+13].

---

[3] `https://www.nature.com/articles/nature16536`
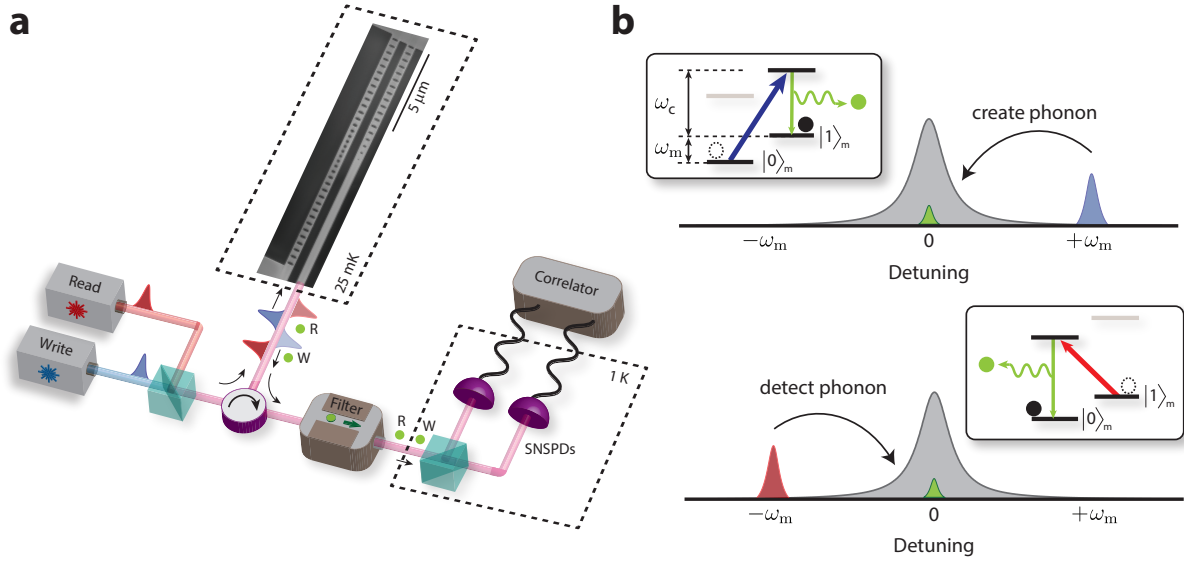
FIGURE 4.2.: **Generation and read-out of photon-phonon pairs. a**, Schematic of the experiment. Two independent lasers (stabilized to a wave-meter) are used to generate a sequence of 'write' and 'read' pulses with tunable time delay δt. They are sent through a circulator and drive a nanomechanical photonic crystal cavity (a scanning electron microscope image of which is shown in the inset) that is mounted inside a dilution refrigerator at a base temperature of 25 mK, which prepares the device in its quantum ground state of motion. For each pulse, Stokes and anti-Stokes Raman scattering creates single photons (green dots) from the write (W) and the read (R) pulse, respectively, that are emitted at a frequency ω_c. The detuned pump fields are strongly suppressed by optical filtering and only the Raman scattered photons are measured by two superconducting nanowire single-photon detectors (SNSPDs) in the output ports of a 50/50 beam-splitter. The time of each photon detection event is recorded and is then correlated in post-processing to obtain both auto- and cross-correlations of the emitted photons. A more detailed explanation of the experimental set-up is provided in the supplementary information (SI). **b**, Pulsed optomechanical interactions in frequency space. A blue-detuned write pulse realizes a two-mode squeezing interaction (blue and green pulses; see text). Cavity-enhanced Stokes Raman scattering generates a single phonon, stored as an excitation on the mechanical resonator, and a single (W) photon, which is emitted from the cavity on resonance (upper panel). Reading out of the phonon utilizes a red-detuned read pulse, which swaps the mechanical excitation onto the optical cavity field, hence creating a single (R) photon (lower panel). The insets depict the relevant energy level diagrams for the two processes, reminiscent of the Λ-schemes in atomic Raman scattering. The grey bars indicate the energy levels that are not involved in the depicted process (Stokes or anti-Stokes), but in the other one.

4.2. Main Text

Over the past few years, nanomechanical devices have been discussed as possible building blocks for quantum information architectures [Sta+10; Wal+09]. Their unique feature is that they combine an engineerable solid-state platform on the nanoscale with the possibility to coherently interact with a variety of physical quantum systems including electronic or nuclear spins, single charges, and photons [PZ12; AKM14]. This feature enables mechanics-based hybrid quantum systems that interconnect different, independent

physical qubits through mechanical modes.

A successful implementation of such quantum transducers requires the ability to create and control quantum states of mechanical motion. The first step – the initialization of micro- and nanomechanical systems in their quantum ground state of motion – has been realized in various mechanical systems either through direct cryogenic cooling [OCo+10; Mee+15] or laser cooling using microwave [Teu+11] and optical cavity fields [Cha+11a]. Further progress in quantum state control has mainly been limited to the domain of electromechanical devices, in which mechanical motion couples to superconducting circuits in the form of qubits and microwave cavities [AKM14]. Recent achievements include single-phonon control of a micromechanical resonator by a superconducting flux qubit [OCo+10], the generation of quantum entanglement between quadratures of a microwave cavity field and micromechanical motion [Pal+13], and the preparation of quantum squeezed micromechanical states [Wol+15; Pir+15; Lec+15].

Interfacing mechanics with optical photons in the quantum regime is highly desirable because it adds important features such as the ability to transfer mechanical excitations over long distances [Sta+10; SP11]. In addition, the available toolbox of single-photon generation and detection allows for remote quantum state control [Kim08]. However, micro- and nano-mechanical quantum control through single optical photons has not yet been demonstrated. One of the outstanding challenges is to achieve single-particle coupling rates that are sufficiently large to alleviate effects of optical and mechanical decoherence in the system, that is, single-photon strong co-operativity. Some of the largest optomechanical couplings have been reported in nanomechanical photonic crystal cavities [Saf+10], but are still two orders of magnitude short of that regime. Although low coupling rates can be overcome in principle by a strong and detuned coherent drive field [AKM14], such measures typically result in unwanted heating of the mechanical device (SI).

Here we take a different approach that allows us to circumvent these problems and to realize quantum control of single phonons through single optical photons. We use a probabilistic scheme based on the well-known DLCZ protocol (Duan, Lukin, Cirac and Zoller) [Dua+01], which, in its original form, uses Raman scattering for efficient generation and read-out of collective spin states of atomic ensembles. In essence, the scheme generates entanglement through single-photon interference and post-selection, which does not require strong coupling [Cab+98]. In the context of mechanical quanta, this protocol has been used in an experiment to entangle high-frequency (40 THz) optical phonons of two bulk diamond lattices [Lee+11]. However, the small interaction and coherence times of such phonons are incompatible with their use in quantum transduction and storage, and so it is necessary to take this approach to the level of chip-scale optomechanical systems. In addition, we minimize absorption heating by using short optical pulses in a cryogenic environment [Mee+15]. The combination of these techniques allows us to overcome the previous limitations and realize a photon-phonon quantum interface.

Our experiment complements previous work on single- and two-mode (opto-)mechanical squeezing in microwave circuits [Pal+13; Wol+15; Pir+15; Lec+15]. Although these experiments were based on the same underlying interactions, they involved homodyne or heterodyne detection of light to access continuous-variable degrees of freedom of a quantum state – specifically, quadrature fluctuations in the mechanical and optical canonical variables. In contrast, the DLCZ scheme uses photon counting, which allows access to discrete quantum variables – here, in form of energy eigenstates (phonons) of the mechan-

ical motion – and thereby enables realistic architectures for entanglement distribution and quantum networking [Kim08].

The mechanical system studied here is a micro-fabricated silicon photonic crystal nanobeam structure (Fig. 4.2a). Such optomechanical crystals co-localize optical and mechanical modes and couple them via a combination of radiation pressure and photostriction [AKM14]. Our device exhibits an optical cavity resonance at wavelength $\lambda_{\mathrm{c}} = 1{,}556$ nm and a mechanical breathing mode at frequency $\omega_{\mathrm{m}}/2\pi = 5.3$ GHz. The cavity decay rate (full-width at half-maximum, FWHM) is $\kappa_{\mathrm{c}}/2\pi = 1.3$ GHz and the mechanical quality factor at cryogenic temperature is $Q_{\mathrm{m}} = 1.1 \cdot 10^6$ (SI). Pulsed optical driving at laser frequency $\omega_{\mathrm{L}} = \omega_{\mathrm{c}} \pm \omega_{\mathrm{m}}$ (in which $\omega_{\mathrm{c}} = 2\pi c/\lambda_{\mathrm{c}}$ is the cavity frequency and c is the vacuum speed of light) allows to realize two different types of interactions on the basis of cavity-enhanced Stokes (+) and anti-Stokes (−) Raman scattering (Fig. 4.2b). A blue-detuned pulse ($\omega_{\mathrm{L}} = \omega_{\mathrm{c}} + \omega_{\mathrm{m}}$) results in two-mode squeezing with interaction Hamiltonian $H_{\mathrm{tms}} \propto \hbar g_0 \left(\hat{a}_{\mathrm{m}}^{\dagger} \hat{a}_{\mathrm{o}}^{\dagger} + \hat{a}_{\mathrm{m}} \hat{a}_{\mathrm{o}} \right)$, in which $\hat{a}_{\mathrm{m}}^{(\dagger)}$ and $\hat{a}_{\mathrm{o}}^{(\dagger)}$ are the creation (annihilation) operators of the mechanical and optical mode, respectively, g_0 is the effective optomechanical coupling rate (here, $g_0/2\pi = 825$ kHz; see SI) and $\hbar$ is the reduced Planck constant. This interaction generates photon-phonon pairs in close analogy to the photon-photon pairs generated in parametric down-conversion [Wu+86]. A red-detuned pulse ($\omega_{\mathrm{L}} = \omega_{\mathrm{c}} - \omega_{\mathrm{m}}$) allows read-out of the mechanical state through the optomechanical beam-splitter interaction $H_{\mathrm{bs}} \propto \hbar g_0 \left(\hat{a}_{\mathrm{m}} \hat{a}_{\mathrm{o}}^{\dagger} + \hat{a}_{\mathrm{m}}^{\dagger} \hat{a}_{\mathrm{o}} \right)$, in which an anti-Stokes scattering event realizes a state swap between the mechanical and optical cavity mode.

Our protocol consists of three distinctive steps. First, we initialize the mechanical system in its quantum ground state of motion by cryogenic cooling. Second, a short blue pulse creates a photon-phonon pair and leaves the originally empty mechanical and optical modes $|0\rangle_{\mathrm{m}}$ and $|0\rangle_{\mathrm{o}}$ at frequencies ω_{m} and ω_{c}, respectively, in the state $|\Phi\rangle_{\mathrm{om}} = |00\rangle + \sqrt{p}|11\rangle + p|22\rangle + \mathcal{O}(p^{3/2})$. Here p is the probability for a single Stokes scattering event to take place. Residual heating through optical absorption introduces additional noise to the state (SI). Finally, a strong red pulse is used to read out the phonon state via emission of an anti-Stokes scattered photon [Coh+15]. We confirm the non-classical photon-phonon correlations on the basis of an observed violation of a Cauchy-Schwarz inequality for the cross-correlation of the coincidence measurements between the Stokes and anti-Stokes photons [Kuz+03].

Precooling of the nanomechanical device is performed using a dilution refrigerator that operates at a base temperature of approximately 25 mK. If the mechanical system is in its quantum ground state of motion, then anti-Stokes processes cannot occur because no additional phonons can be extracted to support the scattering. This is in contrast to Stokes processes, which deposit mechanical energy and hence can always occur. As a consequence, the asymmetry in the scattering rates of these two processes is a direct measurement of the mean thermal phonon occupancy n_{th}. Using such photon-counting based sideband thermometry [Mee+15], we find $n_{\mathrm{th}} \lesssim 0.025$ (see Fig. 4.3).

We create the desired photon-phonon pairs using a blue-detuned 'write' pulse that is sufficiently weak to minimize the effects of residual absorption heating (FWHM, 28.4 ns; energy, 40 fJ). We find the relevant probability to generate a Stokes scattered photon on cavity resonance to be $p \approx 3.0\%$. Subsequently, a red-detuned 'read' pulse (effective length, 55 ns; energy of approximately 50 fJ) is injected at a time delay δt (see Fig. 4.4a), resulting in a phonon-to-photon conversion efficiency of approximately 3.7% (SI).
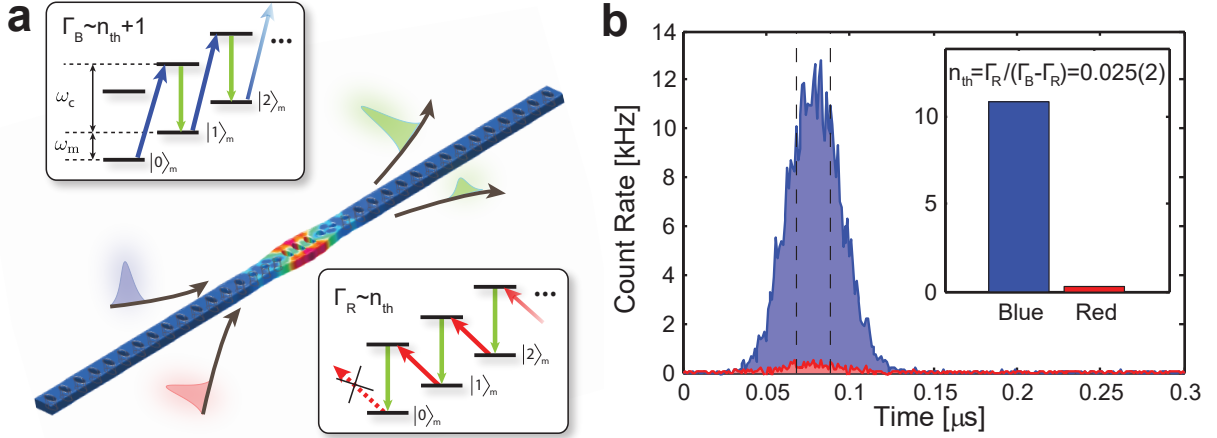
FIGURE 4.3.: **Mechanical quantum ground state preparation. a**, Principle of sideband ther-
mometry. The finite element method simulation depicted in the main panel shows the structure
of the mechanical breathing mode under investigation. The upper (lower) inset shows the en-
ergy level scheme in case of blue- (red-) detuned pumping and the resultant cavity-enhanced
Stokes (anti-Stokes) scattering. The corresponding scattering rates Γ_R and Γ_B are proportional
to thermal occupation of the mechanics n_{th} and $n_{th} + 1$, respectively, and hence show a strong
asymmetry when the mechanics are close to the quantum ground state. **b**, Sideband asymme-
try. The optomechanical device is pumped with a sequence of alternating blue- and red-detuned
optical pulses at frequency $\omega_c \pm \omega_m$ (optical energy per pulse $E_{opt} = 33$ fJ; FWHM of 28.4 ns;
500 μs separation of pulse sequences). Shown are the count rates recorded by the SNSPDs as a
function of the arrival time of the scattered photons (blue, blue-detuned pulse; red, red-detuned
pulse). This data has been corrected for leakage of pump photons through the optical filters,
which was independently measured and subtracted from our data (SI). The inset shows a his-
togram of the total counts that are obtained when averaging over a 20 ns window centred on the
peak (within the dashed lines). The pronounced asymmetry in the rates (of more than a factor
of 40) corresponds to a thermal occupancy of $n_{th} = \Gamma_R/(\Gamma_B - \Gamma_R) = 0.025 \pm 0.002$ and to a
mode temperature of 69 mK.
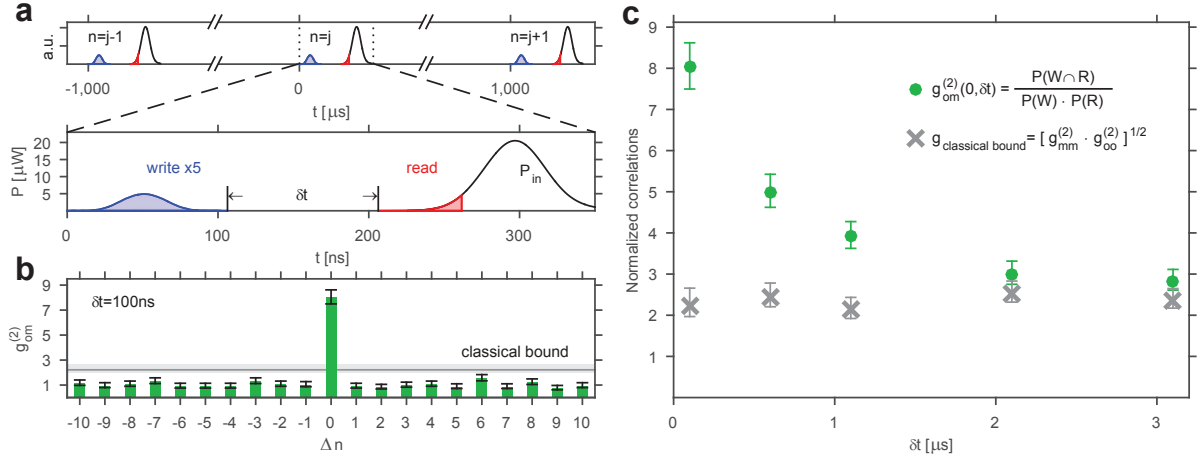
FIGURE 4.4.: **Non-classical photon-phonon correlations. a**, Driving pulse sequence. A pair of one write (blue) and one read (red) pulse is sent to the device every 1 ms. The long idle phase between pulse pairs ensures the ground-state initialization by cryogenic cooling. Each pulse sequence is labelled with a number (n). The read pulse is delayed by δt with respect to the write pulse, and only the first 55 ns, equivalent to a read-pulse power of about 50 fJ, are used for the data evaluation. This reduces the influence of absorption heating while maintaining reasonable state swap fidelity. **b**, Violating a Cauchy-Schwarz inequality. Shown is the cross-correlation (green bars) between the mechanical (read pulse) and optical state (write pulse) for $\delta t = 100$ ns, as well as the classical (Cauchy-Schwarz) bound obtained from the autocorrelations at $\Delta n = 0$ (grey horizontal line, shading indicates a 68% confidence interval; see text). For photon-phonon pairs that emerge from different pulse sequences ($\Delta n \neq 0$) the Cauchy-Schwarz inequality is fulfilled, $\langle g_{\mathrm{om}}^{(2)}(\Delta n \neq 0, 100 \text{ ns}) \rangle = 1.04 \pm 0.04$, consistent with statistical independence. For pulses from the same pair, the cross-correlation $g_{\mathrm{om}}^{(2)}(0, 100 \text{ ns})$ clearly exceeds the classical bound. $g_{\mathrm{om}}^{(2)}$ can be interpreted as the ratio of heralded phonons n_{h} to unheralded (thermal) phonons n_{th} at the time of the read pulse. **c**, Storage of non-classical correlations. Shown is the dependence of the cross-correlation on the time delay δt between the write and read pulses. For each data point, the classical bound is measured independently through the normalized autocorrelation functions of the write (W) and read (R) photons. For increasing δt, the photon-phonon cross-correlations decrease, but stay above the classical limit even beyond 1 μs. The main contribution to the loss of correlation is heating by absorption of the write pulse (SI). All error bars represent a 68% confidence interval.

We correlate the measured Stokes- and anti-Stokes photons via the cross-correlation function $g_{\text{om}}^{(2)}(\Delta n, \delta t) = P(W \cap R)/[P(R)P(W)]$, which is computed for read and write pulses originating from pulse sequences from different trials separated by Δn iterations (see Fig. 4.4). $P(W \cap R)$ is the probability for a joint detection of both a Stokes (W, 'write') and an anti-Stokes (R, 'read') photon from these pulses, and $P(W)$ and $P(R)$ are the unconditional probabilities to detect either of the two photons. For all pair correlations of classical origin, the value of $g_{\text{om}}^{(2)}$ is bounded by a Cauchy-Schwarz inequality of the form [Kuz+03] $g_{\text{om}}^{(2)}(0, \delta t) \leq \left[g_{\text{oo},\delta t}^{(2)}(0) g_{\text{mm},\delta t}^{(2)}(0) \right]^{1/2}$, in which $g_{\text{oo},\delta t}^{(2)}(0)$ and $g_{\text{mm},\delta t}^{(2)}(0)$ are the autocorrelation functions for the optical and mechanical mode, respectively (SI). A violation of this inequality [Kuz+03; Cla74; För+13] is an unambiguous measure for the non-classicality of the generated photon-phonon state. The Cauchy-Schwarz inequality for coincidence detection marks a well-defined border between the quantum and classical domain. It is based on the fact that the Glauber-Sudarshan phase-space function, or P-function, is positive definite for every classical field. This places a fundamental limit on the relative strength of measurable cross-correlations versus autocorrelations between classical fields. Previous applications of this limit include the distinction between the classical and quantum field theoretical predictions for the photoelectric effect [Cla74], and the storage and retrieval of non-classical states in the collective emission from an atomic ensemble [Kuz+03]. A detailed derivation of the Cauchy-Schwarz inequality for the case of non-stationary fields, as are being used here, is provided in ref. [Kuz+03].

We find a clear violation for an extended regime of time delays. Figure 4.4b shows the value of g_{om} at a time delay of 100 ns. For pairs emitted from the same pulse sequence ($\Delta n = 0$) we find that

$$g_{\text{om}}^{(2)}(0, 100 \text{ ns}) = 8.0_{-0.5}^{+0.6} \nleq \sqrt{g_{\text{oo},100 \text{ ns}}^{(2)}(0) g_{\text{mm},100 \text{ ns}}^{(2)}(0)} = 2.09 + 0.23 - 0.16,$$

which obviously violates the classical bound. As expected, pairs emitted from different pulse sequences ($\Delta n \neq 0$) are uncorrelated and hence fulfil the inequality. Upon increasing the time delay further, we find a violation even beyond $\delta t = 1$ μs (see Fig. 4.4c), which demonstrates that we can store and retrieve non-classical states for an extended time interval. Nevertheless, the lifetime of these non-classical correlations is still much shorter than the lifetime of the mechanical excitations, $Q/\omega_{\text{m}} \approx 34$ μs. We attribute this to the fact that the dynamics are dominated by heating caused by absorption of pump photons, which after some onset time drives the mechanical system towards a thermal state (SI). As a consequence, reducing the energy of the write pulse further should allow non-classical correlations to be maintained for much longer times. In addition, upon further reduction of the absorption heating of the read pulse, even higher values for the cross-correlation are obtained.

The cross-correlation is also linked to the autocorrelation of the heralded mechanical state. If one considers two-mode optomechanical squeezing acting on an initial mechanical thermal state, and if $g_{\text{om}}^{(2)} \gg 1$ – as is the case in our experiment – then one obtains $g_{\text{mm,heralded}}^{(2)} \approx 4/\left(g_{\text{om}}^{(2)} - 1 \right)$. The largest value for $g_{\text{om}}^{(2)}$ observed in our experiment was $g_{\text{om}}^{(2)}(0, 100 \text{ ns}) = 19.6 - 2.8 + 3.9$ (using an energy of 1.7 fJ in the first 30 ns of the read pulse; see SI). In other words, our system should allow for a Hanbury Brown and Twiss experiment with phonons yielding $g_{\text{mm,heralded}}^{(2)} \approx 0.22$. A direct measurement of this value

with the current experimental parameters is difficult without a prohibitively large number of pulse sequences.

In summary, we have demonstrated non-classical correlations between single photons and phonons from a nanomechanical resonator. This is a crucial step towards on-chip photon-phonon quantum interfaces, which are relevant for future solid-state based quantum information and communication architectures. For example, the observed photon-phonon correlation of $g_{\mathrm{om}}^{(2)} = 19.6$ suggests that conditional mechanical Fock-state preparation should be possible with fidelities exceeding 85% (SI). The ability to store and retrieve non-classical states over extended storage times that we reported also shows that nano-optomechanical resonators are a promising candidate for quantum memories. The performance of the system we have demonstrated constitutes an improvement of almost two orders of magnitude on previous lifetimes of stored non-classical single-phonon states [OCo+10]. Finally, photon-phonon conversion on the single particle level is required to extend the ongoing efforts on mechanically transduced conversion between microwave and optical fields [Boc+13] into the quantum domain [Bar+12].

References

These are the references cited in the author's version of the manuscript.

[AKM14]   M. Aspelmeyer, T. J. Kippenberg, and F. Marquardt, "Cavity optomechanics", *Rev. Mod. Phys.* 86, 1391 (2014), DOI: `10.1103/RevModPhys.86.1391` (cited on pgs. 66–68).

[Akr+10]   U. Akram, N. Kiesel, M. Aspelmeyer, and G. J. Milburn, "Single-photon opto-mechanics in the strong coupling regime", *New J. Phys.* 12, 083030 (2010) (cited on pg. 79).

[And+14]   R. W. Andrews, R. W. Peterson, T. P. Purdy, K. Cicak, R. W. Simmonds, C. A. Regal, and K. W. Lehnert, "Bidirectional and efficient conversion between microwave and optical light", *Nature Phys.* 10, 321 (2014), DOI: `10.1038/nphys2911` (cited on pg. 79).

[Bag+14]   T. Bagci et al., "Optical detection of radio waves through a nanomechanical transducer.", *Nature* 507, 81 (2014), DOI: `10.1038/nature13029` (cited on pg. 79).

[Bar+12] S. Barzanjeh, M. Abdi, G. J. Milburn, P. Tombesi, and D. Vitali, "Reversible Optical-to-Microwave Quantum Interface", *Phys. Rev. Lett.* 109, 130503 (2012), DOI: 10.1103/PhysRevLett.109.130503 (cited on pgs. 65, 72).

[Boc+13] J. Bochmann, A. Vainsencher, D. D. Awschalom, and A. N. Cleland, "Nanomechanical coupling between microwave and optical photons", *Nature Phys.* 9, 712 (2013), DOI: 10.1038/nphys2748 (cited on pgs. 65, 72, 79).

[Cab+98] C. Cabrillo, J. I. Cirac, P. Garcia-Fernandez, and P. Zoller, "Creation of entangled states of distant atoms by interference", *Phys. Rev. A* 59, 1025 (1998), DOI: 10.1103/PhysRevA.59.1025 (cited on pg. 67).

[Cha+11a] J. Chan, T. P. M. Alegre, A. H. Safavi-naeini, J. T. Hill, A. Krause, S. Groeblacher, and M. Aspelmeyer, "Laser cooling of a nanomechanical oscillator into its quantum ground state", *Nature* 478, 89 (2011), DOI: 10.1038/nature10461 (cited on pg. 67).

[Cha+11b] D. E. Chang, A. H. Safavi-Naeini, M. Hafezi, and O. Painter, "Slowing and stopping light using an optomechanical crystal array", *New J. Phys.* 13, 023003 (2011), DOI: 10.1088/1367-2630/13/2/023003 (cited on pg. 65).

[Cha+12] J. Chan, A. H. Safavi-Naeini, J. T. Hill, S. Meenehan, and O. Painter, "Optimized optomechanical crystal cavity with acoustic radiation shield", *App. Phys. Lett.* 101, 081115 (2012), DOI: 10.1063/1.4747726 (cited on pg. 76).

[Cla74] J. F. Clauser, "Experimental distinction between the quantum and classical field-theoretic predictions for the photoelectric effect", *Phys. Rev. D* 9, 853 (1974), DOI: 10.1103/PhysRevD.9.853 (cited on pg. 71).

[Coh+15] J. D. Cohen, S. M. Meenehan, G. S. MacCabe, S. Gröblacher, A. H. Safavi-Naeini, F. Marsili, M. D. Shaw, and O. Painter, "Phonon counting and intensity interferometry of a nanomechanical resonator", *Nature* 520, 522 (2015), DOI: 10.1038/nature14349 (cited on pg. 68).

[Dua+01] L. M. Duan, M. D. Lukin, J. I. Cirac, and P. Zoller, "Long-distance quantum communication with atomic ensembles and linear optics.", *Nature* 414, 413 (2001), DOI: 10.1038/35106500 (cited on pg. 67).

[Fio+11] V. Fiore, Y. Yang, M. C. Kuzyk, R. Barbour, L. Tian, and H. Wang, "Storing Optical Information as a Mechanical Excitation in a Silica Optomechanical Resonator", *Phys. Rev. Lett.* 107, 133601 (2011), DOI: 10.1103/PhysRevLett.107.133601 (cited on pg. 79).

[För+13] M. Förtsch, J. U. Fürst, C. Wittmann, D. Strekalov, A. Aiello, M. V. Chekhova, C. Silberhorn, G. Leuchs, and C. Marquardt, "A versatile source of single photons for quantum information processing", *Nature Commun.* 4, 1818 (2013), DOI: 10.1038/ncomms2838 (cited on pg. 71).

[Gal+14] C. Galland, N. Sangouard, N. Piro, N. Gisin, and T. J. Kippenberg, "Heralded Single-Phonon Preparation, Storage, and Readout in Cavity Optomechanics", *Phys. Rev. Lett.* 112, 143602 (2014), DOI: 10.1103/PhysRevLett.112.143602 (cited on pg. 84).

[Hen+15]   B. Hensen et al., "Loophole-free Bell inequality violation using electron spins separated by 1.3 kilometres", *Nature* 526, 682 (2015), DOI: `10.1038/nature1 5759` (cited on pg. 65).

[Hof+11]   S. G. Hofer, W. Wieczorek, M. Aspelmeyer, and K. Hammerer, "Quantum entanglement and teleportation in pulsed cavity optomechanics", *Phys. Rev. A* 84, 52327 (2011), DOI: `10.1103/PhysRevA.84.052327` (cited on pgs. 81, 84, 85).

[Kim08]   H. J. Kimble, "The quantum internet", *Nature* 453, 1023 (2008), DOI: `10.1 038/nature07127` (cited on pgs. 65, 67, 68).

[Kuz+03]   A. Kuzmich, W. P. Bowen, A. D. Boozer, A. Boca, C. W. Chou, L.-M. Duan, and H. J. Kimble, "Generation of nonclassical photon pairs for scalable quantum communication with atomic ensembles", *Nature* 423, 731 (2003), DOI: `10.1038/nature01714` (cited on pgs. 65, 68, 71, 81).

[Lec+15]   F. Lecocq, J. B. Clark, R. W. Simmonds, J. Aumentado, and J. D. Teufel, "Quantum Nondemolition Measurement of a Nonclassical State of a Massive Object", *Phys. Rev. X* 5, 041037 (2015), DOI: `10.1103/PhysRevX.5.041037` (cited on pg. 67).

[Lee+11]   K. C. Lee et al., "Entangling macroscopic diamonds at room temperature.", *Science* 334, 1253 (2011), DOI: `10.1126/science.1211914` (cited on pg. 67).

[Mee+14]   S. M. Meenehan, J. D. Cohen, S. Gröblacher, J. T. Hill, A. H. Safavi-Naeini, M. Aspelmeyer, and O. Painter, "Silicon optomechanical crystal resonator at millikelvin temperatures", *Phys. Rev. A* 90, 011803 (2014), DOI: `10.110 3/PhysRevA.90.011803` (cited on pgs. 77, 79).

[Mee+15]   S. M. Meenehan, J. D. Cohen, G. S. MacCabe, F. Marsili, M. D. Shaw, and O. Painter, "Pulsed Excitation Dynamics of an Optomechanical Crystal Resonator near Its Quantum Ground State of Motion", *Phys. Rev. X* 5, 041002 (2015), DOI: `10.1103/PhysRevX.5.041002` (cited on pgs. 67, 68, 77, 79, 80, 84).

[MW95]   L. Mandel and E. Wolf, *Optical Coherence and Quantum Optics*, Cambridge University Press, (1995), ISBN: 9781139644105 (cited on pg. 81).

[NTH12]   C. M. Natarajan, M. G. Tanner, and R. H. Hadfield, "Superconducting nanowire single-photon detectors: physics and applications", *Supercond. Sci. Technol.* 25, 063001 (2012), DOI: `10.1088/0953-2048/25/6/063001` (cited on pg. 81).

[OCo+10]   A. D. O'Connell et al., "Quantum ground state and single-phonon control of a mechanical resonator.", *Nature* 464, 697 (2010), DOI: `10.1038/nature08 967` (cited on pgs. 67, 72).

[Pal+13]   T. A. Palomaki, J. W. Harlow, J. D. Teufel, R. W. Simmonds, and K. W. Lehnert, "Coherent state transfer between itinerant microwave fields and a mechanical oscillator", *Nature* 495, 210 (2013), DOI: `10.1038/nature11915` (cited on pgs. 67, 79).

[Pir+15] J.-M. Pirkkalainen, E. Damskägg, M. Brandt, F. Massel, and M. A. Sillanpää, "Squeezing of Quantum Noise of Motion in a Micromechanical Resonator", *Phys. Rev. Lett.* 115, 243601 (2015), DOI: `10.1103/PhysRevLett.115.243601` (cited on pg. 67).

[PZ12] M. Poot and H. S. J. van der Zant, "Mechanical systems in the quantum regime", *Phys. Rep.* 511, 273 (2012), DOI: `10.1016/j.physrep.2011.12.004` (cited on pg. 66).

[Rom11] O. Romero-Isart, "Quantum superposition of massive objects and collapse models", *Phys. Rev. A* 84, 52121 (2011), DOI: `10.1103/PhysRevA.84.052121` (cited on pg. 65).

[Saf+10] A. H. Safavi-Naeini, T. P. M. Alegre, M. Winger, and O. Painter, "Optomechanics in an ultrahigh-Q slotted 2D photonic crystal cavity", *Appl. Phys. Lett.* 97, 181106 (2010) (cited on pg. 67).

[San+11] N. Sangouard, C. Simon, H. de Riedmatten, and N. Gisin, "Quantum repeaters based on atomic ensembles and linear optics", *Rev. Mod. Phys.* 83, 33 (2011), DOI: `10.1103/RevModPhys.83.33` (cited on pg. 84).

[SP11] A. H. Safavi-Naeini and O. Painter, "Proposal for an optomechanical traveling wave phonon-photon translator", *New J. Phys.* 13, 013017 (2011), DOI: `10.1088/1367-2630/13/1/013017` (cited on pg. 67).

[Sta+10] K. Stannigel, P. Rabl, A. S. Sørensen, P. Zoller, and M. D. Lukin, "Optomechanical Transducers for Long-Distance Quantum Communication", *Phys. Rev. Lett.* 105, 220501 (2010), DOI: `10.1103/PhysRevLett.105.220501` (cited on pgs. 65–67).

[Stu+13] A. Stute, B. Casabone, B. Brandstätter, K. Friebe, T. E. Northup, and R. Blatt, "Quantum-state transfer from an ion to a photon", *Nature Photon.* 7, 219 (2013), DOI: `10.1038/nphoton.2012.358` (cited on pg. 65).

[Teu+11] J. D. Teufel, T. Donner, D. Li, J. W. Harlow, M. S. Allman, K. Cicak, A. J. Sirois, J. D. Whittaker, K. W. Lehnert, and R. W. Simmonds, "Sideband cooling of micromechanical motion to the quantum ground state.", *Nature* 475, 359 (2011), DOI: `10.1038/nature10261` (cited on pg. 67).

[VAK13] M. R. Vanner, M. Aspelmeyer, and M. S. Kim, "Quantum State Orthogonalization and a Toolset for Quantum Optomechanical Phonon Control", *Phys. Rev. Lett.* 110, 10504 (2013), DOI: `10.1103/PhysRevLett.110.010504` (cited on pg. 84).

[Ver+12] E. Verhagen, S. Deleglise, S. Weis, A. Schliesser, and T. J. Kippenberg, "Quantum-coherent coupling of a mechanical oscillator to an optical cavity mode", *Nature* 482, 63 (2012), DOI: `10.1038/nature10787` (cited on pg. 79).

[Wal+03] C. H. van der Wal, M. D. Eisaman, A. André, R. L. Walsworth, D. F. Phillips, A. S. Zibrov, and M. D. Lukin, "Atomic Memory for Correlated Photon States", *Science* 301, 196 (2003), DOI: `10.1126/science.1085946` (cited on pg. 65).

[Wal+09]   M. Wallquist, K. Hammerer, P. Rabl, M. Lukin, and P. Zoller, "Hybrid quantum devices and quantum engineering", *Phys. Scr.* T137, 014001 (2009), DOI: `10.1088/0031-8949/2009/T137/014001` (cited on pg. 66).

[Wil+07]   T. Wilk, S. C. Webster, A. Kuhn, and G. Rempe, "Single-atom single-photon quantum interface", *Science* 317, 488 (2007), DOI: `10.1126/science.1143835` (cited on pg. 65).

[Wol+15]   E. E. Wollman, C. U. Lei, A. J. Weinstein, J. Suh, A. Kronwald, F. Marquardt, A. A. Clerk, and K. C. Schwab, "Quantum squeezing of motion in a mechanical resonator", *Science* 349, 952 (2015), DOI: `10.1126/science.aac5138` (cited on pg. 67).

[Wu+86]   L.-A. Wu, H. J. Kimble, J. L. Hall, and H. Wu, "Generation of Squeezed States by Parametric Down Conversion", *Phys. Rev. Lett.* 57, 2520 (1986), DOI: `10.1103/PhysRevLett.57.2520` (cited on pg. 68).

[YFI10]   S. T. Yilmaz, P. Fallahi, and A. Imamoğlu, "Quantum-Dot-Spin Single-Photon Interface", *Phys. Rev. Lett.* 105, 033601 (2010), DOI: `10.1103/PhysRevLett.105.033601` (cited on pg. 65).

[Zha+09]   B. Zhao, Y.-A. Chen, X.-H. Bao, T. Strassel, C.-S. Chuu, X.-M. Jin, J. Schmiedmayer, Z.-S. Yuan, S. Chen, and J.-W. Pan, "A millisecond quantum memory for scalable quantum networks", *Nature Phys.* 5, 95 (2009), DOI: `10.1038/nphys1153` (cited on pg. 84).

[Zol+04]   P. Zoller, J. I. Cirac, L. Duan, and J. J. García-Ripoll, "Quantum optical implementation of quantum information processing", in: *Quantum Entanglement and Information Processing, École d'été de Physique des Houches Session LXXIX*, ed. by D. Estève, J.-M. Raimond, and J. Dalibard, (2004) (cited on pg. 84).

4.3. Supplementary Information

4.3.1. Device fabrication and characterization

The optomechanical device used for this experiment (see Figure 4.5) is fabricated from a silicon-on-insulator wafer, with a device layer thickness of 250 nm and 3 μm of buried oxide. The structures are patterned using an electron beam writer and are then transferred into the top silicon layer in an SF_6/O_2 atmosphere using a reactive ion-etcher. The devices are finally released and undercut using concentrated hydrofluoric acid. We design the nanobeams such that the fundamental mechanical breathing mode is at 5.3 GHz (cf. Figure 4.3a, main text) and the optical resonance is around 1550 nm (the measured wavelength for the device used here is 1556 nm) [Cha+12]. The optical and the mechanical modes are co-localized in the center of the beam, where we create a defect region of the photonic- and phononic-bandgap, allowing for an optomechanical coupling rate $g_0/2\pi = 825$ kHz. In order to minimize the thermalization time to the surrounding bath we opted, unlike previous designs, to not use any additional phononic shielding. As a consequence, the mechanical quality factors at base temperature are found to be around $1.1 \cdot 10^6$ (see section *Mechanical response to optical pulses*), compared to values above 10^7
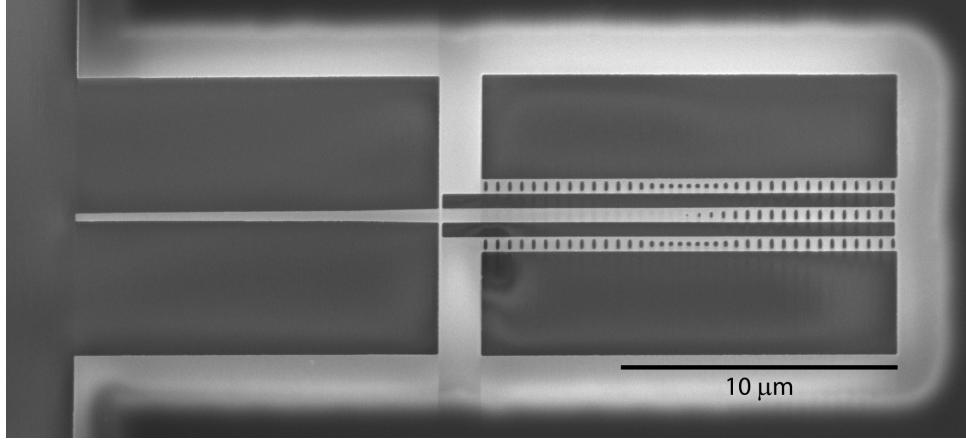
FIGURE 4.5.: **Optomechanical device.** Shown is a scanning electron microscope image of a set of nanobeams, which are fabricated in silicon, as described in the text. Light is coupled into the central, adiabatically tapered waveguide through a lensed optical fiber (not shown) from the left of the image. The field then evanescently couples to each nanobeam (top and bottom). The two devices have slightly different resonance frequency, which makes it possible to distinguish them.

with a phononic shield [Mee+15]. The laser pulses are coupled directly into a tapered waveguide through an optical fiber with a lensed tip [Mee+14], achieving efficencies of about 60%. The optical mode of the nanobeam is evanescently coupled to the waveguide, which is terminated with a periodic array of holes, acting as a mirror, allowing us to collect the light in reflection. For this experiment we chose a critically coupled device (internal losses equal external losses) with an optical linewidth $\kappa_c/2\pi$ of approximately 1.3 GHz. This places us well within the so-called resolved-sideband regime ($\omega_m > \kappa_c$).

4.3.2. Setup

In this section, we provide a detailed description of the experimental setup. It consists of a 'pump part', 'detection part', and the 'electronic control part' (cf. Figure 4.6).
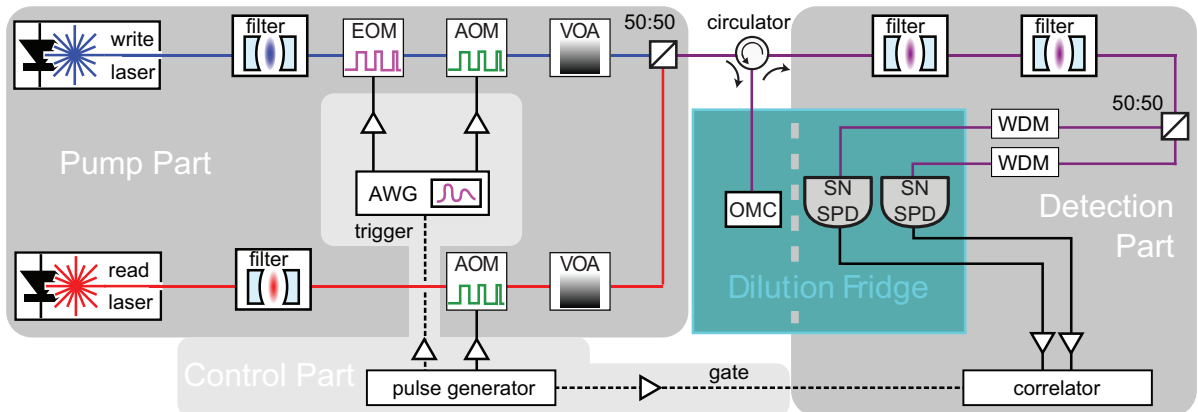

FIGURE 4.6.: **Detailed experimental setup.** See text for a detailed description.

Pump part

We use two identical, tunable continuous-wave (CW) lasers (New Focus 6728) as our light sources. The lasers are detuned and stabilized to the blue and red side respectively of the device's cavity resonance (1556.21 nm). The detuning is set to be the mechanical frequency (5.307 GHz). The two lasers separately pass through voltage-controlled tunable optical filters (MicronOptics FFP-TF2, free spectral range ∼18 GHz, bandwidth ∼50 MHz) to suppress any potential background emissions dispersed in frequency space. In order to create short optical pulses we modulate the filtered CW fields using acousto-optic modulators (AOM; IntraAction) and an additional electro-optic amplitude modulator (EOM; EOSpace). We employ variable optical attenuators (VOA; Sercalo) on each path to control the pulse power. The pulses are combined on a variable optical coupler and then sent to the device in the dilution refrigerator (Vericold E21) via an optical circulator. At the device (OMC; optomechanical crystal), the optomechanical interaction with the blue (red) detuned pulses generates down-(up-) converted photons, whose frequency is on resonance with the device's optical cavity frequency. The scattered photons are reflected back from the OMC into the optical fiber and routed to the detection part through the output port of the circulator.

Detection part

Two voltage-controlled optical filters (MicronOptics FFP-TF2, specification as above) are installed in series at the beginning of the detection path. These filters are tuned on resonance with the OMC cavity frequency such that they only allow (anti-) Stokes scattered photons to be transmitted, while strong off-resonant pump photons are rejected (suppression of about 84 dB). After the filters, a 50:50 beam splitter divides the path. Each output is additionally filtered by broadband wavelength-division multiplexors (WDM), and fiber-coupled to two superconducting nanowire single photon detectors (SNSPD; PhotonSpot, detection efficiency ∼90%, dark count rate <10 Hz). The SNSPDs are mounted on the 1 K plate inside the dilution refrigerator. Upon receiving a photon the SNSPD generates a brief voltage spike, which is then electrically registered by a time-correlated single photon counting module (TCSPC; PicoQuant TimeHarp 260 NANO). The overall efficiency of detecting a photon leaving the OMC is ∼2.7% (see below).

Control part

In order to generate programmable optical pulses and to detect photons synchronously, we use a digital pulse generator (DPG; Highland Technology P400) and an arbitrary waveform generator (AWG; Agilent Technologies 81180A). We first program the DPG to generate a TTL gate voltage signal for the AOM on the read (red) path and to trigger the TCSPC synchronously. The DPG additionally triggers the AWG, which then generates a TTL gate voltage for the AOM and a voltage pulse for the EOM on the write (blue) path.

4.3.3. Mechanical response to optical pulses

Over the past few years, several experiments have demonstrated precise control over optical and mechanical states through continuous optomechanical driving, including coherent
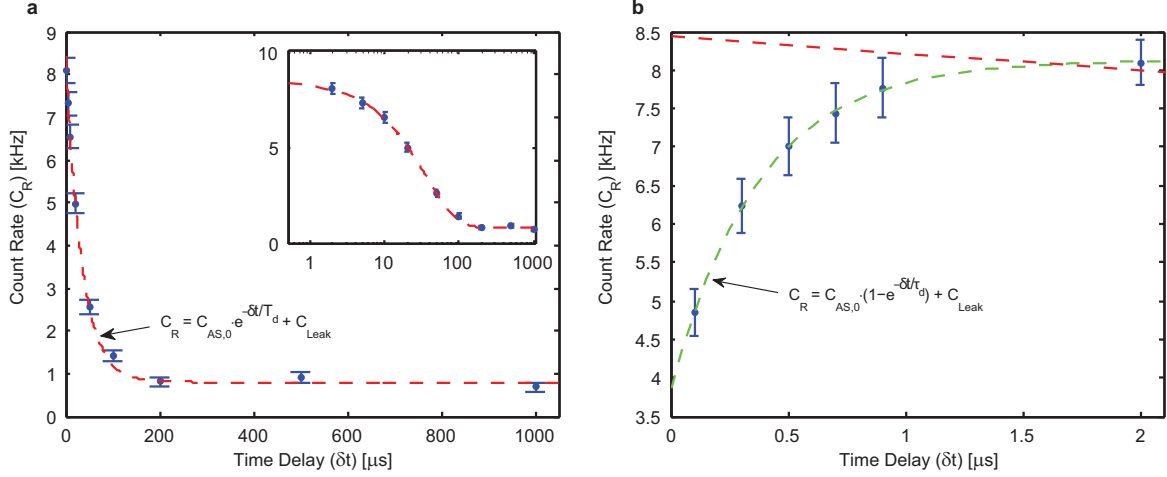
FIGURE 4.7.: **Pump-probe measurement of the mechanical response.** We send in a brief, intense blue detuned optical pulse (pump) and measure the mechanical response via red detuned optical probe pulse as a function of pump-probe time delay (δt). **a** Long-term mechanical response. The result fits well with a simple exponential decay (red dashed line; see the equation in the plot) with a damping time constant (T_d) of 34.4 μs. The inset shows the same data/fit with a logarithmic scale on the x axis. $C_{AS,0}$ is the extrapolated $C_{AS}(\delta t = 0)$. **b** Short-term mechanical response. The data is fitted to a simple exponential curve (green dashed line; see the equation in the plot). The fitted time constant (τ_d) is 0.37 μs. The fit results of long-term response (red dashed line) projected to 0 μs delay is also shown for comparison. As the pump pulse had 5 times stronger energies than the write pulses in the correlation experiment, it is expected that the delayed heating occurs on longer time scale, due to the temperature dependence of the thermal conductivity of silicon [Mee+15]. Error bars in **a** and **b** represent a 68% confidence interval.

state transfer [Pal+13; Fio+11; Ver+12] and microwave-to-optics conversion [Boc+13; And+14; Bag+14]. Due to the unavailability of the regime of single-photon strong co-operativity, strong drive fields have to be used in order to achieve the wanted coupling strength [Akr+10]. This leads to unwanted heating effects, in particular in the optical domain. Since the mechanism of optical absorption couples only indirectly to the mechanical mode of interest [Mee+14], using short optical pulses as nonstationary drive fields can substantially suppress the heating on short time scales – in particular at low temperatures [Mee+15].

Here, we probe the thermal response of the mechanical mode by pump-probe type measurements; we first send a short blue-detuned pump pulse onto the OMC cavity to intentionally heat the mode, and subsequently inject a red-detuned probe pulse to read out the mode's phonon occupancy. By repeating the experiment with varying time delay between the pump and the probe pulses, we monitor time-dependent evolution of the mode's phonon occupancy with a fixed initial impulse heating. The time delay δt is defined as the delay between the end of the pump (blue) pulse and the start of the probe (red) pulse detection window, as indicated in Figure 4.4a in the main text. In that way the probing is performed after the optical absorption of the pump photons is completed. In order to ensure that the mechanical mode fully re-thermalizes to the bath, we set the duty cycle of sending another blue pulse after the red pulse to be one millisecond. For an improved signal to noise ratio, the pulse energies of the blue (200 fJ) and red pulses

(2 pJ) used here are substantially larger than in the cross-correlation measurements.

The effective mode temperature is inferred from the average count rate observed after sending the red pulse (C_R). C_R can be decomposed into three terms: (1) the rate proportional to the (on-resonance) anti-Stokes Raman scattered pump photons (C_{AS}), (2) the term corresponding to pump photons leaked through the optical filters (C_{Leak}), and (3) the additional anti-Stokes scattering term due to heating (ref. [Mee+15]) of the mode during the readout pulse (C_{Heat}). We minimize C_{Heat} by only taking into account the first 30 ns of the red pulse as 'logical' red pulse. C_{Leak} gives a constant offset to the signal. C_{AS} directly reflects the mode's effective temperature, as the anti-Stokes scattering rate is proportional to the average number of phonons (n_m) in the mode (see Figure 4.3a in the main text). To that end, we deduce the following equation

$$C_R(\delta t) = C_{AS}(\delta t) + C_{Leak} = \alpha \cdot n_m(\delta t) + C_{Leak},$$

in which α is the constant of proportionality.

The long-term response of the mechanical mode to the initial blue pump pulse is shown in Figure 4.7a. It exhibits an exponential decay with a time constant of $T_d = 34.4$ μs, which is interpreted as the mechanical damping time. The corresponding mechanical quality factor is then $Q = \omega_m \cdot T_d \approx 1.1 \cdot 10^6$.

In addition, we probe the short-term response of the mechanics within one microsecond after the blue pulse in more detail (Figure 4.7b). We observe an increase of C_R with a time constant of 0.37 μs (fit to a simple exponential curve). This data reveals slow turn-on dynamics of pulse-induced heating, as previously studied in reference [Mee+15]. This time constant is even shorter than the decay of the cross-correlations (see Figure 4.4c in the main text), which we attribute to the increased thermal conductivity of silicon at higher temperatures, caused by absorption of increased optical pump energies.

4.3.4. Characterization of the detection scheme

Detection Efficiency

We first calibrate the fiber-to-chip coupling efficiency (η_{fc}) by sending in light far off-resonant from the OMC cavity and then measure the reflected power ($\eta_{fc} = 60.3\%$ one-way). The device impedance ratio (η_c), i.e. the ratio of external coupling losses κ_{ext} to total losses κ_c, is measured through the depth and the linewidth of the optical resonance, which we find to be $\eta_c = \kappa_{ext}/\kappa_c = 0.5$. The detection efficiency of scattered photons for each detector (η_i; i=1,2) consists of η_{fc}, η_c, the total losses of the remaining detection paths ($\eta_{path,i}$), and the SNSPDs' quantum efficiencies ($\eta_{QE,i}$). To measure η_i, pulses with calibrated energy are sent off-resonantly to the OMC (P_{in}), and the reflected photons transmitted through the optical filters are detected by the SNSPDs (P_{out}). P_{in}/P_{out} corresponds to $\eta_{fc} \cdot \eta_{fc} \cdot \eta_{path,i} \cdot \eta_{QE,i}$, which we measure to be 0.013 for SNSPD1 and 0.019 for SNSPD2. Therefore, we deduce $\eta_i = \eta_c \cdot \eta_{fc} \cdot \eta_{path,i} \cdot \eta_{QE,i}$ to be

$$\eta_1 = 1.1\%$$
$$\eta_2 = 1.6\%.$$

The detection efficiency of SNSPD1 (characterized quantum efficiency $\eta_{QE,1} = 65\%$) is lower than SNSPD2 (characterized quantum efficiency $\eta_{QE,2} = 90\%$), as we needed to

reduce the bias current to prevent the detector from latching [NTH12]. This latching is probably caused by a nearby heater of the dilution refrigerator. It also results in a slow drift in the quantum efficiency of SNSPD1. We note that the deduced $\eta_{\mathrm{path,i}}$ come from the various optical elements in the beam path of the detection part and are in good agreement with their specified insertion losses.

Scattering rates and optomechanical coupling rate

With the total detection efficiency of resonantly generated cavity photons, we can estimate the pair generation probability per write pulse (optical energy $E_{\mathrm{opt}} \sim 40$ fJ) to be $p \sim 3.0\%$, including the effects of a finite starting temperature and leaked pump photons. The latter is calibrated by sending detuned optical pulses ($E_{\mathrm{opt}} \sim 40$ fJ, $\omega_{\mathrm{L}} = \omega_{\mathrm{c}} - \omega_{\mathrm{m}} - 2\pi \cdot 200$ MHz) to the device. The generated optomechanical sidebands are now blocked by the filters and only leaked pump photons are detected. We measure a suppression of the pump pulse by 84 dB compared to an on- resonance transmission. Thus, approximately 1 out of 25 photons detected during the write pulse is a leaked pump photon. Knowing the scattering rate and the energy of the detuned pump pulse, we can determine the single-photon coupling rate of our OMC to be

$$g_0 = \frac{\partial \omega_{\mathrm{c}}}{\partial x} \sqrt{\frac{\hbar}{2m\omega_{\mathrm{m}}}} = 2\pi \cdot 825 \text{ kHz}.$$

With this coupling rate, we can estimate the state-transfer efficiency of the red-detuned optical readout pulse of $E_{\mathrm{opt}} = 50$ fJ to be $\varepsilon_{\mathrm{R}} = 3.7\%$, where

$$\hat{a}_{\mathrm{opt,out}} \approx \sqrt{1 - \varepsilon_{\mathrm{R}}} \hat{a}_{\mathrm{opt,in}} + e^{i\phi} \sqrt{\varepsilon_{\mathrm{R}}} \hat{a}_{\mathrm{mech,in}}.$$

Here, $\hat{a}_{\mathrm{opt,in(out)}}$ are the annihilation operators of the temporal optical input (output) mode of the cavity resonance, $\hat{a}_{\mathrm{mech,in}}$ the mechanical mode before the interaction, and ϕ an arbitrary but fixed phase between the inputs [Hof+11].

4.3.5. Definition and properties of the second order correlation function

We define the normalized second-order correlation function for two, not necessarily different modes α and β, and the respective annihilation operators $\hat{a}_\alpha$ and $\hat{a}_\beta$, to be (references [Kuz+03; MW95] and references therein)

$$g^{(2)}_{\alpha\beta} = \frac{\langle : \hat{a}^\dagger_\alpha \hat{a}_\alpha \hat{a}^\dagger_\beta \hat{a}_\beta : \rangle}{\langle \hat{a}^\dagger_\alpha \hat{a}_\alpha \rangle \langle \hat{a}^\dagger_\beta \hat{a}_\beta \rangle},$$

where $: \hat{O} :$ denotes normal ordering of the operators. For the autocorrelation of the optical field (photons scattered by the write pulse), $\alpha = \beta = \mathrm{o}$, for the mechanical field $\alpha = \beta = \mathrm{m}$ and for the cross-correlation $\alpha = \mathrm{o}$, $\beta = \mathrm{m}$. By introducing effective modes γ, δ it can be seen that this correlation-function is independent of losses in the detection. Assuming the loss angles φ_α and φ_β for detection of modes α, β, we define the annihilation operators of the effectively detected modes γ, δ

$$\hat{a}_{\gamma/\delta} = \cos(\varphi_{\alpha/\beta}) \hat{a}_{\alpha/\beta} + \sin(\varphi_{\alpha/\beta}) \hat{l}_{\alpha/\beta}$$

4. Non-classical correlations between single photons and phonons

by coupling the original modes α, β to modes l_α and l_β represented by the annihilation operator $\hat{l}_{\alpha/\beta}$. As the detected modes γ, δ have frequencies in the optical domain, we can assume the in-coupled modes l_α, l_β to be in their respective ground state. Tracing over l_α, l_β, we find that

$$g^{(2)}_{\gamma\delta} = g^{(2)}_{\alpha\beta}$$

i.e. the second order correlation function is independent of losses or, in the case of the mechanical mode, of "ineffective" partial state-transfer to the cavity mode. Thus, e.g. $g^{(2)}_{\mathrm{mm}}$ is equivalent to the autocorrelation of the photons scattered by the read pulse.

For autocorrelation measurements, we use a Hanbury Brown and Twiss setup, by splitting the mode on a symmetric beamsplitter and sending it to a pair of detectors. We define the modes detected by the individual detectors d_1, d_2 with their annihilation operators

$$\hat{a}_{1/2} = \cos(\theta)\hat{a}_\alpha \pm \sin(\theta)\hat{l}_{\mathrm{d}}$$

with the splitting angle θ of the beam splitter and the annihilation operator $\hat{l}_{\mathrm{d}}$ of the second input of the beamsplitter. The input state can as before be approximated to be in its vacuum state. We find that the autocorrelation of mode α equals the cross-correlation of the two detectors:

$$g^{(2)}_{\alpha\alpha} = g^{(2)}_{12}.$$

For a definition in terms of probabilities, see below.

δt	$0.1\mu s$	$0.6\mu s$	$1.1\mu s$	$2.1\mu s$	$3.1\mu s$	total	$0.1\mu s^*$
$N(R \cap W)$	202	153	144	113	127		34
$N(R_1 \cap R_2)$	13	24	23	36	37		0
$N(W_1 \cap W_2)$	16	15	17	12	20	80	16
$N(R_1)$	13.172	16.523	18.751	18.316	23.629		966
$N(R_2)$	17.490	22.278	25.394	26.122	31.892		1145
$N(W_1)$	12.471	12.061	13.051	11.870	15.032	64.485	12.471
$N(W_2)$	19.409	18.616	20.176	18.329	23.601	100.131	19.409
T	38.806.017	38.829.923	39.958.216	35.712.159	47.964.927	201.271.242	38.806.017

TABLE 4.1.: **Counts of the cross-correlation measurements.** The row label 'N(event)' represents the number of counts for a certain event, e.g. detection of a photon during the measurement window of read pulse on detector 1/2 ($R_{1/2}$), or the coincidence of a detection event of a subsequent write and read pulse on either detector 1 or 2, $R \cap W = (R_1 \cup R_2) \cap (W_1 \cup W_2)$. T denotes the total number of pulse pairs sent to the optomechanical device. For the calculation of the autocorrelation function of the read pulse, only counts from the delay setting δt are used, as the delayed heating of the blue pulse (cf. Figure 4.4) influences the mechanical state. For the autocorrelation function of the write pulse, counts from all delay settings are summed, as the mechanical state is reinitialized by cryogenic cooling before measurement, independent of the delay δt. The numbers for this are summarized in the column labeled 'total'. The highest reported cross-correlation value was obtained by reducing the measurement window of the read pulse from 55 ns to 30 ns, with a delay of $\delta t = 100$ ns between the write and the read pulse. The counts for this evaluation window are presented in the column marked with *. The underlying dataset is the same as for the standard evaluation period of 55 ns, i.e. the first column.

4.3.6. Statistical Analysis

Due to the low detection probability, the uncertainty in the estimation of the second-order correlation functions is completely dominated by the estimation of the coincidence rate $\langle : \hat{a}_\alpha^\dagger \hat{a}_\alpha \hat{a}_\beta^\dagger \hat{a}_\beta : \rangle$ of the two modes α, β. As the absolute number of coincidences is low in some measurements, Gaussian statistics cannot be used for estimating uncertainties. Instead, we use the likelihood function based on the binomial distribution for estimating the probability p of the underlying process, i.e. to obtain N counts in T tries

$$L(p, N, T) = \frac{1}{K} p^N (1-p)^{T-N}.$$

The normalization K is chosen such that $\int_0^1 L(p, N, T) dp = 1$. The upper and lower uncertainty σ_+ and σ_- are chosen numerically, such that they cover a 68% confidence interval around the maximum likelihood estimator $p_{\mathrm{ML}} = N/T$, i.e. $\int_0^{p_{\mathrm{ML}} - \sigma_-} L(p, N, T) dp = 0.16$, $\int_{p_{\mathrm{ML}} + \sigma_+}^1 L(p, N, T) dp = 0.16$.

For the classical bound of the cross-correlation, $g_{\mathrm{cb}}^{(2)} = \sqrt{g_{\mathrm{mm}}^{(2)} \cdot g_{\mathrm{oo}}^{(2)}}$, the likelihood functions of the individual autocorrelations are convoluted. Due to their asymmetry, the maximum likelihood estimator of the classical bound is slightly lower than when using the individual maximum likelihood estimators $g_{\mathrm{cb,ML}}^{(2)} \leq \sqrt{g_{\mathrm{mm,ML}}^{(2)} \cdot g_{\mathrm{oo,ML}}^{(2)}}$.

As estimators for the cross-correlation function, the probabilities P of a coincidence- or single detection event during the read (R) and write pulse (W) were used, with $g_{\mathrm{om}}^{(2)} = P(W \cap R)/P(R)P(W)$. This is valid for low event probabilities $P \ll 1$. Autocorrelations were estimated by probabilities of coincidence- and single detection events on individual SNSPDs (1,2), $g_{\mathrm{yy}}^{(2)} = P(X_1 \cap X_2)/P(X_1)P(X_2)$ during the evaluation periods of the write ($y = \mathrm{o}$, $X = W$) and read ($y = \mathrm{m}$, $X = R$) pulse, respectively. The statistics of the cross-correlation measurements are summarized in Table 4.1.

For the read pulse, only the first 55 ns of the pulse were evaluated (cf. Figure 4.4, main text). A further reduction of the evaluation period to $t_{\mathrm{eval}} = 30$ ns (R^*) has the advantage of reducing the influence of optical absorption of pump photons from the read pulse, while still obtaining solid statistics for the cross-correlation, $g_{\mathrm{om}}^{(2)}(\Delta n = 0, \delta t = 100 \text{ ns}, t_{\mathrm{eval}} = 30 \text{ ns}) = 19.6 - 2.8 + 3.9$. However, this reduction also results in a much lower state transfer efficiency $\varepsilon_{\mathrm{R}}^* \approx 0.1\%$ (compared to $\varepsilon_{\mathrm{R}} = 3.7\%$ above; see section *Characterization of the detection scheme*). As a consequence we cannot obtain independent statistics on the autocorrelation function of the read pulse, as the number of pulse sequences is too low to observe coincidences during the reduced read pulse $N(R_1^* \cap R_2^*) = 0$. Thus, no independent classical bound g_{cb}^* can be obtained for this case. As the measurement is identical to the one with longer evaluation window in the first column of Table 4.1, it is reasonable to assume the same autocorrelation of the mechanical state and thus the same classical limit.

We note that slight differences in the polarization of the two input lasers and the optimal axis of the SNSPDs can lead to different detection rates of leaked pump photons between the read and the write pulse. While this does not influence the cross-correlation measurement, it is important to use the same laser source for the sideband asymmetry measurements.

4.3.7. Interpretation of the cross-correlation measurements

Classical bound

The classical bound $g_{\mathrm{cb,ML}}$ is found to be slightly above 2, the value expected for a thermal state of the mechanical system (cf. Figure 4.4c, main text). Although this increase of the autocorrelation is not significant in our measurements, a behavior like this would be expected in the case of mixed thermal states of different temperatures, caused e.g. by fluctuations in the absorbed power. Effects that usually decrease the measured autocorrelation function of a thermal state, such as dark counts of the detectors and instantaneous heating by the read pulse, do not play a major role in our experiment due to the choice of pulse parameters. In conclusion, the classical bound in the present experiment is slightly elevated compared to cross-correlation experiments in atomic physics or non-linear optics, where the classical bound is usually assumed to be [San+11] below 2.

Decay of cross-correlations due to delayed heating

The cross-correlation can be interpreted as

$$g_{\mathrm{om}}^{(2)} \sim \frac{\langle n_{\mathrm{m}} \rangle_{\mathrm{h}}}{\langle n_{\mathrm{m}} \rangle}$$

where $\langle n_{\mathrm{m}} \rangle_{\mathrm{h}}$ is the average number of mechanical excitations in the state heralded on a detection event of the write pulse (indicating the presence of an anti-Stokes scattered photon), and $\langle n_{\mathrm{m}} \rangle$ the average number of unheralded events (essentially probing the thermal excitation of the system when $p \ll 1$). In case of a delayed heating, the thermal occupation of the system is a function of the delay δt after the write pulse $\langle n_{\mathrm{m,th}} \rangle = \langle n_{\mathrm{m,th}} \rangle (\delta t)$. Assuming our cross-correlation is dominated by the thermal occupation, we obtain for $\delta t \ll T_{\mathrm{d}}$,

$$g_{\mathrm{om}}^{(2)}(\delta t) \sim \frac{1 + \langle n_{\mathrm{m,th}} \rangle (\delta t)}{\langle n_{\mathrm{m,th}} \rangle (\delta t)},$$

which clearly decays in the case of substantial delayed heating as observed here (cf. Figure 4.7). Theoretical models of the complex thermodynamic non-equilibrium processes contain many device dependent parameters [Mee+15], which will be subject of further studies.

Estimation of the heralded single-phonon fidelity

In general, the toolbox of quantum optics provides unique means for quantum state control of various systems [Zol+04]. As an example we discuss the application of single-photon detection for the heralded generation of single-phonon Fock states of our mechanical resonator [Hof+11; VAK13; Gal+14]. To estimate the fidelity of the single-phonon state directly after heralding on the detection of a resonant photon generated by the write pulse, we need to know all contributions to the diagonal of the density matrix, which are not a single phonon. These contributions can either be higher excitations by thermal contribution, multi-pair generation, or vacuum states by false positive heralding events. Higher excitations can be estimated by the auto-correlation function of the heralded state, which is related to the cross-correlations function [Zha+09]. As the target is to

estimate the state immediately after heralding it, we reduce the evaluation window of the read pulse as much as possible, while maintaining reasonable statistics on the cross-correlation (cf. Table 4.1). From measured $g_{\mathrm{om}}^{(2)}(\Delta n = 0, \delta t = 100$ ns$, t_{\mathrm{eval}} = 30$ ns$) = 19.6 - 2.8 + 3.9$, we infer an auto-correlation function for the heralded mechanical state of $g_{\mathrm{mm,heralded}}^{(2)} \approx 0.22 \pm 0.04$, which approximately relates to the ratio of probabilities of higher excitations $p_{n>1}$ to single phonon excitations $p_{n=1}$, $2 \cdot p_{n>1} \approx g_{\mathrm{mm,heralded}}^{(2)} \cdot p_{n=1}^2$. In the meantime, the main contribution for non-zero $p_{n=0}$ (i.e. the probability of the heralded mechanical state being the ground state) is false positive heralding events, i.e. dark counts and leaked pump photons. With the known ratio of true positive to false positive heralding events (cf. section *Characterization of the detection scheme*), we obtain an estimate of $p_{n=0} \sim 1/25$. With these conservative estimates, we obtain a heralded Fock-state fidelity of $p_{n=1} = 87.7 \pm 1.2\%$ on the basis of the standard system Hamiltonian of the optomechanical device [Hof+11].

5. Hanbury Brown and Twiss interferometry of single phonons from an optomechanical resonator

Control over single quanta of energy in a system plays an important role in quantum information science [Win13; Har13]. In a bosonic system, such as an optical or mechanical resonator, states containing a discrete number of excitations are called Fock states. They are the basis of a vast number of quantum information protocols, in particular those Fock states with a single excitation per mode [BB84; GHZ89; CZ95]. Here, I will report on my work on Hanbury Brown and Twiss interferometry of single phonons, first published as reference [Hon+17], preceded by a summary of the scientific context of this manuscript.

Sources of single Fock excitations can be characterized with a Hanbury Brown and Twiss (HBT) interferometer, which refers to a pair of detectors coupled to the emission mode of the source. For a source emitting into a single spatial mode, this can be achieved for example by using a beam splitter, with one detector monitoring the power at each of the two output ports of the beam splitter. As mentioned in the previous chapter, the cross-correlation of the two output ports is equivalent to the normalized autocorrelation

$$g_{aa}^{(2)}(t,\tau) = \frac{\langle :\hat{a}^\dagger(t)\hat{a}(t)\ \hat{a}^\dagger(t+\tau)\hat{a}(t+\tau): \rangle}{\langle \hat{a}^\dagger(t)\hat{a}(t) \rangle \langle \hat{a}^\dagger(t+\tau)\hat{a}(t+\tau) \rangle} \tag{5.1}$$

of the input mode $\hat{a}$, i.e. the second order coherence of the source (with itself).

In their original experiments, Robert Hanbury Brown and Richard Q. Twiss intended to determine the angular diameter of an astronomical object, in their case the star Sirius, while avoiding the requirement of an interferometricaly stable telescope with a large base line[1] [HT56b; HT56a]. Based on earlier work with radio frequency telescopes [HJD52], they realized that the stability criterion in intensity interferometers is based on the coherence length rather than the wavelength of the source, thus easing the requirements for sub-wavelength stabilization of long base lines. Hence, by using a measurement of the spatial autocorrelation to infer the first order coherence, i.e. the potential interference visibility between two spatially separate parts of a wave emitted by a source, they managed to increase the effective base lines such that they were able to resolve the angular diameter of Sirius.[2]

---

[1] The latter is necessary to form an image of the star with great enough resolution to determine its geometrical properties, as the formation of the image in the focal plane of the telescope is based on interference of spatially separate parts of the wave collected by the telescope.

[2] While they were able to realize long base lines with their new method, intensity interferometers require more intensity, respectively integration time, than classical telescopes, as they are based on coincidences in the two detectors. In fact, they state that for this reason, Sirius was the only star bright enough for their experiment.

5. Hanbury Brown and Twiss interferometry of single phonons

While the effect HBT used for their astronomical observations is of classical nature, the quantum treatment of the effect attracted considerable attention. The correlations they observed between two partially coherent light beams seemed to contradict an absence of correlations in an earlier experiment with a very similar configuration [ÁJV55; BF56]. While it was found that both observations were indeed compatible [Pur56; TH57; Ján57], the controversy lead to the realization that HBT type experiments, and more generally the second order coherence, are of great interest to understand the quantum properties of light [Man58]. Glauber's formalism for the treatment of quantum fields [Gla63b; Gla63a] enabled to formulate testable inequalities which distinct the predictions of a classical field theory from those of a quantum field theory. Of those, two inequalities are of great importance [Man86].

First, as the variance of the intensity is always positive, it follows for classical waves that

$$g^{(2)}(t,0) \geq 1. \tag{5.2}$$

In a quantum language this means that a classical field will always exhibit poissonian counting statistics. A quantized field can violate this inequality, for example with a fock state $|n\rangle$ in mode $\hat{a}$ at time t resulting in a subpoissonian autocorrelation of $g_{aa}^{(2)}(t,0) = 1 - 1/n \not\geq 1$. In particular, a Fock state with a single excitation $|1\rangle$ ideally exhibits $g_{aa}^{(2)}(t,0) = 0$. In other words, a single excitation cannot be detected at both outputs of a beam splitter simultaneously. This anti-correlation is a typical particle-like feature occurring naturally in fermionic systems, but representing a genuine quantum feature in bosonic systems[3].

The second relevant inequality is based on the Cauchy Scharz inequality discussed in the previous chapter. For a single mode, it can be reformulated as

$$g^{(2)}(t,0) \geq g^{(2)}(t,\tau) \tag{5.3}$$

for a steady state[4]. This classical property is called bunching in a quantum language, referring to the tendency of bosons to occur together, i.e. in bunches, rather than separate [MM66]. Anti-bunching of bosons, i.e. a tendency of excitations to occur at different times, rather than together, is a genuine feature of a quantum field. Note that the second inequality is independent of the first, though a measurement of the first often implies a violation of the second, with notable exceptions [Man86].

These two effects have been predicted for resonance fluorescence by Carmichael and Walls [CW76]. While anti-bunching was observed soon after [KDM77], anti-correlation in resonance fluorescence could initially only be inferred for the emission of single atoms [KDM78; DM78], but was masked in the optical field by fluctuations in the number of emitting atoms. Sub-Poissonian photon number statistics could eventually be observed by ensuring that only a single atom was present [SM83], or more generally sub-Possonian source number statistics [TS85; TRS87].

The quality of single photon sources was drastically improved by the advent of heralding schemes [ST85; JW85] and the trapping of emitters [DW87]. In a heralding generation of

---

[3] Note that anti-correlations $g_{aa}^{(2)}(t,0) \leq 1$ imply sub-Poissonian photon number statistics [Man79] and vice versa, but strictly speaking they are different measurements.

[4] If the system is not in a steady state, the autocorrelation at different times is not necessarily equal and thus the inequality has the slightly more complex form $\sqrt{g^{(2)}(t,0)g^{(2)}(t+\tau,0)} \geq g^{(2)}(t,\tau)$.

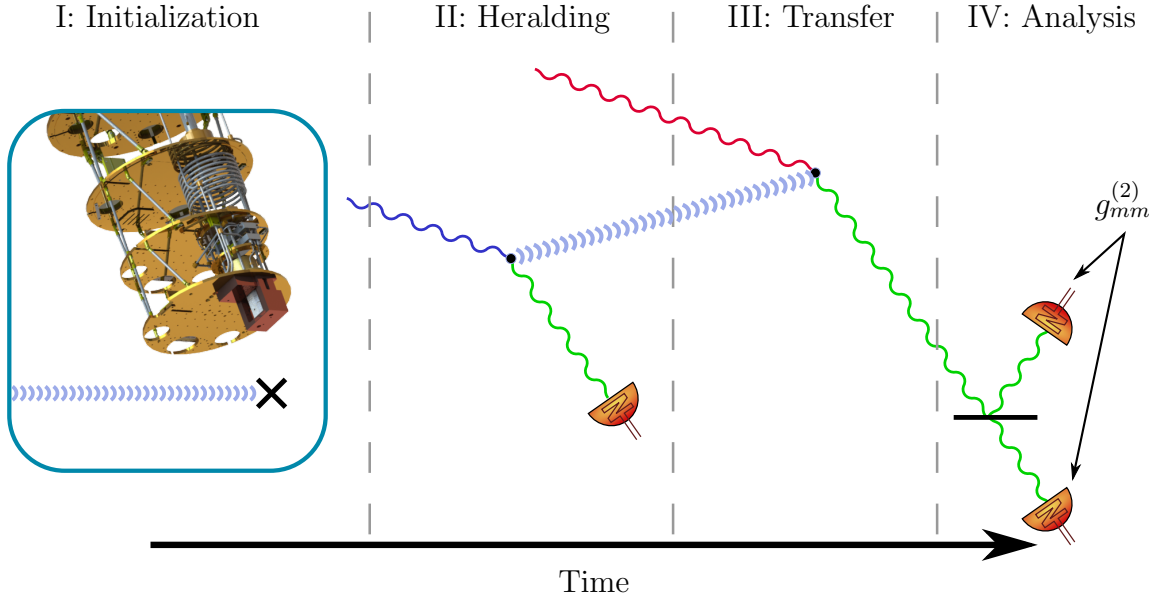| I: Initialization | II: Heralding | III: Transfer | IV: Analysis |

Time

FIGURE 5.1.: **Heralded Single Phonon Generation.** First, the mechanical modes is initialized in its groundstate by cryogenic cooling. The detection of a signal photon from a Stokes scattering event heralds the presence of an idler phonon. The latter is transferred to the optical domain by means of anti-Stokes scattering (step III) and analyzed in a Hanbury Brown and Twiss setup (step IV).

single photons, a photon pair emission process is employed, in which the detection of a first photon (called signal) can be used to herald the presence of a second single photon. Such photon pair processes can be found for example in cascaded fluorescence [GRA86] and spontaneous parametric down conversion [WJ85; HM86]. In contrast, trapping of an emitter allows for exact control over the number of emitters, thereby allowing for high quality single photons from a single fluorescence process [DW87].

With more and more single photon sources emerging [Bas+92; Mic+00; Bro+00], the autocorrelation $g^{(2)}(0)$ became a figure of merit to determine the quality of the single photon states [DW87; DDM96; Bru+99; Bro+00]. Moreover, for solid state emitters, it often is of interest, how many emitters are coupled to the optical mode. As the molecules and crystal defects used as fluorescent single photon sources are drastically smaller than the emitted wavelength, two nearby emitters cannot necessarily be optically resolved. However, a HBT experiment can be used to verify that only a single emitter is present, by demonstrating an autocorrelation $g^{(2)}(0) < 1/2$ below the value of a two photon state [DW87]. State of the art single photon sources can reach extremely low values of $g^{(2)}(0) < 10^{-2}$ [Dal+12; Hig+16].

HBT experiments have also been studied with other bosonic and fermionic systems, including electrons [Oli+99; Hen+99], atoms [YS96; Sch+05; Jel+07], plasmons [Kol+09] and subatomic particles [BGJ90].

For mechanical oscillators, HBT type intensity interferometry was recently realized by Cohen et al. [Coh+15], observing the lasing threshold of optomechanically amplified spontaneous emission. The preparation of single phonons, necessary to observe a violation of either inequality (5.2) or (5.3), can readily be achieved for the motion of trapped ions

5. Hanbury Brown and Twiss interferometry of single phonons

[Mee+96; Lei+03], but remained elusive in massive resonators.

While individual phonons were previously generated by transferring an excitation from a superconducting qubit to a mechanical resonator [OCo+10], the system lacked suitable single microwave photon detectors to perform an autocorrelation measurement. In parallel to the experiment presented in the following, single phonons were generated in electromechanical systems exhibiting longer coherence times [Chu+17; Ree+17], which enabled the tomography of the mechanical state [Sat+18; Chu+18], as was previously realized for the motion of trapped ions [Lei+96].

In the following, I will present my work on a HBT experiment with optically generated heralded single phonons. The experiment in this form was proposed by Galland et al. [Gal+14]. I contributed to this work by conceiving, building and automating the experiment, taking and analyzing the data and writing the manuscript.

In brief, a blue detuned drive pulse was used to probabilistically generate a photon-phonon pair, as characterized in the previous experiment [Rie+16]. The detection of a photon thus heralds the presence of a single phonon in the optomechanical crystal. This is verified by transferring the mechanical state to the optical domain, using a red detuned drive pulse, and analyzing it in a HBT interferometer, see also figure 5.1.

With this experiment, we demonstrated that optomechanical down conversion can be used to generate mechanical states with genuine quantum properties, specifically anti-correlated phonon counting statistics. These single phonons can for example be used to generate on demand single photons in integrated silicon photonics, addressing the question of scalability for photonic quantum computing [GAN14]. Further, they can act as building block for more complex mechanical quantum states, such as mechanical path entanglement [Rie+18].

While the mechanical state prepared here likely also exhibits phonon anti-bunching, the observed anti-correlations are neither necessary nor sufficient to conclude it [Man86; ZM90]. Consequently, a direct observation of this complementary quantum feature is still outstanding. Further, it would be of interest to realize a phononic HBT experiment, i.e. using phononic beam splitters and to separate optomechanical crystals as phonon detectors, in order to directly explore the quantum behavior of the motion.

Hanbury Brown and Twiss interferometry of single phonons from an optomechanical resonator

Sungkun Hong*,ᵃ, Ralf Riedinger*,ᵃ, Igor Marinković*,ᵇ, Andreas Wallucks*,ᵇ, Sebastian G. Hoferᵃ, Richard A. Norteᵇ, Markus Aspelmeyerᵃ, Simon Gröblacherᵇ

* These authors contributed equally to this work.
ᵃ Vienna Center for Quantum Science and Technology (VCQ), Faculty of Physics, University of Vienna
ᵇ Kavli Institute of Nanoscience, Delft University of Technology

5.1. Abstract

Nano- and micromechanical solid-state quantum devices have become a focus of attention. Reliably generating nonclassical states of their motion is of interest both for addressing fundamental questions about macroscopic quantum phenomena and for developing quantum technologies in the domains of sensing and transduction. We used quantum optical control techniques to conditionally generate single-phonon Fock states of a nanomechanical resonator. We performed a Hanbury Brown and Twiss–type experiment that verified the nonclassical nature of the phonon state without requiring full state reconstruction. Our result establishes purely optical quantum control of a mechanical oscillator at the single-phonon level.

5.2. Main Text

Intensity correlations in electromagnetic fields have been pivotal in the development of modern quantum optics. The experiments by Hanbury Brown and Twiss were a particular milestone that connected the temporal and spatial coherence properties of a light source with the second-order intensity autocorrelation function $g^{(2)}(\tau, x)$ [HT56b; HT56a;

---

[5] `http://science.sciencemag.org/content/358/6360/203`

MM66]. In essence, $g^{(2)}$ correlates intensities measured at times differing by τ or at locations differing by x and hence is a measure of their joint detection probability. At the same time, these correlations allow the quantum nature of the underlying field to be inferred directly. For example, a classical light source of finite coherence time can only exhibit positive correlations at a delay of $\tau \approx 0$ in the joint intensity detection probability, leading to bunching in the photon arrival time. This result holds true for all bosonic fields. Fermions, on the other hand, exhibit negative correlations and hence antibunching in the detection events [Hen+99; Oli+99; Jel+07], which is a manifestation of the Pauli exclusion principle. A bosonic system needs to be in a genuine nonclassical state to exhibit antibunching. The canonical example is a single-photon (Fock) state, for which $g^{(2)}(\tau = 0) = 0$ because no joint detection can take place [GRA86]. For this reason, measuring $g^{(2)}$ has become a standard method to characterize the purity of single-photon sources [Eis+11]. In general, $g^{(2)}(\tau)$ carries a wealth of information on the statistical properties of a bosonic field with no classical analogue [ZM90; Dav96] – specifically sub-Poissonian counting statistics [$g^{(2)}(0) < 1$] and antibunching [$g^{(2)}(\tau) \geq g^{(2)}(0)$] – all of which have been demonstrated successfully with quantum states of light [KDM77; SM83].

Over the past decade, motional degrees of freedom (phonons) of solid-state devices have emerged as a quantum resource. Quantum control of phonons was pioneered in the field of trapped ions [BW08], where single excitations of the motion of the ions are manipulated through laser light. These single-phonon states have been used for fundamental studies of decoherence [Lei+96] and for elementary transduction channels in quantum gates for universal quantum computing [CZ95]. Cavity optomechanics [AKM14] has successfully extended these ideas to optically controlling the collective motion of solid-state mechanical systems. It has allowed for remarkable progress in controlling solid-state phonons at the quantum level, including sideband cooling into the quantum ground state of motion [Teu+11; Cha+11], the generation of quantum correlated states between radiation fields and mechanical motion [Pal+13; Lee+11; Rie+16], and the generation of squeezed motional states [Wol+15; Pir+15; Lec+15].

So far single-phonon manipulation of micromechanical systems has exclusively been achieved through coupling to superconducting qubits [OCo+10; Chu+17; Ree+17], and optical control has been limited to the generation of quantum states of bipartite systems [Lee+11; Lee+12; Rie+16]. Here we demonstrate all-optical quantum control of a purely mechanical system, creating phonons at the single quantum level and unambiguously showing their nonclassical nature. We combined optomechanical control of motion and single-phonon counting techniques [Coh+15; Rie+16] to probabilistically generate a single-phonon Fock state from a nanomechanical device. Implementing Hanbury Brown and Twiss interferometry for phonons [Coh+15; Rie+16] (Figure 5.2) allowed us to probe the quantum mechanical character of single-phonons without reconstructing their states. We observed $g^{(2)}(0) < 1$, which is a direct verification of the nonclassicality of the optomechanically generated phonons, highlighting their particle-like behavior.

Our optomechanical crystal [Cha+11] consists of a microfabricated silicon nanobeam patterned so that it simultaneously acts as a photonic and phononic resonator (Figure 5.3). The resulting optical and mechanical modes couple through radiation pressure and the photoelastic effect so that a displacement equivalent to the zero-point fluctuation of the mechanical mode leads to a frequency shift of the optical mode by $g_0/2\pi = 869$ kHz (g_0: optomechanical coupling rate). The optical resonance has a wave-

Step I: create single-phonon Fock state   **Step II:** measure phonon correlation function
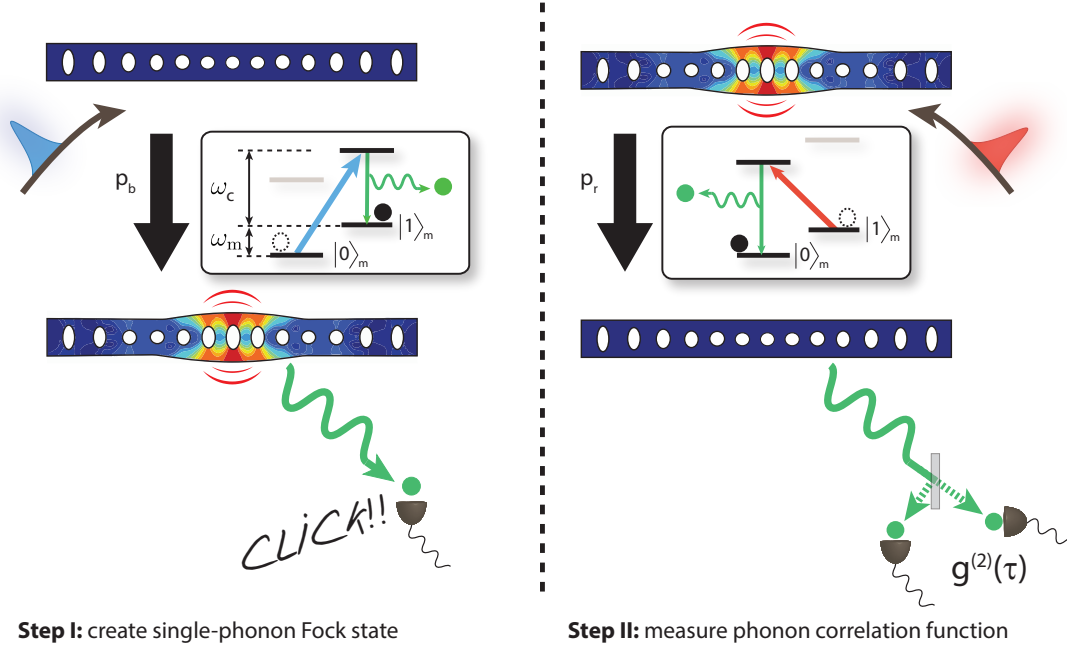
FIGURE 5.2.: **Working principle of the approach used to generate single-phonon states and verify their nonclassicality.** The first step (**left**) starts with a mechanical oscillator in its quantum ground state, followed by pumping the optomechanical cavity with a blue-detuned pulse. The resonator is excited to a single-phonon state with a probability $p_b = 1.2\%$ through the optomechanical interaction, which is accompanied by the emission of a photon on resonance with the cavity. The detection of such a photon in a single-photon detector (indicated by the "Click") allows us to post-select on a purely mechanical Fock state. To verify the quantum state that we created, a red-detuned read pulse is sent onto the optomechanical cavity in the second step (**right**), which performs a partial state transfer between the optics and the mechanics. With a probability of $p_r = 32.5\%$, the mechanical system's excitation is converted into a photon on cavity resonance, returning the mechanics to its ground state. The photon is sent onto a beamsplitter, where we measure the second-order intensity correlation function $g^{(2)}$ by using a pair of single-photon detectors. $g^{(2)}(0) < 1$ confirms the nonclassicality of the generated phonon states. The insets show the equivalent energy level diagrams of the processes.
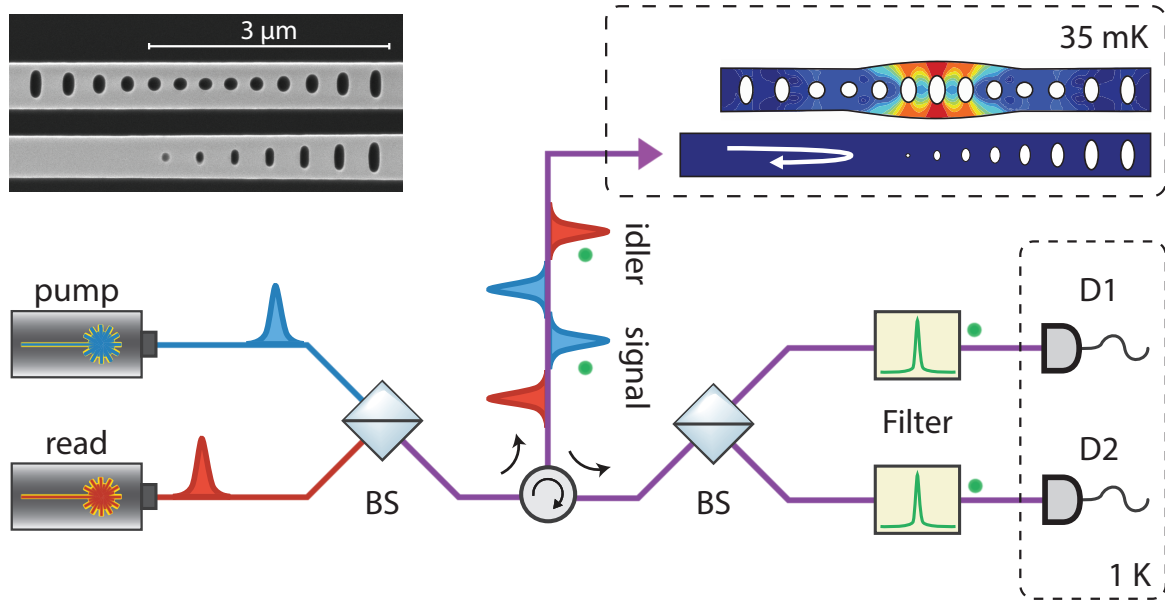
FIGURE 5.3.: **Sketch of the experimental setup used to measure the intensity autocorrelation function** $g^{(2)}$ **of phonons.** Blue-detuned pump pulses are sent into the optomechanical cavity, which is kept at 35 mK. With a small probability p_b, the optomechanical interaction creates a single excitation of the mechanical mode at 5.25 GHz (idler) and at the same time emits a signal photon on resonance with the cavity. The original optical pump field is then filtered and only the signal photon created in the optomechanical down-conversion process is detected in one of the single-photon detectors ($D1$ or $D2$). With a time delay t_d, a red-detuned read pulse is sent into the device, converting any mechanical idler excitation into an idler photon, which again is filtered from the original pump. Conditioned on the detection of a signal photon, we measure the $g^{(2)}$ of the idler photons. Because the red-detuned pulse is equivalent to a state-swap interaction, the $g^{(2)}$ function that we obtain for the photons is a direct measure of the $g^{(2)}$ function of the phonons in the mechanical oscillator. The inset in the top left corner shows a scanning electron microscope image of the device (top) next to a waveguide (bottom). BS, beamsplitter.

length $\lambda = 1554.35$ nm and a critically coupled total quality factor $Q_o = 2.28 \times 10^5$ (cavity energy decay rate $\kappa/2\pi = 846$ MHz), whereas the mechanical resonance has a frequency of $\omega_m/2\pi = 5.25$ GHz and a quality factor of $Q_m = 3.8 \times 10^5$. The device is placed in a dilution refrigerator with a base temperature of $T = 35$ mK. When the device is thermalized, its high frequency guarantees that the mechanical mode is initialized deep in its quantum ground state [Rie+16].

We utilized two types of linearized optomechanical interactions – the parametric down-conversion and the state swap – which can be realized by driving the system with detuned laser beams in the limit of weak coupling ($g_0\sqrt{n_c} \ll \kappa$, where n_c is the intracavity photon number) and resolved sidebands ($\kappa \ll \omega_m$) [AKM14]. The parametric down-conversion interaction has the form $H_{dc} = \hbar g_0\sqrt{n_c}(\hat{a}^\dagger\hat{b}^\dagger + \hat{a}\hat{b})$ where $\hbar$ is the reduced Planck constant; $\hat{b}^\dagger$ and $\hat{b}$ are the phononic creation and annihilation operators, respectively; and $\hat{a}^\dagger$ and $\hat{a}$ are the respective photonic operators. This interaction is selectively turned on by detuning the laser frequency ω_L to the blue side of the cavity resonance ω_c ($\omega_L = \omega_c + \omega_m$). H_{dc}

drives the joint optical and mechanical state, initially in the ground state, into the state $|\psi\rangle_{om} \propto |00\rangle + p_b^{1/2}|11\rangle + p_b|22\rangle + \mathcal{O}(p_b^{3/2})$. For low excitation probabilities $p_b \ll 1$, higher-order terms can be neglected so that the system can be approximated as emitting a pair consisting of a resonant signal photon and an idler phonon with a probability p_b [Hof+11]. Detection of the signal photon emanating from the device heralds a single excitation of the mechanical oscillator $|\psi\rangle_m \approx |1\rangle$, in close analogy to heralded single-photons from spontaneous parametric down-conversion. To read out the phonon state, we send in another laser pulse that is now red-detuned from the cavity resonance by ω_m ($\omega_L = \omega_c - \omega_m$). This realizes a state-swap interaction $H_{swap} = \hbar g_0 \sqrt{n_c}(\hat{a}^\dagger \hat{b} + \hat{a}\hat{b}^\dagger)$, which transfers the mechanical state to the optical mode with efficiency p_r. We can therefore use the scattered light field from this "read" operation to directly measure the second-order intensity correlation function $g^{(2)}$ of the mechanical oscillator mode, which is defined as

$$g^{(2)}(\tau) = \langle \hat{b}^\dagger(0)\hat{b}^\dagger(\tau)\hat{b}(\tau)\hat{b}(0)\rangle / \langle \hat{b}^\dagger(0)\hat{b}(0)\rangle\langle \hat{b}^\dagger(\tau)\hat{b}(\tau)\rangle, \qquad (5.4)$$

where τ is the time between the first and the second detection event. Like for any other bosonic system, $g^{(2)}(0) > 1$ means that the phonons exhibit super-Poissonian (classical) behavior, whereas $g^{(2)}(0) < 1$ is direct evidence of the quantum mechanical nature of the state and implies sub-Poissonian phonon statistics [Dav96].

We implemented the experimental approach (Fig. 5.2) by repeatedly sending a pair of optical pulses, the first one blue-detuned [pump pulse, full width at half maximum (FWHM) ≈ 32 ns] and the second one red-detuned (read pulse, FWHM ≈ 32 ns) with a fixed repetition period $T_r = 50$ μs. Photons generated through the optomechanical interactions were reflected back from the device and analyzed by a Hanbury Brown and Twiss interferometer using two superconducting nanowire single-photon detectors (SNSPDs). We set the mean pump pulse energy to 27 fJ so that $p_b = 1.2\%$, see Supplementary Information (SI). Detection of resonant (signal) photons created by this pulse heralds the preparation of the mechanical oscillator in a single-phonon Fock state, in principle with a probability of 98.8%. Owing to a small amount of initial thermal phonons and residual absorption heating, a fraction of unwanted phonons were incoherently added to the quantum states that we prepared [Rie+16]. After each pump pulse, a red-detuned read pulse was sent to the device with a programmable delay t_d, reading out phonons stored in the device by converting them into photons on resonance with the cavity. The mean read pulse energy is set to 924 fJ, corresponding to a state-swap efficiency $p_r \approx 32.5\%$. Taking into account subsequent optical scattering losses, this yields an absolute quantum efficiency for the detection of phonons of 0.9% (SI). Last, the pulse repetition period of $T_r = 50$ μs, which is long compared with the mechanical damping time of 11 μs, provides ample time for dissipating any excitation or unwanted heating generated by optical absorption. This ensured that each experimental cycle started with the mechanical mode well in the quantum ground state. The pulse sequence was repeated more than 7×10^9 times to acquire enough statistics. Conditioned on heralding events from detector $D1$ by the blue-detuned pulses, we analyzed the coincidence detection probability of photons at $D1$ and $D2$ that are transferred from phonons by the swap operation.

In our first experiment, we set $t_d = 115$ ns and measured $g^{(2)}(0)$ of the heralded phonons. One of our SNSPDs, $D2$, exhibited a longer dead time than t_d (SI) and we therefore only used photon counts from $D1$ for heralding the phonon states. From these measurements, we obtained a $g^{(2)}(0)$ of $0.65^{+0.11}_{-0.08}$ (Figure 5.4C), demonstrating a nonclassical character

A

B   **C**
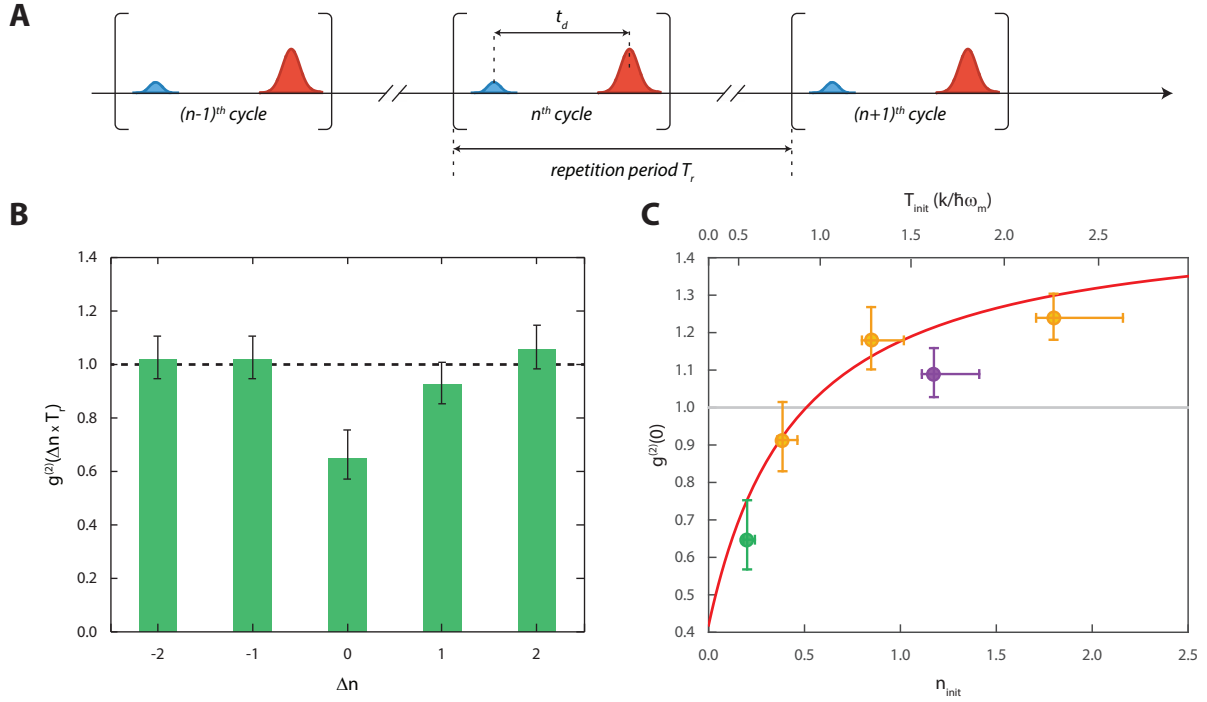
FIGURE 5.4.: **Experimental single-phonon creation and HBT interferometry.** **A** Pulse sequence used in the experiments. Each cycle consists of a blue-detuned pump pulse and a subsequent red-detuned read pulse delayed by t_d. The pulse sequence is repeated with the period T_r. Both t_d and T_r can be adjusted. **B** The measurement result of the second-order correlation function $g^{(2)}(\tau = \Delta n \times T_r)$ of the heralded phonons, with $g^{(2)}(0) < 1$ being a direct measure of their nonclassicality. In this measurement, we set $t_d = 115$ ns and $T_r = 50$ μs. $g^{(2)}(\Delta n \times T_r)$ with $\Delta n \neq 0$ depicts the correlations between phonons read from separate pulse sequences with the cycle difference of Δn. Whereas phonons from independent pulses show no correlation $[g^{(2)}(\Delta n \times T_r; \Delta n \neq 0) \approx 1]$, those from the same read pulse are strongly anticorrelated $[g^{(2)}(\tau = 0) = 0.65^{+0.11}_{-0.08}]$. **C** The influence of an incoherent phonon background on the $g^{(2)}(0)$ of the generated mechanical states. Several measurements are plotted for a range of different effective initial temperatures of the nanomechanical oscillator. The first data point (green) was taken with a delay $t_d = 115$ ns and a repetition period $T_r = 50$ μs. We control the initial mode occupation n_{init} (initial mode temperature T_{init}) by using the long lifetime of the thermally excited phonons stemming from the delayed absorption heating by pump and read pulses. This allows us to increase n_{init} while keeping the bulk temperature and properties of the device constant, causing an increase in $g^{(2)}(0)$, as the state becomes more thermal. The red line shows the simulated $g^{(2)}(0)$ as discussed in (SI). For technical reasons all data points (yellow and purple) except the leftmost (green) were taken with $t_d = 95$ ns. In addition, the second from the right (purple) was taken at an elevated bath temperature of $T_{bath} = 160$ mK.

of the mechanical state.

    The observed $g^{(2)}(0)$ of 0.65 is considerably higher than what we expect in the ideal case $g^{(2)}_{ideal}(0) \approx 4 \times p_b = 0.045$ (SI). We attribute this to heating induced by the absorption of the pump and read pulses. Although a detailed physical mechanism for the absorption and subsequent heat transfer into the mechanical mode is still a subject of study [Rie+16], the influx of thermal phonons $\dot{n}_{abs}$ caused by the absorption of drive laser pulses can be

experimentally deduced from the (unconditional) photon count rates generated by the read pulses (SI). Including an estimation of the initial thermal phonon number n_{init}, which is likewise inferred from the unconditional photon counts associated with the pump and read pulses, we constructed a theoretical model that predicts $g^{(2)}(0)$ as a function of p_b, n_{init}, and $\dot{n}_{abs}$. Given the measured $n_{init} \approx 0.20$ and $\dot{n}_{abs}$ (SI) within the read pulse, our model predicts $g^{(2)}(0) \approx 0.76$, which is consistent with the experimental value.

To further probe the effect of thermal phonons, we performed a set of experiments with reduced repetition periods T_r, while keeping the other settings for the pump pulses the same. This effectively increases n_{init}, because the absorbed heat does not have enough time to dissipate before the next pair of pulses arrives. As expected, as T_r was reduced, we observed an increase in $g^{(2)}(0)$. With the measured n_{init} and $\dot{n}_{abs}$ from the same data set, we can plot the predicted $g^{(2)}(0)$ values. The experimental values and theoretical bounds on $g^{(2)}(0)$ are in good agreement (Fig. 5.4).

We also measured $g^{(2)}(0)$ for $t_d = 350$ ns and found that it increased to $0.84^{+0.07}_{-0.06}$. This increase is consistent with previously observed delayed heating effects of the absorption [Rie+16] and is in good agreement with the theoretical prediction of 0.84. Even for these longer delays, the value is still below 1, demonstrating the potential of our device as a single-phonon quantum memory on the time scale of several hundred nanoseconds.

We experimentally demonstrated the quantum nature of heralded single-phonons in a nanomechanical oscillator by measuring their intensity correlation function $g^{(2)}(0) < 1$. The deviation from a perfect single-phonon state can be modeled by a finite initial thermal occupation and additional heating from our optical cavity fields. We achieved conversion efficiencies between phonons and telecom photons of more than 30%, only limited by our available laser power and residual absorption. Full state reconstruction of the single-phonon state, as demonstrated with phononic states of trapped ions [Lei+96], should be realizable with slightly improved read-out efficiency and through homodyne tomography. The demonstrated fully optical quantum control of a nanomechanical mode, preparing sub-Poissonian phonons, shows that optomechanical cavities are a useful resource for future integrated quantum phononic devices, as both single-phonon sources and detectors. They are also an ideal candidate for storage of quantum information in mechanical excitations and constitute a fundamental building block for quantum information processing involving phonons. Some of the potential applications include quantum noise–limited, coherent microwave-to-optics conversion, as well as studying the quantum behavior of individual phonons of a massive system.

Acknowledgments

5. Hanbury Brown and Twiss interferometry of single phonons

References

These are the references cited in the author's version of the manuscript.

[AKM14] M. Aspelmeyer, T. J. Kippenberg, and F. Marquardt, "Cavity optomechanics", *Rev. Mod. Phys.* 86, 1391 (2014), DOI: `10.1103/RevModPhys.86.1391` (cited on pgs. 92, 94).

[Bar87] A. Barchielli, "Quantum stochastic differential equations: an application to the electron shelving effect", *J. Phys. A* 20, 6341 (1987), DOI: `10.1088/0305-4470/20/18/034` (cited on pg. 107).

[Bar90] A. Barchielli, "Direct and heterodyne detection and other applications of quantum stochastic calculus to quantum optics", *Quantum Opt.* 2, 423 (1990), DOI: `10.1088/0954-8998/2/6/002` (cited on pgs. 107, 109).

[BW08] R. Blatt and D. Wineland, "Entangled states of trapped atomic ions", *Nature* 453, 1008 (2008), DOI: `10.1038/nature07125` (cited on pg. 92).

[Cha+11] J. Chan, T. P. M. Alegre, A. H. Safavi-naeini, J. T. Hill, A. Krause, S. Groeblacher, and M. Aspelmeyer, "Laser cooling of a nanomechanical oscillator into its quantum ground state", *Nature* 478, 89 (2011), DOI: `10.1038/nature10461` (cited on pg. 92).

[Cha12] J. Chan, "Laser cooling of an optomechanical crystal resonator to its quantum ground state of motion", PhD thesis, California Institute of Technology, 2012 (cited on pg. 102).

[Cho+04] C. W. Chou, S. V. Polyakov, A. Kuzmich, and H. J. Kimble, "Single-Photon Generation from Stored Excitation in an Atomic Ensemble", *Phys. Rev. Lett.* 92, 213601 (2004), DOI: `10.1103/PhysRevLett.92.213601` (cited on pg. 102).

[Chu+17] Y. Chu, P. Kharel, W. H. Renninger, L. D. Burkhart, L. Frunzio, P. T. Rakich, and R. J. Schoelkopf, "Quantum acoustics with superconducting qubits.", *Science* 358, 199 (2017), DOI: `10.1126/science.aao1511` (cited on pg. 92).

[Coh+15] J. D. Cohen, S. M. Meenehan, G. S. MacCabe, S. Gröblacher, A. H. Safavi-Naeini, F. Marsili, M. D. Shaw, and O. Painter, "Phonon counting and intensity interferometry of a nanomechanical resonator", *Nature* 520, 522 (2015), DOI: `10.1038/nature14349` (cited on pg. 92).

[CZ95] J. I. Cirac and P. Zoller, "Quantum Computations with Cold Trapped Ions", *Phys. Rev. Lett.* 74, 4091 (1995), DOI: `10.1103/PhysRevLett.74.4091` (cited on pg. 92).

[Dav96]   L. Davidovich, "Sub-Poissonian processes in quantum optics", *Rev. Mod. Phys.* 68, 127 (1996), DOI: `10.1103/RevModPhys.68.127` (cited on pgs. 92, 95).

[Eis+11]   M. D. Eisamana, J. Fan, A. Migdall, and S. V. Polyakov, "Single-photon sources and detectors", *Rev. Sci. Instrum.* 82, 071101 (2011), DOI: `10.1063/1.3610677` (cited on pg. 92).

[FL13]   R. Filip and L. Lachman, "Hierarchy of feasible nonclassicality criteria for sources of photons", *Phys. Rev. A* 88, 043827 (2013), DOI: `10.1103/PhysRevA.88.043827` (cited on pg. 110).

[Gal+14]   C. Galland, N. Sangouard, N. Piro, N. Gisin, and T. J. Kippenberg, "Heralded Single-Phonon Preparation, Storage, and Readout in Cavity Optomechanics", *Phys. Rev. Lett.* 112, 143602 (2014), DOI: `10.1103/PhysRevLett.112.143602` (cited on pgs. 102, 104).

[GRA86]   P. Grangier, G. Roger, and A. Aspect, "Experimental Evidence for a Photon Anticorrelation Effect on a Beam Splitter: A New Light on Single-Photon Interferences", *Europhys. Lett.* 1, 173 (1986), DOI: `10.1209/0295-5075/1/4/004` (cited on pg. 92).

[GZ04]   C. W. Gardiner and P. Zoller, *Quantum Noise*, 3rd ed., Springer, (2004), ISBN: 9783540223016 (cited on pg. 108).

[Hen+99]   M. Henny, S. Oberholzer, C. Strunk, T. Heinzel, K. Ensslin, M. Holland, and C. Schonenberger, "The fermionic hanbury brown and twiss experiment", *Science* 284, 296 (1999), DOI: `10.1126/SCIENCE.284.5412.296` (cited on pg. 92).

[Hof+11]   S. G. Hofer, W. Wieczorek, M. Aspelmeyer, and K. Hammerer, "Quantum entanglement and teleportation in pulsed cavity optomechanics", *Phys. Rev. A* 84, 52327 (2011), DOI: `10.1103/PhysRevA.84.052327` (cited on pgs. 95, 104).

[HT56a]   R. Hanbury Brown and R. Q. Twiss, "A Test of a New Type of Stellar Interferometer on Sirius", *Nature* 178, 1046 (1956), DOI: `10.1038/1781046a0` (cited on pg. 91).

[HT56b]   R. Hanbury Brown and R. Q. Twiss, "Correlation between Photons in two Coherent Beams of Light", *Nature* 177, 27 (1956), DOI: `10.1038/177027a0` (cited on pg. 91).

[IBW88]   W. M. Itano, J. C. Bergquist, and D. J. Wineland, "Photon antibunching and sub-Poissonian statistics from quantum jumps in one and two atoms", *Phys. Rev. A* 38, 559(R) (1988), DOI: `10.1103/PhysRevA.38.559` (cited on pg. 110).

[Jel+07]   T. Jeltes et al., "Comparison of the Hanbury Brown-Twiss effect for bosons and fermions", *Nature* 445, 402 (2007), DOI: `10.1038/nature05513` (cited on pg. 92).

[JNN12]   J. R. Johansson, P. D. Nation, and F. Nori, "QuTiP: An open-source Python framework for the dynamics of open quantum systems", *Comp. Phys. Comm.* 183, 1760 (2012), DOI: `10.1016/j.cpc.2012.02.021` (cited on pg. 110).

[JNN13]   J. R. Johansson, P. D. Nation, and F. Nori, "QuTiP 2: A Python framework for the dynamics of open quantum systems", *Comp. Phys. Comm.* 184, 1234 (2013), DOI: `10.1016/j.cpc.2012.11.019` (cited on pg. 110).

[KDM77]   H. J. Kimble, M. Dagenais, and L. Mandel, "Photon Antibunching in Resonance Fluorescence", *Phys. Rev. Lett.* 39, 691 (1977), DOI: `10.1103/PhysRevLett.39.691` (cited on pg. 92).

[KP70]   W. Kern and D. A. Puotinen, "Cleaning Solutions Based on Hydrogen Peroxide for Use in Silicon Semiconductor Technology", *RCA Rev.* 31, 187 (1970) (cited on pg. 102).

[LDC14]   M.-A. Lemonde, N. Didier, and A. A. Clerk, "Antibunching and unconventional photon blockade with Gaussian squeezed states", *Phys. Rev. A* 90, 063824 (2014), DOI: `10.1103/PhysRevA.90.063824` (cited on pg. 110).

[Lec+15]   F. Lecocq, J. B. Clark, R. W. Simmonds, J. Aumentado, and J. D. Teufel, "Quantum Nondemolition Measurement of a Nonclassical State of a Massive Object", *Phys. Rev. X* 5, 041037 (2015), DOI: `10.1103/PhysRevX.5.041037` (cited on pg. 92).

[Lee+11]   K. C. Lee et al., "Entangling macroscopic diamonds at room temperature.", *Science* 334, 1253 (2011), DOI: `10.1126/science.1211914` (cited on pg. 92).

[Lee+12]   K. C. Lee, B. J. Sussman, M. R. Sprague, P. Michelberger, K. F. Reim, J. Nunn, N. K. Langford, P. J. Bustard, D. Jaksch, and I. A. Walmsley, "Macroscopic non-classical states and terahertz quantum processing in room-temperature diamond", *Nat. Photon.* 6, 41 (2012), DOI: `10.1038/nphoton.2011.296` (cited on pg. 92).

[Lei+96]   D. Leibfried, D. M. Meekhof, B. E. King, C. Monroe, W. M. Itano, and D. J. Wineland, "Experimental Determination of the Motional Quantum State of a Trapped Atom", *Phys. Rev. Lett.* 77, 4281 (1996), DOI: `10.1103/PhysRevLett.77.4281` (cited on pgs. 92, 97).

[Lin76]   G. Lindblad, "On the generators of quantum dynamical semigroups", *Commun. Math. Phys.* 48, 119 (1976), DOI: `10.1007/BF01608499` (cited on pg. 108).

[Mee+14]   S. M. Meenehan, J. D. Cohen, S. Gröblacher, J. T. Hill, A. H. Safavi-Naeini, M. Aspelmeyer, and O. Painter, "Silicon optomechanical crystal resonator at millikelvin temperatures", *Phys. Rev. A* 90, 011803 (2014), DOI: `10.1103/PhysRevA.90.011803` (cited on pg. 106).

[Mee+15]   S. M. Meenehan, J. D. Cohen, G. S. MacCabe, F. Marsili, M. D. Shaw, and O. Painter, "Pulsed Excitation Dynamics of an Optomechanical Crystal Resonator near Its Quantum Ground State of Motion", *Phys. Rev. X* 5, 041002 (2015), DOI: `10.1103/PhysRevX.5.041002` (cited on pgs. 103, 106).

[MM66]   B. L. Morgan and L. Mandel, "Measurement of Photon Bunching in a Thermal Light Beam", *Phys. Rev. Lett.* 16, 1012 (1966), DOI: `10.1103/PhysRevLett.16.1012` (cited on pg. 92).

[OCo+10]   A. D. O'Connell et al., "Quantum ground state and single-phonon control of a mechanical resonator.", *Nature* 464, 697 (2010), DOI: 10.1038/nature08967 (cited on pg. 92).

[Oli+99]   W. D. Oliver, J. Kim, R. C. Liu, and Y. Yamamoto, "Hanbury Brown and Twiss-Type Experiment with Electrons", *Science* 284, 299 (1999), DOI: 10.1126/science.284.5412.299 (cited on pg. 92).

[Pal+13]   T. A. Palomaki, J. W. Harlow, J. D. Teufel, R. W. Simmonds, and K. W. Lehnert, "Coherent state transfer between itinerant microwave fields and a mechanical oscillator", *Nature* 495, 210 (2013), DOI: 10.1038/nature11915 (cited on pg. 92).

[Pat+17]   R. N. Patel, C. J. Sarabalis, W. Jiang, J. T. Hill, and A. H. Safavi-Naeini, "Engineering phonon leakage in nanomechanical resonators", *Phys. Rev. Applied* 8, 041001 (2017), DOI: 10.1103/PhysRevApplied.8.041001 (cited on pg. 102).

[Pir+15]   J.-M. Pirkkalainen, E. Damskägg, M. Brandt, F. Massel, and M. A. Sillanpää, "Squeezing of Quantum Noise of Motion in a Micromechanical Resonator", *Phys. Rev. Lett.* 115, 243601 (2015), DOI: 10.1103/PhysRevLett.115.243601 (cited on pg. 92).

[Ree+17]   A. P. Reed et al., "Faithful conversion of propagating quantum information to mechanical motion", *Nature Phys.* (2017), DOI: 10.1038/nphys4251 (cited on pg. 92).

[Rie+16]   R. Riedinger, S. Hong, R. A. Norte, J. A. Slater, J. Shang, A. G. Krause, V. Anant, M. Aspelmeyer, and S. Gröblacher, "Normal Non-classical correlations between single photons and phonons from a mechanical oscillator", *Nature* 530, 313 (2016), DOI: 10.1038/nature16536 (cited on pgs. 92, 94–97, 102–104, 106).

[SM83]   R. Short and L. Mandel, "Observation of Sub-Poissonian Photon Statistics", *Phys. Rev. Lett.* 51, 384 (1983), DOI: 10.1103/PhysRevLett.51.384 (cited on pgs. 92, 110).

[Teu+11]   J. D. Teufel, T. Donner, D. Li, J. W. Harlow, M. S. Allman, K. Cicak, A. J. Sirois, J. D. Whittaker, K. W. Lehnert, and R. W. Simmonds, "Sideband cooling of micromechanical motion to the quantum ground state", *Nature* 475, 359 (2011), DOI: 10.1038/nature10261 (cited on pg. 92).

[Wil+07]   I. Wilson-Rae, N. Nooshi, W. Zwerger, and T. J. Kippenberg, "Theory of ground state cooling of a mechanical oscillator using dynamical back-action", *Phys. Rev. Lett.* 99, 093901 (2007), DOI: 10.1103/PhysRevLett.99.093901 (cited on pg. 108).

[Wol+15]   E. E. Wollman, C. U. Lei, A. J. Weinstein, J. Suh, A. Kronwald, F. Marquardt, A. A. Clerk, and K. C. Schwab, "Quantum squeezing of motion in a mechanical resonator", *Science* 349, 952 (2015), DOI: 10.1126/science.aac5138 (cited on pg. 92).

[ZM90]   X. T. Zou and L. Mandel, "Photon-antibunching and sub-Poissonian photon statistics", *Phys. Rev. A* 41, 475 (1990), DOI: 10.1103/PhysRevA.41.475 (cited on pg. 92).

5.3. Supplementary Information

Optomechanical devices

The optomechanical device is fabricated from a silicon on insulator wafer (Soitec) with a device layer of 250 nm thickness on top of a 3 μm buried oxide layer. We pattern our chips with an electron beam writer and transfer the structures into the silicon layer in a reactive ion etcher using a SF_6/O_2 plasma. One of the sides of the chip is removed to allow for in-plane access to the lensed fiber couplers. After the resist is removed, the device layer is undercut in 40% hydrofluoric acid. An additional cleaning step using the so-called RCA method [KP70] is performed to remove organic and metallic residuals. The final step is a dip in 2% hydrofluoric acid to remove the oxide layer formed by the RCA cleaning and to terminate the silicon surface with hydrogen atoms.

Unlike in previous device designs [Cha12], we do not use an additional phononic shield around the optomechanical structure as this unnecessarily increases the re-thermalization time and therefore reduces the achievable repetition rate of our experiment [Rie+16]. We reduce the mechanical quality factors of the designed structures further by offsetting the photonic crystal holes laterally from the center of the beam by 30 nm [Pat+17]. This yields a measured quality factor of $Q_m = 3.8 \times 10^5$ at mK temperatures, while otherwise such structures exhibit Q's beyond 10^7.

In order to find particularly good devices on a chip, we characterize them in a pump-probe experiment at cryogenic temperatures (35mK) and select devices with optimal mechanical Q and low optical absorption. We then perform cross-correlation measurements of the photon-phonon pairs scattered by the pump pulse, while varying the repetition period T_r, pump excitation probability p_b and state-swap efficiency p_r. This short two-fold coincidence measurement (~1h) allows us to predict the expectation value of the three-fold coincidence autocorrelation measurement [Cho+04; Gal+14; Rie+16] as well as the time required to obtain enough statistics for a targeted confidence interval. We chose a parameter set, which allows for a statistically significant (p-value < 0.001, see below) demonstration of intensity anticorrelations ($g^{(2)}(0) < 1$) of the phononic state within a realistic measurement time (~100h).

Detection efficiency

We calibrate the total detection efficiencies of optomechanically generated cavity photons ($\eta_i; i = 1, 2$) by performing a series of independent measurements. First, the fiber-to-device coupling efficiency ($\eta_{fc} = 0.48$) is measured by sending light with known power to the photonic crystal and then measuring the reflected power. The extraction efficiency of cavity photons η_{dev} is obtained from the device impedance ratio, $\eta_{dev} = \kappa_e/\kappa$, where κ_e is the external cavity energy decay rate. These values are extracted from the visibility and the linewidth of the optical resonance scan, and we find $\eta_{dev} = 0.5$. Furthermore, we measure the efficiency of detecting photons coming from the device for each SNSPD. We
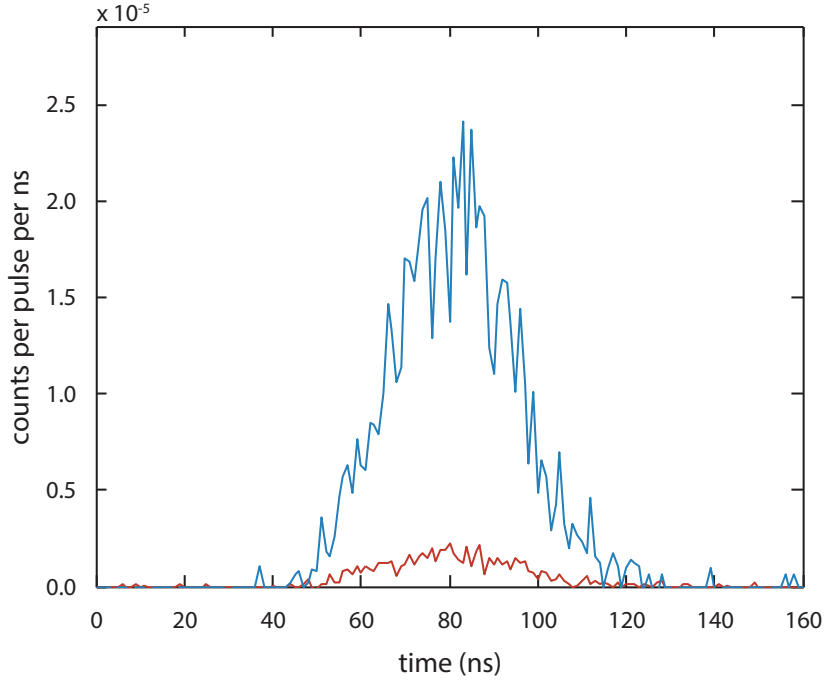
FIGURE 5.5.: A sideband asymmetry measurement is performed to extract the optomechanical coupling rate g_0. For a detailed explanation of the measurement see the text below. We plot the detected photon counts per pulse repetition per nanosecond for a blue-detuned (blue) and a red-detuned beam (red). Unwanted contributions from leaked pump photons and detector dark counts are independently measured and subtracted. Integrating over the whole detection window (i.e. from 30 to 150 ns in the plot) gives the photon counting probabilities C_b and C_r, respectively. From this data, we extract the optomechanical coupling rate $g_0/2\pi = 869$ kHz.

launch weak, off-resonant optical pulses with an average of 5.14 photons to the device and measure the photon count rate of each SNSPD. This measurement gives the quantities $\eta_{fc}^2 \times \eta_{trans,i} \times \eta_{QE,i}$, where $\eta_{trans,i}$ is the transmission efficiency of the detection path to each SNSPD, while $\eta_{QE,i}$ is their quantum efficiency. As η_{fc} is measured independently, $\eta_{trans,i} \times \eta_{QE,i}$ can be calculated from these results. Finally, this allows us to obtain $\eta_i = \eta_{dev} \times \eta_{fc} \times \eta_{trans,i} \times \eta_{QE,i}$, which are $\eta_1 = 1.16\%$ and $\eta_2 = 1.50\%$, respectively.

Optomechanical coupling rate

In order to calibrate the optomechanical coupling rate g_0 between the cavity field and the mechanical mode, we perform a measurement similar to sideband thermometry [Mee+15; Rie+16] (see Figure 5.5). In this measurement, pairs of pump and probe pulses are sent to the device with a repetition period of $T_r = 100$ μs. For this pulse sequence, a blue-detuned pump pulse (190.62 fJ) is sent to intentionally heat the device's mechanical mode, followed by the probe pulse (55.16 fJ) with a long delay of 99.825 μs. We perform two sets of such repetitive measurements, one with red-detuned and the other with blue-detuned probe pulses. From each measurement, we acquire a photon counting probability for the probe pulses, C_r (red-detuned) and C_b (blue-detuned). These can be expressed as $C_r = (\eta_1 + \eta_2) \times p_r \times n_{th}$ and $C_b = (\eta_1 + \eta_2) \times p_b \times (1 + n_{th})$ in the limit of $p_b \ll 1$ and $p_r \ll 1$, where p_b and p_r are equivalent to the photon-phonon pair excitation probability

and state-swap efficiency as introduced in the main text. p_b and p_r can be explicitly written as

$$p_b = \exp(\kappa_e/\kappa \left[4g_0^2 E_p/\hbar\omega_c(\omega_m^2 + (\kappa/2)^2) \right]) - 1, \tag{5.5}$$

$$p_r = 1 - \exp(-\kappa_e/\kappa \left[4g_0^2 E_p/\hbar\omega_c(\omega_m^2 + (\kappa/2)^2) \right]), \tag{5.6}$$

where E_p is the total energy of the incident laser pulses and all the other terms as defined in the main text. We find that $C_r = 0.0064\%$ and $C_b = 0.0697\%$. From these values we extract $n_{th} = 0.104$, $p_r = 2.32\% \ll 1$ and $p_b = 2.37\% \ll 1$, which allows us to directly obtain $g_0/2\pi = 869$ kHz, in good agreement with our simulated value [Rie+16]. With the calibrated value of g_0, the scattering probabilites p_r and p_b can now be directly set by simply choosing the appropriate pulse energies. The average phonon occupation of the mechanical oscillator n_{th} can also be obtained by measuring the count rates with predetermined values of p_b and p_r, without requiring sideband thermometry.

Data analysis

The second order autocorrelation function is defined as

$$g^{(2)}(t_1, t_2) = \frac{\left\langle : \hat{N}(t_1)\hat{N}(t_2) : \right\rangle}{\left\langle \hat{N}(t_2) \right\rangle \left\langle \hat{N}(t_1) \right\rangle}, \tag{5.7}$$

where $\hat{N}(t) = \hat{b}^\dagger(t)\hat{b}(t)$ is the phonon number operator of the mechanical mode at time t after the start of the pulse sequence, and $: :$ is the notation for time and normal ordering of the operators. The mechanical mode is measured by the optical read pulses and the signal, i.e. the scattered photons, are filtered before they are detected by SNSPDs. Consequently, the observed detection events are averaged by the optical filters and weighted with the envelope of the read pulse $n_p(t)$, which holds for the weak coupling (i.e. adiabatic) regime. Further, to gain enough statistics, the events associated with the read pulse are integrated. We define the time interval $[t_a, t_b]$, containing the effective pulse shape $p(t)$, which is obtained from the actual pulse envelope $n_p(t)$ and the filter transfer function. This allows us to express the observed autocorrelation function

$$g^{(2)}_{obs}(\tau) = \frac{\int_{t_a}^{t_b} dt_1 \int_{t_a+\tau}^{t_b+\tau} dt_2 p(t_1)p(t_2) \left\langle : \hat{N}(t_1)\hat{N}(t_2) : \right\rangle}{\left(\int_{t_a}^{t_b} dt_1 p(t_1) \left\langle \hat{N}(t_1) \right\rangle \right) \left(\int_{t_a+\tau}^{t_b+\tau} dt_2 p(t_2) \left\langle \hat{N}(t_2) \right\rangle \right)}, \tag{5.8}$$

for a delay τ between two phonon measurements. This averaging does not influence the validity of the statements about sub-poissonian statistics and nonclassicality of the mechanical state. Strictly speaking, within the averaging window there is a randomization of the phonon statistics due to damping and heating. Thus, a small regression towards $g^{(2)} = 1$ is the expected. Due to the short averaging time, this effect is negligible compared the other uncertainties and systematic effects described below, such that we can safely assume $g^{(2)}(\tau) \equiv g^{(2)}(t_d, t_d + \tau) \approx g^{(2)}_{obs}(\tau)$, with the effective delay of the read pulse $t_d = (t_a + t_b)/2$.

A Hanbury Brown and Twiss setup with two single-photon detectors $D1$ and $D2$ with low count rates allows to measure this second order autocorrelation [Hof+11; Gal+14].

Specifically, for $\tau = 0$, this expression reduces to the cross-correlation between those detectors

$$g^{(2)}(0) \approx g^{(2)}_{E_1,E_2} = P(E_1 \cap E_2)/P(E_1)P(E_2), \tag{5.9}$$

where $P(X)$ describes the probability of the occurrence of event X, and E_n is a detection event at detector D_n ($n = 1, 2$) during the time interval $[t_a, t_b]$. In this notation, it can easily be seen that a rescaling of the detection efficiency of either detector drops out of the expression. Consequently, $g^{(2)}$ is independent of losses in the optical path or the fidelity of the state transfer by the read pulse. However, the value of $g^{(2)}$ can be changed by measurement noise, in our case dominated by false positive detection events (caused by electronic noise, stray light or leaked pump photons). In our setup this gives a negligible systematic error $\delta g^{(2)} = g^{(2)}_{E_1,E_2} - g^{(2)}(0)$ of $0 < \delta g^{(2)} < 3 \times 10^{-4}$. If the state-swap is seen as part of the measurement, heating of the mechanical state by optical absorption of pump photons within the device can also be interpreted as measurement noise. The effect on $g^{(2)}$ depends strongly on the initial effective temperature of the mechanical mode, so that we cannot give a general number for the systematic error. From simulations, we deduce that it spans from about $0 < \delta g^{(2)}_{abs} < 0.17$ for the lowest temperature measurement to $0 < \delta g^{(2)}_{abs} < 0.02$ for the highest initial temperature. The absorption heating in combination with dead time of the SNSPDs, additionally causes a systematic error of $0 < \delta g^{(2)}_{dt} < 0.03$, which is described in detail in the following section. As the heating related effects can also be considered to be part of the actual mechanical state and the other effects are much smaller than the statistical uncertainties, all $g^{(2)}$ values presented in this work are not corrected for these systematic errors. With all $\delta g^{(2)} > 0$, the presented values are upper bounds to the noise free auto-correlation of the mechanical state.

To estimate the statistical uncertainty of our measurement, we use the likelihood function based on a binomial distribution of photon detection events in the limit of low probabilities. The experimentally measurable values for $g^{(2)}_{E_1,E_2}(0)$ are the maximum likelihood values

$$\bar{g}^{(2)}_{E_1,E_2} \equiv \frac{C(E_1 \cap E_2)/N}{(C(E_1)/N)(C(E_2)/N)} \approx g^{(2)}_{E_1,E_2}, \tag{5.10}$$

where $C(E_1)$ ($C(E_2)$) is the number of counts registered at detector $D1$ ($D2$) and $C(E_1 \cap E_2)$ is the number of co-detection events at both detectors, all conditioned on heralding events (i.e. detection events from earlier pump pulses). N refers to the number of such heralding events. In our experiment, the uncertainty of $g^{(2)}_{E_1,E_2}$ is dominated by that of $\bar{P}(E_1 \cap E_2) \equiv C(E_1 \cap E_2)/N$, i.e. the estimated probability of $P(E_1 \cap E_2)$, as $E_1 \cap E_2$ is the rarest event among all the other events. Therefore, we use the likelihood function of $P(E_1 \cap E_2)$ to determine the confidence interval of the given values $g^{(2)}(0) = \bar{g}^{(2)}_{E_1,E_2}{}^{+\sigma_+}_{-\sigma_-}$, such that the likelihood of the actual value of $g^{(2)}_{E_1,E_2}$ is 34% to be within $\left[\bar{g}^{(2)}_{E_1,E_2} - \sigma_-, \bar{g}^{(2)}_{E_1,E_2}\right]$ and 34% to be within $\left[\bar{g}^{(2)}_{E_1,E_2}, \bar{g}^{(2)}_{E_1,E_2} + \sigma_+\right]$. While the low count numbers produce skewed likelihood functions and therefore unequal upper and lower uncertainties $\sigma_\pm$, the counts are high enough such that the rule of thumb of requiring 3σ for statistical significance (p-value< 0.001) still holds. Specifically, our null hypothesis is no correlation between the phonons in the oscillator, i.e. an actual $g^{(2)}_{actual} = 1$. For the delay of the read pulse of $t_d = 115$ ns and $T = 35$ mK, we measured an autocorrelation of $g^{(2)}(0) = 0.647^{+0.105}_{-0.079}$. The p-value, i.e. the probability of observing this or a more extreme result, given that the null
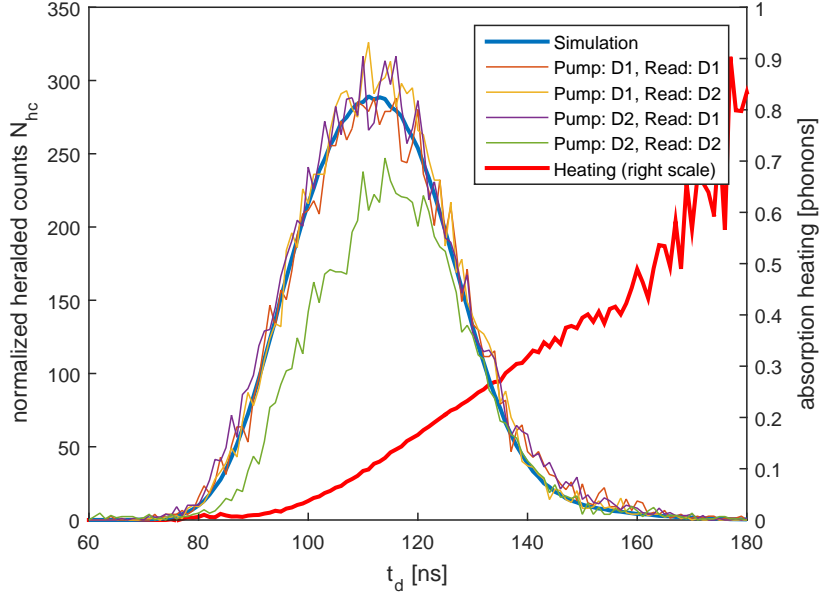
FIGURE 5.6.: Plotted are the heralded counts for various combinations of detection events: In brown, yellow, purple and green are the counts of photons scattered by the read pulse (left axis), heralded on the detection of a photon scattered by the pump pulse. They are normalized to the detection efficiency of events heralded by detector $D1$ and detected by $D2$ (yellow). All combinations involving $D1$ either for heralding or detection match well with the simulated counting distribution (blue). Notably, the combination of heralding and detecting with $D2$ deviates from that. This reduced detection efficiency is caused by the longer dead time of $D2$ compared to $D1$. In addition, the time window over which the pulse averages, is shifted to later times and is more heavily influenced by the cumulative heating $n_{abs}(t)$ (red) by absorbed driving photons from the read pulse. The latter is extracted from the detection of a thermal state and compensated for the optomechanical cooling to obtain the true cumulative number of added phonons $n_{abs}(t)$ (right axis).

hypothesis of no correlation was true, is $p = P\big(\bar{g}^{(2)}_{E_1,E_2} \leq 0.647 \big| g^{(2)}_{\text{actual}} = 1, N = 1.2 \times 10^6\big) < 7 \times 10^{-4}$. In our case this coincides with the probability of falsely rejecting the classical bound $P\big(g^{(2)}_{\text{actual}}(0) \geq 1 \big| \bar{g}^{(2)}(0) = 0.647^{+0.105}_{-0.079}\big) < 7 \times 10^{-4}$. For the delay of $t_d = 370$ ns and $T = 35$ mK, we find the p-value $p < 0.01$ for the observed $g^{(2)}(0) = 0.832^{+0.068}_{-0.058}$, also coinciding with $P\big(g^{(2)}_{\text{actual}}(0) \geq 1 \big| g^{(2)}(0) = 0.832^{+0.068}_{-0.058}\big) < 0.01$.

Dead time effects

In order to reduce the effects of absorption heating on the mechanical state [Mee+14; Mee+15; Rie+16], it is important to measure the state as quickly as possible upon its generation by the pump pulse. For the data shown in Figure 5.4B in the main text, the time delay between the read and the pump pulses is $t_d = 115$ ns. For the measurements in Figure 5.4C, t_d is set to 95 ns, except for the first data point, which represents the result of Figure 5.4B.

In our measurement scheme, we use the same pair of SNSPDs to herald the generation of nonclassical mechanical states as we use to measure $g^{(2)}(0)$ through the read pulses.

After a detection event, the superconducting nanowire is in the normal conducting state and is therefore blind to additional photons arriving during this time, before it cools down and returns into the superconducting state. This so-called dead time for our detectors is nominally on the order of $50 - 70$ ns. If the state is heralded by one of the SNSPDs and its dead time overlaps with the arrival time of the photons from the read pulse, its detection efficiency will be lower than the nominal value. In our experiment this is in fact the case for detector D2 in the measurement of $g^{(2)}(0)$ with $t_d = 115$ ns (cf. Figure 5.6).

To first approximation, this should have no influence on the value of $g^{(2)}(0)$ itself, as the detection probability of the heralded pulses enters equation (5.9) in the numerator $P(E_1 \cap E_2)$ and the denominator $P(E_2)$ in the same way. However, a detected readout pulse with a seemingly distorted shape as in Figure 5.6 effectively measures the mechanical state slightly later than the nominal delay time t_d. Due to absorption heating during the read pulse (cf. Figure 5.6), the mechanical state at later times is corrupted by the influx of thermal phonons $\dot{n}_{abs}(t)$. Therefore, it will increase the observed value of $g^{(2)}(0)$ towards 2, the value of a thermal state. For this reason we discard heralding events from detector D2 for short delays.

A more detailed analysis allows us to quantify the systematic error by the shorter dead time of detector D1. The minor reduction of the detection efficiency for a t_d of 115 ns leads to $0 < \delta g^{(2)}_{dt} < 0.01$, which corresponds to an overestimation of our observed value of $g^{(2)}(0)$ by much less than our statistical uncertainty. For $t_d = 95$ ns, this effect from detector D1 becomes stronger, resulting in 10% reduced detection efficiency. However, thanks to an increased thermal background, it only produces a systematic error of around $0 < \delta g^{(2)}_{dt} < 0.03$, which is again smaller than the statistical uncertainty. As they are negligible in magnitude, we did not account for these systematic errors in the reported values of $g^{(2)}$ in the main text.

Simulation of the correlation function

To calculate the expected value of $g^{(2)}$ we use the formalism developed by Barchielli [Bar87; Bar90]. In order to do this, we require a model of the open-system dynamics of our optomechanical system, describing the coupling to the environment. In addition to the typical assumption that the mechanical system couples to a heat bath of a fixed temperature, we observe in our experiment an additional, time-dependent heating effect that is activated by the strong read pulse. In the absence of a microscopic description of this effect, we adopt a simple phenomenological description and model it as a standard Lindblad dynamics with two parameters γ and n_{bath}, which can be estimated from the singlefold detection events of the exerimental $g^{(2)}$ data for each n_{init}. Note that n_{bath} is not the occupation number determined by the dilution refrigerator and is assumed to be a function of time. In essence, the incoherent (thermal) phonon influx $\dot{n}_{abs} = \gamma n_{bath}(t)$ is the derivative of the cummulative absorbtion heating and can be extracted from singlefold detection events, with calibrated scattering rates from sideband asymmetry measurements (see above) and knowledge of the envelope of the read pulse (cf. Figure 5.6). The mechanical decay rate γ is assumed to be the measured decay rate ω_m/Q_m. The Lindblad dynamics stay identical when coupling to a number of different baths with different coupling strengths, as long as the phonon influx and the mechanical decay rate stay constant. For reasons of simplicity, we therefore work with a single phenomenological phonon influx $\gamma \times n_{bath}(t)$.

5. Hanbury Brown and Twiss interferometry of single phonons

The evolution of the optomechanical quantum state ρ under open-system dynamics can be described by a Lindblad master equation [Lin76] of the form [Wil+07]

$$\dot{\rho} = \mathcal{L}\rho = -\frac{i}{\hbar}[H_{swap}(t), \rho] + \kappa\mathcal{D}[a]\rho + \gamma(n_{bath}(t) + 1)\mathcal{D}[b]\rho + \gamma n_{bath}(t)\mathcal{D}[b^\dagger]\rho, \quad (5.11)$$

where the time dependence in H_{swap} accounts for the time-dependent drive by the light pulses. The Lindblad terms,

$$\mathcal{D}[s]\rho = s\rho s^\dagger - \frac{1}{2}\left(s^\dagger s\rho + \rho s^\dagger s\right), \quad (5.12)$$

describe the coupling of the system to its electromagnetic environment (second term in eq. (5.11)) and the mechanical heat bath with a mean occupation number n_{bath} (third and fourth term in eq. (5.11)). Below we will write the formal solution of eq. (5.11) as $\rho(t) = \mathcal{T}(t, t_0)\rho(t_0)$.

To describe a photon-counting measurement with a quantum efficiency η, we iteratively solve the master equation as [GZ04]

$$\rho(t) = \mathcal{S}(t, t_0)\rho(t_0) + \sum_{m=1}^{\infty} \int_0^t dt_m \cdots \int_0^{t_2} dt_1 \mathcal{S}(t, t_m)\mathcal{J}\mathcal{S}(t, t_{m-1}) \ldots \mathcal{J}\mathcal{S}(t_1, 0)\rho(t_0), \quad (5.13)$$

where we defined the operator $\mathcal{J}\rho = \eta\kappa\, a\rho a^\dagger$ (which corresponds to the emission of one photon from the cavity), and the propagator $\mathcal{S}$ that solves the effective evolution $\dot{\mathcal{S}} = (\mathcal{L} - \mathcal{J})\mathcal{S}$. Equation (5.13) allows for the following interpretation: Assuming that we register m photons on the photo-detector, the *conditional* state of the system is, up to a normalizing factor, given by the m-th term in the sum above. In case no photons are registered, the unnormalized conditional state is given by $\mathcal{S}(t, t_0)\rho(t_0)$ instead. The heralded state of the mechanical system after the blue-detuned write pulse (for a click of the detector at time t_{click}) is thus given by

$$\rho_{click} = \frac{\mathrm{Tr}_{cav}[\mathcal{T}(t_{click}, t_0)\rho(t_0) - \mathcal{S}(t_{click}, t_0)\rho(t_0)]}{\mathrm{Tr}[\mathcal{T}(t_{click}, t_0)\rho(t_0) - \mathcal{S}(t_{click}, t_0)\rho(t_0)]}. \quad (5.14)$$

Note that this state is conditioned on a measurement of *at least* one phonon. For our case where two-fold events are rare, this effectively reduces to the first term in the sum in eq. (5.13), i.e., $\rho_{click} \propto \mathrm{Tr}_{cav}[a^\dagger a\mathcal{S}(t_{click}, t_0)\rho(t_0)]$.

As the evaluation of $g^{(2)}$ is computationally expensive, we first adiabatically eliminate the cavity mode from eq. (5.11), which is possible in the weak-coupling limit $g_0 \times \sqrt{n_c} \ll \kappa$. For the case of the red-detuned read pulse we find the equation (neglecting the very weak optical-spring effect) [Wil+07]

$$\dot{\rho}_m = [\gamma(n_{bath} + 1) + \Gamma_-(t)]\mathcal{D}[b]\rho_m + (\gamma n_{bath} + \Gamma_+(t))\mathcal{D}[b^\dagger]\rho_m, \quad (5.15)$$

for the reduced state of the mechanical system ρ_m, with $\Gamma_\pm(t) = 2\kappa_e/\kappa \times g_0^2 n_c(t)\mathrm{Re}(\eta_\pm)$, $\eta_- = 2/\kappa$, $\eta_+ = 2/(\kappa + 4i\omega_m)$. In this approximation the photo-counting measurement at the cavity resonance frequency is described by $\mathcal{J}(t)\rho = \eta\Gamma_-(t)b\rho b^\dagger$.

To calculate $g^{(2)}$ of the photons emitted from the cavity (after heralding) we need to evaluate time- and normal-ordered expectation values of the cavity output field, which is

readily achieved in this formalism. We find [Bar90]

$$\langle \hat{I}(t_1) \rangle = \text{Tr}[\mathcal{J}(t_1)\mathcal{T}(t_1, t_{click})\rho_{click}], \tag{5.16}$$

$$\langle : \hat{I}(t_1)\hat{I}(t_2) : \rangle = \text{Tr}[\mathcal{J}(t_2)\mathcal{T}(t_2, t_1)\mathcal{J}(t_1)\mathcal{T}(t_1, t_{click})\rho_{click}]. \tag{5.17}$$

To evaluate equations (5.16) and (5.17), we expand the mechanical operators in a number basis up to a maximal phonon number of 50. We assume the mechanical system to initially be in a thermal state with a mean phonon number n_{init}. In optomechanical crystals, the mechanical damping rate γ tends to be a function of the environmental temperature. As $\gamma \times n_{bath}$ is effectively treated as a single parameter $\dot{n}_{abs}$ and the time scale of the simulation is short compared to the mechanical decay time $1/\gamma$, potential changes of γ with the bath temperature by up to one order of magnitude do not influence the simulations significantly.
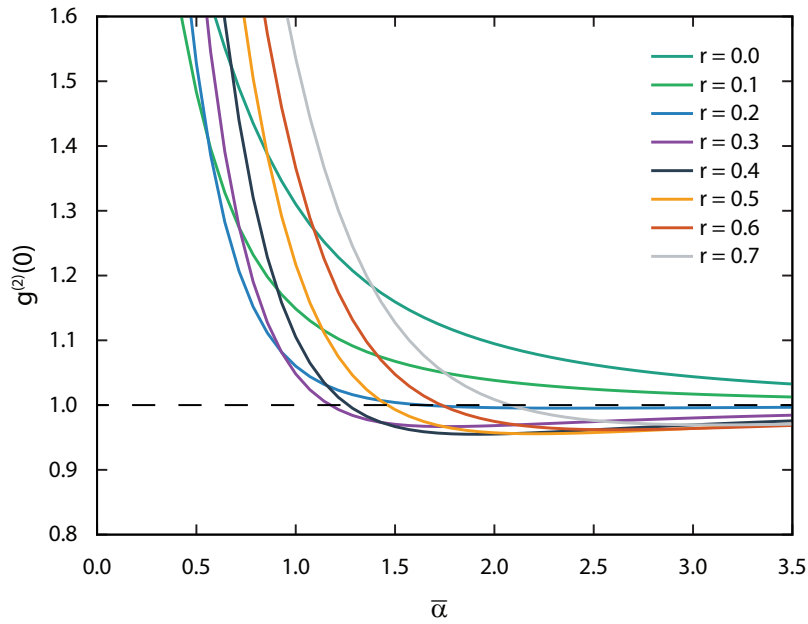

FIGURE 5.7.: Shown is the numerically calculated $g^{(2)}$ function of a squeezed Gaussian state with an initial thermal occupation of $n_{init} = 0.20$ as a function of displacement $\bar{\alpha}$ and squeezing parameter r (color-coded) for $\theta = 2\phi$. Even for the optimal choice of settings $r = 0.44$ and $\bar{\alpha} = 2.00$, such a model cannot explain our data.

Nonclassicality and $g^{(2)}$

The degree of second order coherence $g^{(2)}$ allows to draw various conclusions on the system under investigation. The most prominent use of $g^{(2)}$ is to violate the nonclassicality bound as described in the main text. The physical meaning of this bound can be inferred from the variance of the energy $\hat{H} = \hbar\omega_m \hat{b}^\dagger \hat{b}$ of the free mechanical oscillator.

$$\text{Var}(\hat{H}) = \left\langle \hat{H}^2 \right\rangle - \left\langle \hat{H} \right\rangle^2 = \left(g^{(2)}(0) - 1\right)\left\langle \hat{H} \right\rangle^2 + \hbar\omega_m \left\langle \hat{H} \right\rangle. \tag{5.18}$$

For classical physics, i.e. not applying canonical quantization, $\langle : \hat{H}^2 : \rangle = \langle \hat{H}^2 \rangle$ and therefore the last term, stemming from the commutation relations, drops out. It immediately

follows from $\text{Var}(\hat{H}) \geq 0$ that $g^{(2)}(0) \geq 1$. When using the canonical quantization, we can infer from $g^{(2)}(0) < 1$ that the source had sub-Poissonian phonon statistics. This also classifies the mechanical state as "nonclassical" in the sense that it cannot be represented as an incoherent mixture of coherent states [SM83]. The degree of second order coherence $g^{(2)}$ can be used to test against stricter bounds as well [FL13], some of them depending on the physical system under investigation. For two level systems it is for example important to demonstrate that only a single emitter is present. This can be done by demonstrating $g^{(2)}(0) < 0.5$ [IBW88]. In our case it is sufficient to show $g^{(2)}(0) < 1$ as we only have a single macroscopic oscillator by design.

As we can see from equation (5.18), states possessing a small variance and/or low energies can also exhibit $g^{(2)}(0) < 1$. One set of states, which is interesting to exclude is incoherent mixtures of Gaussian states. In general, linear bosonic systems that involve squeezing can exhibit $g^{(2)}(0) < 1$. This has recently been theoretically shown in the context of optomechanics [LDC14]. Using these models we numerically calculate $g^{(2)}(0)$ for a general mechanical single-mode Gaussian state undergoing squeezing. For this, we use the most favorable parameters observed in our correlation experiments. We start from an initial thermal state $\hat{\rho}_{init}$ with $n_{init} = 0.20$ phonons, which corresponds to the lowest temperature observed in the correlation measurements. The state is assumed to be purely thermal, which is in agreement with the experimentally observed autocorrelation of the pump pulse of $g^{(2)}(0) = 2.0^{+0.1}_{-0.1}$. Neglecting any heating from the optical pulses, we apply displacement $\hat{D}(\alpha) = \exp[\alpha\hat{b}^\dagger - \alpha^*\hat{b}]$ and squeezing operations $\hat{S}(\xi) = \exp[\frac{1}{2}(\xi^*\hat{b}^2 - \xi\hat{b}^{\dagger 2})]$ with variable $\alpha = \bar{\alpha}e^{i\phi}$ and $\xi = re^{i\theta}$ ($\bar{\alpha}, r > 0$). We then numerically minimize $g^{(2)}(0)$ of the resulting states $\hat{\rho} = \hat{D}(\alpha)\hat{S}(\xi)\hat{\rho}_{init}\hat{S}^\dagger(\xi)\hat{D}^\dagger(\alpha)$ as a function of α and ξ using the quantum toolbox QuTiP [JNN12; JNN13]. The minimal correlation we can obtain is $g^{(2)}(0) \approx 0.95$, with $r = 0.44$ and $\bar{\alpha} = 2.00$ for $\theta = 2\phi$, clearly exceeding our experimentally measured value, as shown in Fig. 5.7. This simple model therefore allows us to exclude, with a p-value of 0.002, the possibility that the states we generate are in fact squeezed Gaussian states. When additionally limiting the mean occupation $n = \text{Tr}[\hat{\rho}\hat{b}^\dagger\hat{b}]$ to the experimentally observed occupation number of the heralded states, $1.25 < n < 1.90$, we get a minimum $g^{(2)}(0) \approx 0.99$, rejecting the hypothesis of observing a squeezed state with even stronger statistical confidence.

6. Remote quantum entanglement between two micromechanical oscillators

Entanglement has been called "*the* characteristic trait of quantum mechanics" by Schrödinger in a letter coining the term [Sch35]. He characterized it as the relation of two initially independent systems in pure states, which interact for some time, and thereafter cannot be fully described by two separate wavefunctions. In other words, the quantum state is spread over both systems, making it impossible to capture the full information of the physical reality when describing the systems separately. This phenomenon was initially described by Einstein, Podolsky and Rosen (EPR), citing the counter-intuitive consequences of quantum entanglement as a reason for their doubts about the completeness of a quantum mechanical description of reality [EPR35]. Later on, it was realized that quantum entanglement not only exists [FC72; KUW75; AGR81], but can be employed for efficient simulation of quantum systems [Man80; Fey82], computation [Deu85] and communication [WS83; BB84]. Here, I will report on my work on entanglement of two remote mechanical oscillators, first published as reference [Rie+18], preceded by a summary of the scientific context of this manuscript.

The consequences of entanglement are at variance with the classical definition of "completeness" of a physical theory [EPR35]. In particular, one part of an entangled system cannot completely be described without knowledge of the other part. Conversely, this allows for example for manipulation of the first system by a mere measurement of the second [Sch35]. A proposal by Bell for an experimental test of the EPR paradox [Bel64] triggered a flurry of research on the topic. Bell's inequality and related ones, like the CHSH inequality [Cla+69], are a classical bound for correlation measurements that can only be violated by entangled states. Subsequent experiments demonstrated the existence of entanglement, using photon polarization correlations in cascaded fluorescence [FC72; AGR81] and positron annihilation [KUW75].

In parallel, first ideas were developed for utilizing entanglement beyond the investigation of fundamental test of physics. For example, it became clear that entanglement, as the manifestation of the superposition principle in many-body systems, prevented classical computers from efficiently simulating large quantum systems [Pop75; Fey82]. It was thus proposed to use controlled quantum systems and the entanglement they produce to circumvent this limitation for quantum simulations [Man80; Fey82]. Soon after, it emerged that the computational power of such systems could also be employed for more general computational tasks [Deu85]. Specific problems, such as the prime factorization of numbers [Sho94] or the search of an entry in a database [Gro96] can in principle be treated more efficiently on a quantum computer than on its classical analogue[1]. While these

---

[1] It has been argued that some quantum algorithms do not require entanglement, but merely the super-

algorithms have been realized in proof-of-concept experiments [CGK98; Van+01], the demonstration of a speed advantage over classical computers (called quantum supremacy) remains outstanding [Boi+18].

An alternative approach to exploit the unconventional properties of quantum mechanics came from the field of cryptography [WS83; BB84]. Relying on the superposition principle for the polarization of single photons, as well as the no-cloning theorem for quantum states [WZ82], public keys can be distributed while ensuring that no eavesdropping occurred [BB14; Ben+92]. In complementary protocols, entanglement can be used to share cryptographic keys [Eke91; Eke+92] or teleport quantum information [Ben+93; Bou+97]. While the no-cloning theorem is integral to the security of these quantum communication protocols, it also limits their range. Due to losses in the absorption channel, increasing the distance between the communicating partners requires an exponential increase in resources. In classical communication, this is circumvented by inserting auxiliary nodes in the transmission channel, called repeaters, which recieve and resend the information along the line. As an unknown quantum state cannot be cloned, i.e. received and identically resend, this is not possible in quantum communication.

With theoretical and experimental advances, the two directions merged to form the field of quantum information science [Ben95]. The formalization and standardization of language in the treatment enabled rapid further progress, such as the description of a quantum computation architecture [Llo93; CZ95], quantum information algorithms [Sho94; Sho95; Gro96], and general conditions for quantum computational supremacy [DiV96; Got98].

The corresponding proof-of-principle experiments, like the demonstration of fundamental quantum gates [Mon+95] and the entanglement of two remote atoms [Hag+97], showed the possibility to extend quantum communication from connecting merely two clients, to forming small networks. In such a quantum networks, quantum channels connect several nodes, consisting small quantum processors that can be locally manipulated. In order to achieve an efficient operation of such a network, however, the range limits of quantum communication had to be overcome.

To this end, Briegel et al. proposed the use of quantum repeaters [Bri+98]. In an array of repeater nodes, neighboring sites are entangled and subsequently the ends are connected by entanglement swapping. Including a nested scheme for the purification of the state, this allows to efficiently generate high fidelity entanglement in distant sites, which can then be used to teleport quantum information from the one to the other end of the chain.

Duan, Lukin, Cirac and Zoller (DLCZ) subsequently proposed a scheme to realize a quantum repeater requiring only atomic ensembles[2], linear optics and single photon detectors [Dua+01]. This sparked the experimental investigation into quantum repeater

---

position principle [Kni00]. This relates to the notion of path entanglement, as will be discussed later. In brief, two formally identical quantum states, namely a single excitation being in a superposition of multiple modes, can be considered an entangled state or not, depending on whether these are multiple modes of the same of different systems.

[2]At the time, atomic ensembles seemed to be the most realistic physical system for an implementation of the scheme. In more general terms, it is based on a pair creation process, such as Stokes scattering or spontaneous parametric down conversion, and the storage of one of the created excitations in a quantum memory, which can be read out on demand.

architectures[3], first demonstrating the non-classical correlations between an atomic ensemble and an optical mode [Kuz+03], followed by the generation of remote heralded entanglement in atomic ensembles [Cho+05; Yua+08], trapped ions [Moe+07], and single neutral atoms [Hof+12]. In order to simplify the requirement, solid state quantum memories were employed, like optical phonons in diamond [Lee+11], ensembles of rare earth ions doped in host crystals [Usm+12], nitrogen vacancy centers in diamond [Ber+13] and semiconductor quantum dots [Del+16].

To efficiently make use of low-loss optical fibers, the quantum memories should be coupled to photons in the telecommunication band, a wavelength range with notoriously few natural resonances. Storage of entangled states coupled to telecom photons was demonstrated in erbium doped fibers [Sag+15] and could be performed in lattice vibrations in diamond [Lee+11], which does not rely on an optical resonance. In addition, artificial resonances in the telecom range were created using semiconductor quantum dots [Miy+05; Olb+17]. In all three systems, however, the life time of the excitations is prohibitively short, preventing network applications. Longer storage times, though only for coherent states, were recently achieved in erbium doped crystals [Ran+17], at the cost of a narrow optical resonance. In order to realize high entanglement rates, however, it is desirable to use a significant part of the bandwith of optical fibers, e.g. by wavelength division multiplexing [Bra90; Tow97; Tan+08; Sas+11; Yos+12]. Operating in multiple densely spaced frequency channels in the telecom range could be realized for example by wavelength conversion, transferring visible photons that are interfaced with quantum memories to the infrared range [Mar+14a; Mar+17].

Optomechanical crystals, on the other hand, couple directly to telecom photons [Rie+16] and can be designed to work in any specific frequency channel in the conventional telecommunication band. An additional intriguing feature is that they are based on integrated silicon photonics. The small form factor and compatibility with industry standard microfabrication procedures [Ben+17] in principle allows for mass fabrication and deployment of these devices. The demonstration of remote heralded entanglement presented here is thus a major step towards silicon photonics based scalable quantum networks [Rie+18].

Beyond quantum communication applications, the entanglement of macroscopic resonators also is of fundamental interest. Demonstrating this core principle of quantum theory for large objects pushes the boundary between the microscopic quantum domain and the classical physics we see every day. Previously, entanglement was demonstrated involving large numbers of electrons, e.g. in a superconducting electrical circuits [Ste+06; Ans+09], or as a spin wave in atomic ensembles [JKP01; Cho+05; Usm+12], as well as large numbers of photons [DSV08; Lvo+13]. In terms of mass, the largest systems where entanglement was previously observed are lattice vibrations in bulk diamond [Lee+11] and entanglement between a microwave field and an aluminum drum [Pal+13b]. In parallel with the experiment presented here, entanglement between the motion of two such drums was reported [Ock+18]. However, despite the differences between quantum mechanics and our classical experience of physics in everyday life, there is no intrinsic limit to quantum theory, neither in terms of mass, nor numbers of particles. For this reason, there is no single clear measure of how macroscopic a certain state or system is, but rather a large parameter space to be explored [Leg02; DSC02; MAD08; Ved08; LJ11; FD12; NH13;

---

[3] Note that there has also been complementary research on quantum networking without repeaters, e.g. entangling remote atomic systems [Mat+06b; Rit+12].

I: Initialization II: Heralding III: Ent. IV: Analysis

$$\frac{|A\rangle + e^{i\phi}|B\rangle}{\sqrt{2}}$$
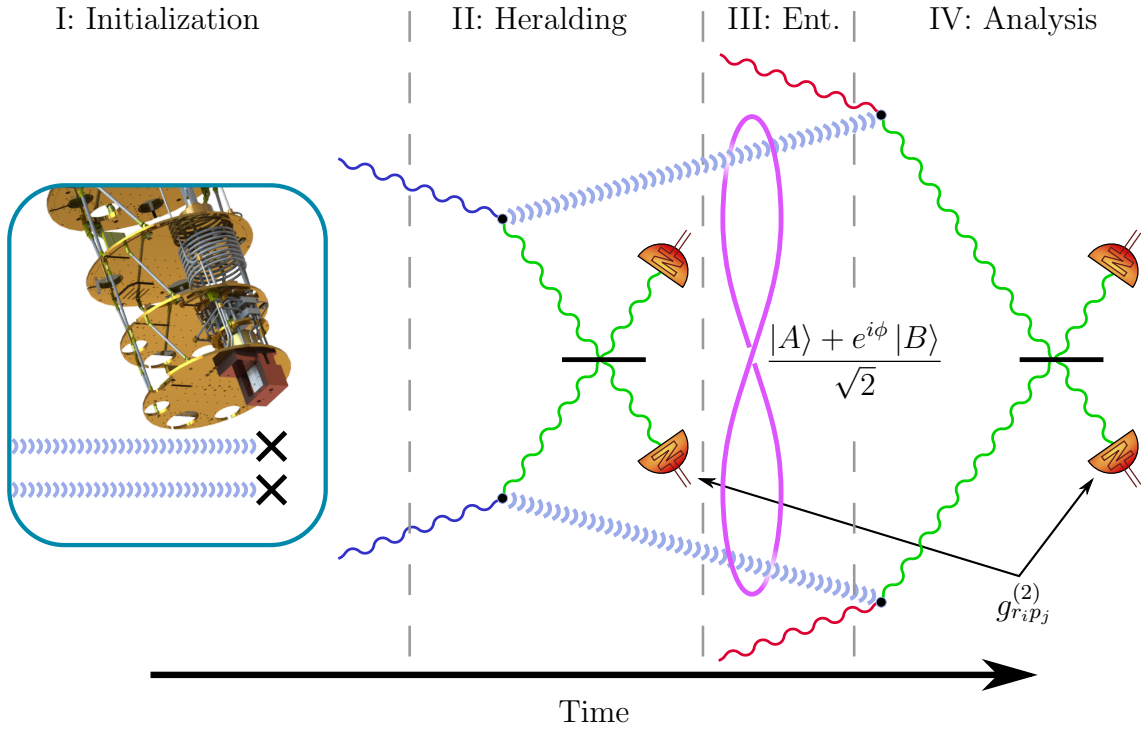
$g_{r_i p_j}^{(2)}$

Time

FIGURE 6.1.: **Mechanical Path Entanglement.** First, the two devices are cryogenically initialized in their groundstates (step I). Then, a weak drive pulse induces a Stokes scattering event creating a photon-phonon pair either in device A (top half) or B (bottom half). The optical paths are overlapped on a beamsplitter, such that the heralding detection event contains no information about where the scattering took place (step II). Consequently, the single phonon is in a superposition between device A $|A\rangle$ and device B $|B\rangle$, i.e. the mechanical oscillators are entangled (step III). Finally the state is transfered to the optical domain by anti-Stokes scattering and interferometrically analyzed (step IV).

Zar+17].

Before transitioning to the experimental part of this chapter, I would like to introduce the notion of entanglement witnesses, which is of importance for the understanding of this work. While initially entanglement was mostly discussed in the context of the EPR paradox and Bell's theorem, it was found that only a sub-set of entangled states violate Bell type inequalities [Wer89]. More specifically, in the spirit of Schrödingers definition, two subsystems a and b are considered to be entangled if they are not separable, i.e. the density matrix ρ cannot be factorized in the form

$$\rho = \sum_i p_i \rho_{a,i} \otimes \rho_{b,i}. \tag{6.1}$$

The sum over instances i, with positive probabilities p_i and the density matrices $\rho_{a,i}$ ($\rho_{b,i}$) of subsystem a (b), accounts for classical correlations, see e.g. [Wer89; Per96]. Determining whether a state is entangled consequently is a non-trivial problem. To tackle it, various necessary conditions for the separability of states were found [Per96; HHH96]. When a measurement contradicts such a condition, it can be concluded that the systems are entangled. Separability conditions, which do not require a full reconstruction of the compound quantum state are called entanglement witnesses, with the Bell or CHSH inequality being

I: Initialization | II: Correlation | III: Ent. | IV: Analysis

$$\frac{|AA\rangle + e^{i\phi}|BB\rangle}{\sqrt{2}}$$
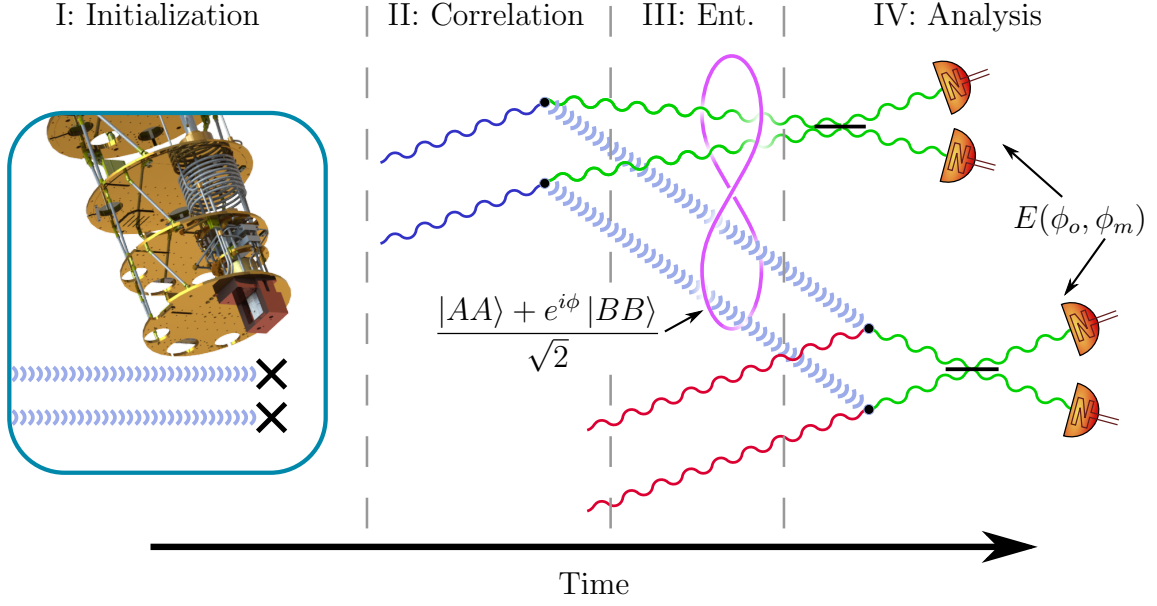
$E(\phi_o, \phi_m)$

Time

FIGURE 6.2.: **Entanglement of the Optical and Mechanical Mode.** The devices are initialize (step I) and a single photon-phonon pair is generated by Stokes scattering (step II). Before any detection takes place, the pair is in a superposition of path A with state $|AA\rangle$ or in path B with state $|BB\rangle$. This corresponds to entanglement between the local mechanical two-mode-system and the flying optical two-mode-system (step III). The entanglement is verified by a Bell test, using the anti-Stokes process to transfer the mechanical part to the optical domain (step IV). For details see reference [Mar+18]

two specific examples thereof [Hor+09]. As for the Bell inequality, witnesses typically only can identify a subset of all entangled states, i.e. fulfilling a certain separability condition is not sufficient to prove that the systems are indeed separable. In this work, we use a witness proposed by Børkje et al., which was tailored to optomechanical systems [BNG11]. The witness $R \sim g^{(2)}/V$, described in detail below, can be approximated[4] as the ratio of the intensity autocorrelation of both systems $g^{(2)}$ to the visibility V of the interference between the states of the two systems, see also appendix B.4. The separability condition $R \geq 1$ can be violated for example by a single phonon in a coherent superposition of being in either device.

In the following, I will present my work on the entanglement of two remote mechanical oscillators. I contributed to this work by conceiving, building and automating the experiment, taking and analyzing the data and writing the manuscript.

In brief, a blue detuned drive pulse probabilistically creates a photon-phonon pair in either of two nearly identical devices. The information, where the Stokes scattering took place is erased by overlapping the paths of the signal modes. Consequently, when the detection of a signal photon indicates the presence of a phonon, located in a superposition of the two devices [Cab+99; Dua+01]. The non-separable nature of the mechanical state is verified by transferring it to the optical domain, using a red detuned drive pulse, and performing a single photon interference experiment, see also figure 6.1.

The entangled state generated in this scheme can be referred to as path entanglement,

---

[4]For small excitation numbers in the mechanical oscillators.

with the phonon in a coherent superposition of being located in path, or more precisely device A or B, i.e. its wavefunction can be approximated as $|\psi\rangle = |A\rangle + e^{i\phi} |B\rangle$. Here the state $|A\rangle = |10\rangle$ ($|B\rangle = |01\rangle$) describes the location of the phonon. This type of entanglement was first demonstrated by Grangier et al. [GRA86], though in a different context. From a formal point of view, this state is equivalent to a photon being in superposition of horizontal and vertical polarization, mapping each polarization to a path (e.g. $A \to H$ and $B \to V$). Thus, while constituting entanglement, as multiple systems are inseparably involved, the state is effectively equivalent to the degrees of freedom of a single polarization qubit[5]. This was pointed out in the proposal by DLCZ [Dua+01], where a pair of memories was required at every node. The advantage is, however, that the auxiliary $|0\rangle$-$|1\rangle$ qubit basis is intrinsically used for state purification. In other words, when no photon is detected, it is clear that the entanglement operation failed.

The emission of the Stokes photons is correlated with the location of the phonon [Rie+16]. Thus, prior to the detection of the Stokes photon, the four mode state can be written as $|\psi\rangle = |AA\rangle + e^{i\phi} |BB\rangle$, with the state describing the location of the Stokes phonon and photon, see figure 6.2. This is equivalent to the state used in photonic realizations of the EPR paradox with "polarization" [AGR82] or "path qubits" [RT90], with the important difference, that it describes entanglement between a photonic and a *phononic* "path" qubit. We recently reported the observation of this type of entanglement in reference [Mar+18]. Notably, the optomechanical Bell experiment is the first demonstration of entanglement between the motion of a massive oscillator and photons in the optical domain.

---

[5] The reason is that for the phononic state, as well as for photons, the $|0\rangle$-$|1\rangle$ basis cannot be effectively employed, due to its intolerance against loss.

Remote quantum entanglement between two micromechanical oscillators

Ralf Riedinger*,ᵃ, Andreas Wallucks*,ᵇ, Igor Marinković*,ᵇ, Clemens Löschnauerᵃ, Markus Aspelmeyerᵃ, Sungkun Hongᵃ, Simon Gröblacherᵇ
* These authors contributed equally to this work.
ᵃ Vienna Center for Quantum Science and Technology (VCQ), Faculty of Physics, University of Vienna
ᵇ Kavli Institute of Nanoscience, Delft University of Technology

6.1. Abstract

Entanglement, an essential feature of quantum theory that allows for inseparable quantum correlations to be shared between distant parties, is a crucial resource for quantum networks [Kim08]. Of particular importance is the ability to distribute entanglement between remote objects that can also serve as quantum memories. This has been previously realized using systems such as warm [Jen+11; Rei+11] and cold atomic vapours [Cho+05; Mat+06], individual atoms [Rit+12] and ions [Moe+07; Jos+09], and defects in solid-state systems [Usm+12; Sag+15; Hen+15]. Practical communication applications require a combination of several advantageous features, such as a particular operating wavelength, high bandwidth and long memory lifetimes. Here we introduce a purely micro-machined solid-state platform in the form of chip-based optomechanical resonators made of nanostructured silicon beams. We create and demonstrate entanglement between two micromechanical oscillators across two chips that are separated by 20 centimetres. The entangled quantum state is distributed by an optical field at a designed wavelength near 1550 nanometres. Therefore, our system can be directly incorporated in a realistic fibre-optic quantum network operating in the conventional optical telecommunication band. Our results are an important step towards the development of large-area quantum networks based on silicon photonics.

6.2. Main Text

In recent years, nanofabricated mechanical oscillators have emerged as a promising platform for quantum information processing. The field of opto- and electromechanics has seen great progress, including ground-state cooling [Teu+11; Cha+11], quantum interfaces to optical or microwave modes [Pal+13; Rie+16], mechanical squeezing [Wol+15; Pir+15; Lec+15] and single-phonon manipulation [OCo+10; Chu+17; Hon+17; Ree+17]. Demonstrations of distributed mechanical entanglement, however, have so far been limited to intrinsic material resonances [Lee+11] and the motion of trapped ions [Jos+09]. Entanglement of engineered (opto-)mechanical resonances, on the other hand, would provide a route towards scalable quantum networks. The freedom of designing and choosing optical resonances would allow operation in the entire frequency range of the technologically important C-, S- and L-bands of fibre-optic telecommunications. Together with dense wavelength-division multiplexing (on the ITU-T grid), this could enable quantum nodes separated by long distances (about 100 km) that can communicate at large bandwidths. State-of-the-art engineered mechanical elements have energy lifetimes that typically range between micro- [Rie+16] and milliseconds [Mee+15], which would allow entanglement distribution on a regional level [RPL09]. In addition, these entangled mechanical systems could be interfaced with microwaves [Boc+13], opening up the possibility of integrating superconducting quantum processors in the local nodes of the network.

Here we report on the observation of distributed entanglement between two nanomechanical resonators, mediated by telecommunication-wavelength photons. We use the DLCZ protocol [Dua+01], which was experimentally pioneered with ensembles of cold atoms [Cho+05]. The entanglement is generated probabilistically through the conditional preparation of a single phonon, heralded by the detection of a signal photon that could originate from either of two identical optomechanical oscillators. Fabrication imperfections have previously limited the use of artificial structures, requiring external tuning mechanisms to render such systems indistinguishable. Here we demonstrate not only that obtaining sufficiently identical devices is in fact possible through nanofabrication, but also that our method could in principle be applied to more than two systems.

The mechanical oscillators that we use in our experiment are nano-structured silicon beams with co-localized mechanical and optical resonances. Radiation pressure forces and the photoelastic effect couple the optical and mechanical modes with a rate g_0, causing the optical frequency to shift under the displacement of the mechanical oscillator [Cha12]. This effect can be used to selectively address Stokes and anti-Stokes transitions by driving the optical resonance with detuned laser beams, resulting in a linear optomechanical interaction. As was recently shown, this technique can be used to create non-classical mechanical and optomechanical states at the single-quantum level for individual devices by using photon counting and post-selection [Rie+16; Hon+17].

To apply the DLCZ scheme to the entanglement of two separate optomechanical crystals, a critical requirement is that the photons emitted from the optomechanical cavities must be indistinguishable. This can be achieved by creating a pair of nanobeams with identical optical and mechanical resonances. Until now, however, fabrication variations have inhibited the deterministic generation of identical devices and the design of current oscillators does not include any tuning capabilities. Considering the optical mode alone, typical fabrication runs result in a spread of the resonance frequency of about 2 nm
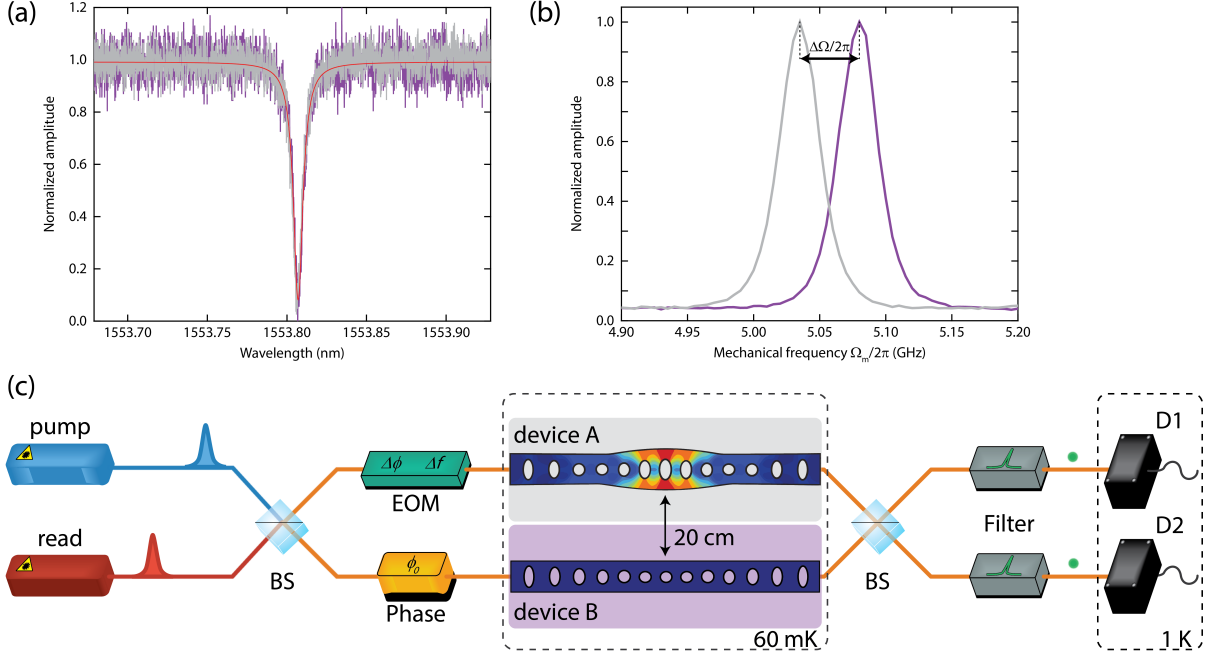
FIGURE 6.3.: **Devices and experimental setup. a**, Optical resonances of device A (grey) and device B (magenta). The Lorentzian fit result (red line) yields a quality factor of $Q = 2.2 \times 10^5$ for each cavity. **b**, Mechanical resonances of device A (grey) and device B (magenta). The normalized mechanical resonances are measured through the optomechanical sideband scattering rates. The linewidth is limited by the bandwidth of the optical pulses and filters. The frequencies of the devices differ by $\Delta\Omega_\mathrm{m}/2\pi = 45$ MHz, which could result in distinguishable photons, potentially reducing the entanglement in the system. We compensate for this shift by tuning the optical pump fields accordingly through serrodyning, erasing any information that could lead to a separable state. **c**, Experimental setup. We create optical pulses using two lasers, which are detuned to the Stokes (pump) and anti-Stokes (read) transition of the optomechanical cavities. The lasers are then combined on a 50/50 beam splitter (BS), which forms an interferometer with a second combining beam splitter. Each arm of the interferometer contains one of the mechanical oscillators, cooled to its ground state using a dilution refrigerator (central dashed rectangle). The phase of the interferometer, ϕ_0, is stabilized using a fibre stretcher (labelled 'phase'), while the phase difference between the pulses, $\Delta\phi$, is controlled using an electro-optic modulator (EOM). The same EOM is also used for serrodyning. Optical filters in front of two superconducting single-photon detectors (D1, D2) ensure that only photons scattered onto the cavity resonance are detected, whereas the original laser pulses are completely suppressed. The mechanical devices are physically separated by 20 cm and their optical separation is around 70 m.

around the centre wavelength. Therefore, finding a pair of matching optical resonances on two chips close to a target frequency currently relies on fabricating a large enough set, in which the probability of obtaining an identical pair is sufficiently high. In fact, this is achievable with a few hundred devices per chip, see Supplementary Information (SI) for details. In addition, a small mismatch in the mechanical frequencies, which is typically around 1%, can readily be compensated by appropriate manipulation of the optical pulse frequencies in the experiment.

For the experiments presented here, we chose a pair of devices with optical resonances at wavelength $\lambda = 1553.8$ nm (optical quality factor $Q = 2.2 \times 10^5$ and $g_0/2\pi = 550$ kHz and 790 kHz for devices A and B, respectively; see Fig. 6.3). For these structures, the mechanical resonance frequencies are centred around $\Omega_\mathrm{m}/2\pi \approx 5.1$ GHz and have a difference of $\Delta\Omega_\mathrm{m}/2\pi = 45$ MHz. The two chips are mounted 20 cm apart in a dilution refrigerator. Although we use a single cryostat, there is in principle no fundamental or technical reason for keeping the devices in a common cold environment. For our setup, if the telecommunication fibres linking the two devices were to be unwrapped, our setup would already allow us to bridge a separation of about 70 m between the two chips without further modification.

The protocol [Dua+01] for the creation and verification of the remote mechanical entanglement consists of three steps (for a schematic, see Fig. 6.4). First, the two mechanical resonators are cryogenically cooled, and thus initialized close to their quantum ground states [Mee+15; Rie+16; Hon+17] (see SI). Second, a weak 'pump' pulse tuned to the upper mechanical sideband (at frequency $\omega_\mathrm{pump} = 2\pi c/\lambda + \Omega_\mathrm{m}$, where c is the speed of light), is sent into a phase-stabilized interferometer (with a fixed phase difference ϕ_0, see Fig. 6.3 and SI) with one device in each arm. This drives the Stokes process–that is, the scattering of a pump photon into the cavity resonance while simultaneously creating a phonon [Rie+16]. The presence of a single phonon is heralded by the detection of a scattered Stokes photon in one of our superconducting nanowire single-photon detectors. The two optical paths of the interferometer are overlapped on a beam splitter, and a variable optical attenuator is set on one of the arms so that a scattered photon from either device is equally likely to reach either detector. The heralding detection event therefore contains no information about which device the scattering took place in and thus where the phonon was created. The energy of the pulse is tuned to ensure that the scattering probability $p_\mathrm{pump} \approx 0.7\%$ is low, making the likelihood of simultaneously creating phonons in both devices negligible. The heralding measurement therefore projects the mechanical state into a superposition of a single-excitation state in device A ($|A\rangle = |1\rangle_\mathrm{A}|0\rangle_\mathrm{B}$) or device B ($|B\rangle = |0\rangle_\mathrm{A}|1\rangle_\mathrm{B}$), with the other device remaining in the ground state. The joint state of the two mechanical systems

$$|\Psi\rangle = \frac{1}{\sqrt{2}} \left(|1\rangle_\mathrm{A}|0\rangle_\mathrm{B} \pm e^{i\theta_\mathrm{m}(0)}|0\rangle_\mathrm{A}|1\rangle_\mathrm{B} \right) \tag{6.2}$$

is therefore entangled, where $\theta_\mathrm{m}(0) = \phi_0$ is the phase with which the mechanical state is initialized at delay $\tau = 0$. This phase is determined from the relative phase difference that the pump beam acquires in the two interferometer arms [Cho+05], which we can choose using our interferometer lock. However, because the two mechanical frequencies differ by $\Delta\Omega_\mathrm{m}$, the phase of the entangled state will continue to evolve as $\theta_\mathrm{m}(\tau) = \phi_0 + \Delta\Omega_\mathrm{m}\tau$. The sign in equation (6.2) reflects which detector is used for heralding, with +

($-$) corresponding to the positive (negative) detector, as defined by the sign convention of the interferometer phase ϕ_0.

In the third step of our protocol, we experimentally verify the entanglement between the two mechanical oscillators. To achieve this, we map the mechanical state onto an optical field using a 'read' pulse after a variable delay τ. This relatively strong pulse is tuned to the lower mechanical sideband of the optical resonance ($\omega_{\mathrm{read}} = 2\pi c/\lambda - \Omega_m$). At this detuning, the field drives the anti-Stokes transition–that is, a pump photon is scattered onto the cavity resonance while annihilating a phonon [Rie+16]. Ideally, this state transfer will convert $|\Psi\rangle$ into

$$|\Phi\rangle = \frac{1}{\sqrt{2}} \left(|1\rangle_{\mathrm{r_A}}|0\rangle_{\mathrm{r_B}} \pm e^{i(\theta_{\mathrm{r}} + \theta_{\mathrm{m}}(\tau))}|0\rangle_{\mathrm{r_A}}|1\rangle_{\mathrm{r_B}} \right), \tag{6.3}$$

where $\mathrm{r_A}$ and $\mathrm{r_B}$ are the optical modes in the two interferometer arms. The state of the optical field now contains the mechanical phase as well as the phase difference θ_{r} acquired by the read pulse. We can add an additional phase offset $\Delta\phi$ to the read pulse in one of the interferometer arms so that $\theta_{\mathrm{r}} = \phi_0 + \Delta\phi$ by using an electro-optic phase modulator, as shown in Fig. 6.3. Sweeping $\Delta\phi$ allows us to probe the relative phase $\theta_{\mathrm{m}}(\tau)$ between the superpositions $|A\rangle$ and $|B\rangle$ of the mechanical state for fixed delays τ. To avoid substantial absorption heating creating thermal excitations in the oscillators, we limit the energy of the read pulse to a state-swap fidelity of about 3.4%, reducing the number of added incoherent phonons to about 0.07 at a delay of $\tau = 123$ ns (see SI).

So far we have neglected the consequence of slightly differing mechanical resonance frequencies for our heralding scheme. To compensate for the resulting frequency offset in the scattered (anti-) Stokes photons and to erase any available 'which device' information, we shift the frequency of the laser pulses by means of serrodyning (see SI). Specifically, we use the electro-optic phase modulator, which controls the phase offset $\Delta\phi$, to also shift the frequency of the pump (read) pulses to device A by $+\Delta\Omega_{\mathrm{m}}$ ($-\Delta\Omega_{\mathrm{m}}$). The frequency differences of the pulses in the two opposing paths cancel out their mechanical frequency differences exactly, ensuring that the scattered photons at the output of the interferometer are indistinguishable.

To confirm that the measured state is indeed entangled, we need to distinguish it from all possible separable states, that is, the set of all states for which systems A and B can be described independently. A specifically tailored measure that can be used to verify this nonseparability of the state is called an 'entanglement witness'. Here we use a witness that is designed for optomechanical systems [BNG11]. In contrast to other path-entanglement witnesses based on partial state tomography, such as concurrence, this approach replaces measurements of third-order coherences, $g^{(3)}$, by expressing them as second-order coherences, $g^{(2)}$, assuming linear interactions between Gaussian states. This greatly simplifies the requirements and reduces the measurement times for our experiments. Because the coherences refer to the unconditional states, the nonlinear detection and state projection do not contradict these assumptions. The above assumptions are satisfied for our system because the initial mechanical states of our devices are in fact thermal states close to the corresponding quantum ground states (step 1 of our protocol; see SI) and we use linearized optomechanical interactions (described in steps 2 and 3) [Wie+15]. The upper

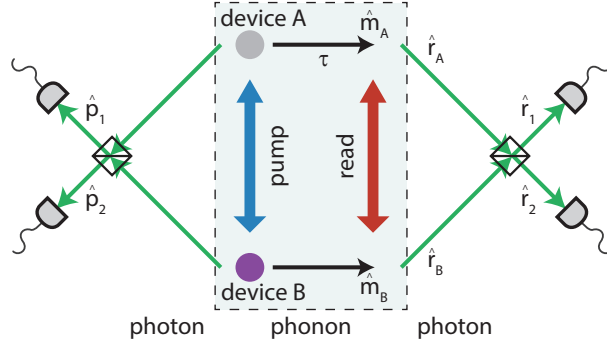## 6. Remote quantum entanglement between two micromechanical oscillators

FIGURE 6.4.: **Creation and detection of entanglement between two remote mechanical oscillators.** A pump pulse detuned to the Stokes sideband of two identical optomechanical resonators is sent into an interferometer, creating a single excitation in either device A or B. This process emits a photon on resonance with one of the cavities, and the two possible paths are superimposed using a beam splitter (black square) when exiting the interferometer (left). Detection of this photon in one of the single-photon detectors projects the two mechanical systems into an entangled state, in which neither device can be described separately. To verify this non-separable state, an optical read pulse tuned to the anti-Stokes sideband is sent into the interferometer with a delay of τ, de-exciting the mechanical systems and emitting another on-resonance photon into modes r_i ($i = $ A,B) with operators $\hat{r}_i$. The two optical paths are again superimposed on the same beam splitter (right), and the photon is detected, allowing us to measure various second-order correlation functions, which are used to test an entanglement witness. The operators $\hat{p}_j$ and $\hat{r}_j$, with $j = 1, 2$, denote the optical modes created from the pump and the read pulses, respectively, after recombination on the beam splitter and $\hat{m}_i$ ($i = $ A,B) are the operators of the mechanical modes. We note that in our experiment, the detectors used for the pump and read photons are identical (see Fig. 6.3).

bound for this witness of mechanical entanglement is given by [BNG11] (see SI).

$$R_{\mathrm{m}}(\theta, j) = 4 \cdot \frac{g^{(2)}_{r_1,p_j}(\theta) + g^{(2)}_{r_2,p_j}(\theta) - 1}{(g^{(2)}_{r_1,p_j}(\theta) - g^{(2)}_{r_2,p_j}(\theta))^2}, \tag{6.4}$$

in a symmetric setup. In equation (6.4), $\theta = \theta_{\mathrm{r}} + \theta_{\mathrm{m}}$, $j = 1, 2$ denotes the heralding detectors and $g^{(2)}_{r_i,p_j} = \langle \hat{r}^{\dagger}_i \hat{p}^{\dagger}_j \hat{r}_i \hat{p}_j \rangle / \langle \hat{r}^{\dagger}_i \hat{r}_i \rangle \langle \hat{p}^{\dagger}_j \hat{p}_j \rangle$ is the second-order coherence between the photons scattered by the pump pulse (with $\hat{p}^{\dagger}_j$ and $\hat{p}_j$ the creation and annihilation operators, respectively, of the mode going to detector j) and the converted phonons from the read pulse (with $\hat{r}^{\dagger}_j$ and $\hat{r}_j$ the creation and annihilation operators, respectively, of the mode going to detector j). For all separable states of the mechanical oscillators A and B, the witness yields $R_{\mathrm{m}}(\theta, j) \geq 1$ for any θ and j. Hence, if there exists a θ and j for which $R_{\mathrm{m}}(\theta, j) < 1$, the mechanical systems must be entangled.

Although entanglement witnesses are designed to be efficient classifiers, they typically depend on the individual characteristics of the experimental setup. If, for example, the second beam splitter (see Fig. 6.3) were to malfunction and act as a perfect mirror–that is, if all photons from device A (B) were transmitted to detector 1 (2)–then $R_{\mathrm{m}}(\theta, j)$ could still be less than 1 for separable states. This is because the witness in equation (6.4) estimates the visibility of the interference between $|A\rangle$ and $|B\rangle$ from a single measurement, without
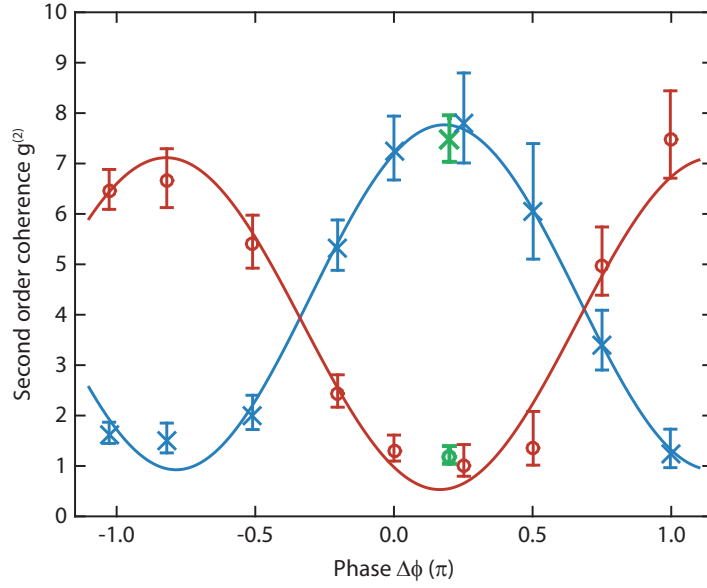
FIGURE 6.5.: **Phase sweep of the entangled state.** We vary the phase difference between the pump and the read pulses, $\Delta\phi$, and measure the second-order coherence $g^{(2)}$ of the Raman-scattered photons for a fixed delay of $\tau = 123$ ns between the pulses. Blue crosses represent measurements of $g^{(2)}_{r_i,p_j,i\neq j}$ and red circles are the results for $g^{(2)}_{r_i,p_i}$, where $i,j \in \{1,2\}$. We fit simple sine functions (shown as solid lines) to each of the datasets as guides to the eye. The sinusoidal dependence on the phase clearly highlights the coherence of the entangled mechanical state. We observe a periodicity of 1.95π, in good agreement with the expected value of 2π for single-particle interference (see equation (6.3)) [BNG11]. The phase sweep allows us to identify the optimal phase $\Delta\phi = 0.2\pi$ for maximum visibility, at which we acquire additional data (green cross and circle) to determine the entanglement witness with sufficient statistical significance. All error bars represent a 68% confidence interval.

requiring a full phase scan of the interference fringe. To ensure the applicability of the witness, we therefore verify experimentally that our system fulfills its assumptions. We first check whether our setup is balanced by adjusting the energy of the pump pulses in each arm, as described above. This guarantees that the scattered photon fluxes impinging on the beam splitter from both arms are equal (see SI). To make the detection symmetric, we use heralding detection events from both superconducting nanowire single-photon detectors–that is, we obtain the actual bound on the entanglement witness $R_{\mathrm{m,sym}}(\theta)$ from averaging measurements of $R_{\mathrm{m}}(\theta,1)$ and $R_{\mathrm{m}}(\theta,2)$ (see SI). By choosing a phase θ such that the correlations between different detectors exceed the correlations at the same detector, $g^{(2)}_{r_i,p_j,i\neq j} > g^{(2)}_{r_i,p_i}$ with $i,j \in \{1,2\}$, we avoid our measurements' susceptibility to unequal splitting ratios applied by the beam splitter.

In Fig. 6.5, we show a series of measurements of the second-order coherence $g^{(2)}$, performed by sweeping $\Delta\phi$ with a readout delay of $\tau = 123$ ns, which verify the coherence between $|A\rangle$ and $|B\rangle$. Using these data, we chose an optimal phase setting $\theta = \theta_{\mathrm{opt}}$ with $\Delta\phi = 0.2\pi$ for the main experiment. We obtain $R_{\mathrm{m,sym}}(\theta_{\mathrm{opt}}) = 0.74^{+0.12}_{-0.06}$, which is well below the separability bound of 1. By including measurements at the non-optimal adjacent phases $\Delta\phi = 0$ and 0.25π, the statistical uncertainty improves, and we obtain
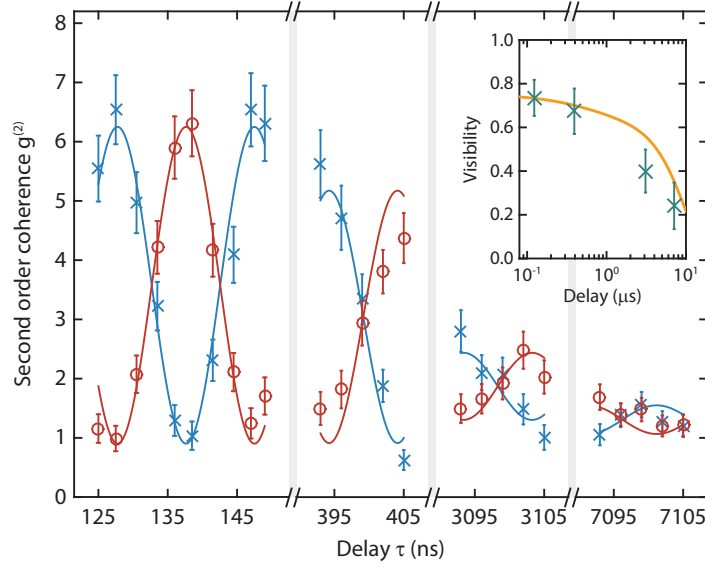
FIGURE 6.6.: **Time sweep of the entangled state.** Shown is the interference of the entangled mechanical state at different delays τ between the pump and read pulses, with the phase of the interferometer, ϕ_0, and the phase difference between the pump and read pulses, $\Delta\phi$, fixed. The blue crosses represent the measurements of $g^{(2)}_{r_i,p_j,i\neq j}$ and red circles are the results for $g^{(2)}_{r_i,p_i}$, where $i,j \in \{1,2\}$. The solid lines are sinusoidal fits averaged over the two out-of-phase components for each delay window and serve as a guide to the eye. The coherence of the entangled state is reduced over time, which can be seen by the decay of the interference visibility (inset). This decoherence is consistent with a delayed optical absorption heating and the mechanical decay time of about 4 μs of device A. The inset shows the visibility of the interference (green crosses) and the expected upper bound on the visibility due to heating and mechanical decay (orange line; see SI). All error bars represent a 68% confidence interval.

$R_{\mathrm{m,sym}}([\theta_{\mathrm{opt}}-0.2\pi, \theta_{\mathrm{opt}}+0.05\pi]) = 0.74^{+0.08}_{-0.05}$. Hence, we experimentally observe entanglement between the two remote mechanical oscillators with a confidence level above 99.8%.

The coherence properties of the generated state can be characterized through the decay of the visibility

$$V = \frac{\max(g^{(2)}_{r_i,p_j}) - \min(g^{(2)}_{r_i,p_j})}{\max(g^{(2)}_{r_i,p_j}) + \min(g^{(2)}_{r_i,p_j})}. \tag{6.5}$$

We therefore sweep the delay time τ between the pump pulse and the read pulse. The mechanical frequency difference $\Delta\Omega_m$ allows us to sweep a full interference fringe by changing the delay τ by 22 ns. Owing to the technically limited hold time of our cryostat, this sweep had to be performed at a higher bath temperature of about $80 - 90$ mK (see Fig. 6.3), yielding a slightly lower, thermally limited visibility at short delays when compared to the data in Fig. 6.5. By varying the delay further, we observe interference between $|A\rangle$ and $|B\rangle$ ($V > 0$) up to $\tau \approx 3$ μs (see Fig. 6.6). The loss of coherence can be explained by absorption heating and mechanical decay (see SI) and appears to be limited at long delays τ by the lifetime $1/\Gamma_A \approx 4$ μs of device A, which has the shorter lifetime of the two devices.

We have experimentally demonstrated entanglement between two engineered mechan-

ical oscillators separated spatially by 20 cm and optically by 70 m. Imperfections in the fabrication process and the resulting small deviations of optical and mechanical frequencies for nominally identical devices are overcome through the statistical selection of devices and optical frequency shifting using a serrodyne approach. The mechanical systems do not interact directly at any point, but are interfaced remotely through optical photons in the telecommunication-wavelength band. The coherence time of the entangled state is several microseconds and appears to be limited by the mechanical lifetime of the devices and by absorption heating. Both of these limitations can be considerably mitigated. On the one hand, optical absorption can be substantially suppressed by using intrinsic, desiccated silicon [Asa+17]. Mechanical lifetimes, on the other hand, can be greatly increased by adding a phononic bandgap shield [Mee+15]. Although our devices are engineered to have short mechanical lifetimes [Hon+17; Pat+17], earlier designs including such a phononic shield have reached [Mee+15] $1/\Gamma \approx 0.5$ ms and could still be further improved. Combined with reduced optical absorption, which would allow efficient laser cooling, such lifetimes can potentially put our devices on par with other state-of-the-art quantum systems [Mar+17].

Our experiment demonstrates a protocol for realistic, fibre telecommunication-compatible entanglement distribution using engineered mechanical quantum systems. With the current parameters of our system, a device separation of 75 km using commercially available telecommunication fibres would result in a drop of less than 5% in the interference visibility (see discussion in SI for more details). The system presented here is directly scalable to include more devices (see SI) and could be integrated into a real quantum network. Combining our results with those of optomechanical devices capable of transferring quantum information from the optical to the microwave domain, which is a highly active field of research [Boc+13; Rue+16; Hig+18], could provide a backbone for a future quantum internet based on superconducting quantum computers.

References

These are the references cited in the author's version of the manuscript.

[Asa+17]   T. Asano, Y. Ochi, Y. Takahashi, K. Kishimoto, and S. Noda, "Photonic crystal nanocavity with a Q factor exceeding eleven million", *Opt. Express* 25, 1769 (2017), DOI: `10.1364/OE.25.001769` (cited on pg. 125).

[BNG11]   K. Børkje, A. Nunnenkamp, and S. M. Girvin, "Proposal for Entangling Remote Micromechanical Oscillators via Optical Measurements", *Phys. Rev. Lett.* 107, 123601 (2011), DOI: `10.1103/PhysRevLett.107.123601` (cited on pgs. 121–123, 133).

[Boc+13]   J. Bochmann, A. Vainsencher, D. D. Awschalom, and A. N. Cleland, "Nanomechanical coupling between microwave and optical photons", *Nature Phys.* 9, 712 (2013), DOI: `10.1038/nphys2748` (cited on pgs. 118, 125).

[Cha+11]   J. Chan, T. P. M. Alegre, A. H. Safavi-naeini, J. T. Hill, A. Krause, S. Groeblacher, and M. Aspelmeyer, "Laser cooling of a nanomechanical oscillator into its quantum ground state", *Nature* 478, 89 (2011), DOI: `10.1038/nature10461` (cited on pg. 118).

[Cha12]   J. Chan, "Laser cooling of an optomechanical crystal resonator to its quantum ground state of motion", PhD thesis, California Institute of Technology, 2012 (cited on pg. 118).

[Cho+05]   C. W. Chou, H. de Riedmatten, D. Felinto, S. V. Polyakov, S. J. van Enk, and H. J. Kimble, "Measurement-induced entanglement for excitation stored in remote atomic ensembles", *Nature* 438, 828 (2005), DOI: `10.1038/nature04353` (cited on pgs. 117, 118, 120).

[Chu+17]   Y. Chu, P. Kharel, W. H. Renninger, L. D. Burkhart, L. Frunzio, P. T. Rakich, and R. J. Schoelkopf, "Quantum acoustics with superconducting qubits.", *Science* 358, 199 (2017), DOI: `10.1126/science.aao1511` (cited on pg. 118).

[Cum57]   R. C. Cumming, "The Serrodyne Frequency Translator", *Proc. IRE* 45, 175 (1957), DOI: `10.1109/JRPROC.1957.278387` (cited on pg. 132).

[Dua+01]   L. M. Duan, M. D. Lukin, J. I. Cirac, and P. Zoller, "Long-distance quantum communication with atomic ensembles and linear optics.", *Nature* 414, 413 (2001), DOI: `10.1038/35106500` (cited on pgs. 118, 120).

[Fan+17]   K. Fang, J. Luo, A. Metelmann, M. H. Matheny, F. Marquardt, A. A. Clerk, and O. Painter, "Generalized non-reciprocity in an optomechanical circuit via synthetic magnetism and reservoir engineering", *Nature Phys.* 13, 465 (2017), DOI: `10.1038/nphys4009` (cited on pg. 130).

[Hen+15]   B. Hensen et al., "Loophole-free Bell inequality violation using electron spins separated by 1.3 kilometres", *Nature* 526, 682 (2015), DOI: `10.1038/nature15759` (cited on pg. 117).

[Hig+18]   A. P. Higginbotham, P. S. Burns, M. D. Urmey, R. W. Peterson, N. S. Kampel, B. M. Brubaker, G. Smith, K. W. Lehnert, and C. A. Regal, "Harnessing electro-optic correlations in an efficient mechanical converter", *Nature Physics*, 1 (2018), DOI: `10.1038/s41567-018-0210-0` (cited on pg. 125).

[Hof+11]   S. G. Hofer, W. Wieczorek, M. Aspelmeyer, and K. Hammerer, "Quantum entanglement and teleportation in pulsed cavity optomechanics", *Phys. Rev. A* 84, 52327 (2011), DOI: `10.1103/PhysRevA.84.052327` (cited on pg. 133).

[Hon+17]   S. Hong, R. Riedinger, I. Marinković, A. Wallucks, S. G. Hofer, R. A. Norte, M. Aspelmeyer, and S. Gröblacher, "Hanbury Brown and Twiss interferometry of single phonons from an optomechanical resonator", *Science* 358, 203 (2017), DOI: `10.1126/science.aan7939` (cited on pgs. 118, 120, 125, 129, 133, 136).

[Hor+09]   R. Horodecki, P. Horodecki, M. Horodecki, and K. Horodecki, "Quantum entanglement", *Rev. Mod. Phys.* 81, 865 (2009), DOI: `10.1103/RevModPhys.81.865` (cited on pg. 132).

[HW97]   S. Hill and W. K. Wootters, "Entanglement of a Pair of Quantum Bits", *Phys. Rev. Lett.* 78, 5022 (1997), DOI: `10.1103/PhysRevLett.78.5022` (cited on pg. 133).

[Jen+11]   K. Jensen, W. Wasilewski, H. Krauter, T. Fernholz, B. M. Nielsen, M. Owari, M. B. Plenio, A. Serafini, M. M. Wolf, and E. S. Polzik, "Quantum memory for entangled continuous-variable states", *Nature Phys.* 7, 13 (2011), DOI: `10.1038/nphys1819` (cited on pg. 117).

[Jos+09]   J. D. Jost, J. P. Home, J. M. Amini, D. Hanneke, R. Ozeri, C. Langer, J. J. Bollinger, D. Leibfried, and D. J. Wineland, "Entangled mechanical oscillators", *Nature* 459, 683 (2009), DOI: `10.1038/nature08006` (cited on pgs. 117, 118).

[Kim08]   H. J. Kimble, "The quantum internet", *Nature* 453, 1023 (2008), DOI: `10.1038/nature07127` (cited on pg. 117).

[Kuz+03]   A. Kuzmich, W. P. Bowen, A. D. Boozer, A. Boca, C. W. Chou, L.-M. Duan, and H. J. Kimble, "Generation of nonclassical photon pairs for scalable quantum communication with atomic ensembles", *Nature* 423, 731 (2003), DOI: `10.1038/nature01714` (cited on pg. 135).

[Lec+15]   F. Lecocq, J. B. Clark, R. W. Simmonds, J. Aumentado, and J. D. Teufel, "Quantum Nondemolition Measurement of a Nonclassical State of a Massive Object", *Phys. Rev. X* 5, 041037 (2015), DOI: `10.1103/PhysRevX.5.041037` (cited on pg. 118).

[Lee+11]   K. C. Lee et al., "Entangling macroscopic diamonds at room temperature.", *Science* 334, 1253 (2011), DOI: `10.1126/science.1211914` (cited on pg. 118).

[Lee12]   K. C. Lee, "Generation of room-temperature entanglement in diamond with broadband pulses", PhD thesis, University of Oxford, 2012 (cited on pg. 136).

[Mar+17]   N. Maring, P. Farrera, K. Kutluer, M. Mazzera, G. Heinze, and H. de Riedmatten, "Photonic quantum state transfer between a cold atomic gas and a crystal", *Nature* 551, 485 (2017), DOI: `10.1038/nature24468` (cited on pg. 125).

[Mat+06]   D. N. Matsukevich, T. Chanelieère, S. D. Jenkins, S.-Y. Lan, T. A. B. Kennedy, and A. Kuzmich, "Entanglement of Remote Atomic Qubits", *Phys. Rev. Lett.* 96, 030405 (2006), DOI: `10.1103/PhysRevLett.96.030405` (cited on pg. 117).

[Mee+15]   S. M. Meenehan, J. D. Cohen, G. S. MacCabe, F. Marsili, M. D. Shaw, and O. Painter, "Pulsed Excitation Dynamics of an Optomechanical Crystal Resonator near Its Quantum Ground State of Motion", *Phys. Rev. X* 5, 041002 (2015), DOI: `10.1103/PhysRevX.5.041002` (cited on pgs. 118, 120, 125, 133).

[Moe+07]   D. L. Moehring, P. Maunz, S. Olmschenk, K. C. Younge, D. N. Matsukevich, L.-M. Duan, and C. Monroe, "Entanglement of single-atom quantum bits at a distance", *Nature* 449, 68 (2007), DOI: `10.1038/nature06118` (cited on pg. 117).

[OCo+10]   A. D. O'Connell et al., "Quantum ground state and single-phonon control of a mechanical resonator.", *Nature* 464, 697 (2010), DOI: `10.1038/nature08967` (cited on pg. 118).

[Pal+13]   T. A. Palomaki, J. W. Harlow, J. D. Teufel, R. W. Simmonds, and K. W. Lehnert, "Coherent state transfer between itinerant microwave fields and a mechanical oscillator", *Nature* 495, 210 (2013), DOI: `10.1038/nature11915` (cited on pg. 118).

[Pat+17]   R. N. Patel, C. J. Sarabalis, W. Jiang, J. T. Hill, and A. H. Safavi-Naeini, "Engineering phonon leakage in nanomechanical resonators", *Phys. Rev. Applied* 8, 041001 (2017), DOI: `10.1103/PhysRevApplied.8.041001` (cited on pg. 125).

[Pir+15]   J.-M. Pirkkalainen, E. Damskägg, M. Brandt, F. Massel, and M. A. Sillanpää, "Squeezing of Quantum Noise of Motion in a Micromechanical Resonator", *Phys. Rev. Lett.* 115, 243601 (2015), DOI: `10.1103/PhysRevLett.115.243601` (cited on pg. 118).

[Ree+17]   A. P. Reed et al., "Faithful conversion of propagating quantum information to mechanical motion", *Nature Phys.* (2017), DOI: `10.1038/nphys4251` (cited on pg. 118).

[Rei+11]   K. F. Reim, P. Michelberger, K. C. Lee, J. Nunn, N. K. Langford, and I. A. Walmsley, "Single-Photon-Level Quantum Memory at Room Temperature", *Phys. Rev. Lett.* 107, 053603 (2011), DOI: `10.1103/PhysRevLett.107.053603` (cited on pg. 117).

[Rie+16]   R. Riedinger, S. Hong, R. A. Norte, J. A. Slater, J. Shang, A. G. Krause, V. Anant, M. Aspelmeyer, and S. Gröblacher, "Normal Non-classical correlations between single photons and phonons from a mechanical oscillator", *Nature* 530, 313 (2016), DOI: `10.1038/nature16536` (cited on pgs. 118, 120, 121, 133, 134, 136).

[Rit+12]   S. Ritter, C. Nölleke, C. Hahn, A. Reiserer, A. Neuzner, M. Uphoff, M. Mücke, E. Figueroa, J. Bochmann, and G. Rempe, "An elementary quantum network of single atoms in optical cavities", *Nature* 484, 195 (2012), DOI: `10.1038/nature11023` (cited on pg. 117).

[RPL09]   M. Razavi, M. Piani, and N. Lütkenhaus, "Quantum repeaters with imperfect memories: Cost and scalability", *Phys. Rev. A* 80, 032301 (2009), DOI: `10.1103/PhysRevA.80.032301` (cited on pg. 118).

[Rue+16]   A. Rueda et al., "Efficient microwave to optical photon conversion: an electrooptical realization", *Optica* 3, 597 (2016), DOI: `10.1364/OPTICA.3.000597` (cited on pg. 125).

[Sag+15]   E. Saglamyurek, J. Jin, V. B. Verma, M. D. Shaw, F. Marsili, S. W. Nam, D. Oblak, and W. Tittel, "Quantum storage of entangled telecom-wavelength photons in an erbium-doped optical fibre", *Nature Photon.* 9, 83 (2015), DOI: `10.1038/nphoton.2014.311` (cited on pg. 117).

[Teu+11]   J. D. Teufel, T. Donner, D. Li, J. W. Harlow, M. S. Allman, K. Cicak, A. J. Sirois, J. D. Whittaker, K. W. Lehnert, and R. W. Simmonds, "Sideband cooling of micromechanical motion to the quantum ground state.", *Nature* 475, 359 (2011), DOI: `10.1038/nature10261` (cited on pg. 118).

[Usm+12]   I. Usmani, C. Clausen, F. Bussières, N. Sangouard, M. Afzelius, and N. Gisin, "Heralded quantum entanglement between two crystals", *Nature Photon.* 6, 234 (2012), DOI: `10.1038/nphoton.2012.34` (cited on pg. 117).

[Wie+15]   W. Wieczorek, S. G. Hofer, J. Hoelscher-Obermaier, R. Riedinger, K. Hammerer, and M. Aspelmeyer, "Optimal State Estimation for Cavity Optomechanical Systems", *Phys. Rev. Lett.* 114, 223601 (2015), DOI: `10.1103/PhysRevLett.114.223601` (cited on pgs. 121, 133).

[Wol+15]   E. E. Wollman, C. U. Lei, A. J. Weinstein, J. Suh, A. Kronwald, F. Marquardt, A. A. Clerk, and K. C. Schwab, "Quantum squeezing of motion in a mechanical resonator", *Science* 349, 952 (2015), DOI: `10.1126/science.aac5138` (cited on pg. 118).

[WRW82]   K. K. Wong, R. M. D. L. Rue, and S. Wright, "Electro-optic-waveguide frequency translator in LiNbO$_3$ fabricated by proton exchange", *Opt. Lett.* 7, 546 (1982), DOI: `10.1364/OL.7.000546` (cited on pg. 132).

6.3. Supplementary Information

6.3.1. Device fabrication and characterization

The devices in the main part are fabricated as described in reference [Hon+17]. The most crucial steps for generating two identical chips are the electron beam lithography and the inductively coupled plasma reactive ion etching. We beamwrite and etch on a single proto-chip containing two sets of devices. This chip is then diced into two halves, each with several hundred nominally identical resonators. The structures are subsequently released in 40% hydrofluoric acid and cleaned with the RCA method, followed by a dip in
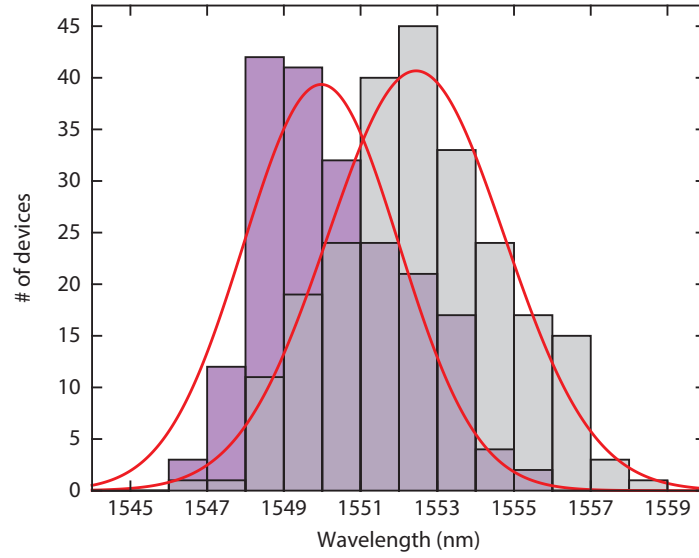
FIGURE 6.7.: **Distribution of optical wavelengths.** We plot a histogram (bin size 1 nm) of the optical resonance wavelengths for a large set of devices on each of the chips containing devices A (gray) and B (magenta). The fits of a Gaussian distribution to the data sets (red solid lines) give a standard deviation of 2.3 nm and 2.0 nm, respectively. The large overlap of the optical resonance frequencies highlights the feasibility of extending the entanglement to even more optomechanical devices in the future.

2% hydrofluoric acid. When characterizing the two chips, we find the center wavelengths to be 1552.4 nm on chip A and 1550.0 nm on chip B (see Figure 6.7). The standard deviation on the spread of the optical resonances is around 2 nm on both chips. For the experiments in the main text, we search for resonances that overlap to within 10% of their linewidth, which is equal to around 100 MHz. We find a total of 5 pairs fulfilling this requirement within 234 devices tested per chip.

In order to verify that finding identical devices is not just lucky coincidence and that this can even be done with a smaller sample size per chip, one can estimate the number of devices needed for a birthday paradox type approach. Therefore, we assume a pair of chips with 234 devices each that are centered at the same target wavelength. Taking similar parameters as found in our actual chips, we use a spread in resonance wavelength of 2 nm and we define resonances to be identical if they match to within 100 MHz. While the probability of obtaining a single device exactly at the center wavelength is only 0.03%, the probability of finding two matching devices at any wavelength within this distribution is 99.9996%. This is reduced if an offset in the mean wavelength of the two chips is introduced. For an offset of 2.5 nm, the probability is 99.98%, and for 5 nm, it is still 92.7%. By extending this approach to, for example, four chips, with the same parameters as above, no offset in the center wavelength and 500 devices per chip, we calculate the probability of finding four identical resonances to be 51.6%. Such a quartet would directly enable experiments on entanglement swapping and tests of a Bell inequality, as proposed by DLCZ. Further improvements could include post-fabrication wavelength tuning, as has recently been demonstrated for similar devices [Fan+17]. This could significantly improve the prospect of scalability of our approach, as it would allow
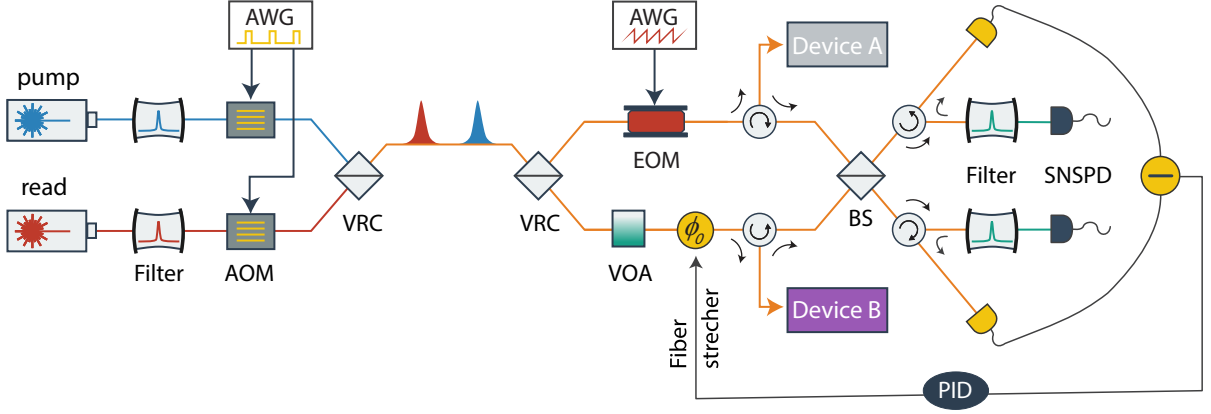
FIGURE 6.8.: **Experimental setup.** A detailed schematics of our setup is shown here and described in the text. AOM are the acousto-optic modulators, AWG the arbitrary waveform generators, VRC the variable ratio couplers, EOM the electro-optic modulator, VOA the variable optical attenuator, BS the 50/50 beamsplitter and SNSPD the superconducting nanowire single-photon detectors.

to fabricate identical devices more deterministically.

In addition, the mechanical resonances are also susceptible to fabrication errors and vary by up to 50 MHz for our devices. To overcome this mismatch, we use serrodyne frequency shifting (see sections below).

6.3.2. Experimental setup

A detailed drawing of the experimental setup is shown in Figure 6.8. The light sources for our pump and read beams are two New Focus 6728 CW lasers, tuned and stabilized on their respective sideband of the optical resonance. The beams are filtered by MicronOptics FFP-TF2 tunable optical filters in order to reduce the laser phase noise in the GHz regime. We then proceed to generate the actual pump and read pulses by driving acousto-optic modulators (Gooch&Housego T-M110-0.2C2J-3-F2S) with an arbitrary function generator (Tektronic AFG3152C). These pulses are then combined on a variable ratio coupler (Newport F-CPL-1550-N-FA). The combined optical mode is subsequently split by another variable ratio coupler and fed into the Mach Zehnder interferometer. The coupling ratio is adjusted to primarily compensate for a small difference in total losses between two paths. The power in the interferometer arms can additionally be balanced by an electrically driven variable optical attenuator (Sercalo VP1). We reflect the pulses from the two devices via optical circulators and recombine on a 50/50 coupler (measured deviation of 0.6%, see below). The strong pump pulses are filtered with two MicronOptics FFP-TF2 fiber filters per detection arm, tuned to transmit only the scattered (anti-) Stokes photons (bandwidth 50 MHz). We detect the resonant photons with superconducting nanowire single photon detectors (Photonspot) and register their arrival times on a TimeHarp 260 NANO correlation board.

6.3.3. Serrodyne frequency shifting

In our experiment, the mechanical frequency of device B ($\Omega_{\mathrm{m,B}}$) is greater than of device A ($\Omega_{\mathrm{m,A}}$) by $\Delta\Omega_{\mathrm{m}} = 2\pi \cdot 45$ MHz. If we were to send pump pulses with exactly the same frequency ω_{pump} to both of the devices, they would produce scattered photons with frequencies $\omega_{\mathrm{o,A}} = \omega_{\mathrm{pump}} - \Omega_{\mathrm{m,A}}$ and $\omega_{\mathrm{o,B}} = \omega_{\mathrm{pump}} - \Omega_{\mathrm{m,B}} = \omega_{\mathrm{o,A}} - \Delta\Omega_{\mathrm{m}}$. This frequency mismatch of scattered photons from the two devices would make them distinguishable, therefore preventing the entangled state. A simple solution is to shift the frequency of the pump pulse going to the device A by $\Delta\Omega_{\mathrm{m}}$, i.e. $\omega_{\mathrm{pump,A}} = \omega_{\mathrm{pump}} - \Delta\Omega_{\mathrm{m}}$. We experimentally realize this by electrically driving the electro-optic phase modulator on the path to device A, with a sawtooth waveform. This so-called serrodyne modulation with frequency $\omega_{\mathrm{s}} = \Delta\Omega_{\mathrm{m}}$ and peak-to-peak phase amplitude of 2π results in an optical frequency shift of ω_{s} [Cum57; WRW82]. We use an arbitrary waveform generator (Agilent 81180A, bandwidth DC to 600 MHz) to generate the sawtooth voltage signal, amplify it with a broadband amplifier (Minicircuits TVA-R5-13A+, bandwidth 0.5 to 1000 MHz) and apply it to the optical phase modulator (Photline MPZ-LN-10-P-P-FA-FA-P, bandwidth DC to 12 GHz). We also apply an additional DC-bias to the serrodyne signal in order to generate a fixed phase offset $\Delta\phi$ in the interferometer arms. Due to the high analog bandwidth of the AWG compared to the frequency shift of 45 MHz, higher order sidebands were negligible and were not observed in the experiment.

6.3.4. Phase stabilization of the interferometer

For stabilizing the phase of the interferometer, we use an additional laser pulse ~ 5 μs after the read pulse. To produce these auxiliary pulses, we also use the red-detuned laser that generates the read pulses and send them along the same beam paths. After being reflected from the optical filters in the detection line, the pulses are re-routed by optical circulators and picked up by a balanced detector (see Figure 6.8). These signals are then sent to a PID controller, which regulates a fiber stretcher to stabilize the relative path length and therefore locking the phase of the interferometer on a slow timescale (i.e. with the experiment repetition period of 50 μs).

In principle, the read or pump pulses that are reflected off the filter cavities could also be used for the phase locking. However, the serrodyne modulation during pump and read results in a beat signal of the pulses behind the beam splitter. This beating requires more sophisticated signal processing, which we avoid by using the auxiliary pulses, during which the serrodyne modulation is off. We note that the auxiliary pulses also induce some absorption heating of the devices. However, the 50 μs repetition period is sufficiently long compared to the decay times of the devices for the extra heating not to influence our experimental result.

6.3.5. Entanglement witness and Systematic Errors

The entanglement witness [Hor+09]

$$R(\tau, j) = \frac{\left\langle \hat{m}_{\mathrm{A}}^{\dagger}(\tau)\hat{m}_{\mathrm{A}}(\tau)\hat{m}_{\mathrm{B}}^{\dagger}(\tau)\hat{m}_{\mathrm{B}}(\tau) \right\rangle_j}{\left| \left\langle \hat{m}_{\mathrm{A}}^{\dagger}(\tau)\hat{m}_{\mathrm{B}}(\tau) \right\rangle_j \right|^2} \tag{6.6}$$

derived in reference [BNG11] is based on the concurrence [HW97] of the bipartite mechanical system. Here, the conditional average $\langle \hat{o} \rangle_j = \langle \hat{o} \, \hat{p}_j^\dagger \hat{p}_j \rangle / \langle \hat{p}_j^\dagger \hat{p}_j \rangle$ for an operator $\hat{o}$ is its expectation value of the state heralded by a Stokes photon detected by detector j. The $\hat{m}_i$ ($\hat{m}_i^\dagger$) are the mechanical annihilation (creation) operators of device $i = \mathrm{A}, \mathrm{B}$. While R is experimentally not directly accessible, the upper bound to this witness R_m, see Eq. (6.4), is a measurable quantity in our interferometry setup. The derivation of the inequality $R_\mathrm{m} \geq R$, as described in reference [BNG11] and its supplementary material, is based on several of assumptions: The unheralded state must be Gaussian at all times, and the interference on the combining beamsplitter must be symmetric. In this section, we would like to discuss the validity of each of these assumptions in more detail.

To obtain R_m, threefold coincidence measurements are re-expressed as twofold coincidences, which can be done for Gaussian states. Note that as the degrees of second order coherence in Eq. (6.4) are measured between the pump and the read pulse, they are applied to this Gaussian state, not to the heralded, non-Gaussian entangled state $|\Psi\rangle \sim |A\rangle + e^{i\theta}|B\rangle$. We ensure that the mechanical states at the beginning of our protocol are Gaussian by allowing sufficiently long thermalization times (7x the mechanical decay time) prior to any optical manipulations. Consequently, the initial state is thermal, which for a bosonic system [Rie+16; Hon+17] implies Gaussian quadrature statistics [Wie+15]. Next, all optomechanical interactions involved in our protocol are linear [Hof+11], therefore conserving the Gaussianity of the state [Wie+15]. Specifically, the Stokes process is described by the linear interaction Hamiltonian $\hat{H}_S \propto g_0 \hat{m}_i^\dagger \hat{o}_i^\dagger + h.c.$ and the anti-Stokes process by $\hat{H}_{AS} \propto g_0 \hat{m}_i \hat{o}_i^\dagger + h.c.$ for device $i = \mathrm{A}, \mathrm{B}$ with the annihilation (creation) operator of optical resonance $\hat{o}_i$ ($\hat{o}_i^\dagger$).

Unintentional interactions, like absorption heating, happen probabilistically and in a remote frequency regime, such that it effectively acts as a Gaussian thermal bath [Mee+15; Hon+17]. Though not strictly contributing to the mechanical state, we also consider false positive detection events: drive photons leaking through the filter stages can be described by a coherent state (with Gaussian intensity fluctuations). Detection of stray photons and electrically caused false positive events are rare ($\sim 0.3\%$ of the total count rate in the detection window) and uncorrelated (autocorrelation $g^{(2)}(0) = 1.05 \pm 0.09$), such that it is reasonable to model them as a Gaussian process as well. More specifically, we observe an average added noise of ~ 0.14 phonons during the measurement, from which the individual contributions of leaked drive photons, background detection events, and optical absorption heating can be estimated with additional measurements (for details see the section on "Second Order Coherence and Entanglement"). With the latter being a thermal process and therefore yielding Gaussian quadrature statistics, and an estimation of the initial thermal occupation from the nominal cryostat temperature, this leaves $\sim 4^{+2.8}_{-2.7} \cdot 10^{-2}$ phonons in device A and $\sim 0^{+1.4}_{-0} \cdot 10^{-2}$ in device B of unidentified origin. These are likely thermal phonons stemming from the non-ideal thermalization of the chips with their environment [Rie+16; Hon+17].

For the modes leaving the interferometer $\hat{r}_\mathrm{j}$, $\hat{p}_\mathrm{j}$, reference [BNG11] assumes an ideal 50/50 beamsplitter with equal powers on each input. Small experimental deviations from this idealized scenario result in quadratic corrections to the witness. For example, when the ratio of read photons at the beamsplitter originating from devices A and B is $1 + \delta$, the measurable upper bound changes to $R_\mathrm{m}(1 + \delta^2/2) \geq R$ for small δ. In our experimental setup, we choose a fused fiber beamsplitter with a measured deviation of

0.6%, leading to a relative correction on the order of 10^{-5}. Experimentally, we cannot achieve power balancing at the input of the beamsplitter for photons scattered from the pump and the read pulses at the same time because the devices have slightly different thermal occupation. We choose to match the detection rates of heralding photons, i.e. photons scattered by the pump pulse. This preserves the unknown origin of the heralding photons. Differences in the optomechanical coupling strength and optical losses on the path from the device to the combining beamsplitter are compensated by adjusting the drive power in each path. After the balancing procedure, the relative difference in count rates of heralding photons is below 2%, limited by the measurement precision during the balancing run and laser power fluctuations during the measurements. This leads to a relative correction of the witness below 10^{-3}. The slightly different heating dynamics between devices A and B result in a measured flux ratio deviation of the scattered readout photons of $\delta \sim 5 - 10\%$. It can easily be seen from Equation (6.4) that an increased heating will increase the witness R_{m}, and therefore the heating induced imbalance does not limit the validity of the witness. Yet, neglecting the thermal origin of the imbalancing, employing the correction $R_{\mathrm{m}}(1 + \delta^2/2) \geq R$, we obtain a relative systematic correction of 0.5% to our result in the worst case scenario. Adding all systematic errors, we obtain a conservative upper bound of all relative systematic corrections of $\sim$0.5%. Consequently, we use a reduced classicality bound of $R_m \geq 0.995$ instead of 1, reducing the confidence level slightly from 99.84% to 99.82%.

6.3.6. Statistical Analysis

Results in the text and figures are given as maximum likelihood values and, where applicable, with a confidence interval of $\pm 34\%$ around this value. For the second order coherences $g^{(2)}_{ri,pj}$, $(i, j = 1, 2)$, we apply binomial statistics based on the number of counted two-fold coincidences, which dominates the statistical uncertainty [Rie+16]. The entanglement witness $R_{\mathrm{m}}(\theta, j)$ in Eq. (6.4) is a non-trivial function of multiple such $g^{(2)}_{ri,pj}$, expressed here as $R_{\mathrm{m}}(\theta, j) \equiv \mathcal{R}_{\mathrm{m}}\left(g^{(2)}_{r1,pj}(\theta), g^{(2)}_{r2,pj}(\theta)\right)$. To estimate its confidence intervals, we discretize the probability density function of the second order coherences $P(g^{(2)}_{ri,pj} \in [a; a+\delta a])$ at equidistant $a = n\delta a, n \in \mathbb{N}$. The probabilities for finding R_{m} in an interval $[f, f + \delta f]$ is then given by $P(R_{\mathrm{m}} \in [f, f+\delta f]) = \sum_{(a,b)\in\mathcal{M}} P(g^{(2)}_{r1,pj} \in [a, a+\delta a])P(g^{(2)}_{r2,pj} \in [b, b+\delta b])$ on the set $\mathcal{M}$ for which $\mathcal{R}_{\mathrm{m}}(a, b) \in [f, f+\delta f]\forall (a, b) \in \mathcal{M}$. For the optimal read phase θ_{opt} we obtain as maximum likelihood values for the witness bounds $R_{\mathrm{m}}(\theta_{\mathrm{opt}}, 1) = 0.612^{+0.152}_{-0.057}$ and $R_{\mathrm{m}}(\theta_{\mathrm{opt}}, 2) = 0.846^{+0.210}_{-0.090}$. We obtain the symmetrized witness by treating the experimentally observed $R_{\mathrm{m}}(\theta_{\mathrm{opt}}, 1)$ and $R_{\mathrm{m}}(\theta_{\mathrm{opt}}, 2)$ as two independent measurements of the expectation value $R_{\mathrm{m, sym}}(\theta) \equiv \langle R_{\mathrm{m}}(\theta, 1)\rangle \overset{!}{=} \langle R_{\mathrm{m}}(\theta, 2)\rangle$ of the optomechanical state in a symmetric setup with no detector noise. For a realistic setup with detectors exhibiting different noise properties, without loss of generality, let detector j have more false positive detection events than detector i. We then find the symmetrized witness $\langle R_{\mathrm{m}}(\theta_{\mathrm{opt}}, i)\rangle \leq R_{\mathrm{m, sym}} \leq \langle R_{\mathrm{m}}(\theta_{\mathrm{opt}}, j)\rangle$ to be an upper bound to the entanglement witness of the state heralded by the better detector i. Consequently $1 > R_{\mathrm{m, sym}} \geq R_{\mathrm{m}}(\theta_{\mathrm{opt}}, i) \geq R$ implies entanglement between the two remote mechanical oscillators. The observed values yield a confidence level for $R_{\mathrm{m, sym}} < 1$ of 98.4%. When correcting for the conservative upper bound of systematic errors, see above, the confidence level for having observed

entanglement remains at 98.3%.

The complete counting statistics of the witness measurement at θ_{opt} are accumulated over $N = 1.114 \cdot 10^9$ trials (i.e. sets of pulses). We obtain $C(p_1) = 111134$ and $C(p_2) = 184114$ counts for photons scattered by the pump pulse on detectors $i = 1, 2$ and $C(r_1) = 108723$ and $C(r_2) = 167427$ counts from the read pulse. This yields the coincidence counts $C_{ri,pj}$, $(i, j = 1, 2)$ for counts on detector i, heralded by detector j, $C_{r1,p1} = 9$, $C_{r2,p1} = 130$, $C_{r1,p2} = 129$, $C_{r2,p2} = 37$.

For non-optimal phases $\theta \neq \theta_{\text{opt}}$, $R_{\text{m}}(\theta, i) \geq R_{\text{m}}(\theta_{\text{opt}}, i)$. Consequently, by adding the photon counts of measurements from an interval $[\theta_1, \theta_2]$, the resulting $R_{\text{m}}([\theta_1, \theta_2], i) \geq R_{\text{m}}(\theta \in [\theta_1, \theta_2], i)$ serves as an upper bound to any phase θ within that interval. Including the measurements at the non-optimal phase $\Delta\phi = 0$, we obtain $R_{\text{m}}([\theta_{\text{opt}} - 0.2\pi, \theta_{\text{opt}}], 1) = 0.66^{+0.114}_{-0.055}$ and $R_{\text{m}}([\theta_{\text{opt}} - 0.2\pi, \theta_{\text{opt}}], 2) = 0.806^{+0.129}_{-0.071}$, resulting in $R_{\text{m, sym}}([\theta_{\text{opt}} - 0.2\pi, \theta_{\text{opt}}]) = 0.74^{+0.08}_{-0.05} \geq R_{\text{m, sym}}(\theta_{\text{opt}})$. The confidence level for $R_{\text{m, sym}} < 1$ is 99.84%, dropping to 99.82% when correcting for the conservative upper bound for systematic errors. Note that for states heralded only with the more efficient detector 1, we already have a confidence level for entanglement between the two mechanical oscillators of 99.50%, including corrections for systematic errors.

The statistics of the witness within the extended phase region are obtained from $N = 1.949 \cdot 10^9$ experimental trials. We get $C(p_1) = 196080$ and $C(p_2) = 322608$ counts for photons scattered by the pump pulse on detectors $i = 1, 2$ and $C(r_1) = 194023$ and $C(r_2) = 300373$ counts from the read pulse. This yields the coincidence counts $C_{ri,pj}$, $(i, j = 1, 2)$ for counts on detector i, heralded by detector j, $C_{r1,p1} = 16$, $C_{r2,p1} = 223$, $C_{r1,p2} = 242$, $C_{r2,p2} = 67$.

6.3.7. Second Order Coherence and Entanglement

The second order coherence between the scattered photons from the pump pulse and signal phonons transfered by the read pulse after a delay t, $g^{(2)}_{i,rp}(t) = \langle \hat{r}^\dagger_j \hat{p}^\dagger_j \hat{r}_j \hat{p}_j \rangle / \langle \hat{r}^\dagger_j \hat{r}_j \rangle \langle \hat{p}^\dagger_j \hat{p}_j \rangle$, of the individual devices $i = A, B$, allows to us quantify the total noise contribution limiting the interference visibility. The measurements are performed the same way as described in the main text, however with the optical path to the other device blocked (see Fig. 6.4). Though there is no fundamental difference between the detectors $j = 1, 2$, we only use detector $j = 2$ for the single device measurements. Following [Kuz+03] and starting from a thermal state for the mechanical system ρ_m and vacuum $|0\rangle\langle 0|_o$ in the optical sidebands we obtain in the low temperature limit

$$g^{(2)}_{i,rp}(t) \approx 1 + \frac{e^{-\Gamma_i t}}{n_{i,\text{th}}(t) + p_{\text{pump},i} \cdot e^{-\Gamma_i t} + n_{\text{leak}} + n_{\text{bg}}}, \tag{6.7}$$

where $n_{i,\text{th}} \ll 1$ is the mean phonon occupation of the device, $p_{\text{pump},i} \ll n_{\text{th}}$ is the Stokes excitation probability, $n_{\text{leak}} \ll n_{\text{th}}$ is the average number of leaked pump photons per transfered phonon, and $n_{\text{bg}} \ll n_{\text{th}}$ is the average number of background counts per detected phonon. At a delay of $\tau = 123$ ns $\ll 1/\Gamma_i$ we measure $g^{(2)}_{A,rp} = 7.1^{+1.2}_{-0.9}$ and $g^{(2)}_{B,rp} = 9.6^{+1.1}_{-0.9}$. With calibrated rates of $n_{\text{bg}} = 3 \cdot 10^{-3}$, $p_{\text{pump},A} = 0.56 \cdot 10^{-2}$, $p_{\text{pump},B} = 0.80 \cdot 10^{-2}$ and leaks at detector 1 $n_{\text{leak},1} = 4.2 \cdot 10^{-2}$ and detector 2 $n_{\text{leak},2} = 3.2 \cdot 10^{-2}$ we can estimate the number of incoherent phonons to be $n_{\text{th},A} = 11.9^{+2.8}_{-2.7} \cdot 10^{-2}$ for device A and $n_{\text{th},B} = 6.9^{+1.4}_{-1.3} \cdot 10^{-2}$ for device B. In a more detailed analysis, including the mechanical
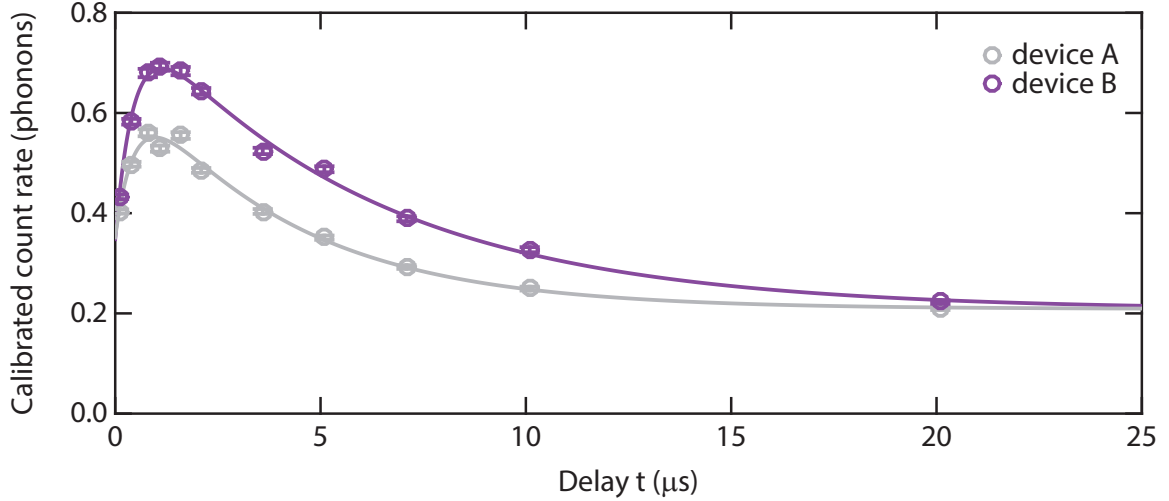
FIGURE 6.9.: **Pump-probe experiment.** The experiment reveals the response of the devices mechanical modes to the initial optical pump. See text for details. Error bars are s.d.

decay measurement (see below), we can estimate that absorption by the pump pulse contributes $n_{\mathrm{pump}} \sim 3 \cdot 10^{-2}$ phonons and absorption from the read pulse contributes $n_{\mathrm{read}} \sim 5 \cdot 10^{-2}$ phonons. This suggest, that the performance of device A is limited by imperfect thermalization with the cryostat at a temperature of 60 mK.

The interference contrast of the entangled state, i.e.

$$C_{\mathrm{e}}(t) = \max\left(g_{ri,pj}^{(2)}(t, \theta)\right) - \min(g_{ri,pj}^{(2)}(t, \theta))$$

is bound by the cross-correlation of the individual devices [Lee12] $C_{\mathrm{e,max}}(t) \approx \min(g_{\mathrm{A},rp}^{(2)}(t), g_{\mathrm{B},rp}^{(2)}(t)) - 1$. A pump-probe measurement of the thermal response of the devices [Rie+16] allows us to predict the cross correlations and thus an upper bound to the interference contrast. We excite the devices with a blue detuned pump pulse with $p_{\mathrm{pump,A}} = 2.8\%$ ($p_{\mathrm{pump,B}} = 4.0\%$) and vary the delay of a read (or probe) pulse with 5.6% (8.0%) state swap fidelity for device A (B). Note that for this experiment, we deliberately choose pulse energies higher than for the interference experiments in order to reduce the measurement time. As is done for sideband asymmetry [Rie+16; Hon+17], the scattering rate of the probe pulse can be converted into the number of phonons at time t, when using the rate of the pump pulse (after scaling the signal according to the pump-to-probe power ratio) as a reference signal of single-phonon strength. This is only valid when $n_{\mathrm{th}} \ll 1$ at the time of pump pulse, which we find is the case later in the section. The results of these measurements are shown in Figure 6.9. We observe an initial rise in phonon occupation after the pump pulse, followed by a decay to an equilibrium state. The delayed heating can be understood by the presence of long lived high frequency phonons, which weakly couple to the 5 GHz modes under investigation. We model these high frequency phonons by an effective thermal bath, exponentially decaying with rate γ_i. This results in the rate equation $\dot{n}_i(t) = -\Gamma_i n_i(t) + k_i e^{-\gamma_i t} + \Gamma_i n_{i,\mathrm{init}}$ of the mean occupation number n_i of device $i = $ A,B. The additional bath couples with strength k_i, and the thermal environment of the chip has an equilibrium temperature of $n_{i,\mathrm{init}}$. The detected signal of the probe pulse

$d_i(t) = n_{i,\text{pump}}(t) + n_{i,\text{final}}$ contains the average phonon number $n_{i,\text{pump}}(t) = n_i(t) - n_{i,\text{init}}$ induced by the pump beam, as well as a constant offset $n_{i,\text{final}} = n_{i,\text{init}} + n_{i,\text{probe}} + n_{\text{leak}} + n_{\text{bg}}$ given by the thermal environment $n_{i,\text{init}}$, the false positive events n_{leak} and n_{bg} and the heating during the probe pulse itself $n_{i,\text{probe}}$. Consequently, we fit the pump-probe data with the general solution of the above differential equation $d_i(t) = a_i \cdot e^{-\Gamma_i t} - b_i \cdot e^{-\gamma_i t} + n_{i,\text{final}}$, with a_i, b_i fitting parameters and including the offset $n_{i,\text{final}}$ of the probe pulse detection rate. We obtain $1/\Gamma_A = 4.0$ μs, $1/\Gamma_B = 5.8$ μs, $1/\gamma_A = 0.5$ μs and $1/\gamma_B = 0.5$ μs. Using the calibrated false positive detection rates and estimating the equilibrium occupation from the thermal environment $n_{i,\text{init}} \sim 1/(e^{\hbar\Omega/k_B T} - 1)$, with the Boltzmann constant k_B and cryostat temperature T, we can obtain the individual contributions to the absorption heating by the pump ($n_{i,\text{pump}}$) and the probe pulse ($n_{i,\text{probe}}$) for any given delay t. Adapting the number of phonons added by the optical drive pulses $n_{i,\text{pump}}$ and $n_{i,\text{probe}}$ for the lower energies, under the assumption of linear absorption and optomechanical processes, we obtain an estimate of the thermal occupation $n_{i,\text{th}}(t) = n_i(t) + n_{i,\text{probe}} - p_{\text{pump},i} e^{-\Gamma_i t}$ during the entanglement experiment. Using the calibrated rates and equation (6.7), we can obtain an upper bound to the interference contrast $C_{\text{e,max}}$ (see above) and therefore also for the visibility $V_{\text{max}} = C_{\text{e,max}}/(C_{\text{e,max}} + 2)$, which is shown in Figure 6.6.

6.3.8. Rates and Extrapolation of Results

In order to highlight the scalability of the mechanical entanglement, we recapitulate the detection rates in the entanglement witness measurement. The experiment is repeated every 50 μs, limited by the thermalization time of the mechanical modes. Using the counting statistics of the measurement at the optimal phase θ_{opt}, see above, we have a probability of $p_{\text{herald}} \approx 2.7 \cdot 10^{-4}$ and the unconditional probability to also detect the anti-Stokes photon from the readout pulse of $p_{\text{read}} \approx 2.8 \cdot 10^{-7}$. These probabilities contain the optomechanically generated photons, leaked pump photons and background counts. In the current setup these rates are limited by losses in the filtering setup and low optomechanical scattering rates to retain the effects of absorption heating. When the two mechanical devices are placed in two separate refrigerators and placed in different locations, additional fiber would be inserted, causing additional losses. While the detection rate of leaked pump photons reduces in the same manner as the of the optomechanical photons, the rate of background counts stays the same. Consequently, the signal-to-noise ratio reduces, lowering the normalized cross-correlation between Stokes and anti-Stokes photons. In the present measurements, the inverse signal-to-background ratio is $n_{\text{bg},1} = 2.9 \cdot 10^{-3}$ ($n_{\text{bg},2} = 3.2 \cdot 10^{-3}$) for detectors 1 (2). The most reliable estimate of the second order coherence of device A, which has worse properties, can be extracted from the observed interference contrast, resulting in $g_{A,\text{rp}}^{(2)} \sim 7.5 \pm 0.35$, as it has better statistics than the direct measurement. For device B, we use the direct measurement $g_{B,\text{rp}}^{(2)} = 9.6_{-0.9}^{+1.1}$. To maintain an interference contrast of 95% of the current level, the second order coherence of both devices is allowed to decrease to ~7.1. With equation (6.7) we can estimate that an additional loss of 5.4 dB (10.6 dB) loss in the optical path from device A (B) to the combining beamsplitter decreases the signal-to-background ratio, such that $g_{A,rp}^{(2)} \approx g_{B,rp}^{(2)} \approx 7.1$. Using the nominal attenuation of commercial low-loss telecom fiber (Corning SMF-28 ULL ~0.17 dB/km), we can estimate that an additional fiber length of 94_{-12}^{+8} km could be inserted between the devices. The projected entanglement witness in this configuration

is $R_m \sim 0.76$ and would need roughly the same number of coincidence events to clear the classicality bound of 1 by 3 standard deviations. Including the reduced scattering rates from matching both paths, this would require $\sim$170 days of integration time, including a 15% overhead time for stabilization of filters and interferometer as well as data management. Reducing the separation distance to 75 km, i.e. an additional fiber length of 32 km (43 km) between device A (B) and the beamsplitter, requires 38 days of continuous measurement time for a statistically significant demonstration of remote entanglement. While our cryostat currently only allows for a few weeks of measurements at a time due to technical limitations, much longer times should in principle be easily achievable.

7. Outlook

In this thesis, I presented three classic quantum optics experiments using single phonons in silicon optomechanical crystals. In reference [Rie+16] and chapter 4, we observed the violation of a classical Cauchy–Scharz inequality for cross-correlations [Cla74], and thereby demonstrated that the mechanical memory operates in the quantum regime [Kuz+03]. Using these optomechanical quantum correlations, we created heralded single phonon Fock states in reference [Hon+17] and chapter 5. The mechanical state exhibited the genuine quantum feature [SM83] of phonon anti-correlations, which were measured by Hanbury Brown and Twiss interferometry. Employing two nearly identical devices in reference [Rie+18] and chapter 6, we reported mechanical path entanglement of a single phonon [GRA86; RT90]. This demonstrated that the optomechanical memory elements have the functionality required for quantum repeater nodes [Dua+01; Cho+05].

The intriguing feature of optomechanical crystals, which distinguishes them from the plethora of readily available quantum systems, is that they are engineered and integrated devices. The freedom of design allows to choose virtually any wavelength in the infrared telecommunication bands as optical resonance. This allows for high speed applications through wavelength division multiplexing, while maintaining long mechanical memory life times. In addition, the compatibility with silicon photonics enables the integration of large parts of the optical setup on chip. With small individual footprints, large numbers of devices can be located and interfaced on a single chip. Complex optical quantum networks, e.g. featuring hundreds of deterministic single photon sources, can potentially be realized on chip and connected to remote locations by low loss optical fibers. In principle, the mechanical modes can also be coupled to superconducting circuits, e.g. using piezoelectric transducers. This opens up the perspective of a hybrid infrared-mechanical-microwave architecture, which combines the advantages of superconducting circuits, mechanical memory elements and high speed infrared communication to form powerful local nodes of a large quantum network. Intriguingly, all elements of such a system are artificial, macroscopic devices, which can be engineered to be compatible with each other and to excel in their respective task.

Clearly, these visions require intense further development of the systems before they can be realized. Primarily, the influence of absorption heating in the optomechanical crystals needs to be reduced. Further, the basic elements of silicon photonics, such as tunable filters, need to be made compatible with a cryogenic environment, and phonon mediated electro-optic conversion ought to be demonstrated in the quantum regime.

Fortunately, very encouraging steps in these directions have recently been reported. Optomechanical crystals were extended to two dimensional geometries [Saf+14], yielding the promise of better thermalization and thus operating them in the strong cooperativity regime. Furthermore, tuning mechanisms for photonic crystal cavities were explored [Sip+16; Pfe+16], with the prospect of generating large arrays of identical devices, together with matched integrated filters [Bek+18]. Mechanical transduction between pho-

tons at microwave and infrared frequencies is a very active field of research, inching ever closer to the quantum domain [Vai+16; Hig+18]. In addition, our recent demonstration of entanglement between an optical and a mechanical system [Mar+18] is an important step towards quantum communication applications with an optomechanical back bone.

In conclusion, my work on single phonon quantum optics highlighted the potential of optomechanical crystals for quantum information applications. Due to their unique and designable properties, the are a promising extension to the arsenal of quantum devices.

Bibliography

[AC05]   J. S. Aldridge and A. N. Cleland, "Noise-Enabled Precision Measurements of a Duffing Nanomechanical Resonator", *Physical Review Letters* 94, 156403 (2005), DOI: 10.1103/PhysRevLett.94.156403 (cited on pg. 7).

[AGR81]   A. Aspect, P. Grangier, and G. Roger, "Experimental Tests of Realistic Local Theories via Bell's Theorem", *Physical Review Letters* 47, 460 (1981), DOI: 10.1103/PhysRevLett.47.460 (cited on pgs. 1, 111).

[AGR82]   A. Aspect, P. Grangier, and G. Roger, "Experimental Realization of Einstein-Podolsky-Rosen-Bohm Gedankenexperiment : A New Violation of Bell's Inequalities", *Physical Review Letters* 49, 91 (1982), DOI: 10.1103/PhysRevLett.49.91 (cited on pg. 116).

[ÁJV55]   A. Ádám, L. Jánossy, and P. Varga, "Beobachtungen mit dem Elektronenvervielfacher an kohärenten Lichtstrahlen", *Annalen der Physik* 451, 408 (1955), DOI: 10.1002/andp.19554510515 (cited on pgs. 61, 88).

[Aka+03]   Y. Akahane, T. Asano, B.-S. Song, and S. Noda, "Erratum: High-Q photonic nanocavity in a two-dimensional photonic crystal", *Nature* 425, 944 (2003), DOI: 10.1038/nature02063 (cited on pg. 59).

[AKM14]   M. Aspelmeyer, T. J. Kippenberg, and F. Marquardt, "Cavity optomechanics", *Reviews of Modern Physics* 86, 1391 (2014), DOI: 10.1103/RevModPhys.86.1391 (cited on pgs. 1, 6, 7, 23, 24).

[Ale+11]   T. P. M. Alegre, A. Safavi-Naeini, M. Winger, and O. Painter, "Quasi-two-dimensional optomechanical crystals with a complete phononic bandgap", *Optics Express* 19, 5658 (2011), DOI: 10.1364/OE.19.005658 (cited on pg. 59).

[And+14]   R. W. Andrews, R. W. Peterson, T. P. Purdy, K. Cicak, R. W. Simmonds, C. A. Regal, and K. W. Lehnert, "Bidirectional and efficient conversion between microwave and optical light", *Nature Physics* 10, 321 (2014), DOI: 10.1038/nphys2911 (cited on pg. 2).

[Ans+09]   M. Ansmann et al., "Violation of Bell's inequality in Josephson phase qubits", *Nature* 461, 504 (2009), DOI: 10.1038/nature08363 (cited on pg. 113).

[Arc+06]   O. Arcizet, P.-F. Cohadon, T. Briant, M. Pinard, and A. Heidmann, "Radiation-pressure cooling and optomechanical instability of a micromirror", *Nature* 444, 71 (2006), DOI: 10.1038/nature05244 (cited on pgs. 2, 60).

[ARW73]   D. K. Anderson, R. T. Robiscoe, and J. M. Wessner, "More tests of QED", *Physics Today* 26, 13 (1973), DOI: 10.1063/1.3127942 (cited on pg. 61).

Bibliography

[AS71]   R. R. Alfano and S. L. Shapiro, "Optical Phonon Lifetime Measured Directly with Picosecond Pulses", *Physical Review Letters* 26, 1247 (1971), DOI: 10 .1103/PhysRevLett.26.1247 (cited on pg. 40).

[Ash70]   A. Ashkin, "Acceleration and Trapping of Particles by Radiation Pressure", *Physical Review Letters* 24, 156 (1970), DOI: 10.1103/PhysRevLett.24.156 (cited on pg. 1).

[AW01a]   S. Adhikari and J. Woodhouse, "Identification of Damping: Part 1, Non-Viscous Damping", *Journal of Sound and Vibration* 243, 63 (2001), DOI: 10.1006/JSVI.2000.3392 (cited on pg. 24).

[AW01b]   S. Adhikari and J. Woodhouse, "Identification of Damping: Part 1, Viscous Damping", *Journal of Sound and Vibration* 243, 43 (2001), DOI: 10.1006 /JSVI.2000.3391 (cited on pg. 24).

[Bar+12]   T. Barois, A. Ayari, A. Siria, S. Perisanu, P. Vincent, P. Poncharal, and S. T. Purcell, "Ohmic electromechanical dissipation in nanomechanical cantilevers", *Physical Review B* 85, 075407 (2012), DOI: 10.1103/PhysRevB.85 .075407 (cited on pg. 24).

[Bar90]   A. Barchielli, "Direct and heterodyne detection and other applications of quantum stochastic calculus to quantum optics", *Quantum Optics: Journal of the European Optical Society Part B* 2, 423 (1990), DOI: 10.1088/0954-8998/2/6/002 (cited on pg. 10).

[Bas+13]   R. Bassiri, K. Evans, K. Borisenko, M. Fejer, J. Hough, I. MacLaren, I. Martin, R. Route, and S. Rowan, "Correlations between the mechanical loss and atomic structure of amorphous TiO2-doped Ta2O5 coatings", *Acta Materialia* 61, 1070 (2013), DOI: 10.1016/J.ACTAMAT.2012.10.009 (cited on pg. 24).

[Bas+92]   T. Basché, W. E. Moerner, M. Orrit, and H. Talon, "Photon antibunching in the fluorescence of a single dye molecule trapped in a solid", *Physical Review Letters* 69, 1516 (1992), DOI: 10.1103/PhysRevLett.69.1516 (cited on pg. 89).

[BB14]   C. H. Bennett and G. Brassard, "Quantum cryptography: Public key distribution and coin tossing", *Theoretical Computer Science* 560, 7 (2014), DOI: 10.1016/J.TCS.2014.05.025 (cited on pg. 112).

[BB84]   C. H. Bennett and G. Brassard, "An Update on Quantum Cryptography", in: *Advances in Cryptology*, Springer Berlin Heidelberg, (1984), 475, DOI: 10.1007/3-540-39568-7_39 (cited on pgs. 87, 111, 112).

[Bek+18]   C. Bekker, C. G. Baker, R. Kalra, H.-H. Cheng, B.-B. Li, V. Prakash, and W. P. Bowen, "Free spectral range electrical tuning of a high quality on-chip microcavity" (2018), arXiv: 1808.01908 (cited on pg. 139).

[Bel64]   J. S. Bell, "On the Einstein Podolsky Rosen Paradox", *Physics* 1, 195 (1964) (cited on pgs. 1, 111).

[Ben+17] R. Benevides, F. G. S. Santos, G. O. Luiz, G. S. Wiederhecker, and T. P. M. Alegre, "Ultrahigh-Q optomechanical crystal cavities fabricated in a CMOS foundry", *Scientific Reports* 7, 2491 (2017), DOI: `10.1038/s41598-017-02515-4` (cited on pg. 113).

[Ben+92] C. Bennett, F. Bessette, G. Brassard, L. Salvail, and J. Smolin, "Experimental quantum cryptography", *Journal of Cryptology* 5, 3 (1992), DOI: `10.1007/BF00191318` (cited on pg. 112).

[Ben+93] C. H. Bennett, G. Brassard, C. Crépeau, R. Jozsa, A. Peres, and W. K. Wootters, "Teleporting an unknown quantum state via dual classical and Einstein-Podolsky-Rosen channels", *Physical Review Letters* 70, 1895 (1993), DOI: `10.1103/PhysRevLett.70.1895` (cited on pg. 112).

[Ben95] C. H. Bennett, "Quantum Information and Computation", *Physics Today* 48, 24 (1995), DOI: `10.1063/1.881452` (cited on pg. 112).

[Ber+13] H. Bernien et al., "Heralded entanglement between solid-state qubits separated by three metres", *Nature* 497, 86 (2013), DOI: `10.1038/nature12016` (cited on pg. 113).

[Bet36] R. A. Beth, "Mechanical Detection and Measurement of the Angular Momentum of Light", *Physical Review* 50, 115 (1936), DOI: `10.1103/PhysRev.50.115` (cited on pg. 1).

[BF56] E. Brannen and H. I. S. Ferguson, "The Question of Correlation between Photons in Coherent Light Rays", *Nature* 178, 481 (1956), DOI: `10.1038/178481a0` (cited on pg. 88).

[BGJ90] D. H. Boal, C.-K. Gelbke, and B. K. Jennings, "Intensity interferometry in subatomic physics", *Reviews of Modern Physics* 62, 553 (1990), DOI: `10.1103/RevModPhys.62.553` (cited on pg. 89).

[Bie74] D. K. Biegelsen, "Photoelastic Tensor of Silicon and the Volume Dependence of the Average Gap", *Physical Review Letters* 32, 1196 (1974), DOI: `10.1103/PhysRevLett.32.1196` (cited on pg. 60).

[Bil+17] C. R. Billman, J. P. Trinastic, D. J. Davis, R. Hamdan, and H.-P. Cheng, "Origin of the second peak in the mechanical loss function of amorphous silica", *Physical Review B* 95, 014109 (2017), DOI: `10.1103/PhysRevB.95.014109` (cited on pg. 24).

[BNG11] K. Børkje, A. Nunnenkamp, and S. M. Girvin, "Proposal for Entangling Remote Micromechanical Oscillators via Optical Measurements", *Physical Review Letters* 107, 123601 (2011), DOI: `10.1103/PhysRevLett.107.123601` (cited on pgs. 44, 49, 52, 115, 180, 183).

[Boc+09] E. Bocquillon, C. Couteau, M. Razavi, R. Laflamme, and G. Weihs, "Coherence measures for heralded single-photon sources", *Physical Review A* 79, 035801 (2009), DOI: `10.1103/PhysRevA.79.035801` (cited on pg. 62).

[Boi+18] S. Boixo, S. V. Isakov, V. N. Smelyanskiy, R. Babbush, N. Ding, Z. Jiang, M. J. Bremner, J. M. Martinis, and H. Neven, "Characterizing quantum supremacy in near-term devices", *Nature Physics* 14, 595 (2018), DOI: `10.1038/s41567-018-0124-x` (cited on pg. 112).

Bibliography

[Bou+97] D. Bouwmeester, J.-W. Pan, K. Mattle, M. Eibl, H. Weinfurter, and A. Zeilinger, "Experimental quantum teleportation", *Nature* 390, 575 (1997), DOI: 10.1038/37539 (cited on pg. 112).

[Bra90] C. Brackett, "Dense wavelength division multiplexing networks: principles and applications", *IEEE Journal on Selected Areas in Communications* 8, 948 (1990), DOI: 10.1109/49.57798 (cited on pg. 113).

[Bri+98] H.-J. Briegel, W. Dür, J. I. Cirac, and P. Zoller, "Quantum Repeaters: The Role of Imperfect Local Operations in Quantum Communication", *Physical Review Letters* 81, 5932 (1998), DOI: 10.1103/PhysRevLett.81.5932 (cited on pgs. 2, 62, 112).

[Bro+00] R. Brouri, A. Beveratos, J.-P. Poizat, and P. Grangier, "Photon antibunching in the fluorescence of individual color centers in diamond", *Optics Letters* 25, 1294 (2000), DOI: 10.1364/OL.25.001294 (cited on pg. 89).

[Bru+99] C. Brunel, B. Lounis, P. Tamarat, and M. Orrit, "Triggered Source of Single Photons based on Controlled Single Molecule Fluorescence", *Physical Review Letters* 83, 2722 (1999), DOI: 10.1103/PhysRevLett.83.2722 (cited on pg. 89).

[BSV01] V. Braginsky, S. Strigin, and S. Vyatchanin, "Parametric oscillatory instability in Fabry-Perot interferometer", *Physics Letters A* 287, 331 (2001), DOI: 10.1016/S0375-9601(01)00510-2 (cited on pgs. 19, 30, 40).

[Bus+14] F. Bussières et al., "Quantum teleportation from a telecom-wavelength photon to a solid-state quantum memory", *Nature Photonics* 8, 775 (2014), DOI: 10.1038/nphoton.2014.215 (cited on pg. 2).

[BVK78] V. B. Braginsky, Y. I. Vorontsov, and F. Y. Khalili, "Optimal quantum measurements in detectors of gravitation radiation", *JETP Lett.* 27, 276 (1978) (cited on pg. 53).

[BVT80] V. B. Braginsky, Y. I. Vorontsov, and K. S. Thorne, "Quantum nondemolition measurements.", *Science (New York, N.Y.)* 209, 547 (1980), DOI: 10.1126/science.209.4456.547 (cited on pgs. 44, 53, 54).

[BW70] D. C. Burnham and D. L. Weinberg, "Observation of Simultaneity in Parametric Production of Optical Photon Pairs", *Physical Review Letters* 25, 84 (1970), DOI: 10.1103/PhysRevLett.25.84 (cited on pgs. 1, 31, 40, 62).

[Cab+99] C. Cabrillo, J. I. Cirac, P. García-Fernández, and P. Zoller, "Creation of entangled states of distant atoms by interference", *Physical Review A* 59, 1025 (1999), DOI: 10.1103/PhysRevA.59.1025 (cited on pg. 115).

[Cag+17] G. Cagnoli et al., "Mode-dependent mechanical losses in disc resonators", *Physics Letters A* 382, 2165 (2017), DOI: 10.1016/J.PHYSLETA.2017.05.065 (cited on pg. 24).

[Cam+70] C. Camhy-Val, A. Dumont, M. Dreux, and R. Vitry, "Absolute measures of mean lifetimes of excited states using the method of correlated photons in cascade", *Physics Letters A* 32, 233 (1970), DOI: 10.1016/0375-9601(70)90295-1 (cited on pg. 62).

[Cav80]   C. M. Caves, "Quantum-Mechanical Radiation-Pressure Fluctuations in an Interferometer", *Physical Review Letters* 45, 75 (1980), DOI: `10.1103/PhysRevLett.45.75` (cited on pgs. 29, 60).

[CG04]   A. N. Cleland and M. R. Geller, "Superconducting Qubit Storage and Entanglement with Nanomechanical Resonators", *Phys. Rev. Lett.* 93, 070501 (2004), DOI: `10.1103/PhysRevLett.93.070501` (cited on pg. 2).

[CG69]   K. Cahill and R. Glauber, "Ordered Expansions in Boson Amplitude Operators", *Physical Review* 177, 1857 (1969), DOI: `10.1103/PhysRev.177.1857` (cited on pg. 14).

[CGK98]   I. L. Chuang, N. Gershenfeld, and M. Kubinec, "Experimental Implementation of Fast Quantum Searching", *Physical Review Letters* 80, 3408 (1998), DOI: `10.1103/PhysRevLett.80.3408` (cited on pg. 112).

[Cha+05]   T. Chanelière, D. N. Matsukevich, S. D. Jenkins, S.-Y. Lan, T. A. B. Kennedy, and A. Kuzmich, "Storage and retrieval of single photons transmitted between remote quantum memories", *Nature* 438, 833 (2005), DOI: `10.1038/nature04315` (cited on pg. 62).

[Cha+11a]   J. Chan, T. P. M. Alegre, A. H. Safavi-naeini, J. T. Hill, A. Krause, S. Groeblacher, and M. Aspelmeyer, "Laser cooling of a nanomechanical oscillator into its quantum ground state", *Nature* 478, 89 (2011), DOI: `10.1038/nature10461` (cited on pgs. 2, 4, 29, 47, 57).

[Cha+11b]   D. E. Chang, A. H. Safavi-Naeini, M. Hafezi, and O. Painter, "Slowing and stopping light using an optomechanical crystal array", *New Journal of Physics* 13, 023003 (2011), DOI: `10.1088/1367-2630/13/2/023003` (cited on pg. 2).

[Cha+12]   J. Chan, A. H. Safavi-Naeini, J. T. Hill, S. Meenehan, and O. Painter, "Optimized optomechanical crystal cavity with acoustic radiation shield", *Applied Physics Letters* 101, 081115 (2012), DOI: `10.1063/1.4747726` (cited on pgs. 3, 4, 57, 59, 60).

[Cho+05]   C. W. Chou, H. de Riedmatten, D. Felinto, S. V. Polyakov, S. J. van Enk, and H. J. Kimble, "Measurement-induced entanglement for excitation stored in remote atomic ensembles", *Nature* 438, 828 (2005), DOI: `10.1038/nature04353` (cited on pgs. 113, 139, 182, 183).

[Chu+17]   Y. Chu, P. Kharel, W. H. Renninger, L. D. Burkhart, L. Frunzio, P. T. Rakich, and R. J. Schoelkopf, "Quantum acoustics with superconducting qubits.", *Science* 358, 199 (2017), DOI: `10.1126/science.aao1511` (cited on pgs. 3, 90).

[Chu+18]   Y. Chu, P. Kharel, T. Yoon, L. Frunzio, P. T. Rakich, and R. J. Schoelkopf, "Climbing the phonon Fock state ladder" (2018), arXiv: `1804.07426` (cited on pg. 90).

[Cir+93]   J. I. Cirac, A. S. Parkins, R. Blatt, and P. Zoller, ""Dark" squeezed states of the motion of a trapped ion", *Phys. Rev. Lett.* 70, 556 (1993), DOI: `10.1103/PhysRevLett.70.556` (cited on pg. 44).

Bibliography

[CJ69]   M. D. Crisp and E. T. Jaynes, "Radiative Effects in Semiclassical Theory", *Physical Review* 179, 1253 (1969), DOI: `10.1103/PhysRev.179.1253` (cited on pg. 61).

[Cla+69]   J. F. Clauser, M. A. Horne, A. Shimony, and R. A. Holt, "Proposed Experiment to Test Local Hidden-Variable Theories", *Physical Review Letters* 23, 880 (1969), DOI: `10.1103/PhysRevLett.23.880` (cited on pg. 111).

[Cla+88]   J. Clarke, A. N. Cleland, M. H. Devoret, D. Esteve, and J. M. Martinis, "Quantum Mechanics of a Macroscopic Variable: The Phase Difference of a Josephson Junction", *Science* 239, 992 (1988), DOI: `10.1126/science.239.4843.992`, eprint: `http://science.sciencemag.org/content/239/4843/992.full.pdf` (cited on pg. 1).

[Cla72]   J. F. Clauser, "Experimental Limitations to the Validity of Semiclassical Radiation Theories", *Physical Review A* 6, 49 (1972), DOI: `10.1103/PhysRevA.6.49` (cited on pg. 61).

[Cla74]   J. F. Clauser, "Experimental distinction between the quantum and classical field-theoretic predictions for the photoelectric effect", *Physical Review D* 9, 853 (1974), DOI: `10.1103/PhysRevD.9.853` (cited on pgs. 1, 48, 61, 139).

[CMJ08]   A. A. Clerk, F. Marquardt, and A. Jacobs, "Back-action evasion and squeezing of a mechanical resonator using a cavity detector", *New Journal of Physics* 10, 095010 (2008), DOI: `http://dx.doi.org/10.1088/1367-2630/10/9/095010` (cited on pg. 44).

[Coh+15]   J. D. Cohen, S. M. Meenehan, G. S. MacCabe, S. Gröblacher, A. H. Safavi-Naeini, F. Marsili, M. D. Shaw, and O. Painter, "Phonon counting and intensity interferometry of a nanomechanical resonator", *Nature* 520, 522 (2015), DOI: `10.1038/nature14349` (cited on pgs. 3, 4, 31, 40, 89).

[Col+11]   G. D. Cole, I. Wilson-Rae, K. Werbach, M. R. Vanner, and M. Aspelmeyer, "Phonon-tunnelling dissipation in mechanical resonators", *Nature Communications* 2, 231 (2011), DOI: `10.1038/ncomms1212` (cited on pg. 24).

[Col+14]   G. D. Cole et al., "Tensile-strained In_X Ga_1-X P membranes for cavity optomechanics", *Applied Physics Letters* 104, 201908 (2014), DOI: `10.1063/1.4879755` (cited on pg. 27).

[Cor+06]   T. Corbitt, D. Ottaway, E. Innerhofer, J. Pelc, and N. Mavalvala, "Measurement of radiation-pressure-induced optomechanical dynamics in a suspended Fabry-Perot cavity", *Physical Review A* 74, 021802 (2006), DOI: `10.1103/PhysRevA.74.021802` (cited on pg. 19).

[CPB59]   M. Cardona, W. Paul, and H. Brooks, "Dielectric constant of germanium and silicon as a function of volume", *Journal of Physics and Chemistry of Solids* 8, 204 (1959), DOI: `10.1016/0022-3697(59)90316-6` (cited on pg. 60).

[CR02]   A. N. Cleland and M. L. Roukes, "Noise processes in nanomechanical resonators", *Journal of Applied Physics* 92, 2758 (2002), DOI: `10.1063/1.1499745` (cited on pgs. 24, 27).

[Cri+18a]   J. Cripe, N. Aggarwal, R. Lanza, A. Libson, R. Singh, P. Heu, D. Follman, G. D. Cole, N. Mavalvala, and T. Corbitt, "Observation of a room-temperature oscillator's motion dominated by quantum fluctuations over a broad audio-frequency band" (2018), arXiv: 1802.10069 (cited on pg. 24).

[Cri+18b]   J. Cripe, N. Aggarwal, R. Singh, R. Lanza, A. Libson, M. J. Yap, G. D. Cole, D. E. McClelland, N. Mavalvala, and T. Corbitt, "Radiation-pressure-mediated control of an optomechanical cavity", *Physical Review A* 97, 013827 (2018), DOI: 10.1103/PhysRevA.97.013827 (cited on pg. 19).

[CW76]   H. J. Carmichael and D. F. Walls, "Proposal for the measurement of the resonant Stark effect by photon correlation techniques", *Journal of Physics B: Atomic and Molecular Physics* 9, L43 (1976), DOI: 10.1088/0022-3700/9/4/001 (cited on pg. 88).

[CZ95]   J. I. Cirac and P. Zoller, "Quantum Computations with Cold Trapped Ions", *Physical Review Letters* 74, 4091 (1995), DOI: 10.1103/PhysRevLett.74.4091 (cited on pgs. 87, 112).

[Dal+12]   D. Dalacu, K. Mnaymneh, J. Lapointe, X. Wu, P. J. Poole, G. Bulgarini, V. Zwiller, and M. E. Reimer, "Ultraclean Emission from InAsP Quantum Dots in Defect-Free Wurtzite InP Nanowires", *Nano Letters* 12, 5919 (2012), DOI: 10.1021/nl303327h (cited on pg. 89).

[DDM96]   F. De Martini, G. Di Giuseppe, and M. Marrocco, "Single-Mode Generation of Quantum Photon States by Excited Single Molecules in a Microcavity Trap", *Physical Review Letters* 76, 900 (1996), DOI: 10.1103/PhysRevLett.76.900 (cited on pg. 89).

[Del+16]   A. Delteil, Z. Sun, W.-b. Gao, E. Togan, S. Faelt, and A. Imamoğlu, "Generation of heralded entanglement between distant hole spins", *Nature Physics* 12, 218 (2016), DOI: 10.1038/nphys3605 (cited on pg. 113).

[Deu85]   D. Deutsch, "Quantum Theory, the Church-Turing Principle and the Universal Quantum Computer", *Proceedings of the Royal Society A: Mathematical, Physical and Engineering Sciences* 400, 97 (1985), DOI: 10.1098/rspa.1985.0070 (cited on pg. 111).

[Die+89]   F. Diedrich, J. C. Bergquist, W. M. Itano, and D. J. Wineland, "Laser Cooling to the Zero-Point Energy of Motion", *Physical Review Letters* 62, 403 (1989), DOI: 10.1103/PhysRevLett.62.403 (cited on pgs. 1, 47).

[DiV96]   D. P. DiVincenzo, "Topics in Quantum Computers" (1996), arXiv: cond-mat/9612126 [cond-mat] (cited on pg. 112).

[DM78]   M. Dagenais and L. Mandel, "Investigation of two-time correlations in photon emissions from a single atom", *Physical Review A* 18, 2217 (1978), DOI: 10.1103/PhysRevA.18.2217 (cited on pg. 88).

[Dor+83]   A. Dorsel, J. D. McCullen, P. Meystre, E. Vignes, and H. Walther, "Optical Bistability and Mirror Confinement Induced by Radiation Pressure", *Physical Review Letters* 51, 1550 (1983), DOI: 10.1103/PhysRevLett.51.1550 (cited on pg. 15).

Bibliography

[DSC02]   W. Dür, C. Simon, and J. I. Cirac, "Effective Size of Certain Macroscopic Quantum Superpositions", *Physical Review Letters* 89, 210402 (2002), DOI: `10.1103/PhysRevLett.89.210402` (cited on pg. 113).

[DSV08]   F. De Martini, F. Sciarrino, and C. Vitelli, "Entanglement Test on a Microscopic-Macroscopic System", *Physical Review Letters* 100, 253601 (2008), DOI: `10.1103/PhysRevLett.100.253601` (cited on pg. 113).

[Dua+01] L.-M. Duan, M. D. Lukin, J. I. Cirac, and P. Zoller, "Long-distance quantum communication with atomic ensembles and linear optics", *Nature* 414, 413 (2001), DOI: `10.1038/35106500` (cited on pgs. 2, 3, 31, 62, 112, 115, 116, 139, 182).

[DW87]   F. Diedrich and H. Walther, "Nonclassical radiation of a single stored ion", *Physical Review Letters* 58, 203 (1987), DOI: `10.1103/PhysRevLett.58.203` (cited on pgs. 88, 89).

[Ede+78] W. A. Edelstein, J. Hough, J. R. Pugh, and W. Martin, "Limits to the measurement of displacement in an interferometric gravitational radiation detector", *Journal of Physics E: Scientific Instruments* 11, 710 (1978), DOI: `10.1088/0022-3735/11/7/030` (cited on pg. 29).

[Edg+16] M. P. Edgar, J. Macarthur, B. W. Barr, S. Hild, S. Huttner, B. Sorazu, and K. A. Strain, "Demonstration of an optical spring in the 100 g mirror regime", *Classical and Quantum Gravity* 33, 075007 (2016), DOI: `10.1088/0264-9381/33/7/075007` (cited on pg. 19).

[EFV05]   D. Englund, I. Fushman, and J. Vučković, "General recipe for designing photonic crystal cavities", *Optics Express* 13, 5961 (2005), DOI: `10.1364/OPEX.13.005961` (cited on pg. 58).

[Eic+09] M. Eichenfield, J. Chan, R. M. Camacho, K. J. Vahala, and O. Painter, "Optomechanical crystals", *Nature* 462, 78 (2009), DOI: `10.1038/nature08524` (cited on pgs. 3, 4, 57, 59).

[Eke+92] A. K. Ekert, J. G. Rarity, P. R. Tapster, and G. Massimo Palma, "Practical quantum cryptography based on two-photon interferometry", *Physical Review Letters* 69, 1293 (1992), DOI: `10.1103/PhysRevLett.69.1293` (cited on pg. 112).

[Eke91]   A. K. Ekert, "Quantum cryptography based on Bell's theorem", *Physical Review Letters* 67, 661 (1991), DOI: `10.1103/PhysRevLett.67.661` (cited on pg. 112).

[EPR35]   A. Einstein, B. Podolsky, and N. Rosen, "Can Quantum-Mechanical Description of Physical Reality Be Considered Complete?", *Physical Review* 47, 777 (1935), DOI: `10.1103/PhysRev.47.777` (cited on pgs. 1, 111).

[ER05]   K. L. Ekinci and M. L. Roukes, "Nanoelectromechanical systems", *Review of Scientific Instruments* 76, 061101 (2005), DOI: `10.1063/1.1927327` (cited on pg. 24).

[Eti+03] S. Etienne, S. Elkoun, L. David, and L. B. Magalas, "Mechanical Spectroscopy and other Relaxation Spectroscopies", *Solid State Phenomena* 89, 31 (2003), DOI: `10.4028/www.scientific.net/SSP.89.31` (cited on pg. 24).

[EYR04]   K. L. Ekinci, Y. T. Yang, and M. L. Roukes, "Ultimate limits to inertial mass sensing based upon nanoelectromechanical systems", *Journal of Applied Physics* 95, 2682 (2004), DOI: `10.1063/1.1642738` (cited on pgs. 24, 27).

[Fan+16]   K. Fang, M. H. Matheny, X. Luan, and O. Painter, "Optical transduction and routing of microwave phonons in cavity-optomechanical circuits", *Nature Photonics* 10, 489 (2016), DOI: `10.1038/nphoton.2016.107` (cited on pg. 4).

[Fan+17]   K. Fang, J. Luo, A. Metelmann, M. H. Matheny, F. Marquardt, A. A. Clerk, and O. Painter, "Generalized non-reciprocity in an optomechanical circuit via synthetic magnetism and reservoir engineering", *Nature Physics* 13, 465 (2017), DOI: `10.1038/nphys4009` (cited on pg. 4).

[FC72]   S. J. Freedman and J. F. Clauser, "Experimental Test of Local Hidden-Variable Theories", *Physical Review Letters* 28, 938 (1972), DOI: `10.1103/PhysRevLett.28.938` (cited on pgs. 1, 111).

[FD12]   F. Fröwis and W. Dür, "Measures of macroscopicity for quantum spin systems", *New Journal of Physics* 14, 093039 (2012), DOI: `10.1088/1367-2630/14/9/093039` (cited on pg. 113).

[Fel+05]   D. Felinto, C. W. Chou, H. de Riedmatten, S. V. Polyakov, and H. J. Kimble, "Control of decoherence in the generation of photon pairs from atomic ensembles", *Physical Review A* 72, 053809 (2005), DOI: `10.1103/PhysRevA.72.053809` (cited on pg. 62).

[Fey82]   R. P. Feynman, "Simulating physics with computers", *International Journal of Theoretical Physics* 21, 467 (1982), DOI: `10.1007/BF02650179` (cited on pg. 111).

[Fio+11]   V. Fiore, Y. Yang, M. C. Kuzyk, R. Barbour, L. Tian, and H. Wang, "Storing Optical Information as a Mechanical Excitation in a Silica Optomechanical Resonator", *Phys. Rev. Lett.* 107, 133601 (2011), DOI: `10.1103/PhysRevLett.107.133601` (cited on pg. 2).

[För+13]   M. Förtsch, J. U. Fürst, C. Wittmann, D. Strekalov, A. Aiello, M. V. Chekhova, C. Silberhorn, G. Leuchs, and C. Marquardt, "A versatile source of single photons for quantum information processing", *Nature Communications* 4, 1818 (2013), DOI: `10.1038/ncomms2838` (cited on pg. 62).

[Gal+14]   C. Galland, N. Sangouard, N. Piro, N. Gisin, and T. J. Kippenberg, "Heralded Single-Phonon Preparation, Storage, and Readout in Cavity Optomechanics", *Physical Review Letters* 112, 143602 (2014), DOI: `10.1103/PhysRevLett.112.143602` (cited on pgs. 52, 90, 181, 184).

[GAN14]   I. M. Georgescu, S. Ashhab, and F. Nori, "Quantum simulation", *Reviews of Modern Physics* 86, 153 (2014), DOI: `10.1103/RevModPhys.86.153` (cited on pg. 90).

[Gav28]   E. Gaviola, "An Experimental Test of Schrödinger's Theory", *Nature* 122, 772 (1928), DOI: `10.1038/122772a0` (cited on pg. 61).

Bibliography

[GC85]   C. W. Gardiner and M. J. Collett, "Input and output in damped quantum systems: Quantum stochastic differential equations and the master equation", *Physical Review A* 31, 3761 (1985), DOI: `10.1103/PhysRevA.31.3761` (cited on pgs. 10, 11).

[GCS73]   H. M. Gibbs, G. G. Churchill, and G. J. Salamo, "Contradictions with the Neoclassical Theory of Radiation in Weakly Excited Multilevel Systems", *Physical Review A* 7, 1766 (1973), DOI: `10.1103/PhysRevA.7.1766` (cited on pg. 61).

[GHZ89]   D. M. Greenberger, M. A. Horne, and A. Zeilinger, "Going Beyond Bell's Theorem", in: *Bell's Theorem, Quantum Theory and Conceptions of the Universe*, ed. by M. Kafatos, Springer Netherlands, (1989), 69, DOI: `10.1007/978-94-017-0849-4_10` (cited on pg. 87).

[Gib72]   H. M. Gibbs, "Spontaneous Decay of Coherently Excited Rb", *Physical Review Letters* 29, 459 (1972), DOI: `10.1103/PhysRevLett.29.459` (cited on pg. 61).

[Gig+06]   S. Gigan, H. R. Böhm, M. Paternostro, F. Blaser, G. Langer, J. B. Hertzberg, K. C. Schwab, D. Bäuerle, M. Aspelmeyer, and A. Zeilinger, "Self-cooling of a micromirror by radiation pressure.", *Nature* 444, 67 (2006), DOI: `10.1038/nature05273` (cited on pgs. 2, 29).

[Giu+15]   M. Giustina et al., "Significant-Loophole-Free Test of Bell's Theorem with Entangled Photons", *Physical Review Letters* 115, 250401 (2015), DOI: `10.1103/PhysRevLett.115.250401` (cited on pg. 40).

[Gla63a]   R. J. Glauber, "Coherent and Incoherent States of the Radiation Field", *Physical Review* 131, 2766 (1963), DOI: `10.1103/PhysRev.131.2766` (cited on pgs. 14, 88).

[Gla63b]   R. J. Glauber, "The Quantum Theory of Optical Coherence", *Physical Review* 130, 2529 (1963), DOI: `10.1103/PhysRev.130.2529` (cited on pgs. 48, 61, 88, 173).

[GNQ13]   J. Gieseler, L. Novotny, and R. Quidant, "Thermal nonlinearities in a nanomechanical oscillator", *Nature Physics* 9, 806 (2013), DOI: `10.1038/nphys2798` (cited on pgs. 7, 27).

[Gor+05]   T. Gorishnyy, M. Maldovan, C. Ullal, and E. Thomas, "Sound ideas", *Physics World* 18, 24 (2005), DOI: `10.1088/2058-7058/18/12/30` (cited on pg. 59).

[Got98]   D. Gottesman, "The Heisenberg Representation of Quantum Computers" (1998), arXiv: `quant-ph/9807006 [quant-ph]` (cited on pg. 112).

[GPI12]   Y. Greenberg, Y. A. Pashkin, and E. Il'ichev, "Nanomechanical resonators", *Physics-Uspekhi* 55, 382 (2012), DOI: `10.3367/UFNe.0182.201204c.0407` (cited on pg. 24).

[GRA86]   P. Grangier, G. Roger, and A. Aspect, "Experimental Evidence for a Photon Anticorrelation Effect on a Beam Splitter: A New Light on Single-Photon Interferences", *Europhysics Letters* 1, 173 (1986), DOI: `10.1209/0295-5075/1/4/004` (cited on pgs. 89, 116, 139).

[Grö+09]   S. Gröblacher, K. Hammerer, M. R. Vanner, and M. Aspelmeyer, "Observation of strong coupling between a micromechanical resonator and an optical cavity field", *Nature* 460, 4 (2009), DOI: `10.1038/nature08171` (cited on pgs. 2, 30, 38).

[Gro96]   L. K. Grover, "A fast quantum mechanical algorithm for database search", in: *Proceedings of the twenty-eighth annual ACM symposium on Theory of computing - STOC '96*, ACM Press, (1996), 212, DOI: `10.1145/237814.237866` (cited on pgs. 111, 112).

[Gru+10]   I. S. Grudinin, H. Lee, O. Painter, and K. J. Vahala, "Phonon Laser Action in a Tunable Two-Level System", *Physical Review Letters* 104, 083901 (2010), DOI: `10.1103/PhysRevLett.104.083901` (cited on pgs. 31, 40).

[Gru+97]   A. Gruber, A. Dräbenstedt, C. Tietz, L. Fleury, J. Wrachtrup, and C. von Borczyskowski, "Scanning Confocal Optical Microscopy and Magnetic Resonance on Single Defect Centers", *Science* 276, 2012 (1997), DOI: `10.1126/science.276.5321.2012` (cited on pg. 1).

[GZ04]   C. W. Gardiner and P. Zoller, *Quantum Noise*, 3rd ed., Springer, (2004), chap. 3, ISBN: 9783540223016 (cited on pgs. 10, 15).

[Hag+97]   E. Hagley, X. Maître, G. Nogues, C. Wunderlich, M. Brune, J. M. Raimond, and S. Haroche, "Generation of Einstein-Podolsky-Rosen Pairs of Atoms", *Physical Review Letters* 79, 1 (1997), DOI: `10.1103/PhysRevLett.79.1` (cited on pg. 112).

[Har13]   S. Haroche, "Nobel Lecture: Controlling photons in a box and exploring the quantum to classical boundary", *Reviews of Modern Physics* 85, 1083 (2013), DOI: `10.1103/RevModPhys.85.1083` (cited on pg. 87).

[Hen+99]   M. Henny, S. Oberholzer, C. Strunk, T. Heinzel, K. Ensslin, M. Holland, and C. Schonenberger, "The fermionic hanbury brown and twiss experiment", *Science* 284, 296 (1999), DOI: `10.1126/SCIENCE.284.5412.296` (cited on pg. 89).

[HHH96]   R. Horodecki, M. Horodecki, and P. Horodecki, "Teleportation, Bell's inequalities and inseparability", *Physics Letters A* 222, 21 (1996), DOI: `10.1016/0375-9601(96)00639-1` (cited on pg. 114).

[Hig+16]   D. B. Higginbottom, L. Slodička, G. Araneda, L. Lachman, R. Filip, M. Hennrich, and R. Blatt, "Pure single photons from a trapped atom source", *New Journal of Physics* 18, 093038 (2016), DOI: `10.1088/1367-2630/18/9/093038` (cited on pg. 89).

[Hig+18]   A. P. Higginbotham, P. S. Burns, M. D. Urmey, R. W. Peterson, N. S. Kampel, B. M. Brubaker, G. Smith, K. W. Lehnert, and C. A. Regal, "Harnessing electro-optic correlations in an efficient mechanical converter", *Nature Physics*, 1 (2018), DOI: `10.1038/s41567-018-0210-0` (cited on pg. 140).

[Hil+12]   J. T. Hill, A. H. Safavi-Naeini, J. Chan, and O. Painter, "Coherent optical wavelength conversion via cavity optomechanics", *Nature Communications* 3, 1196 (2012), DOI: `10.1038/ncomms2201` (cited on pg. 4).

Bibliography

[HJD52]   R. Hanbury Brown, R. C. Jennison, and M. K. Das Gupta, "Apparent Angular Sizes of Discrete Radio Sources: Observations at Jodrell Bank, Manchester", *Nature* 170, 1061 (1952), DOI: `10.1038/1701061a0` (cited on pg. 87).

[HM13]   R. Hamerly and H. Mabuchi, "Coherent controllers for optical-feedback cooling of quantum oscillators", *Physical Review A* 87, 013815 (2013), DOI: `10.1103/PhysRevA.87.013815` (cited on pg. 29).

[HM86]   C. K. Hong and L. Mandel, "Experimental realization of a localized one-photon state", *Physical Review Letters* 56, 58 (1986), DOI: `10.1103/PhysRevLett.56.58` (cited on pgs. 1, 31, 40, 89).

[HNK10]   M. A. Hopcroft, W. D. Nix, and T. W. Kenny, "What is the Young's Modulus of Silicon?", *Journal of Microelectromechanical Systems* 19, 229 (2010), DOI: `10.1109/JMEMS.2009.2039697` (cited on pg. 59).

[Hof+11]   S. Hofer, W. Wieczorek, M. Aspelmeyer, and K. Hammerer, "Quantum entanglement and teleportation in pulsed cavity optomechanics", *Physical Review A* 84, 10 (2011), DOI: `10.1103/PhysRevA.84.052327` (cited on pgs. 17, 20, 31, 32, 40, 174).

[Hof+12]   J. Hofmann, M. Krug, N. Ortegel, L. Gérard, M. Weber, W. Rosenfeld, and H. Weinfurter, "Heralded entanglement between widely separated atoms.", *Science* 337, 72 (2012), DOI: `10.1126/science.1221856` (cited on pg. 113).

[Hof15]   S. G. Hofer, "Quantum Control of Optomechanical Systems", PhD thesis, Universität Wien, 2015 (cited on pgs. 12, 15, 19, 24, 32, 33, 174, 177).

[Hon+17]   S. Hong, R. Riedinger, I. Marinković, A. Wallucks, S. G. Hofer, R. A. Norte, M. Aspelmeyer, and S. Gröblacher, "Hanbury Brown and Twiss interferometry of single phonons from an optomechanical resonator", *Science* 358, 203 (2017), DOI: `10.1126/science.aan7939` (cited on pgs. 3, 4, 10, 31, 40, 48, 63, 87, 139).

[Hor+09]   R. Horodecki, P. Horodecki, M. Horodecki, and K. Horodecki, "Quantum entanglement", *Reviews of Modern Physics* 81, 865 (2009), DOI: `10.1103/RevModPhys.81.865` (cited on pg. 115).

[HT56a]   R. Hanbury Brown and R. Q. Twiss, "A Test of a New Type of Stellar Interferometer on Sirius", *Nature* 178, 1046 (1956), DOI: `10.1038/1781046a0` (cited on pg. 87).

[HT56b]   R. Hanbury Brown and R. Q. Twiss, "Correlation between Photons in two Coherent Beams of Light", *Nature* 177, 27 (1956), DOI: `10.1038/177027a0` (cited on pg. 87).

[HW97]   S. Hill and W. K. Wootters, "Entanglement of a Pair of Quantum Bits", *Physical Review Letters* 78, 5022 (1997), DOI: `10.1103/PhysRevLett.78.5022` (cited on pg. 183).

[Jai+16]   V. Jain, J. Gieseler, C. Moritz, C. Dellago, R. Quidant, and L. Novotny, "Direct Measurement of Photon Recoil from a Levitated Nanoparticle", *Physical Review Letters* 116, 243601 (2016), DOI: `10.1103/PhysRevLett.116.243601` (cited on pg. 27).

[Ján57]   L. Jánossy, "On the classical fluctuation of a beam of light", *Il Nuovo Cimento* 6, 111 (1957), DOI: `10.1007/BF02827762` (cited on pg. 88).

[Jel+07]   T. Jeltes et al., "Comparison of the Hanbury Brown-Twiss effect for bosons and fermions", *Nature* 445, 402 (2007), DOI: `10.1038/nature05513` (cited on pg. 89).

[JKP01]   B. Julsgaard, A. Kozhekin, and E. S. Polzik, "Experimental long-lived entanglement of two macroscopic objects.", *Nature* 413, 400 (2001), DOI: `10.1038/35096524` (cited on pg. 113).

[Joa+08]   J. D. Joannopoulos, S. G. Johnson, J. N. Winn, and R. D. Meade, *Photonic crystals : molding the flow of light*, Princeton University Press, (2008), ISBN: 9780691124568 (cited on pgs. 57, 58).

[Joh+02]   S. G. Johnson, M. Ibanescu, M. A. Skorobogatiy, O. Weisberg, J. D. Joannopoulos, and Y. Fink, "Perturbation theory for Maxwell's equations with shifting material boundaries", *Physical Review E* 65, 066611 (2002), DOI: `10.1103/PhysRevE.65.066611` (cited on pg. 60).

[Joh87]   S. John, "Strong localization of photons in certain disordered dielectric superlattices", *Physical Review Letters* 58, 2486 (1987), DOI: `10.1103/PhysRevLett.58.2486` (cited on pg. 57).

[JW85]   E. Jakeman and J. Walker, "Analysis of a method for the generation of light with sub-poissonian photon statistics", *Optics Communications* 55, 219 (1985), DOI: `10.1016/0030-4018(85)90051-3` (cited on pg. 88).

[KA11]   K. Kunal and N. R. Aluru, "Akhiezer damping in nanostructures", *Physical Review B* 84, 245450 (2011), DOI: `10.1103/PhysRevB.84.245450` (cited on pg. 24).

[Kal60]   R. E. Kalman, "A New Approach to Linear Filtering and Prediction Problems", *Journal of Basic Engineering* 82, 35 (1960), DOI: `10.1115/1.3662552` (cited on pg. 31).

[Kas+15]   M. Kasperczyk, A. Jorio, E. Neu, P. Maletinsky, and L. Novotny, "Stokes-anti-Stokes correlations in diamond", *Optics Letters* 40, 2393 (2015), DOI: `10.1364/OL.40.002393` (cited on pg. 44).

[Kas+16]   M. Kasperczyk, F. S. de Aguiar Júnior, C. Rabelo, A. Saraiva, M. F. Santos, L. Novotny, and A. Jorio, "Temporal Quantum Correlations in Inelastic Light Scattering from Water", *Physical Review Letters* 117, 243603 (2016), DOI: `10.1103/PhysRevLett.117.243603` (cited on pg. 44).

[Kas50]   A. Kastler, "Quelques suggestions concernant la production optique et la détection optique d'une inégalité de population des niveaux de quantifigation spatiale des atomes. Application à l'expérience de Stern et Gerlach et à la résonance magnétique", *Journal de Physique et le Radium* 11, 255 (1950), DOI: `10.1051/jphysrad:01950001106025500` (cited on pg. 1).

[KDM77]   H. J. Kimble, M. Dagenais, and L. Mandel, "Photon Antibunching in Resonance Fluorescence", *Physical Review Letters* 39, 691 (1977), DOI: `10.1103/PhysRevLett.39.691` (cited on pgs. 1, 62, 88).

Bibliography

[KDM78]   H. J. Kimble, M. Dagenais, and L. Mandel, "Multiatom and transit-time ef-
          fects on photon-correlation measurements in resonance fluorescence", *Phys-
          ical Review A* 18, 201 (1978), DOI: `10.1103/PhysRevA.18.201` (cited on
          pg. 88).

[Kha+10] F. Khalili, S. Danilishin, H. Miao, H. Müller-Ebhardt, H. Yang, and Y. Chen,
          "Preparing a Mechanical Oscillator in Non-Gaussian Quantum States", *Phys-
          ical Review Letters* 105, 070403 (2010), DOI: `10.1103/PhysRevLett.105.0
          70403` (cited on pg. 53).

[Kie+13] N. Kiesel, F. Blaser, U. Delic, D. Grass, R. Kaltenbaek, and M. Aspelmeyer,
          "Cavity cooling of an optically levitated submicron particle.", *PNAS* 110,
          14180 (2013), DOI: `10.1073/pnas.1309167110` (cited on pg. 60).

[Kip+05] T. J. Kippenberg, H. Rokhsari, T. Carmon, A. Scherer, and K. J. Vahala,
          "Analysis of Radiation-Pressure Induced Mechanical Oscillation of an Opti-
          cal Microcavity", *Physical Review Letters* 95, 033901 (2005), DOI: `10.1103
          /PhysRevLett.95.033901` (cited on pgs. 2, 19, 30, 40).

[Kni00]   P. Knight, "Quantum Information Processing Without Entanglement", *Sci-
          ence* 287, 441 (2000), DOI: `10.1126/science.287.5452.441` (cited on
          pg. 112).

[Kok+87] K. Kokubun, M. Hirata, M. Ono, H. Murakami, and Y. Toda, "Unified for-
          mula describing the impedance dependence of a quartz oscillator on gas
          pressure", *Journal of Vacuum Science & Technology A: Vacuum, Surfaces,
          and Films* 5, 2450 (1987), DOI: `10.1116/1.574869` (cited on pg. 24).

[Kol+09] R. Kolesov, B. Grotz, G. Balasubramanian, R. J. Stöhr, A. A. L. Nicolet,
          P. R. Hemmer, F. Jelezko, and J. Wrachtrup, "Wave-particle duality of single
          surface plasmon polaritons", *Nature Physics* 5, 470 (2009), DOI: `10.1038
          /nphys1278` (cited on pg. 89).

[Kra+12] A. G. Krause, M. Winger, T. D. Blasius, Q. Lin, and O. Painter, "A high-
          resolution microchip optomechanical accelerometer", *Nature Photonics* 6,
          768 (2012), DOI: `10.1038/nphoton.2012.245` (cited on pgs. 24, 59).

[KSG13]   T. J. Kippenberg, A. Schliesser, and M. L. Gorodetsky, "Phase noise mea-
          surement of external cavity diode lasers and implications for optomechanical
          sideband cooling of GHz mechanical modes", *New Journal of Physics* 15,
          015019 (2013), DOI: `10.1088/1367-2630/15/1/015019` (cited on pg. 48).

[KUW75]   L. R. Kasday, J. Ullman, and C. S. Wu, "Angular correlation of compton-
          scattered annihilation photons and hidden variables", *Il Nuovo Cimento B
          Series 11* 25, 633 (1975), DOI: `10.1007/BF02724742` (cited on pg. 111).

[Kuz+03] A. Kuzmich, W. P. Bowen, A. D. Boozer, A. Boca, C. W. Chou, L.-M.
          Duan, and H. J. Kimble, "Generation of nonclassical photon pairs for scalable
          quantum communication with atomic ensembles.", *Nature* 423, 731 (2003),
          DOI: `10.1038/nature01714` (cited on pgs. 40, 48, 62, 113, 139, 180).

[Lau+06] J. Laurat, H. de Riedmatten, D. Felinto, C.-W. Chou, E. W. Schomburg, and H. J. Kimble, "Efficient retrieval of a single excitation stored in an atomic ensemble", *Optics Express* 14, 6912 (2006), DOI: `10.1364/OE.14.006912` (cited on pg. 62).

[Lau+07] J. Laurat, K. S. Choi, H. Deng, C. W. Chou, and H. J. Kimble, "Heralded Entanglement between Atomic Ensembles: Preparation, Decoherence, and Scaling", *Physical Review Letters* 99, 180504 (2007), DOI: `10.1103/PhysRevLett.99.180504` (cited on pgs. 62, 184).

[Lau+10] B. Lauritzen, J. Minář, H. de Riedmatten, M. Afzelius, N. Sangouard, C. Simon, and N. Gisin, "Telecommunication-Wavelength Solid-State Memory at the Single Photon Level", *Phys. Rev. Lett.* 104, 080502 (2010), DOI: `10.1103/PhysRevLett.104.080502` (cited on pg. 2).

[Lec+15a] F. Lecocq, J. B. Clark, R. W. Simmonds, J. Aumentado, and J. D. Teufel, "Quantum Nondemolition Measurement of a Nonclassical State of a Massive Object", *Physical Review X* 5, 041037 (2015), DOI: `10.1103/PhysRevX.5.041037` (cited on pg. 44).

[Lec+15b] F. Lecocq, J. D. Teufel, J. Aumentado, and R. W. Simmonds, "Resolving the vacuum fluctuations of an optomechanical system using an artificial atom", *Nature Physics* 11, 635 (2015), DOI: `10.1038/nphys3365` (cited on pgs. 31, 40).

[Lee+11] K. C. Lee et al., "Entangling Macroscopic Diamonds at Room Temperature", *Science* 334, 1253 (2011) (cited on pgs. 3, 44, 62, 113).

[Lee+12] K. C. Lee, B. J. Sussman, M. R. Sprague, P. Michelberger, K. F. Reim, J. Nunn, N. K. Langford, P. J. Bustard, D. Jaksch, and I. A. Walmsley, "Macroscopic non-classical states and terahertz quantum processing in room-temperature diamond", *Nature Photonics* 6, 41 (2012), DOI: `10.1038/nphoton.2011.296` (cited on pgs. 44, 62).

[Leg02] A. J. Leggett, "Testing the limits of quantum mechanics: motivation, state of play, prospects", *Journal of Physics: Condensed Matter* 14, R415 (2002), DOI: `10.1088/0953-8984/14/15/201` (cited on pg. 113).

[Lei+03] D. Leibfried, R. Blatt, C. Monroe, and D. Wineland, "Quantum dynamics of single trapped ions", *Reviews of Modern Physics* 75, 281 (2003), DOI: `10.1103/RevModPhys.75.281` (cited on pg. 90).

[Lei+96] D. Leibfried, D. M. Meekhof, B. E. King, C. Monroe, W. M. Itano, and D. J. Wineland, "Experimental Determination of the Motional Quantum State of a Trapped Atom", *Physical Review Letters* 77, 4281 (1996), DOI: `10.1103/PhysRevLett.77.4281` (cited on pg. 90).

[Lin76] G. Lindblad, "On the generators of quantum dynamical semigroups", *Communications in Mathematical Physics* 48, 119 (1976), DOI: `10.1007/BF01608499` (cited on pg. 10).

[LJ11] C.-W. Lee and H. Jeong, "Quantification of Macroscopic Quantum Superpositions within Phase Space", *Physical Review Letters* 106, 220401 (2011), DOI: `10.1103/PhysRevLett.106.220401` (cited on pg. 113).

Bibliography

[LLK72]   A. Laubereau, D. von der Linde, and W. Kaiser, "Direct Measurement of the Vibrational Lifetimes of Molecules in Liquids", *Physical Review Letters* 28, 1162 (1972), DOI: `10.1103/PhysRevLett.28.1162` (cited on pg. 40).

[Llo93]   S. Lloyd, "A potentially realizable quantum computer.", *Science* 261, 1569 (1993), DOI: `10.1126/science.261.5128.1569` (cited on pg. 112).

[LMH04]   P. Lalanne, S. Mias, and J. P. Hugonin, "Two physical mechanisms for boosting the quality factor to cavity volume ratio of photonic crystal microcavities", *Optics Express* 12, 458 (2004), DOI: `10.1364/OPEX.12.000458` (cited on pg. 58).

[Lou80]   R. Loudon, "Non-classical effects in the statistical properties of light", *Reports on Progress in Physics* 43, 913 (1980), DOI: `10.1088/0034-4885/43/7/002` (cited on pg. 61).

[LR00]   R. Lifshitz and M. L. Roukes, "Thermoelastic damping in micro- and nanomechanical systems", *Physical Review B* 61, 5600 (2000), DOI: `10.1103/PhysRevB.61.5600` (cited on pg. 24).

[Lvo+13]   A. I. Lvovsky, R. Ghobadi, A. Chandra, A. S. Prasad, and C. Simon, "Observation of micro-macro entanglement of light", *Nature Physics* 9, 541 (2013), DOI: `10.1038/nphys2682` (cited on pg. 113).

[Mac+13]   E. R. MacQuarrie, T. A. Gosavi, N. R. Jungwirth, S. A. Bhave, and G. D. Fuchs, "Mechanical Spin Control of Nitrogen-Vacancy Centers in Diamond", *Physical Review Letters* 111, 227602 (2013), DOI: `10.1103/PhysRevLett.111.227602` (cited on pg. 24).

[MAD08]   F. Marquardt, B. Abel, and J. von Delft, "Measuring the size of a quantum superposition of many-body states", *Physical Review A* 78, 012109 (2008), DOI: `10.1103/PhysRevA.78.012109` (cited on pg. 113).

[Mag+18]   L. Magrini, R. A. Norte, R. Riedinger, I. Marinković, D. Grass, U. Delić, S. Gröblacher, S. Hong, and M. Aspelmeyer, "Nanophotonic near-field levitated optomechanics" (2018), arXiv: `1804.06676` (cited on pgs. 56, 60).

[Mal+18]   D. Malz, L. D. Tóth, N. R. Bernier, A. K. Feofanov, T. J. Kippenberg, and A. Nunnenkamp, "Quantum-Limited Directional Amplifiers with Optomechanics", *Physical Review Letters* 120, 023601 (2018), DOI: `10.1103/PhysRevLett.120.023601` (cited on pgs. 31, 40).

[Man58]   L. Mandel, "Fluctuations of Photon Beams and their Correlations", *Proceedings of the Physical Society* 72, 1037 (1958), DOI: `10.1088/0370-1328/72/6/312` (cited on pg. 88).

[Man79]   L. Mandel, "Sub-Poissonian photon statistics in resonance fluorescence", *Optics Letters* 4, 205 (1979), DOI: `10.1364/OL.4.000205` (cited on pg. 88).

[Man80]   Y. Manin, "Computable and Uncomputable", *Sovetskoye Radio Press, Moscow* (1980), arXiv: `quant-ph/9903008 [arXiv:quant-ph]` (cited on pg. 111).

[Man86]   L. Mandel, "Non-Classical States of the Electromagnetic Field", *Physica Scripta* T12, 34 (1986), DOI: `10.1088/0031-8949/1986/T12/005` (cited on pgs. 88, 90).

[Mar+14a] N. Maring, K. Kutluer, J. Cohen, M. Cristiani, M. Mazzera, P. M. Ledingham, and H. de Riedmatten, "Storage of up-converted telecom photons in a doped crystal", *New Journal of Physics* 16, 113021 (2014), DOI: `10.1088/1367-2630/16/11/113021` (cited on pg. 113).

[Mar+14b] I. W. Martin et al., "Low temperature mechanical dissipation of an ion-beam sputtered silica film", *Classical and Quantum Gravity* 31, 035019 (2014), DOI: `10.1088/0264-9381/31/3/035019` (cited on pg. 24).

[Mar+16] D. V. Martynov et al., "Sensitivity of the Advanced LIGO detectors at the beginning of gravitational wave astronomy", *Physical Review D* 93, 112004 (2016), DOI: `10.1103/PhysRevD.93.112004` (cited on pg. 24).

[Mar+17] N. Maring, P. Farrera, K. Kutluer, M. Mazzera, G. Heinze, and H. de Riedmatten, "Photonic quantum state transfer between a cold atomic gas and a crystal", *Nature* 551, 485 (2017), DOI: `10.1038/nature24468` (cited on pg. 113).

[Mar+18] I. Marinkovic, A. Wallucks, R. Riedinger, S. Hong, M. Aspelmeyer, and S. Gröblacher, "An optomechanical Bell test" (2018), arXiv: `1806.10615` (cited on pgs. 63, 115, 116, 140).

[Mas+11] F. Massel, T. T. Heikkilä, J.-M. Pirkkalainen, S. U. Cho, H. Saloniemi, P. J. Hakonen, and M. A. Sillanpää, "Microwave amplification with nanomechanical resonators.", *Nature* 480, 351 (2011), DOI: `10.1038/nature10628` (cited on pgs. 31, 40).

[Mat+05] D. N. Matsukevich, T. Chanelière, M. Bhattacharya, S.-Y. Lan, S. D. Jenkins, T. A. B. Kennedy, and A. Kuzmich, "Entanglement of a Photon and a Collective Atomic Excitation", *Physical Review Letters* 95, 040405 (2005), DOI: `10.1103/PhysRevLett.95.040405` (cited on pg. 62).

[Mat+06a] D. N. Matsukevich, T. Chanelière, S. D. Jenkins, S.-Y. Lan, T. A. B. Kennedy, and A. Kuzmich, "Deterministic Single Photons via Conditional Quantum Evolution", *Physical Review Letters* 97, 013601 (2006), DOI: `10.1103/PhysRevLett.97.013601` (cited on pg. 62).

[Mat+06b] D. N. Matsukevich, T. Chanelière, S. D. Jenkins, S.-Y. Lan, T. A. B. Kennedy, and A. Kuzmich, "Entanglement of Remote Atomic Qubits", *Physical Review Letters* 96, 030405 (2006), DOI: `10.1103/PhysRevLett.96.030405` (cited on pg. 113).

[Mee+14] S. M. Meenehan, J. D. Cohen, S. Gröblacher, J. T. Hill, A. H. Safavi-Naeini, M. Aspelmeyer, and O. Painter, "Silicon optomechanical crystal resonator at millikelvin temperatures", *Physical Review A* 90, 011803 (2014), DOI: `10.1103/PhysRevA.90.011803` (cited on pg. 3).

[Mee+15] S. M. Meenehan, J. D. Cohen, G. S. MacCabe, F. Marsili, M. D. Shaw, and O. Painter, "Pulsed Excitation Dynamics of an Optomechanical Crystal Resonator near Its Quantum Ground State of Motion", *Physical Review X* 5, 041002 (2015), DOI: `10.1103/PhysRevX.5.041002` (cited on pgs. 3, 4).

Bibliography

[Mee+96]   D. M. Meekhof, C. Monroe, B. E. King, W. M. Itano, and D. J. Wineland, "Generation of Nonclassical Motional States of a Trapped Atom", *Physical Review Letters* 76, 1796 (1996), DOI: `10.1103/PhysRevLett.76.1796` (cited on pgs. 1, 90).

[MG83]   K. J. McNeil and C. W. Gardiner, "Quantum statistics of parametric oscillation", *Physical Review A* 28, 1560 (1983), DOI: `10.1103/PhysRevA.28.1560` (cited on pg. 61).

[Mic+00]   P. Michler, A. Imamoğlu, M. D. Mason, P. J. Carson, G. F. Strouse, and S. K. Buratto, "Quantum correlation among photons from a single quantum dot at room temperature", *Nature* 406, 968 (2000), DOI: `10.1038/35023100` (cited on pg. 89).

[Miy+05]   T. Miyazawa, K. Takemoto, Y. Sakuma, S. Hirose, T. Usuki, N. Yokoyama, M. Takatsu, and Y. Arakawa, "Single-Photon Generation in the 1.55-u m Optical-Fiber Band from an InAs/InP Quantum Dot", *Japanese Journal of Applied Physics* 44, L620 (2005), DOI: `10.1143/JJAP.44.L620` (cited on pg. 113).

[MM66]   B. L. Morgan and L. Mandel, "Measurement of Photon Bunching in a Thermal Light Beam", *Physical Review Letters* 16, 1012 (1966), DOI: `10.1103/PhysRevLett.16.1012` (cited on pg. 88).

[Moe+07]   D. L. Moehring, P. Maunz, S. Olmschenk, K. C. Younge, D. N. Matsukevich, L.-M. Duan, and C. Monroe, "Entanglement of single-atom quantum bits at a distance", *Nature* 449, 68 (2007), DOI: `10.1038/nature06118` (cited on pg. 113).

[Mol73]   B. R. Mollow, "Photon Correlations in the Parametric Frequency Splitting of Light", *Physical Review A* 8, 2684 (1973), DOI: `10.1103/PhysRevA.8.2684` (cited on pg. 31).

[Møl97]   K. Mølmer, "Optical coherence: A convenient fiction", *Physical Review A* 55, 3195 (1997), DOI: `10.1103/PhysRevA.55.3195` (cited on pg. 13).

[Mon+95]   C. Monroe, D. M. Meekhof, B. E. King, W. M. Itano, and D. J. Wineland, "Demonstration of a Fundamental Quantum Logic Gate", *Physical Review Letters* 75, 4714 (1995), DOI: `10.1103/PhysRevLett.75.4714` (cited on pg. 112).

[MSW64]   L. Mandel, E. C. G. Sudarshan, and E. Wolf, "Theory of photoelectric detection of light fluctuations", *Proceedings of the Physical Society* 84, 435 (1964), DOI: `10.1088/0370-1328/84/3/313` (cited on pg. 61).

[MW95]   L. Mandel and E. Wolf, *Optical coherence and quantum optics*, Cambridge University Press, (1995), ISBN: 9781139644105 (cited on pg. 48).

[NH13]   S. Nimmrichter and K. Hornberger, "Macroscopicity of Mechanical Quantum Superposition States", *Physical Review Letters* 110, 160403 (2013), DOI: `10.1103/PhysRevLett.110.160403` (cited on pg. 113).

[Nor14]   R. A. Norte, "Nanofabrication for On-Chip Optical Levitation, Atom-Trapping, and Superconducting Quantum Circuits", PhD thesis, California Institute of Technology, 2014 (cited on pg. 19).

[NPT99]   Y. Nakamura, Y. A. Pashkin, and J. S. Tsai, "Coherent control of macro-scopic quantum states in a single-Cooper-pair box", *Nature* 398, 786 (1999), DOI: 10.1038/19718 (cited on pg. 1).

[Num+02]   K. Numata, S. Otsuka, M. Ando, and K. Tsubono, "Intrinsic losses in various kinds of fused silica", *Classical and Quantum Gravity* 19, 1697 (2002), DOI: 10.1088/0264-9381/19/7/363 (cited on pg. 24).

[Nun+14]   A. Nunnenkamp, V. Sudhir, A. K. Feofanov, A. Roulet, and T. J. Kippen-berg, "Quantum-Limited Amplification and Parametric Instability in the Reversed Dissipation Regime of Cavity Optomechanics", *Physical Review Letters* 113, 023604 (2014), DOI: 10.1103/PhysRevLett.113.023604 (cited on pgs. 31, 40).

[Ock+18]   C. F. Ockeloen-Korppi, E. Damskägg, J.-M. Pirkkalainen, M. Asjad, A. A. Clerk, F. Massel, M. J. Woolley, and M. A. Sillanpää, "Stabilized entan-glement of massive mechanical oscillators", *Nature* 556, 478 (2018), DOI: 10.1038/s41586-018-0038-x (cited on pg. 113).

[OCo+10]   A. D. O'Connell et al., "Quantum ground state and single-phonon control of a mechanical resonator.", *Nature* 464, 697 (2010), DOI: 10.1038/nature08967 (cited on pgs. 3, 90).

[Olb+17]   F. Olbrich, J. Höschele, M. Müller, J. Kettler, S. Luca Portalupi, M. Paul, M. Jetter, and P. Michler, "Polarization-entangled photons from an InGaAs-based quantum dot emitting in the telecom C-band", *Applied Physics Letters* 111, 133106 (2017), DOI: 10.1063/1.4994145 (cited on pg. 113).

[Oli+99]   W. D. Oliver, J. Kim, R. C. Liu, Y. Yamamoto, K. Ensslin, M. Holland, and C. Schönenberger, "Hanbury Brown and Twiss-type experiment with electrons", *Science* 284, 299 (1999), DOI: 10.1126/science.284.5412.299 (cited on pg. 89).

[Ou+90]   Z. Y. Ou, L. J. Wang, X. Y. Zou, and L. Mandel, "Evidence for phase memory in two-photon down conversion through entanglement with the vacuum", *Phys. Rev. A* 41, 566 (1990), DOI: 10.1103/PhysRevA.41.566 (cited on pg. 33).

[Ova+14]   P. Ovartchaiyapong, K. W. Lee, B. A. Myers, and A. C. B. Jayich, "Dy-namic strain-mediated coupling of a single diamond spin to a mechanical resonator", *Nature Communications* 5, 4429 (2014), DOI: 10.1038/ncomms5429 (cited on pg. 24).

[Pal+13a] T. A. Palomaki, J. D. Teufel, R. W. Simmonds, and K. W. Lehnert, "Entan-gling Mechanical Motion with Microwave Fields.", *Science* 342, 710 (2013), DOI: 10.1126/science.1244563 (cited on pg. 31).

[Pal+13b] T. A. Palomaki, J. W. Harlow, J. D. Teufel, R. W. Simmonds, and K. W. Lehnert, "Coherent state transfer between itinerant microwave fields and a mechanical oscillator", *Nature* 495, 210 (2013), DOI: 10.1038/nature11915 (cited on pgs. 2, 20, 40, 113).

Bibliography

[Pal07a]   G. Palasantzas, "Adsorption-desorption noise influence on mass sensitivity and dynamic range of nanoresonators with rough surfaces", *Journal of Applied Physics* 101, 076103 (2007), DOI: `10.1063/1.2714792` (cited on pgs. 24, 27).

[Pal07b]   G. Palasantzas, "Random surface roughness influence on gas damped nanoresonators", *Applied Physics Letters* 90, 041914 (2007), DOI: `10.1063/1.2435328` (cited on pg. 24).

[Par+15]   T. K. Paraïso, M. Kalaee, L. Zang, H. Pfeifer, F. Marquardt, and O. Painter, "Position-Squared Coupling in a Tunable Photonic Crystal Optomechanical Cavity", *Physical Review X* 5, 041024 (2015), DOI: `10.1103/PhysRevX.5.041024` (cited on pg. 7).

[Pat+17]   R. N. Patel, C. J. Sarabalis, W. Jiang, J. T. Hill, and A. H. Safavi-Naeini, "Engineering Phonon Leakage in Nanomechanical Resonators", *Physical Review Applied* 8, 041001 (2017), DOI: `10.1103/PhysRevApplied.8.041001` (cited on pg. 60).

[Pat+18]   R. N. Patel, Z. Wang, W. Jiang, C. J. Sarabalis, J. T. Hill, and A. H. Safavi-Naeini, "Single-Mode Phononic Wire", *Physical Review Letters* 121, 040501 (2018), DOI: `10.1103/PhysRevLett.121.040501` (cited on pgs. 4, 60).

[Per96]   A. Peres, "Separability Criterion for Density Matrices", *Physical Review Letters* 77, 1413 (1996), DOI: `10.1103/PhysRevLett.77.1413` (cited on pg. 114).

[Pfe+16]   H. Pfeifer, T. Paraïso, L. Zang, and O. Painter, "Design of tunable GHz-frequency optomechanical crystal resonators", *Opt. Express* 24, 11407 (2016), DOI: `10.1364/OE.24.011407` (cited on pg. 139).

[Pir+15]   J.-M. Pirkkalainen, E. Damskägg, M. Brandt, F. Massel, and M. A. Sillanpää, "Squeezing of Quantum Noise of Motion in a Micromechanical Resonator", *Physical Review Letters* 115, 243601 (2015), DOI: `10.1103/PhysRevLett.115.243601` (cited on pg. 44).

[Pop75]   R. P. Poplavskiĭ, "Thermodynamic models of information processes", *Soviet Physics Uspekhi* 18, 222 (1975), DOI: `10.1070/PU1975v018n03ABEH001955` (cited on pg. 111).

[PPR13]   T. P. Purdy, R. W. Peterson, and C. A. Regal, "Observation of Radiation Pressure Shot Noise on a Macroscopic Object", *Science* 339, 801 (2013), DOI: `10.1126/science.1231282` (cited on pgs. 2, 15, 29).

[Pur+17]   T. P. Purdy, K. E. Grutter, K. Srinivasan, and J. M. Taylor, "Quantum correlations from a room-temperature optomechanical cavity.", *Science* 356, 1265 (2017), DOI: `10.1126/science.aag1407` (cited on pg. 4).

[Pur56]   E. M. Purcell, "The Question of Correlation between Photons in Coherent Light Rays", *Nature* 178, 1449 (1956), DOI: `10.1038/1781449a0` (cited on pg. 88).

[PZ12]   M. Poot and H. S. van der Zant, "Mechanical systems in the quantum regime", *Physics Reports* 511, 273 (2012), DOI: `10.1016/j.physrep.2011.12.004` (cited on pg. 24).

[QDL10]   Q. Quan, P. B. Deotare, and M. Loncar, "Photonic crystal nanobeam cavity strongly coupled to the feeding waveguide", *Applied Physics Letters* 96, 203102 (2010), DOI: `10.1063/1.3429125` (cited on pg. 58).

[Qiu+18]   L. Qiu, I. Shomroni, M. A. Ioannou, D. Malz, A. Nunnenkamp, and T. Kippenberg, "Motional Sideband Asymmetry in Quantum Optomechanics in the Presence of Kerr-type Nonlinearities" (2018), arXiv: `1805.12364` (cited on pg. 44).

[QL11]   Q. Quan and M. Loncar, "Deterministic design of wavelength scale, ultra-high Q photonic crystal nanobeam cavities", *Optics Express* 19, 18529 (2011), DOI: `10.1364/OE.19.018529` (cited on pg. 58).

[Rab+10]   P. Rabl, S. J. Kolkowitz, F. H. L. Koppens, J. G. E. Harris, P. Zoller, and M. D. Lukin, "A quantum spin transducer based on nanoelectromechanical resonator arrays", *Nature Physics* 6, 602 (2010), DOI: `10.1038/nphys1679` (cited on pg. 2).

[Ran+17]   M. Rančić, M. P. Hedges, R. L. Ahlefeldt, and M. J. Sellars, "Coherence time of over a second in a telecom-compatible quantum memory storage material", *Nature Physics* 14, 50 (2017), DOI: `10.1038/nphys4254` (cited on pg. 113).

[Ree+17]   A. P. Reed et al., "Faithful conversion of propagating quantum information to mechanical motion", *Nature Physics* 13, 1163 (2017), DOI: `10.1038/nphys4251` (cited on pgs. 3, 90).

[Ric+17]   F. Ricci, R. A. Rica, M. Spasenović, J. Gieseler, L. Rondin, L. Novotny, and R. Quidant, "Optically levitated nanoparticle as a model system for stochastic bistable dynamics", *Nature Communications* 8, 15141 (2017), DOI: `10.1038/ncomms15141` (cited on pg. 7).

[Rie+06]   H. de Riedmatten, J. Laurat, C. W. Chou, E. W. Schomburg, D. Felinto, and H. J. Kimble, "Direct Measurement of Decoherence for Entanglement between a Photon and Stored Atomic Excitation", *Physical Review Letters* 97, 113603 (2006), DOI: `10.1103/PhysRevLett.97.113603` (cited on pgs. 52, 62).

[Rie+16]   R. Riedinger, S. Hong, R. A. Norte, J. A. Slater, J. Shang, A. G. Krause, V. Anant, M. Aspelmeyer, and S. Gröblacher, "Non-classical correlations between single photons and phonons from a mechanical oscillator", *Nature* 530, 313 (2016), DOI: `10.1038/nature16536` (cited on pgs. 3, 4, 27, 31, 48, 52, 61, 62, 90, 113, 116, 139).

[Rie+18]   R. Riedinger, A. Wallucks, I. Marinković, C. Löschnauer, M. Aspelmeyer, S. Hong, and S. Gröblacher, "Remote quantum entanglement between two micromechanical oscillators", *Nature* 556, 473 (2018), DOI: `10.1038/s41586-018-0036-z` (cited on pgs. 4, 31, 63, 90, 111, 113, 139).

[Rit+12]   S. Ritter, C. Nölleke, C. Hahn, A. Reiserer, A. Neuzner, M. Uphoff, M. Mücke, E. Figueroa, J. Bochmann, and G. Rempe, "An elementary quantum network of single atoms in optical cavities", *Nature* 484, 195 (2012), DOI: `10.1038/nature11023` (cited on pg. 113).

Bibliography

[Ros+18]   M. Rossi, D. Mason, J. Chen, Y. Tsaturyan, and A. Schliesser, "Measurement-based quantum control of mechanical motion" (2018), arXiv: `1805.05087` (cited on pg. 55).

[RT90]   J. G. Rarity and P. R. Tapster, "Experimental violation of Bell's inequality based on phase and momentum", *Phys. Rev. Lett.* 64, 2495 (1990), DOI: `10.1103/PhysRevLett.64.2495` (cited on pgs. 116, 139).

[RW84]   M. D. Reid and D. F. Walls, "Violation of Bell's Inequalities in Quantum Optics", *Physical Review Letters* 53, 955 (1984), DOI: `10.1103/PhysRevLett.53.955` (cited on pg. 61).

[RW86]   M. D. Reid and D. F. Walls, "Violations of classical inequalities in quantum optics", *Physical Review A* 34, 1260 (1986), DOI: `10.1103/PhysRevA.34.1260` (cited on pg. 61).

[Saf+11]   A. H. Safavi-Naeini, T. P. Mayer Alegre, J. Chan, M. Eichenfield, M. Winger, Q. Lin, J. T. Hill, D. E. Chang, and O. Painter, "Electromagnetically induced transparency and slow light with optomechanics.", *Nature* 472, 69 (2011), DOI: `10.1038/nature09933` (cited on pgs. 2, 59).

[Saf+12]   A. Safavi-Naeini, J. Chan, J. Hill, T. Alegre, A. Krause, and O. Painter, "Observation of Quantum Motion of a Nanomechanical Resonator", *Physical Review Letters* 108, 033602 (2012), DOI: `10.1103/PhysRevLett.108.033602` (cited on pgs. 4, 47).

[Saf+13a]   A. H. Safavi-Naeini, S. Gröblacher, J. T. Hill, J. Chan, M. Aspelmeyer, and O. Painter, "Squeezed light from a silicon micromechanical resonator", *Nature* 500, 185 (2013), DOI: `10.1038/nature12307` (cited on pg. 59).

[Saf+13b]   A. H. Safavi-Naeini, J. Chan, J. T. Hill, S. Gröblacher, H. Miao, Y. Chen, M. Aspelmeyer, and O. Painter, "Laser noise in cavity-optomechanical cooling and thermometry", *New Journal of Physics* 15, 035007 (2013), DOI: `10.1088/1367-2630/15/3/035007` (cited on pg. 48).

[Saf+14]   A. H. Safavi-Naeini, J. T. Hill, S. Meenehan, J. Chan, S. Gröblacher, and O. Painter, "Two-Dimensional Phononic-Photonic Band Gap Optomechanical Crystal Cavity", *Physical Review Letters* 112, 153603 (2014), DOI: `10.1103/PhysRevLett.112.153603` (cited on pgs. 4, 59, 139).

[Sag+15]   E. Saglamyurek, J. Jin, V. B. Verma, M. D. Shaw, F. Marsili, S. W. Nam, D. Oblak, and W. Tittel, "Quantum storage of entangled telecom-wavelength photons in an erbium-doped optical fibre", *Nature Photonics* 9, 83 (2015), DOI: `10.1038/nphoton.2014.311` (cited on pgs. 2, 113).

[Sak05]   K. Sakoda, *Optical properties of photonic crystals*, Springer, (2005), ISBN: 9783540269656 (cited on pg. 57).

[San+10]   J. C. Sankey, C. Yang, B. M. Zwickl, A. M. Jayich, and J. G. E. Harris, "Strong and tunable nonlinear optomechanical coupling in a low-loss system", *Nature Physics* 6, 707 (2010), DOI: `10.1038/nphys1707` (cited on pg. 7).

[Sas+11]   M. Sasaki et al., "Field test of quantum key distribution in the Tokyo QKD Network", *Optics Express* 19, 10387 (2011), DOI: `10.1364/OE.19.010387` (cited on pg. 113).

[Sat+18]   K. J. Satzinger et al., "Quantum control of surface acoustic wave phonons" (2018), arXiv: `1804.07308` (cited on pg. 90).

[Sau90]   P. R. Saulson, "Thermal noise in mechanical experiments", *Physical Review D* 42, 2437 (1990), DOI: `10.1103/PhysRevD.42.2437` (cited on pg. 24).

[Sch+05]   M. Schellekens, R. Hoppeler, A. Perrin, J. V. Gomes, D. Boiron, A. Aspect, and C. I. Westbrook, "Hanbury Brown Twiss effect for ultracold quantum gases.", *Science* 310, 648 (2005), DOI: `10.1126/science.1118024` (cited on pg. 89).

[Sch+06]   A. Schliesser, P. Del'Haye, N. Nooshi, K. J. Vahala, and T. J. Kippenberg, "Radiation Pressure Cooling of a Micromechanical Oscillator Using Dynamical Backaction", *Physical Review Letters* 97, 243905 (2006), DOI: `10.1103/PhysRevLett.97.243905` (cited on pg. 2).

[Sch+08]   A. Schliesser, R. Rivière, G. Anetsberger, O. Arcizet, and T. J. Kippenberg, "Resolved-sideband cooling of a micromechanical oscillator", *Nature Physics* 4, 415 (2008), DOI: `10.1038/nphys939` (cited on pgs. 29, 30).

[Sch+16]   C. Schäfermeier, H. Kerdoncuff, U. B. Hoff, H. Fu, A. Huck, J. Bilek, G. I. Harris, W. P. Bowen, T. Gehring, and U. L. Andersen, "Quantum enhanced feedback cooling of a mechanical oscillator using nonclassical light", *Nature Communications* 7, 13628 (2016), DOI: `10.1038/ncomms13628` (cited on pg. 27).

[Sch35]   E. Schrödinger, "Discussion of Probability Relations between Separated Systems", *Mathematical Proceedings of the Cambridge Philosophical Society* 31, 555 (1935), DOI: `10.1017/S0305004100013554` (cited on pg. 111).

[Sha85]   J. Shapiro, "Quantum noise and excess noise in optical homodyne and heterodyne receivers", *IEEE Journal of Quantum Electronics* 21, 237 (1985), DOI: `10.1109/JQE.1985.1072640` (cited on pgs. 35, 36, 47).

[Sho94]   P. Shor, "Algorithms for quantum computation: discrete logarithms and factoring", in: *Proceedings 35th Annual Symposium on Foundations of Computer Science*, IEEE Comput. Soc. Press, (1994), 124, DOI: `10.1109/SFCS.1994.365700` (cited on pgs. 111, 112).

[Sho95]   P. W. Shor, "Scheme for reducing decoherence in quantum computer memory", *Physical Review A* 52, R2493 (1995), DOI: `10.1103/PhysRevA.52.R2493` (cited on pg. 112).

[Sip+16]   A. Sipahigil et al., "An integrated diamond nanophotonics platform for quantum optical networks", *Science* (2016), DOI: `10.1126/science.aah6875` (cited on pg. 139).

[SM83]   R. Short and L. Mandel, "Observation of Sub-Poissonian Photon Statistics", *Physical Review Letters* 51, 384 (1983), DOI: `10.1103/PhysRevLett.51.384` (cited on pgs. 88, 139).

Bibliography

[SP02]   K. Srinivasan and O. Painter, "Momentum space design of high-Q photonic crystal optical cavities", *Optics Express* 10, 670 (2002), DOI: `10.1364/OE.1 0.000670` (cited on pg. 58).

[SP03]   K. Srinivasan and O. Painter, "Fourier space design of high-Q cavities in standard and compressed hexagonal lattice photonic crystals", *Optics Express* 11, 579 (2003), DOI: `10.1364/OE.11.000579` (cited on pg. 58).

[SP10]   A. H. Safavi-Naeini and O. Painter, "Design of optomechanical cavities and waveguides on a simultaneous bandgap phononic-photonic crystal slab", *Optics Express* 18, 14926 (2010), DOI: `10.1364/OE.18.014926` (cited on pgs. 59, 60).

[ST85]   B. Saleh and M. Teich, "Sub-Poisson light generation by selective deletion from cascaded atomic emissions", *Optics Communications* 52, 429 (1985), DOI: `10.1016/0030-4018(86)90344-5` (cited on pg. 88).

[Ste+06] M. Steffen, M. Ansmann, R. C. Bialczak, N. Katz, E. Lucero, R. McDermott, M. Neeley, E. M. Weig, A. N. Cleland, and J. M. Martinis, "Measurement of the entanglement of two superconducting qubits via state tomography.", *Science* 313, 1423 (2006), DOI: `10.1126/science.1130886` (cited on pg. 113).

[Suh+14] J. Suh, A. J. Weinstein, C. U. Lei, E. E. Wollman, S. K. Steinke, P. Meystre, A. A. Clerk, and K. C. Schwab, "Mechanically detecting and avoiding the quantum fluctuations of a microwave field", *Science* 344, 1262 (2014), DOI: `10.1126/science.1253258` (cited on pg. 44).

[Tan+08] A. Tanaka et al., "Ultra fast quantum key distribution over a 97 km installed telecom fiber with wavelength division multiplexing clock synchronization", *Optics Express* 16, 11354 (2008), DOI: `10.1364/OE.16.011354` (cited on pg. 113).

[Tei+14] J. Teissier, A. Barfuss, P. Appel, E. Neu, and P. Maletinsky, "Strain Coupling of a Nitrogen-Vacancy Center Spin to a Diamond Mechanical Oscillator", *Physical Review Letters* 113, 020503 (2014), DOI: `10.1103/PhysRevLett.1 13.020503` (cited on pg. 24).

[Teu+08] J. D. Teufel, J. W. Harlow, C. A. Regal, and K. W. Lehnert, "Dynamical Backaction of Microwave Fields on a Nanomechanical Oscillator", *Physical Review Letters* 101, 197203 (2008), DOI: `10.1103/PhysRevLett.101.197203` (cited on pg. 19).

[Teu+11a] J. D. Teufel, T. Donner, D. Li, J. W. Harlow, M. S. Allman, K. Cicak, A. J. Sirois, J. D. Whittaker, K. W. Lehnert, and R. W. Simmonds, "Sideband cooling of micromechanical motion to the quantum ground state.", *Nature* 475, 359 (2011), DOI: `10.1038/nature10261` (cited on pgs. 2, 29, 46).

[Teu+11b] J. D. Teufel, D. Li, M. S. Allman, K. Cicak, A. J. Sirois, J. D. Whittaker, and R. W. Simmonds, "Circuit cavity electromechanics in the strong-coupling regime.", *Nature* 471, 204 (2011), DOI: `10.1038/nature09898` (cited on pgs. 2, 30, 38).

[TG65]   U. M. Titulaer and R. J. Glauber, "Correlation Functions for Coherent Fields", *Physical Review* 140, B676 (1965), DOI: `10.1103/PhysRev.140.B676` (cited on pg. 61).

[TH57]   R. Q. Twiss and R. Hanbury Brown, "The Question of Correlation between Photons in Coherent Beams of Light", *Nature* 179, 1128 (1957), DOI: `10.1038/1791128a0` (cited on pg. 88).

[Tho+08] J. D. Thompson, B. M. Zwickl, A. M. Jayich, F. Marquardt, S. M. Girvin, and J. G. E. Harris, "Strong dispersive coupling of a high-finesse cavity to a micromechanical membrane", *Nature* 452, 72 (2008), DOI: `10.1038/nature06715` (cited on pgs. 2, 7, 60).

[Tho+78] K. S. Thorne, R. W. P. Drever, C. M. Caves, M. Zimmermann, and V. D. Sandberg, "Quantum Nondemolition Measurements of Harmonic Oscillators", *Physical Review Letters* 40, 667 (1978), DOI: `10.1103/PhysRevLett.40.667` (cited on pg. 53).

[Tow97]   P. Townsend, "Simultaneous quantum cryptographic key distribution and conventional data transmission over installed fibre using wavelength-division multiplexing", *Electronics Letters* 33, 188 (1997), DOI: `10.1049/el:19970147` (cited on pg. 113).

[TRA09]   R. Tabrizian, M. Rais-Zadeh, and F. Ayazi, "Effect of phonon interactions on limiting the f.Q product of micromechanical resonators", in: *TRANSDUCERS 2009 - 2009 International Solid-State Sensors, Actuators and Microsystems Conference*, IEEE, (2009), 2131, DOI: `10.1109/SENSOR.2009.5285627` (cited on pg. 24).

[TRS87]   P. R. Tapster, J. G. Rarity, and J. S. Satchell, "Generation of Sub-Poissonian Light by High-Efficiency Light-Emitting Diodes", *Europhysics Letters (EPL)* 4, 293 (1987), DOI: `10.1209/0295-5075/4/3/007` (cited on pg. 88).

[TS85]   M. C. Teich and B. E. A. Saleh, "Observation of sub-Poisson Franck-Hertz light at 253.7 nm", *Journal of the Optical Society of America B* 2, 275 (1985), DOI: `10.1364/JOSAB.2.000275` (cited on pg. 88).

[Tsa+17] Y. Tsaturyan, A. Barg, E. S. Polzik, and A. Schliesser, "Ultracoherent nanomechanical resonators via soft clamping and dissipation dilution", *Nature Nanotechnology* 12, 776 (2017), DOI: `10.1038/nnano.2017.101` (cited on pg. 59).

[UFK10]   Q. P. Unterreithmeier, T. Faust, and J. P. Kotthaus, "Damping of Nanomechanical Resonators", *Physical Review Letters* 105, 027205 (2010), DOI: `10.1103/PhysRevLett.105.027205` (cited on pg. 24).

[Usm+12] I. Usmani, C. Clausen, F. Bussières, N. Sangouard, M. Afzelius, and N. Gisin, "Heralded quantum entanglement between two crystals", *Nature Photonics* 6, 234 (2012), DOI: `10.1038/nphoton.2012.34` (cited on pgs. 52, 62, 113).

[Vai+16] A. Vainsencher, K. J. Satzinger, G. A. Peairs, and A. N. Cleland, "Bi-directional conversion between microwave and optical frequencies in a piezo-electric optomechanical device", *Applied Physics Letters* 109, 033107 (2016), DOI: `10.1063/1.4955408` (cited on pgs. 2, 4, 140).

Bibliography

[Van+01]   L. M. K. Vandersypen, M. Steffen, G. Breyta, C. S. Yannoni, M. H. Sherwood, and I. L. Chuang, "Experimental realization of Shor's quantum factoring algorithm using nuclear magnetic resonance", *Nature* 414, 883 (2001), DOI: 10.1038/414883a (cited on pg. 112).

[Van+11]   M. R. Vanner, I. Pikovski, G. D. Cole, M. S. Kim, C. Brukner, K. Hammerer, G. J. Milburn, and M. Aspelmeyer, "Pulsed quantum optomechanics", *PNAS* 108, 16182 (2011), DOI: 10.1073/pnas.1105098108 (cited on pgs. 17, 53).

[Van+13]   M. R. Vanner, J. Hofer, G. D. Cole, and M. Aspelmeyer, "Cooling-by-measurement and mechanical state tomography via pulsed optomechanics.", *Nature Communications* 4, 2295 (2013), DOI: 10.1038/ncomms3295 (cited on pgs. 53, 55).

[Vas+15]   G. Vasilakis, H. Shen, K. Jensen, M. Balabas, D. Salart, B. Chen, and E. S. Polzik, "Generation of a squeezed state of an oscillator by stroboscopic back-action-evading measurement", *Nature Physics* 11, 389 (2015), DOI: 10.1038/nphys3280 (cited on pg. 53).

[Ved08]   V. Vedral, "Quantifying entanglement in macroscopic systems", *Nature* 453, 1004 (2008), DOI: 10.1038/nature07124 (cited on pg. 113).

[Ver+12]   E. Verhagen, S. Deleglise, S. Weis, A. Schliesser, and T. J. Kippenberg, "Quantum-coherent coupling of a mechanical oscillator to an optical cavity mode", *Nature* 482, 63 (2012), DOI: 10.1038/nature10787 (cited on pgs. 2, 38).

[Vit+07]   D. Vitali, S. Gigan, A. Ferreira, H. Böhm, P. Tombesi, A. Guerreiro, V. Vedral, A. Zeilinger, and M. Aspelmeyer, "Optomechanical Entanglement between a Movable Mirror and a Cavity Field", *Physical Review Letters* 98, 030405 (2007), DOI: 10.1103/PhysRevLett.98.030405 (cited on pg. 44).

[VS14]   L. G. Villanueva and S. Schmid, "Evidence of Surface Loss as Ubiquitous Limiting Damping Mechanism in SiN Micro- and Nanomechanical Resonators", *Physical Review Letters* 113, 227201 (2014), DOI: 10.1103/PhysRevLett.113.227201 (cited on pg. 24).

[Vuc+02]   J. Vuckovic, M. Loncar, H. Mabuchi, and A. Scherer, "Optimization of the Q factor in photonic crystal microcavities", *IEEE Journal of Quantum Electronics* 38, 850 (2002), DOI: 10.1109/JQE.2002.1017597 (cited on pg. 58).

[Wal+03]   C. H. van der Wal, M. D. Eisaman, A. André, R. L. Walsworth, D. F. Phillips, A. S. Zibrov, and M. D. Lukin, "Atomic memory for correlated photon states.", *Science* 301, 196 (2003), DOI: 10.1126/science.1085946 (cited on pg. 62).

[Wal+04a] A. Wallraff, D. I. Schuster, A. Blais, L. Frunzio, R.-. S. Huang, J. Majer, S. Kumar, S. M. Girvin, and R. J. Schoelkopf, "Strong coupling of a single photon to a superconducting qubit using circuit quantum electrodynamics", *Nature* 431, 162 (2004), DOI: 10.1038/nature02851 (cited on pg. 1).

[Wal+04b] P. Walther, J.-W. Pan, M. Aspelmeyer, R. Ursin, S. Gasparoni, and A. Zeilinger, "De Broglie wavelength of a non-local four-photon state", *Nature* 429, 158 (2004), DOI: 10.1038/nature02552 (cited on pg. 40).

[Wal+05]   P. Walther, K. J. Resch, T. Rudolph, E. Schenck, H. Weinfurter, V. Vedral, M. Aspelmeyer, and A. Zeilinger, "Experimental one-way quantum computing", *Nature* 434, 169 (2005), DOI: `10.1038/nature03347` (cited on pg. 40).

[WAR72]   J. M. Wessner, D. K. Anderson, and R. T. Robiscoe, "Radiative Decay of the 2 P State of Atomic Hydrogen: A Test of the Exponential Decay Law", *Physical Review Letters* 29, 1126 (1972), DOI: `10.1103/PhysRevLett.29.1126` (cited on pg. 61).

[Wei+10]   S. Weis, R. Rivière, S. Deléglise, E. Gavartin, O. Arcizet, A. Schliesser, and T. J. Kippenberg, "Optomechanically induced transparency.", *Science (New York, N.Y.)* 330, 1520 (2010), DOI: `10.1126/science.1195596` (cited on pg. 35).

[Wei+14]   A. J. Weinstein, C. U. Lei, E. E. Wollman, J. Suh, A. Metelmann, A. A. Clerk, and K. C. Schwab, "Observation and Interpretation of Motional Sideband Asymmetry in a Quantum Electromechanical Device", *Physical Review X* 4, 041003 (2014), DOI: `10.1103/PhysRevX.4.041003` (cited on pg. 47).

[Wer89]   R. F. Werner, "Quantum states with Einstein-Podolsky-Rosen correlations admitting a hidden-variable model", *Physical Review A* 40, 4277 (1989), DOI: `10.1103/PhysRevA.40.4277` (cited on pg. 114).

[Wie+15]   W. Wieczorek, S. G. Hofer, J. Hoelscher-Obermaier, R. Riedinger, K. Hammerer, and M. Aspelmeyer, "Optimal State Estimation for Cavity Optomechanical Systems", *Physical Review Letters* 114, 223601 (2015), DOI: `10.1103/PhysRevLett.114.223601` (cited on pgs. 2, 31, 55).

[Wil08]   I. Wilson-Rae, "Intrinsic dissipation in nanomechanical resonators due to phonon tunneling", *Physical Review B* 77, 245418 (2008), DOI: `10.1103/PhysRevB.77.245418` (cited on pg. 24).

[Win13]   D. J. Wineland, "Nobel Lecture: Superposition, entanglement, and raising Schrödinger's cat", *Reviews of Modern Physics* 85, 1103 (2013), DOI: `10.1103/RevModPhys.85.1103` (cited on pg. 87).

[WJ85]   J. Walker and E. Jakeman, "Photon-antibunching by Use of a Photoelectron-event-triggered Optical Shutter", *Optica Acta: International Journal of Optics* 32, 1303 (1985), DOI: `10.1080/713821672` (cited on pg. 89).

[Wol+15]   E. E. Wollman, C. U. Lei, A. J. Weinstein, J. Suh, A. Kronwald, F. Marquardt, A. A. Clerk, and K. C. Schwab, "Quantum squeezing of motion in a mechanical resonator.", *Science* 349, 952 (2015), DOI: `10.1126/science.aac5138` (cited on pg. 44).

[Woo98]   W. K. Wootters, "Entanglement of Formation of an Arbitrary State of Two Qubits", *Physical Review Letters* 80, 2245 (1998), DOI: `10.1103/PhysRevLett.80.2245` (cited on pg. 183).

[WS83]   S. Wiesner and Stephen, "Conjugate coding", *SIGACT News* 15, 78 (1983), DOI: `10.1145/1008908.1008920` (cited on pgs. 111, 112).

[WZ82]   W. K. Wootters and W. H. Zurek, "A single quantum cannot be cloned", *Nature* 299, 802 (1982), DOI: `10.1038/299802a0` (cited on pg. 112).

Bibliography

[Yab87]   E. Yablonovitch, "Inhibited Spontaneous Emission in Solid-State Physics and Electronics", *Physical Review Letters* 58, 2059 (1987), DOI: `10.1103/PhysRevLett.58.2059` (cited on pg. 57).

[Yab93]   E. Yablonovitch, "Photonic band-gap structures", *Journal of the Optical Society of America B* 10, 283 (1993), DOI: `10.1364/JOSAB.10.000283` (cited on pg. 57).

[YG89]   E. Yablonovitch and T. J. Gmitter, "Photonic band structure: The face-centered-cubic case", *Physical Review Letters* 63, 1950 (1989), DOI: `10.1103/PhysRevLett.63.1950` (cited on pg. 57).

[Yos+12]   K.-i. Yoshino et al., "High-speed wavelength-division multiplexing quantum key distribution system", *Optics Letters* 37, 223 (2012), DOI: `10.1364/OL.37.000223` (cited on pg. 113).

[YS96]   M. Yasuda and F. Shimizu, "Observation of Two-Atom Correlation of an Ultracold Neon Atomic Beam", *Physical Review Letters* 77, 3090 (1996), DOI: `10.1103/PhysRevLett.77.3090` (cited on pg. 89).

[Yu+14]   P.-L. Yu, K. Cicak, N. S. Kampel, Y. Tsaturyan, T. P. Purdy, R. W. Simmonds, and C. A. Regal, "A phononic bandgap shield for high-Q membrane microresonators", *Applied Physics Letters* 104, 023510 (2014), DOI: `10.1063/1.4862031` (cited on pg. 59).

[Yua+08]   Z.-S. Yuan, Y.-A. Chen, B. Zhao, S. Chen, J. Schmiedmayer, and J.-W. Pan, "Experimental demonstration of a BDCZ quantum repeater node", *Nature* 454, 1098 (2008), DOI: `10.1038/nature07241` (cited on pg. 113).

[Yur85]   B. Yurke, "Wideband photon counting and homodyne detection", *Physical Review A* 32, 311 (1985), DOI: `10.1103/PhysRevA.32.311` (cited on pgs. 35, 36, 47).

[Zar+17]   P. Zarkeshian et al., "Entanglement between more than two hundred macroscopic atomic ensembles in a solid", *Nature Communications* 8, 906 (2017), DOI: `10.1038/s41467-017-00897-7` (cited on pg. 114).

[Zen37]   C. Zener, "Internal Friction in Solids. I. Theory of Internal Friction in Reeds", *Physical Review* 52, 230 (1937), DOI: `10.1103/PhysRev.52.230` (cited on pg. 24).

[ZH46]   C. Zener and J. H. Hollomon, "Problems in Non-Elastic Deformation of Metals", *Journal of Applied Physics* 17, 69 (1946), DOI: `10.1063/1.1707696` (cited on pg. 24).

[ZM90]   X. T. Zou and L. Mandel, "Photon-antibunching and sub-Poissonian photon statistics", *Physical Review A* 41, 475 (1990), DOI: `10.1103/PhysRevA.41.475` (cited on pg. 90).

[Zub82]   M. Zubairy, "Nonclassical effects in a two-photon laser", *Physics Letters A* 87, 162 (1982), DOI: `10.1016/0375-9601(82)90102-5` (cited on pg. 61).

Appendices

A. Notations

Symbol	Description	Unit or Typical Value	See pg.
$[\hat{A}, \hat{B}]$	commutator $\hat{A}\hat{B} - \hat{B}\hat{A}$	[AB]	8
$\hat{O}\dagger$	Hermetian conjugate of operator $\hat{O}$	[O]	7
$\hat{\mathcal{H}}$	Hamiltonian operator	J	7
$\hbar = h/2\pi$	reduced Planck constant	Js	7
$\int_{-\infty}^{\infty} \frac{dt}{\sqrt{2\pi}} f(t)$	Fourier transform of function $f(t)$	[f]s	17
$\hat{D}_{\hat{a}}(\alpha)$	Displacement operator for mode $\hat{a}$	1	14
$\hat{O}_\omega$	Operator $\hat{O}$ in frame rotating with ω	$[\hat{O}]$	14
m_{eff}	effective mass of the mechanical mode	kg	7
$\hat{P}_p$	Physical momentum of the mechancial mode	kg m/s	7
$\hat{X}_p$	Physical displacement of the mechancial mode	m	7
$\hat{P}$	Momentum quadrature of the mechancial mode	$\sqrt{\text{phonon}}$	8
$\hat{X}$	Displacement quadrature of the mechancial mode	$\sqrt{\text{phonon}}$	8
$\hat{m}\ (\hat{m}^\dagger)$	mechanical annihilation (creation) operator	$\sqrt{\text{phonon}}$	8
$\hat{c}^\dagger\ (\hat{c})$	creation (annihilation) operator of the optical cavity mode	$\sqrt{\text{photon}}$	7
$\hat{A}$	Amplitude quadrature of the optical mode	$\sqrt{\text{photon}}$	8
$\hat{Y}$	Phase quadrature of the optical mode	$\sqrt{\text{photon}}$	8
$\hat{o}_{\text{in}}\ (\hat{o}_{\text{out}})$	Optical input (output) field of the cavity	$\sqrt{\text{photon}/s}$	11
$\hat{o}_{\text{loss}}$	Incoupled loss channel of the cavity	$\sqrt{\text{photon}/s}$	11
$\hat{o}_{\text{loss,out}}$	Outcoupled loss channel of the cavity	$\sqrt{\text{photon}/s}$	11
$\hat{a}_{\text{in}}$	Discrete wave-packet inbound to cavity	$\sqrt{\text{photon}}$	33
$\hat{a}_{\text{out}}$	Discrete wave-packet outbound from cavity	$\sqrt{\text{photon}}$	34
$\chi_{\text{L}}\ (\chi_{\text{M}})$	Optical (mechanical) susceptibility	$2\pi \cdot$s	18/25
$g_{ab}^{(2)}$	Intensity cross-correlation between system a and b	1	48

TABLE A.1.: Important operators and functions.

Symbol	Description	Unit or Typical Value	See pg.
G	optomechanical transduction	Hz/m	7
g_0	Optomechanical single photon coupling strength	$2\pi\cdot825\,\text{kHz}$	9
Ω	Angular mechanical frequency	$2\pi\cdot5.2\,\text{GHz}$	7
Q_{mech}	Mechanical quality factor	10^5 to 10^7	25
Γ	Mechanical energy decay rate	$2\pi\,\text{Hz}$	12
ω_c	Angular optical resonance frequency	$2\pi\cdot193\,\text{THz}$	7
Q_{opt}	Optical quality factor	$220\cdot10^3$	23
κ	Optical amplitude decay rate	$2\pi\cdot450\,\text{MHz}$	11
ω_{L}	Angular frequency of the drive laser	$2\pi\cdot193\,\text{THz}$	14
ϵ_{P}	Stokes scattering constant, pair creation probability	1	39
ϵ_{R}	Anti-Stokes scattering constant, transfer efficiency	1	36

TABLE A.2.: Important system parameters and typical values.

B. Theory

B.1. The Thermal Mechanical State

A mechanical oscillator with viscous damping in contact with a thermal bath in thermal equilibrium is in a thermal state. The following section intends to show how this thermal state is connected with the equations of motion (2.22) derived in paragraph 2.1.3.

In order to achieve this, we adapt a matrix formalism of describing the equation of motions of the mechanical oscillator, that is neglecting the optical field and the optomechanical coupling $g \sim 0$. We start by noting that we defined the mean value of all degrees of freedom in equilibrium to be zeros, that is for the state vector

$$\langle \vec{X} \rangle = \langle (\hat{X}, \hat{P})^T \rangle = (0, 0)^T. \tag{B.1}$$

The equations of motion can be expressed as the matrix equation

$$\frac{\mathrm{d}}{\mathrm{d}t} \vec{X} = \mathbf{B} \vec{X} = \begin{pmatrix} 0 & \Omega \\ -\Omega & -\Gamma \end{pmatrix} \begin{pmatrix} \hat{X} \\ \hat{P} \end{pmatrix}. \tag{B.2}$$

In order to describe the thermal state, we will first derive the cross-correlation[1] spectral density (CSD) $\mathbf{S}_{XX}(\omega)$ will then obtain the covariance matrix $\mathbf{P} = \langle \vec{X} \vec{X}^\dagger \rangle$ of the quadratures by integrating over it.

From the system dynamics we can deduce the transfer function of the thermal noise input by going into Fourier transforming (B.2)

$$- i\omega \tilde{\vec{X}}(\omega) = \mathbf{B} \tilde{\vec{X}}(\omega) + \mathbf{\Lambda} \tilde{\vec{\xi}}(\omega) \tag{B.3}$$

with the noise input vector $\vec{\xi} = (0, \hat{P}_{\text{loss}})$ and the coupling matrix $\mathbf{\Lambda} = \mathrm{diag}(0, \sqrt{2\Gamma})$. Thus the CSD is

$$\mathbf{S}_{XX}(\omega) = \tilde{\vec{X}}(\omega) \tilde{\vec{X}}^\dagger(\omega) = (i\omega - B)^{-1} \Lambda S_{\xi\xi}(\omega) \Lambda^T \left\{ (i\omega - B)^{-1} \right\}^\dagger \tag{B.4}$$

The CSD is Hermetian, but can contain complex values, corresponding to time correlations. As they are of no relevance for the covariance, consequently the CSD is symmetrized, i.e. its real part is taken, before the integration[2]

$$\mathbf{P}_{\text{th}} = \int_{-\infty}^{\infty} \frac{\mathrm{d}\omega}{2\pi} \, \mathcal{R}e(\mathbf{S}_{XX}(\omega)) \,. \tag{B.5}$$

---

[1] Not to confuse with the normalized cross-correlation, which is short for the degree of second-order coherence as defined by reference [Gla63b].

[2] For practical applications, that is if only a one sided frequency spectrum is available, this corresponds to $\mathbf{P}_{\text{init}} = 2 \int_0^\infty \mathrm{d}f \, \mathcal{R}e(\mathbf{S}_{XX}(f))$.

B. Theory

In the following, we will evaluate this integral analytically.

We calculate the transfer function between the noise input and the state vector

$$- (i\omega + B)^{-1} = \underbrace{\frac{1}{\Omega^2 - \omega^2 - i\omega\Gamma_k}}_{\chi_{\mathrm{M}}(\omega)/\Omega} \begin{pmatrix} -i\omega + \Gamma & \Omega \\ -\Omega & -i\omega \end{pmatrix} \tag{B.6}$$

to obtain the cross spectral density

$$S_{kk}(\omega) = (i\omega + B)^{-1} \Lambda S_{\xi\xi}(\omega)\Lambda^T \left[(i\omega + B)^{-1}\right]^\dagger \tag{B.7}$$

$$= \frac{|\chi_{\mathrm{M}}(\omega)|^2}{\Omega^2} \begin{pmatrix} \Omega^2 & i\omega\Omega \\ -i\omega\Omega & \omega^2 \end{pmatrix} 2\Gamma \left(n_{\mathrm{th}} + \frac{1}{2}\right) \tag{B.8}$$

The off diagonal terms are purely imaginary, i.e. they do not play a role for the covariance matrix. We further simplify the system by assuming a high Q oscillator, which allows to approximate the inverse absolute square of the determinant as a δ distribution, with the normalization

$$\int_{-\infty}^{\infty} \frac{d\omega}{2\pi} |\chi_{\mathrm{M}}(\omega)|^2 = \frac{1}{2\Gamma} \tag{B.9}$$

$$\Rightarrow \quad |\chi_{\mathrm{M}}(\omega)|^2 \approx \frac{\delta(\omega - \Omega) + \delta(\omega + \Omega)}{4\Gamma}. \tag{B.10}$$

We thus find the covariance matrix

$$\mathbf{P}_{\mathrm{th}} = \int_{-\infty}^{\infty} \omega \frac{d\omega}{2\pi} \mathcal{R}e(\mathbf{S}_{XX}(\omega)) = \begin{pmatrix} n_{\mathrm{th}} + \frac{1}{2} & 0 \\ 0 & n_{\mathrm{th}} + \frac{1}{2} \end{pmatrix}, \tag{B.11}$$

recovering as expected the energy equipartition between the quadratures and a thermal equilibrium with the environment.

B.2. Emitted Mode Envelope in a Quasi-Continuously Driven System

Here we will discuss the mode envelope of the waves emitted from an optomechanical system driven by a quasi-continous way, as described in section 2.3. The derivation will closely follow [Hof+11; Hof15], generalizing them to arbitrary envelopes of the drive pulse.

For the input wavelet mode, we found in equation (2.52)

$$\hat{a}_{\mathrm{in}} = \frac{1}{\sqrt{\pm \left(1 - e^{-2\tilde{G}_\pm(T)}\right)}} \int_{-\infty}^{\infty} \frac{d\omega}{\sqrt{2\pi}} \int_0^T d\tau \, \frac{\chi_{\omega_{\mathrm{L}}}(\omega \mp \tilde{\Omega})}{|\chi_{\omega_{\mathrm{L}}}(\mp\tilde{\Omega})|} \hat{\tilde{o}}_{\omega_{\mathrm{L}}}(\omega \mp \tilde{\Omega}) e^{-\tilde{G}_\pm(\tau)} \sqrt{2\tilde{s}_\pm(\tau)} e^{-i\omega\tau}. \tag{B.12}$$

For the output we expect a similar integration kernel, as it should also be located at the optomechanical sideband and in the weak coupling case follow the drive pulse envelope.

In order to find an expression for the output field, we rephrase the expression for the cavity field (2.24) with the general parametrization[3] and in the limit of a single sideband

$$\sqrt{2\kappa}\hat{c}_{\omega_{\mathrm{L}}} = ie^{\pm i\phi_{\pm}}\sqrt{2\tilde{s}_{\pm}}\frac{\chi_{\omega_{\mathrm{L}}}(\mp\Omega)}{|\chi_{\omega_{\mathrm{L}}}(\mp\Omega)|}\hat{m}_{\tilde{\Omega}}^{\pm}e^{\pm i\tilde{\Omega}t} + 2\kappa\int_{-\infty}^{\infty}\frac{\mathrm{d}\omega}{\sqrt{2\pi}}\,\chi_{\omega_{\mathrm{L}}}(\omega)\hat{\bar{o}}_{\omega_{\mathrm{L}}}(\omega)e^{-i\omega t} \qquad (\text{B.13})$$

Using the cavity input output relation (2.12) we can define the continuous output field as

$$\hat{u}_{\omega_{\mathrm{L}}} = \hat{o}_{\omega_{\mathrm{L}}} - \sqrt{2\kappa}\hat{c}_{\omega_{\mathrm{L}}} \qquad (\text{B.14})$$

$$= -ie^{\pm i\phi_{\pm}}\sqrt{2\tilde{s}_{\pm}}\frac{\chi_{\omega_{\mathrm{L}}}(\mp\Omega)}{|\chi_{\omega_{\mathrm{L}}}(\mp\Omega)|}\hat{m}_{\tilde{\Omega}}^{\pm}e^{\pm i\tilde{\Omega}t} - \int_{-\infty}^{\infty}\frac{\mathrm{d}\omega}{\sqrt{2\pi}}\frac{\chi_{\omega_{\mathrm{L}}}(\omega)}{\chi_{\omega_{\mathrm{L}}}(\omega)^{\dagger}}\hat{\bar{o}}_{\omega_{\mathrm{L}}}(\omega)e^{-i\omega t}. \qquad (\text{B.15})$$

This expression is still dependent on the time evolution of the mechanical operator. In order to obtain an expression, which only depends on the initial mechanical operator, we can use equation (2.50)[4], such that we obtain

$$\hat{u}_{\omega_{\mathrm{L}}}(t) = -ie^{\pm i\phi_{\pm}}\sqrt{2\tilde{s}_{\pm}}\frac{\chi_{\omega_{\mathrm{L}}}(\mp\Omega)}{|\chi_{\omega_{\mathrm{L}}}(\mp\Omega)|}e^{\pm i\tilde{\Omega}t}e^{\tilde{G}_{\pm}(t)}\hat{m}_{\tilde{\Omega}}^{\pm}(0) \qquad (\text{B.16a})$$

$$\mp\sqrt{2\tilde{s}_{\pm}}\frac{\chi_{\omega_{\mathrm{L}}}(\mp\Omega)}{|\chi_{\omega_{\mathrm{L}}}(\mp\Omega)|}e^{\pm i\tilde{\Omega}t}e^{\tilde{G}_{\pm}(t)}$$

$$\cdot\int_{0}^{t}\mathrm{d}\tau\int_{-\infty}^{\infty}\frac{\mathrm{d}\omega}{\sqrt{2\pi}}\,e^{-\tilde{G}_{\pm}(\tau)}\sqrt{2\tilde{s}_{\pm}(\tau)}\frac{\chi_{\omega_{\mathrm{L}}}(\omega\mp\tilde{\Omega})}{|\chi_{\omega_{\mathrm{L}}}(\mp\tilde{\Omega})|}\hat{\bar{o}}_{\omega_{\mathrm{L}}}(\omega\mp\tilde{\Omega})e^{-i\omega\tau} \qquad (\text{B.16b})$$

$$-\int_{-\infty}^{\infty}\frac{\mathrm{d}\omega}{\sqrt{2\pi}}\frac{\chi_{\omega_{\mathrm{L}}}(\omega)}{\chi_{\omega_{\mathrm{L}}}(\omega)^{\dagger}}\hat{\bar{o}}_{\omega_{\mathrm{L}}}(\omega)e^{-i\omega t}. \qquad (\text{B.16c})$$

The first line of this rather bulky expression shows the pulse shape of the emitted photon to have the envelope $\sqrt{2\tilde{s}_{\pm}(t)}e^{\tilde{G}_{\pm}(t)}$ and is shifted in frequency by $\pm\tilde{\Omega}$ compared to the drive frequency. Hence, we make an Ansatz for the output mode

$$\hat{a}_{\mathrm{out}} = \int_{-\infty}^{\infty}\frac{\mathrm{d}\omega}{\sqrt{2\pi}}\int_{0}^{T}\mathrm{d}\tau\,\mathcal{W}_{(\pm)}^{\mathrm{out}}(\omega,\tau)\hat{\tilde{u}}_{\omega_{\mathrm{L}}}(\omega\mp\tilde{\Omega}) \qquad (\text{B.17a})$$

$$\mathcal{W}_{(\pm)}^{\mathrm{out}}(\omega,\tau) = \frac{1}{\sqrt{\pm(e^{2\tilde{G}_{\pm}(T)}-1)}}\frac{\chi_{\omega_{\mathrm{L}}}(\omega\mp\Omega)^{\dagger}}{|\chi_{\omega_{\mathrm{L}}}(\mp\Omega)|}e^{\tilde{G}_{\pm}(\tau)}\sqrt{2\tilde{s}_{\pm}(\tau)}e^{-i\omega\tau}, \qquad (\text{B.17b})$$

with $\hat{\tilde{u}}_{\omega_{\mathrm{L}}}$ the Fourier transform of $\hat{u}_{\omega_{\mathrm{L}}}$. In the limit of large κ, we can see that this mode is normalized, in analogy to the optical inputmode (2.52).

---

[3] Here we use the same notation as in section 2.3, that is, the coupling strength is

$$\mu_{\pm} = -g^{\mp}\sqrt{\kappa}|\chi_{\omega_{\mathrm{L}}}(\mp\tilde{\Omega})| = \sqrt{\tilde{s}_{\pm}}e^{i\phi_{\pm}}.$$

[4] For reference, we fully expand the expression for the evolution of the mechanical annihilation operator:

$$\hat{m}(t) = e^{\tilde{G}_{\pm}(T)}\hat{m}_{\tilde{\Omega}}(0)$$

$$+ ie^{i\phi_{\pm}}e^{\tilde{G}_{\pm}(t)}\int_{-\infty}^{\infty}\frac{\mathrm{d}\omega}{\sqrt{2\pi}}\int_{0}^{t}\mathrm{d}\tau\,e^{-\tilde{G}_{\pm}(\tau)}\sqrt{2\tilde{s}_{\pm}(\tau)}\frac{\chi_{\omega_{\mathrm{L}}}^{\pm}(\omega\mp\tilde{\Omega})}{|\chi_{\omega_{\mathrm{L}}}(\mp\tilde{\Omega})|}\hat{o}_{\omega_{\mathrm{L}}}^{\pm}(\omega\mp\tilde{\Omega})e^{\pm i\omega\tau}$$

B. Theory

We will now analyze the contribution of (B.16) to the output mode line by line in order to obtain an equation for the interaction in terms of modes.

$$
\hat{a}_{\text{out}} = \int_{-\infty}^{\infty} \frac{\mathrm{d}\omega}{\sqrt{2\pi}} \int_0^T \mathrm{d}\tau \, \mathcal{W}_{(\pm)}^{\text{out}}(\omega, \tau) \int_{-\infty}^{\infty} \frac{\mathrm{d}t}{\sqrt{2\pi}} \, \hat{u}_{\omega_{\text{L}}}(t) e^{-i(\omega \mp \tilde{\Omega})t}
$$

$$
= \int_{-\infty}^{\infty} \frac{\mathrm{d}\omega}{\sqrt{2\pi}} \int_0^T \mathrm{d}\tau \int_{-\infty}^{\infty} \frac{\mathrm{d}t}{\sqrt{2\pi}} \, \mathcal{W}_{(\pm)}^{\text{out}}(\omega, \tau) e^{-i(\omega \mp \tilde{\Omega})t} \Big[\underbrace{(\text{B.16a})}_{\to \text{①}} + \underbrace{(\text{B.16b})}_{\to \text{②}} + \underbrace{(\text{B.16c})}_{\to \text{③}} \Big]
$$

For this, we will repeatedly make a couple of approximations: due to the slow time envelope in the mode definition (B.17), we we can see that the mode is peaked very narrowly around the mechanical sidebands, i.e. at $\omega \sim 0$. As the bandwidth of the cavity is large compared to the pulse bandwidth, we can approximate $\chi_{\omega_{\text{L}}}(\omega \mp \Omega) \sim \chi_{\omega_{\text{L}}}(\mp\Omega)$, the cavity response will in essence correspond to an effective phase shift. We apply the above approximation in the first term

$$
\text{①} = -\frac{1}{\sqrt{\pm(e^{2\tilde{G}_{\pm}(T)} - 1)}} \int_{-\infty}^{\infty} \frac{\mathrm{d}\omega}{\sqrt{2\pi}} \int_0^T \mathrm{d}\tau \, \frac{\chi_{\omega_{\text{L}}}(\omega \mp \Omega)^{\dagger}}{|\chi_{\omega_{\text{L}}}(\mp\Omega)|} e^{\tilde{G}_{\pm}(\tau)} \sqrt{2\tilde{s}_{\pm}(\tau)} e^{-i\omega\tau}
$$

$$
\int_{-\infty}^{\infty} \frac{\mathrm{d}t}{\sqrt{2\pi}} \, i e^{\pm i\phi_{\pm}} \sqrt{2\tilde{s}_{\pm}(t)} \frac{\chi_{\omega_{\text{L}}}(\mp\Omega)}{|\chi_{\omega_{\text{L}}}(\mp\Omega)|} e^{\tilde{G}_{\pm}(t)} \hat{m}_{\tilde{\Omega}}^{\pm}(0) e^{i\omega t}
$$

$$
= -i e^{\pm i\phi_{\pm}} \sqrt{\pm(e^{2\tilde{G}_{\pm}(T)} - 1)} \hat{m}_{\tilde{\Omega}}^{\pm}(0), \tag{B.18}
$$

simplifying the ω-integral to a Dirac delta distribution $\delta(t - \tau)$. Note that the boundaries of the τ-integral can equivalently be set to $[-\infty, \infty]$, as the integrand is zero outside the original bounds of $[0, T]$. Hence, it can be resolved with the distribution, eventually resulting in the same type of t-integral as already encoutered in the normalization of mode shape (B.17). Employing the same steps, we can resolve the first two integrals of the second term, and then simplify the remaining three integrals using the equality $\int_0^T \mathrm{d}t \int_0^t \mathrm{d}\tau \, f(t, \tau) = \int_0^T \mathrm{d}\tau \int_{\tau}^T \mathrm{d}t \, f(t, \tau)$, which can be applied to integrable functions f

[Hof15]:

$$\circled{2} = \mp \frac{1}{\sqrt{\pm(e^{2\tilde{G}_\pm(T)} - 1)}} \int_0^T \mathrm{d}t\ e^{2\tilde{G}_\pm(t)} 2\tilde{s}_\pm(t)$$

$$\int_{-\infty}^{\infty} \frac{\mathrm{d}\omega}{\sqrt{2\pi}} \int_0^t \mathrm{d}\tau\ e^{-\tilde{G}_\pm(\tau)} \sqrt{2\tilde{s}_\pm(\tau)} \frac{\chi_{\omega_\mathrm{L}}(\omega \mp \tilde{\Omega})}{|\chi_{\omega_\mathrm{L}}(\mp\tilde{\Omega})|} \hat{o}_{\omega_\mathrm{L}}(\omega \mp \tilde{\Omega}) e^{-i\omega\tau}$$

$$= \mp \frac{1}{\sqrt{\pm(e^{2\tilde{G}_\pm(T)} - 1)}} \int_0^T \mathrm{d}\tau \int_\tau^T \mathrm{d}t\ e^{2\tilde{G}_\pm(t)} 2\tilde{s}_\pm(t)$$

$$e^{-\tilde{G}_\pm(\tau)} \sqrt{2\tilde{s}_\pm(\tau)} \int_{-\infty}^{\infty} \frac{\mathrm{d}\omega}{\sqrt{2\pi}} \frac{\chi_{\omega_\mathrm{L}}(\omega \mp \tilde{\Omega})}{|\chi_{\omega_\mathrm{L}}(\mp\tilde{\Omega})|} \hat{o}_{\omega_\mathrm{L}}(\omega \mp \tilde{\Omega}) e^{-i\omega\tau}$$

$$= -\frac{e^{\tilde{G}_\pm(T)}}{\sqrt{\pm\left(1 - e^{-2\tilde{G}_\pm(T)}\right)}} \int_{-\infty}^{\infty} \frac{\mathrm{d}\omega}{\sqrt{2\pi}} \frac{\chi_{\omega_\mathrm{L}}(\omega \mp \tilde{\Omega})}{|\chi_{\omega_\mathrm{L}}(\mp\tilde{\Omega})|} \hat{o}_{\omega_\mathrm{L}}(\omega \mp \tilde{\Omega}) \int_0^T \mathrm{d}\tau\ e^{-\tilde{G}_\pm(\tau)} \sqrt{2\tilde{s}_\pm(\tau)} e^{-i\omega\tau}$$

$$+ \frac{1}{\sqrt{\pm(e^{2\tilde{G}_\pm(T)} - 1)}} \int_0^T \mathrm{d}\tau\ e^{\tilde{G}_\pm(\tau)} \sqrt{2\tilde{s}_\pm(\tau)} \int_{-\infty}^{\infty} \frac{\mathrm{d}\omega}{\sqrt{2\pi}} \frac{\chi_{\omega_\mathrm{L}}(\omega \mp \tilde{\Omega})}{|\chi_{\omega_\mathrm{L}}(\mp\tilde{\Omega})|} \hat{o}_{\omega_\mathrm{L}}(\omega \mp \tilde{\Omega}) e^{-i\omega\tau}$$

$$= -e^{\tilde{G}_\pm(T)} \hat{a}_\mathrm{in} - \circled{3}. \tag{B.19}$$

Going from the second to the third line, we use the definition (2.47) of the cummulative coupling $\mathrm{d}/\mathrm{d}t\ \tilde{G}_\pm(t) = \pm\tilde{s}_\pm(t)$ to resolve the t-integral over the interval $[\tau, T]$. We can thus eliminate the third term, yielding equation (2.54) for the output mode

$$\hat{a}_\mathrm{out} = -ie^{\pm i\phi_\pm} \sqrt{\pm\left(e^{2\tilde{G}_\pm(T)} - 1\right)} \hat{m}_{\tilde{\Omega}}^\pm(0) - e^{\tilde{G}_\pm(T)} \hat{a}_\mathrm{in}. \tag{B.20}$$

B.3. The Cross-Correlation in an Optomechanical System

In paragraph 2.4.2, the normalized cross-correlation between the optical and the mechanical mode of an optomechanical system was introduced, and its relation to the cross-correlation between the counting measurements of the Stokes and the anti-Stokes scattered photons was discussed. Here, this relation is investigated in a more formal way, and the relation between the measured cross-correlation and typical noise processes is treated.

B.3.1. Measurement Operators and Initial State

In a real experiment, we do not have access to the ideal number operators $\hat{m}^\dagger\hat{m}$ and $\hat{a}_\mathrm{wg,out}^\dagger \hat{a}_\mathrm{wg,out}$, but instead use single photon detectors as estimators, which are partially corrupted by measurement noise. We define the approximate measurement operator[5] for

---

[5] Note that typical single photon detectors can not resolve the number of excitations excitations. Therefore, they are best described by $\mathbb{1} - |0\rangle\langle 0|_{\hat{b}}$ for a mode $\hat{b}$. When the average photon number is low, e.g. in the presence of a significant loss channel, higher excitation numbers are negligible and thus $\hat{b}^\dagger\hat{b}$ is a good approximation, with $\langle\mathbb{1} - |0\rangle\langle 0|_{\hat{b}}\rangle \sim \langle\hat{b}^\dagger\hat{b}\rangle$.

B. Theory

the Stokes ($\hat{D}_o$) and anti-Stokes ($\hat{D}_m$) scattered photons

$$\hat{D}_o = \hat{d}_{\mathrm{w}}^\dagger \hat{d}_{\mathrm{w}} + \hat{f}_o^\dagger \hat{f}_o \tag{B.21a}$$

$$\hat{D}_m = \hat{d}_{\mathrm{r}}^\dagger \hat{d}_{\mathrm{r}} + \hat{f}_m^\dagger \hat{f}_m. \tag{B.21b}$$

The detection modes $\hat{d}_{\mathrm{w}}$ and $\hat{d}_{\mathrm{r}}$ are defined as in paragraph 2.4.2 and equation (2.70) modeling the transmission losses from the device to the detector with the absolute quantum efficiency for the Stokes photons η_{d} and the transferred phonons $\eta_{\mathrm{d}}\epsilon_{\mathrm{R}}$[6]. The number operator $\hat{f}_o^\dagger \hat{f}_o$ ($\hat{f}_m^\dagger \hat{f}_m$) summarizes the origins of false positive counts, with $\langle \hat{f}_o^\dagger \hat{f}_o \rangle$ ($\langle \hat{f}_m^\dagger \hat{f}_m \rangle$) corresponding to the mean number of false positive detection events during the time gate associated with the Stokes (anti-Stokes) scattered photons. We further assume that the noise channel $\hat{f}$ and the loss channel vacuum port $\hat{l}$ and the Markovian thermal environment are uncorrelated with the initial optomechanical system, i.e. we can decompose the density matrix $\hat{\rho} \approx \hat{\rho}_{o,m} \otimes \hat{\rho}_{f,l,t}$. The first factor $\hat{\rho}_{o,m}$ is the density matrix of the initial optomechanical system before any interaction takes place, and the second factor $\hat{\rho}_{f,l,t}$ represents the auxiliary systems at that time.

This allows to define the estimators of the optomechanical system as

$$\hat{M}_o = \mathrm{Tr}_{\hat{l},\hat{f},\hat{T}}(\hat{D}_o \hat{\rho}_{f,l,t})/\eta_{\mathrm{d}} \approx \hat{a}_{\mathrm{wg,out}}^\dagger \hat{a}_{\mathrm{wg,out}} + P_{\mathrm{fpo}}\mathbb{1} \tag{B.22a}$$

$$\hat{M}_m = \mathrm{Tr}_{\hat{l},\hat{f},\hat{T}}(\hat{D}_m \hat{\rho}_{f,l,t})/(\eta_{\mathrm{d}}\epsilon_{\mathrm{R}}) \approx \hat{m}^\dagger \hat{m} + P_{\mathrm{fpm}}\mathbb{1}, \tag{B.22b}$$

with the normalized false positive detection probability $P_{\mathrm{fpo}} = \langle \hat{f}_o^\dagger \hat{f}_o \rangle/\eta_{\mathrm{d}}$. The mechanical phonon number estimator is defined in close analogy for detection events during the time gate associated with the anti-Stokes scattered photons and $P_{\mathrm{fpm}} = \langle \hat{f}_m^\dagger \hat{f}_m \rangle/(\eta_{\mathrm{d}}\epsilon_{\mathrm{R}})$ corrected for the finite state transfer fidelity ϵ_{R}. The indexes of the trace operator $\mathrm{Tr}_{\hat{l},\hat{f},\hat{T}}$ indicate that the trace is only taken over the loss channel $\hat{l}$ and the noise channels $\hat{f}$ of both Stokes and anti-Stokes drive pulses, as well as the initial thermal environment, represented by the abstract operator $\hat{T}$. Due to including the latter, the normalized false positive rate of the readout pulse P_{fpm} also includes the thermally generated phonons in the system after the initial interaction.

The initial state of the optomechanical system is

$$\hat{\rho}_i = \hat{\rho}_{o,m} = \hat{\rho}_{\mathrm{th}} \otimes |0\rangle \langle 0|_{\mathrm{opt}}, \tag{B.23}$$

with the vacuum state $|0\rangle \langle 0|_{\mathrm{opt}}$ in the optical resonator and a thermal state $\hat{\rho}_{\mathrm{th}}$ in the mechanical oscillator. The latter is characterized by the mean number of phonons

$$\mathrm{Tr}\left(\hat{m}^\dagger \hat{m}\rho_i\right) = n_i \tag{B.24}$$

and autocorrelation $g_{mm}^{(2)} = 2$ in the initial state.

B.3.2. The Heralded State

The 'write' pulse drives the Stokes transition and is represented by the unitary transformation

$$\hat{U} = \exp\left[i\sqrt{p}\left(\hat{a}_{\mathrm{wg,out}}^\dagger \hat{m}^\dagger + \hat{a}_{\mathrm{wg,out}} \hat{m}\right)\right], \tag{B.25}$$

---

[6] As a reminder, $\eta_{\mathrm{d}} = \eta_{\mathrm{qe}}\eta_{\mathrm{path}}\kappa_{\mathrm{in}}/\kappa$, with the quantum efficiency η_{qe} of the detector, η_{path} the transmission of the optical path from the device to the detector, and $\kappa_{\mathrm{in}}/\kappa$ the loss due to the cavity impedance.

with the small probability $p = \epsilon_P \ll 1$ of a Stokes scattering event, see also paragraph 2.3.3. This yields the state after the write pulse in the interaction picture $\hat{\rho}_p = \hat{U}\hat{\rho}_i\hat{U}^\dagger$.

Here, we want to estimate the cross-correlation between the read and the write pulse in the limit of $p, n_i \ll 1$. In order to obtain an expression of the leading terms of the cross-correlation, we need to include the process of creating two photon-phonon pairs[7]. We thus expand the state up to the quadratic terms $\mathcal{O}(p^2)$ in the Stokes pair creation probability. As the counting measurements are not sensitive to the coherences of the state, we can further neglect the off-diagonal terms in the density matrix.

In this approximation[8] the state after the Stokes interaction is

$$
\begin{aligned}
\hat{\rho}_p \approx &\hat{\rho}_i + p(\hat{m}^\dagger \hat{a}^\dagger_{\mathrm{wg,out}}\hat{\rho}_i \hat{a}_{\mathrm{wg,out}}\hat{m}) - \frac{p}{2}\hat{m}\hat{m}^\dagger\hat{\rho}_i - \frac{p}{2}\hat{\rho}_i \hat{m}\hat{m}^\dagger \\
&+ \frac{p^2}{4}(\hat{m}^{\dagger 2}\hat{a}^{\dagger 2}_{\mathrm{wg,out}}\hat{\rho}_i \hat{a}^2_{\mathrm{wg,out}}\hat{m}^2) + \frac{p^2}{4}\hat{m}\hat{m}^\dagger\hat{\rho}_i \hat{m}\hat{m}^\dagger \\
&- \frac{p^2}{6}\left[\left(3\hat{m}^\dagger\hat{m} + 2\right)\hat{m}^\dagger\hat{a}^\dagger_{\mathrm{wg,out}}\hat{\rho}_i \hat{a}_{\mathrm{wg,out}}\hat{m} + \mathrm{h.c.}\right] \\
&+ \frac{p^2}{24}\left[\left(2\hat{m}^2\hat{m}^{\dagger 2} + (\hat{m}\hat{m}^\dagger)^2\right)\hat{\rho}_i + \mathrm{h.c.}\right].
\end{aligned}
\tag{B.26}
$$

The expectation value for the photon and phonon measurement of this state yield

$$
\mathrm{Tr}(\hat{M}_o\hat{\rho}_p) = P_{\mathrm{fpo}} + p(1 + n_i) - p^2\frac{2 + 5n_i + 3n_i^2}{3}
\tag{B.27a}
$$

$$
\mathrm{Tr}(\hat{M}_m\hat{\rho}_p) = P_{\mathrm{fpm}} + n_i + p(1 + n_i) + \mathcal{O}(p^2) \equiv \bar{M},
\tag{B.27b}
$$

where we used the expression for the autocorrelation of the thermal state $\langle\hat{m}^{\dagger 2}\hat{m}^2\rangle = g^{(2)}_{mm}n_i^2 \approx 2n_i^2$. The measured mean phonon number is an important figure of merit, and is therefore noted as $\langle\hat{M}_m\rangle \equiv \bar{M}$.

We can now express the mechanical state heralded by the detection of a signal photon from the write pulse. In essence, the heralding process selects those mechanical states, for which a photon was detected by the detector represented by $\hat{M}_o$, i.e. the state is proportional to the trace over the optical part of the system $\mathrm{Tr}_o(\hat{M}_o\hat{\rho}_p)$, including the photo-detection. As this process is not unitary, the density matrix of the heralded state

---

[7] For this reason, the following equalities for bosonic ladder operators $\hat{a} = \hat{m}, \hat{a}_{\mathrm{wg,out}}$ will be used frequently, and are therefore given here as reference:

$$
\begin{aligned}
\hat{a}\hat{a}^\dagger &= \hat{a}^\dagger\hat{a} + 1 & \hat{a}^2\hat{a}^{\dagger 2} &= \hat{a}^{\dagger 2}\hat{a}^2 + 4\hat{a}^\dagger\hat{a} + 2 \\
\hat{a}\hat{a}^\dagger\hat{a}\hat{a}^\dagger &= \hat{a}^{\dagger 2}\hat{a}^2 + 3\hat{a}^\dagger\hat{a} + 1 & \hat{a}^2\hat{a}^\dagger\hat{a}\hat{a}^{\dagger 2} &= \hat{a}^{\dagger 3}\hat{a}^3 + 8\hat{a}^{\dagger 2}\hat{a}^2 + 14\hat{a}^\dagger\hat{a} + 4
\end{aligned}
$$

[8] The relevant terms of the unitary transformation of the write pulse are thus

$$
\begin{aligned}
\hat{U} = &1 + i\sqrt{p}\hat{a}^\dagger_{\mathrm{wg,out}}\hat{m}^\dagger - \frac{p}{2}\hat{m}\hat{m}^\dagger - \frac{p}{2}\hat{a}^{\dagger 2}_{\mathrm{wg,out}}\hat{m}^{\dagger 2} \\
&- i\frac{p^{3/2}}{6}\left(2\hat{m}\hat{m}^{\dagger 2} + \hat{m}^\dagger\hat{m}\hat{m}^\dagger\right)\hat{a}^\dagger_{\mathrm{wg,out}} + \frac{p^2}{24}\left(2\hat{m}^2\hat{m}^{\dagger 2} + \hat{m}\hat{m}^\dagger\hat{m}\hat{m}^\dagger\right).
\end{aligned}
$$

B. Theory

$\hat{\rho}_H = \mathrm{Tr}_o(\hat{M}_o\hat{\rho}_p)/\mathrm{Tr}(\hat{M}_o\hat{\rho}_p)$ needs to be normalized. This leads to the expression

$$\hat{\rho}_H = \frac{P_{\mathrm{fpoR}}\mathrm{Tr}_o(\hat{\rho}_p) + \hat{m}^\dagger\hat{\rho}_{\mathrm{th}}\hat{m} + \frac{p}{2}\hat{m}^{\dagger 2}\hat{\rho}_{\mathrm{th}}\hat{m}^2 - \frac{p}{6}\left[\left(3\hat{m}^\dagger\hat{m} + 2\right)\hat{m}^\dagger\hat{\rho}_{\mathrm{th}}\hat{m} + \mathrm{h.c.}\right]}{P_{\mathrm{fpoR}} + (1 + n_i) - p\frac{2 + 5n_i + 3n_i^2}{3}}, \quad \text{(B.28)}$$

where we introduced the relative false positive detection rate of the write pulse $P_{\mathrm{fpoR}} = P_{\mathrm{fpo}}/p$. It describes the ratio between false positive detection events and intended ones, and is therefore comparable with the expression for the read pulse. This will be discussed more extensively in the following paragraph.

For negligible noise figures $P_{\mathrm{fpoR}}, p, n_i \ll 1$, we find that the dominant term in the heralded state is $\hat{m}^\dagger\hat{\rho}_i\hat{m}$, i.e. a single phonon is added to the initial thermal state $\hat{\rho}_{\mathrm{th}}$.

B.3.3. The Cross-Correlation

We found in paragraph 2.4.2, that the crosscorrelation $g_{om}^{(2)} = \langle\hat{M}_m\hat{M}_o\rangle/(\langle\hat{M}_m\rangle\langle\hat{M}_o\rangle)$ is equivalent to the ratio of tha apparent phonon numbers in the heralde versus the unheralded state $g_{om}^{(2)} = \mathrm{Tr}(\hat{M}_m\hat{\rho}_H)/\mathrm{Tr}(\hat{M}_m\hat{\rho}_p)$. With the previously derived expressions (B.27) and (B.28) we obtain the the cross-correlation

$$g_{om}^{(2)} = \frac{1 + 3n_i + 2n_i^2 + p(\frac{1}{3} - 2n_i) + P_{\mathrm{fpm}}\left[1 + n_i - \frac{p}{3}(2 + 5n_i)\right] + P_{\mathrm{fpoR}}\bar{M}}{(1 + n_i + p(1 + 2n_i) - \frac{p}{3}(5 + 11n_i) + P_{\mathrm{fpoR}})\bar{M}}, \quad \text{(B.29)}$$

where we neglected terms of a higher order than $\mathcal{O}(pn_i)$. In order to identify the dominant terms, we linearize the denominator $1/(1+S) \sim 1-S$ with $S = P_{\mathrm{fpoR}}+n_i-p(2+5n_i)/3 \ll 1$. Keeping only the dominant terms in the numerator[9] we arrive at

$$g_{om}^{(2)} = \frac{1 + \bar{M} + n_i - P_{\mathrm{fpoR}} + P_{\mathrm{fpm}}\left[n_i - \frac{2p}{3}\right] + g_{ff}^{(2)}P_{\mathrm{fpm}}P_{\mathrm{fpoR}}}{\bar{M}} \quad \text{(B.30a)}$$

$$= \frac{1 + n_i - P_{\mathrm{fpoR}}}{\bar{M}} + 1. \quad \text{(B.30b)}$$

In the first line, we included the possibility of correlation $g_{ff}^{(2)}$ of the background noise processes for the read and write pulse. For uncorrelated noise $g_{ff}^{(2)} = 1$. In the second line we further assumed low readout noise $P_{\mathrm{fpm}} \ll 1$, resulting in exclusively linear terms in the numerator. This expression can be used to reproduce corresponding results from the literature: For negligible noise in the detectors $P_{\mathrm{fpm}}, P_{\mathrm{fpoR}} \sim 0$ and no thermal background $n_i \sim 0$, we find $\bar{M} \sim p$, resulting in the expression $g_{om}^{(2)} \approx 1 + 1/p$ from reference [Kuz+03]. Again neglecting detection noise and a weak drive strength $p \ll n_i$, the expression $g_{om}^{(2)} \approx 2 + 1/n_i$ from reference [BNG11] is recovered.

---

[9] This includes terms which are linear in the noise figures p, n_i, $P_{\mathrm{fpoR}} \ll 1$. As P_{fpm} includes the the mean number of phonons induced absorption heating, it is not in general small, and higher orders are kept.

B.3.4. Noise Processes

We now have a closer look at the false positive detection probabilities. They are defined normalized to equivalent phonon numbers

$$P_{\text{fpoR}} = \langle \hat{f}_o^\dagger \hat{f}_o \rangle / (\eta_{\text{d}} \epsilon_{\text{P}}) \tag{B.31}$$

$$P_{\text{fpm}} = \langle \hat{f}_m^\dagger \hat{f}_m \rangle / (\eta_{\text{d}} \epsilon_{\text{R}}). \tag{B.32}$$

In the limit of weak state transfer fidelities, the scattering constants ϵ_{R} and ϵ_{P} are proportional to the respective drive pulse energy. Consequently, the contribution of leaked drive photons to the detector noise is equivalent for the write and read pulse, with

$$P_{\text{leak}} = \eta_f \frac{\kappa^2}{\kappa_{\text{in}}^2} \frac{\tilde{\Omega}^2 + \kappa^2}{4g_0^2} \tag{B.33}$$

in the resolved sideband regime, compare equation (2.79). The second contribution to the false positive detection events are background counts, related e.g. to the detection of stray photons, thermal photons or related to electronic noise. The expectation value of background counts during the gate times for either pulse $P(\text{background})$ is typically negligible compared to leaked photons $P(\text{background})/(\eta_{\text{d}} \epsilon_{\text{P}}) \ll P_{\text{leak}}$. For the read pulse, the third noise source is phonon related to absorption heating caused by drive photons, with the expectation value n_{heating}. In summary, we can approximate the normalized false positive rates as

$$P_{\text{fpoR}} = P_{\text{leak}} + P(\text{background})/(\eta_{\text{d}} \epsilon_{\text{P}}) \tag{B.34a}$$

$$P_{\text{fpm}} = P_{\text{leak}} + P(\text{background})/(\eta_{\text{d}} \epsilon_{\text{R}}) + n_{\text{heating}}. \tag{B.34b}$$

Neglecting background counts $P(\text{background}) \sim 0$ and defining the total average occupation during the read pulse

$$n_f = n_i + p + n_{\text{heating}} \tag{B.35}$$

we can rewrite the cross-correlation (B.30b) as

$$g_{om}^{(2)} = \frac{1 + n_f + n_i}{n_f + P_{\text{leak}}} \tag{B.36}$$

Finally we take into account the time dependence of the mechanical state. One the one hand, the state generated in the heralding process will decay, on the other hand, phonons from the thermal environment will leak into the system. Including these effects, the time dependent expression for the optomechanical cross-correlation becomes

$$g_{om}^{(2)}(t) = \frac{1 + n_i - P_{\text{leak}}}{n_f(t) + P_{\text{leak}}} e^{-\Gamma t} + 1. \tag{B.37}$$

Note that in most cases treated in the experimental part of this thesis, $n_i, P_{\text{fpoR}} \ll 1$ and therefore can be neglected.

Further, we can investigate the autocorrelation of the heralded state. Using the density matrix (B.28), we find that

$$g_{mm,\text{H}}^{(2)} = \frac{\text{Tr}(:\hat{M}_m \hat{M}_m \hat{\rho}_H:)}{\text{Tr}(\hat{M}_m \hat{\rho}_H)^2} \approx 2n_i + 2\bar{M} \approx 2(n_i + n_f + P_{\text{leak}}) \tag{B.38}$$

in a linear approximation. For negligible heating and other false positive detection events, this reproduces the result $g_{mm,\text{H}}^{(2)} = 4n_i$ from reference [Gal+14].

B.4. Generation and Verification of Remote Mechanical Entanglement

In chapter 6, the generation and characterization of remote mechanical entanglement is reported. Here, additional information on the generated state and the verification of entanglement is provided. First, the phase relation of the mechanical state is investigated. Thereafter, the entanglement witness is discussed, providing a more intuitive understanding of its meaning.

B.4.1. The Role of Drive Laser Phase for Remote Mechanical Entanglement

The entanglement between two mechanical elements is generated by the DLCZ protocol [Dua+01]. In brief, spontaneous optomechanical downconversion creates a single photon-phonon pair. The information, in which device the Stokes scattering event took place is erased, overlaping the optical paths on a beamsplitter before detecting the heralding photon. Thereby, the phonon is projected in a superposition of being located in device A or B, see also [Cho+05]. Here, we discuss the relation of the phases between the different modes involved in the experiment.

In order to keep the discussion as simple as possible, we restrict it to the subset of states where a single scattering event took place, neglecting dissipation, absorption and damping in either mode. As discussed in sections 2.3.2 and 2.3.3, we adopt an effective nonlinear interaction picture of the optomechanical scattering processes. For the blue detuned 'write' pulse, one photon from the drive mode $\hat{d}_j^\dagger$ is scattered onto resonance $\hat{o}_j^\dagger$, while creating a phonon in the mechanical oscillator $\hat{m}_j^\dagger$ in either one of the interfereometer arms $j = A, B$. Keeping only the terms where a single scattering event took place, we thus obtain the 'write' interaction $\sqrt{\varepsilon_1}\hat{W}_j = \sqrt{\varepsilon_1}\hat{d}_j\hat{o}_j^\dagger\hat{m}_j^\dagger$, with the single photon scattering probability $\varepsilon_1 = \frac{\kappa_{\text{in}}}{\kappa}\frac{4g_0^2}{\bar{\Omega}^2+\kappa^2}$, compare equation (2.64a).

For the read pulses the anti-Stokes interaction then is equivalently $\sqrt{\varepsilon_1}\hat{R}_j = \sqrt{\varepsilon_1}\hat{d}_j\hat{o}_j^\dagger\hat{m}_j$, compare equation (2.60b). The six modes of the system are described by the wavefunction

$$|\Psi\rangle = |\psi_{\text{drive, A}}, \psi_{\text{mech,A}}, \psi_{\text{opt,A}}, \psi_{\text{drive, B}}, \psi_{\text{mech,B}}, \psi_{\text{opt,B}}\rangle, \tag{B.39}$$

with the optical drive pulse $\psi_{\text{drive, j}}$, mechanical $\psi_{\text{mech, j}}$ and the resonant optical field $\psi_{\text{opt,j}}$ in path $j = A, B$. Initially, we assume all resonances to be in their respective vacuum state. In the first step of the protocol, we drive the Stokes transition, sending coherent pulses with equal amplitudes $|\Psi(t)\rangle = |\alpha(t), 0, 0, \alpha(t)e^{i\phi_0}, 0, 0\rangle$ into the interferometer. A controlled phase offset ϕ_0 is added to arm B. The coherent state oscillates with its optical frequency, i.e. $\alpha(t) = \alpha_0 \cdot e^{-i\omega_{\text{write}}t}$.

Without loss of generality, we assume that both pulses arrive at equal times t_0 at the optomechanical resonators, driving the Stokes transition. The amplitude α_0 is chosen such that the integrated scattering probability $\epsilon_P \ll 1$ of the process is low. Neglecting higher order excitations, the state after the Stokes interaction is $|\Psi_p(t_0)\rangle \propto (1+i\varepsilon\hat{W}_A)(1+i\varepsilon\hat{W}_B)|\Psi(t_0)\rangle$. Selecting only states where a single scattering event took place, we thus

find

$$|\Psi_p(t_0)\rangle \propto (\hat{W}_A + \hat{W}_B)\,|\Psi(t_0)\rangle \tag{B.40a}$$

$$\propto \alpha(t_0)\,|\alpha(t_0), 1, 1, \alpha(t_0)e^{i\phi_0}, 0, 0\rangle + \alpha(t_0)e^{i\phi_0}\,|\alpha(t_0), 0, 0, \alpha(t_0)e^{i\phi_0}, 1, 1\rangle \tag{B.40b}$$

After the interaction, the resonant optical and mechanical excitation acquire phases according to their eigenenergies, i.e. with frequencies ω_c respectively Ω. At time t_1 the signal photons interfere on the combining beamsplitter. Adding the phases of all modes, we find that the phase $\phi_t A, B$ in each arm is equivalent to the phase of the drive beam $\alpha(t_1)$, e.g. for arm A we find $\phi_A = \omega_{\text{write}}t_0 + \omega_c(t_1 - t_0) + \Omega(t_1 - t_0) = \omega_{\text{pump}}t_1$, as $\omega_{\text{write}} = \omega_c + \Omega$. Consequently, the relative phase of the superposition $\theta_m = \phi_0$ is given by the relative phase of the drive beams in the two interferometer arms.

The detectors $i = 1, 2$ on the output of the interferometer beamsplitter are described by the annihilation operators $\hat{p}_i = (\hat{o}_A \pm \hat{o}_B)/\sqrt{2}$ for an ideal 50/50 beamsplitter. Heralding on a detection event in detector i and tracing over the optical modes, see also appendix B.3, we obtain

$$|\Psi_{i,\text{H}}\rangle = |\psi_{mech,A}, \psi_{mech,B}\rangle = (|1, 0\rangle \pm e^{i\theta_m}|0, 1\rangle)/\sqrt{2}. \tag{B.41}$$

At time t_2 we send in the read pulses with amplitudes $\beta(t) = \beta_0 e^{-i\omega_{\text{read}}t}$. After adding an phase offset $-\Delta\phi$ to arm A and ϕ_0 to arm B, they arrive at time t_3 at the optomechanical resonators, yielding the state

$$\begin{aligned}|\Psi(t_3)\rangle \propto{}& e^{-i\Omega(t_3-t_1)}\,|\beta(t_3)e^{-i\Delta\phi}, 1, 0, \beta(t_3)e^{i\phi_0}, 0, 0\rangle \\ &\pm e^{i\phi_0 - i\Omega(t_3-t_1)}\,|\beta(t_3)e^{-i\Delta\phi}, 0, 0, \beta(t_3)e^{i\phi_0}, 1, 0\rangle\end{aligned} \tag{B.42}$$

prior to the interaction.

The anti-Stokes transition acts as a state transfer between the mechanical and resonant optical mode. As there is at maximum a single phonon in either mechanical oscillator, we can again neglect higher order terms. Thus, the state after the anti-Stokes interaction is $|\Psi_r(t_3)\rangle \tilde{\propto} \left(1 + i\varepsilon\hat{R}_A\right)\left(1 + i\varepsilon\hat{R}_B\right)|\Psi(t_3)\rangle$. We further neglect all branches, where no state transfer happened, as we will later on only register states containing photons. Consequently we find for $t > t_3$ the effective state

$$\begin{aligned}|\Psi_{r,\text{eff}}(t)\rangle \propto{}& e^{-i\omega_c(t-t_3)}(\hat{R}_A + \hat{R}_B)\,|\Psi(t_3)\rangle \tag{B.43a}\\ \propto{}& \beta(t_3)e^{-i\Delta\phi - i\Omega(t_3-t_1) - i\omega_c(t-t_3)}\,|\beta, 0, 1, \beta, 0, 0\rangle \\ &\pm \beta(t_3)e^{i\theta_m + i\phi_0 - i\Omega(t_3-t_1) - i\omega_c(t-t_3)}\,|\beta, 0, 0, \beta, 0, 1\rangle.\end{aligned}$$

When the photons arrive at time t_4 at the beamsplitter, we find that the relative phase between the superposition state is equivalent to the sum of the initial mechanical phase θ_m and the phase of an of an optical field at frequency ω_c traveling through the interferometer. This is a consequence of the sideband frequency relation $\omega_{\text{read}} + \Omega = \omega_c$, resulting in the optical phase $\theta_r = \phi_0 + \Delta\phi$. Consequently, the optical effective optical state at the beam splitter is $|\Psi_{\text{read}}\rangle \propto |1, 0\rangle + e^{i(\theta_r + \theta_m)}|0, 1\rangle$.

B.4.2. the witness

The entanglement witness (6.4) developed by Børkje et al. [BNG11] is based on another witness called 'concurrence' [HW97; Woo98; Cho+05]. The concurrence requires a partial state tomography of the entangled state, with one entry being the probability p_{11}

of finding an excitation in both devices. Directly determining this quantity requires a threefold coincidence measurement, with one heralding detection of a Stokes scattered photon and two independent phonon detections, similarly to the Hanbury Brown and Twiss interferometry presented in chapter 5.

The witness (6.4) replaces the direct threefold coincidence measurement by a more resource efficient twofold coincidence measurement. As the initial state is thermal, exhibiting a Gaussian quasi-probability distribution, and all interactions are linear, the final unheralded state is still Gaussian. Thus, higher order statistical momenta, such as p_{11} can be derived from the mean value and covariance of the distribution, or the first and second order degree of coherence.

At the ideal relative phase $\theta = \theta_{\mathrm{opt}}$ between the two mechanical oscillators, the maximum cross-correlation between the Stokes and anti-Stokes photons for either detector combination $\max_{i,j=(1,2)} \left(g_{r_i,p_j}^{(2)} \right)$ can be approximated by the lower cross-correlation of the individual devices $g_{om}^{(2)} = \min_{\mathrm{dev}=(A,B)} \left(g_{om}^{(2)}(\mathrm{dev}) \right)$ [Lau+07]. The witness can be expressed as $R_{\mathrm{m}} \approx 4 \cdot g_{om}^{(2)}/(g_{om}^{(2)} - 1)^2$, requiring $R_{\mathrm{m}} \geq 1$ for separable states.

For $g_{om}^{(2)} \gg 1$ we can thus approximate the visibility of the interference fringes as $V \approx (g_{om}^{(2)} - 1)/(g_{om}^{(2)} + 1) \approx (g_{om}^{(2)} - 1)/g_{om}^{(2)}$. Further, we find with equation (B.36), that the mean number of phonons in the unheralded state is $n_f \approx 1/(g_{om}^{(2)} - 1) \ll 1$. Therefore, we obtain

$$R_{\mathrm{m}} \approx \frac{4n_f}{V} \approx \frac{g_{mm,\mathrm{H}}^{(2)}}{V} \tag{B.44}$$

using the autocorrelation of the heralded state $g_{mm,\mathrm{H}}^{(2)}$ in either one of the devices. In the last step, we neglected readout noise of the phononic state, see also equation (B.38) or reference [Gal+14]. The quantity n_f can be interpreted as the noise in the system expressed as an average phonon number. In a classically correlated state, e.g. two identical coherent states in both oscillators, the mechanical shot noise $n_f \sim 1/2$ will ensure $R_{\mathrm{m}} \geq 1$[10]. In other words, the witness requires stronger correlations than classically possible to demonstrate that the two mechanical oscillators are entangled.

The final expression of (B.44) further clarifies the meaning of witness. A violation of the separability criterion, i.e. $R_{\mathrm{m}} < 1$ requires (1) $g_{mm,\mathrm{H}}^{(2)} < 1$ as well as (2) a large visibility V. The first condition (1) ensure that only a single phonon is present in the system. The second condition (2) demonstrates that the state of both mechanical oscillators is coherent. In other words, the single phonon must be in a coherent superposition of being located in device A and B, corresponding to path entanglement, as described in equation (B.41).

---

[10] Note that (B.44) is only valid for $n_f \ll 1$, i.e. it is not directly applicable for $n_f \sim 1/2$.

C. Curriculum Vitae

Education

Oct 2013 - Sep 2018	**Doctoral Studies in Physics**, University of Vienna, Austria
Oct 2011 - Sep 2013	**M.Sc. in Physics**, Philipps University Marburg, Germany and University of Vienna, Austria
Oct 2008 - Sep 2011	**B.Sc. in Physics**, Philipps University Marburg, Germany and Université Joseph Fourier, Grenoble, France
Sep 1999 - Jun 2008	**Abitur**, Humboldt Gymnasium Vaterstetten, Germany

Research Experience

Oct 2013 - Sep 2018	**Research Assistant** Prof. Markus Aspelmeyer Lab, University of Vienna, Austria Topic: Single phonon quantum optics
Jun 2017 - Aug 2017	**Secondment** Prof. Simon Gröblacher Lab, TU Delft, Netherlands Topic: Suspendend photonic crystals in silicon on insulator
Oct 2012 - Sep 2013	**Project Student** Prof. Markus Aspelmeyer Lab, University of Vienna, Austria Topic: Optomechanical state reconstruction
Oct 2010 - Feb 2011	**Project Student** Prof. Martin Koch Lab, Philipps University Marburg, Germany Topic: Tunable waveguide optics for THz radiation

Teaching Experience

Oct 2017 - Feb 2018	**Teaching Assistant** Exercise to "Introduction to Physics 3", B.Sc. curriculum
Oct 2016 - Feb 2017	**Teaching Assistant** Exercise to "Introduction to Physics 3", B.Sc. curriculum
Mar 2016 - Sep 2016	**Teaching Assistant** Seminar "Problems and Solutions in Experimental Physics", Ph.D. Curriculum

Other Work Experience

Aug 2011 - Sep 2011	**Internship, German Parliament**, Berlin, Germany
Apr 2011 - Jun 2011	**Internship, European Parliament**, Brussels, Belgium

Honors and Awards

Oct 2014 - Sep 2018	**Affiliation with CoQuS Doctoral School** (Doctoral school for research in Complex Quantum Systems)
Jan 2016 - Mar 2018	**DOC Scholarship** by the Austrian Academy of Science (OEAW)
Jan 2009 - Sep 2013	**Scholarship Studienstiftung des deutschen Volkes** (German Academic Scholarship Foundation)

Publications

[Hon+17]   S. Hong, R. Riedinger, I. Marinković, A. Wallucks, S. G. Hofer, R. A. Norte, M. Aspelmeyer, and S. Gröblacher, "Hanbury Brown and Twiss interferometry of single phonons from an optomechanical resonator", *Science* 358, 203 (2017), DOI: `10.1126/science.aan7939` (cited on pgs. 3, 4, 10, 31, 40, 48, 63, 87, 139).

[Mag+18]   L. Magrini, R. A. Norte, R. Riedinger, I. Marinković, D. Grass, U. Delić, S. Gröblacher, S. Hong, and M. Aspelmeyer, "Nanophotonic near-field levitated optomechanics" (2018), arXiv: `1804.06676` (cited on pgs. 56, 60).

[Mar+18]   I. Marinkovic, A. Wallucks, R. Riedinger, S. Hong, M. Aspelmeyer, and S. Gröblacher, "An optomechanical Bell test" (2018), arXiv: `1806.10615` (cited on pgs. 63, 115, 116, 140).

[Rie+16]   R. Riedinger, S. Hong, R. A. Norte, J. A. Slater, J. Shang, A. G. Krause, V. Anant, M. Aspelmeyer, and S. Gröblacher, "Non-classical correlations between single photons and phonons from a mechanical oscillator", *Nature* 530, 313 (2016), DOI: `10.1038/nature16536` (cited on pgs. 3, 4, 27, 31, 48, 52, 61, 62, 90, 113, 116, 139).

[Rie+18]   R. Riedinger, A. Wallucks, I. Marinković, C. Löschnauer, M. Aspelmeyer, S. Hong, and S. Gröblacher, "Remote quantum entanglement between two micromechanical oscillators", *Nature* 556, 473 (2018), DOI: `10.1038/s41586-018-0036-z` (cited on pgs. 4, 31, 63, 90, 111, 113, 139).

[Wie+15]   W. Wieczorek, S. G. Hofer, J. Hoelscher-Obermaier, R. Riedinger, K. Hammerer, and M. Aspelmeyer, "Optimal State Estimation for Cavity Optomechanical Systems", *Physical Review Letters* 114, 223601 (2015), DOI: `10.1103/PhysRevLett.114.223601` (cited on pgs. 2, 31, 55).

Acknowledgments